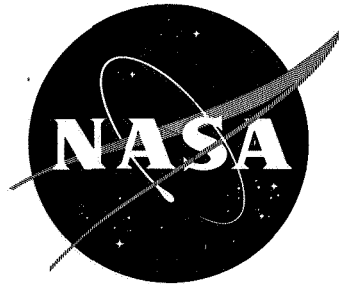LMSC-D352380

FINAL REPORT

DEVELOPMENT OF TECHNIQUES AND ASSOCIATED INSTRUMENTATION FOR HIGH TEMPERATURE EMISSIVITY MEASUREMENTS

Contract NAS8-26304

CASE FILE COPY

Prepared for

NATIONAL AERONAUTICS AND SPACE ADMINISTRATION

FINAL REPORT

DEVELOPMENT OF TECHNIQUES
AND ASSOCIATED INSTRUMENTATION
FOR HIGH TEMPERATURE
EMISSIVITY MEASUREMENTS

CONTRACT NAS 8-26304

June 1973

PREPARED FOR

NATIONAL AERONAUTICS AND SPACE ADMINISTRATION
GEORGE C. MARSHALL SPACE FLIGHT CENTER
MARSHALL SPACE FLIGHT CENTER, ALABAMA

BY G. R. CUNNINGTON, A. I. FUNAI AND P. E. CASSADY

ENGINEERING SCIENCES

FOREWORD

This report was prepared by the Lockheed Palo Alto Research Laboratory, Lockheed Missiles & Space Company, Inc., for the George C. Marshall Space Flight Center of the National Aeronautics and Space Administration as the final report of the research activities carried out under Contract NAS 8-26304 from July 1970 to June 1973. The NASA Project Manager was Mr. Roger Harwell, George C. Marshall Space Flight Center, Materials Division, Astronautics Laboratory.

ABSTRACT

Studies were made to develop a test apparatus for the measurement of
total emittance of materials under repeated exposure to simulated earth
entry conditions. As no existing test facility met the emittance measure-
ment and entry simulation goals, a new apparatus was designed, fabricated
and checked out. This apparatus has the capability of performing total and
spectral emittance measurements during cyclic temperature and pressure
exposure under sonic and supersonic flow conditions. Emittance measure-
ments were performed on a series of oxidized superalloys, silicide coated
columbium alloys and ceramic coatings.

v

CONTENTS

ILLUSTRATIONS

TABLES

xvii

SYMBOLS

A   Area (cm^2)

c_1 First radiation constant $(3.7405 \times 10^{-12} \text{ watt-cm}^2)$

c_2 Second radiation constant $(1.4388 \text{ cm-}°K)$

E   Total emissive power of a surface (watts/cm^2)

NOTE: For a blackbody, $E_b = \sigma T^4$

E_λ Spectral emissive power of a surface (watts/cm^3)

NOTE: For a blackbody, $E_{\lambda b} = c_1/\lambda^5 (e^{c_2 \lambda T} - 1)$

e   Natural logarithm base $(2.718...)$

$K, \overline{K}$ Detection system or radiometer response constants

M   Mach number

M_∞ Free stream Mach Number

N   Radiance of a surface $(\text{watts/cm}^2\text{-sr})$

N_λ Spectral radiance of a surface $(\text{watts/cm}^3\text{-sr})$

P   Pressure (torr), or Power (watts)

P_c Test chamber pressure

P_t Upstream pressure to sonic and supersonic flow nozzles

P_s, P_m Total pressure at sample surface in sonic or supersonic flow environments, measured pressure with flat calibrating test plate (see Section 6.1)

P_{in} Input heating power to test-section area of sample (watts)

P_L Non-radiative power loss from the test-section area of sample (watts)

q_c Convective heat flux (watts/m^2)

q_r Radiative heat flux (watts/m^2)

q Aerodynamic heat flux (watts/m^2)

S Radiometer signal for a particular target (volts); e. g. , S_s when viewing sample, S_r when viewing radiometer reference cavity, S_b when viewing blackbody target

T Temperature (°K)

U Boundary layer velocity (km/sec)

V Radiometer output signal for a particular target (volts), e. g. ,
$$V_s = S_s - S_r$$

α Absorptance

α_λ Spectral absorptance

α_s Solar absorptance

δ Boundary layer thickness (meters)

ϵ Emittance

ϵ_λ Spectral emittance

ϵ_{TN} Total normal emittance

ϵ_{TH} Total hemispherical emittance

$\epsilon_A, \epsilon_{\lambda A}$ Used to designate assumed values of total and spectral emittance in figures 9, 10, 11

λ Wavelength (μm)

θ, Φ Direction angles for emitted radiation (pp 5) or incident radiation (pp 6)

θ', Φ' Direction angles for reflected radiation (pp 6)

ρ Reflectance

ρ_λ Spectral reflectance

σ Stefan–Boltzmann constant (5.6697×10^{-12} watts/cm^2-$^\circ$K^4)

τ Transmittance

τ_λ Spectral transmittance

Subscripts

b   Designates property of blackbody

s   Designates property of sample

c, ch, r, w, o   Used in Section 5 to designate properties of the test chamber walls, chopper blade, reference cavity, window and ambient temperature surrounds, respectively

t   Total

Section 1
INTRODUCTION

Design of radiatively cooled thermal protection systems for reusable earth entry vehicles is dependent upon an accurate knowledge of the total emittance of the exterior surface material as a function of temperature, and the stability of this property during exposure to the entry environment. Because of the reusability factor, the emittance of the high-temperature materials should be evaluated for repeated exposures to cyclic temperatures in an oxidizing atmosphere at total pressures from less than 1 torr to nearly atmospheric pressure. Considerations must also be given to the effects of the gas stream in terms of velocity, angle of incidence on the surface, composition, and its temperature in relation to that of the surface. Because of the complexity introduced by the environmental simulation aspect the selection of the technique and experimental apparatus was made after the completion of a study of the exposure conditions required to reasonably duplicate the behavior of the radiative properties of candidate materials under entry conditions. Investigations were then made into the potential of using existing facilities to perform emittance studies for this application. As none met the requirements for simulation together with adequate emittance measurement capability, a new facility was prepared. This apparatus has the capability for total and spectral emittance measurements on metals and ceramic coatings to 1900° K at pressures of 10^{-6} to 760 torr in a static atmosphere or with a flow of air directed onto the test surface. The air velocity may be varied from subsonic to Mach 3, and the apparatus is designed such that provision can be made for heating the air stream to 2200° K using an r-f plasma.

The objectives of this program were to develop an experimental apparatus for emittance measurements under simulated entry conditions and to perform measurements on a series of candidate space shuttle thermal protection system materials under

repeated simulated entry exposure conditions. The capabilities of the experimental apparatus are:

- Total and spectral normal emittance from 500° to 1900° K in static air and during exposure to free stream Mach numbers to 3 (air)

- Total hemispherical emittance in vacuum (10^{-5} torr) for electrical conductors or surfaces on electrical conductors to 1900° K

- Total pressure on specimens from 1 to 760 torr during flow testing

- Flow system adaptable to hot gas source using r-f air plasma and hypersonic Mach numbers

The materials investigated during the measurements phase of the program were:

- Anodized Ti-6Al-4V alloy, maximum test temperature of 700° K.

- Solar SP-93A-I coating on René 41 and oxidized René 41, maximum test temperature of 1143° K.

- Oxidized HS-188, maximum test temperature of 1360° K.

- Oxidized TD Ni Cr, maximum test temperature of 1470° K.

- VH 101 coating on Cb 129Y, maximum test temperature of 1640° K.

- R512E coating on Cb 752, maximum test temperature of 1640° K.

- Lockheed Missiles and Space Co., Inc. 0042 coating.

- McDonnell-Douglas HCF coating.

Emittance measurements were made in vacuum for the anodized Ti-6Al-4V alloy, coated René 41 alloy, and six oxidized René 41 samples as discussed in Appendix A. Static air as well as sonic and supersonic flow tests were conducted on oxidized René 41 and all of the remaining high temperature alloy materials. No significant differences in total emittance were observed between static, sonic and supersonic exposures. Some changes in emittance between the as prepared and post-environmental

exposure conditions were observed, but these generally occurred during the initial exposure cycle. Static and sonic flow exposure tests were conducted on the RSI coatings and no significant changes in the emittance properties of either material were observed.

Discussions of the test facility development, checkout and measurement phases of the program are given in the following sections.

Section 2
SURVEY OF REQUIREMENTS AND FACILITIES

2.1 BACKGROUND

During the initial phase of the program a survey was made to determine the current
state-of-the-art in high temperature emittance measurement methods and available
test facilities which had environmental simulation capability. This survey was based
upon a comprehensive literature review and contacts with a number of industry,
government, and university personnel. Two computerized information retrieval
services, NASA/RECON and the Defense Documentation Center, were utilized for the
literature review. Using subject descriptors such as high temperature emittance,
materials, measurements, reentry vehicles, simulation, and radiant heat transfer
approximately 1300 references to technical journal articles and NASA and DOD
contractor's reports were obtained. From this total, 170 references were pertinent
to the materials and measurements problems of the program (Ref. 1). As a result of
the literature survey questionnaires were sent to 28 laboratories and research organi-
zations regarding experimental facilities. From the response to these questionnaires
visits were made to 10 laboratories to discuss measurement and simulation methods
and existing test facilities. The results of the survey and discussions were reviewed
in terms of measurement methods and simulation requirements, and an evaluation was
made of the existing test facilities.

Numerous experimental techniques have been used for determining the emittance of
opaque materials over a wide range of temperatures. Direct methods of emittance
measurement employ either calorimetric (total hemispherical emittance) or radiomet-
ric (total or spectral directional) techniques. Emittance is also computed (indirect
method) from the measured reflectance properties of a surface. Before proceeding
to a discussion of the measurement methods the radiant properties are briefly
summarized.

Emittance — This is defined as the ratio of radiant power per unit area emitted by a surface (from thermal excitation only) to that from a perfect emitter (a blackbody) over all half-space above the surface. For the monochromatic case the surface emittance is $\epsilon_\lambda = E_\lambda/E_{\lambda b}$. Total emittance is defined in the same manner, where the emissive powers of the surface and the blackbody are integrated over all wavelengths. These are then respectively the monochromatic and total hemispherical emittances of a surface.

Real surfaces exhibit a directional nonuniformity of energy distribution, and the degree of nonuniformity is a function of both intrinsic material properties and surface characteristics. Polished metals, for example, emit significantly more strongly at grazing angles while dielectrics emit slightly more energy in a normal direction (Ref. 2). Thus, to describe the emittance properties of a real surface the emittance is defined in terms of the spherical coordinates (θ, Φ) of a directional beam from that surface. Integration of the surface radiant power per unit area over all angles and wavelengths and dividing this by the blackbody power results in the total emittance of a directional surface.

Reflectance — Of the total radiant flux incident on an opaque surface, a fraction is reflected and the remainder absorbed. From Kirchhoff's law, the absorptance and emittance are equal provided that the energy absorbed or emitted is created by the same temperature (i.e., surface in thermal equilibrium with its surroundings and at the same temperature as the surroundings). For the condition where the source and surface are at different temperatures it can be shown through an extension of Kirchhoff's law that the monochromatic absorptance and emittance are equal ($\alpha_\lambda = \epsilon_\lambda$), and monochromatic emittance can be derived from

$$\epsilon_\lambda = 1 - \rho_\lambda$$

which also applies to directional properties.

The primary reflectance properties (Ref. 3) which may be used for computing emittance are:

- Bihemispherical reflectance, ratio of energy reflected into hemisphere above the surface to that diffusely incident over the hemisphere ($\epsilon_\lambda = 1 - \rho_\lambda$).

- Directional hemispherical reflectance, ratio of energy reflected into the hemispherical space above the surface to that incident in an elemental cone around θ, Φ. Hemispherical emittance, ϵ_λ, computed from integration over all angles of incidence.

- Bidirectional reflectance, ratio of energy reflected into an elemental cone in the direction θ', Φ' to the energy incident within an elemental cone in direction θ, Φ. Many measurements are required to obtain ϵ_λ and the time required becomes very cumbersome for transient studies.

2.2 THERMAL RADIATION PROPERTIES MEASUREMENT METHODS

As the radiation property of prime importance to the thermal protection system design is total hemispherical emittance the ideal experimental method would be one which measures this property directly. However, the environmental simulation require-ments present several serious difficulties in utilizing this approach. Calorimetric emittance measurements are based upon an energy balance with the surroundings, and consequently, the convective heat transfer from the sample must be very accurately known. Radiometric measurements of a nearly hemispherical emittance may also be made, but the large collecting optical system interferes with the flow simulation. Although radiometric measurements of directional emittance do not require optical systems which are incompatible with the environmental requirements, the hemispher-ical value must be obtained by either integration of the directional data or by assuming a ratio of normal to hemispherical emittance for the surface. Reflectance measure-ments also have been utilized for high temperature studies of emittance properties of materials, but again, this approach is not compatible with the flow simulation re-quirements because of the presence of optical elements within the test chamber which are subject to contamination by the environment and interfere with the gas flow.

The experimental methods which are most applicable to this program are the calor-imetric or radiometric measurements of emittance. The success of the calorimetric method is dependent upon the accuracy to which the convective heat transfer is known. The radiometric method requires a calibrated detector and optical viewing system for determining the quantity and quality of radiation emitted from the surface of a test specimen relative to the radiation emitted by a blackbody at the same temperature. The general test conditions and measurement parameters required for each of these methods are reviewed below.

2.2.1 Calorimetric Methods

Calorimetric methods have been developed to determine the total hemispherical emit-tance of specimens at temperatures as low as 20° K to temperatures as high as 3000° K. The procedure involves a determination of the net energy lost by radiation from a sample heated to a steady state test temperature. It is the most direct approach for total hemispherical emittance determinations since directional effects need not be considered in performing the energy balance. Heating of the sample can be accom-plished with a variety of techniques, although at temperature above ambient levels it is most common to use electrical power. For an electrically conducting material, a current can be passed through the sample itself, while for insulators it is necessary to place them on a substrate which is heated either electrically or by some other means such as by a heater totally enclosed within the specimen.

As the calorimetric method is based upon an energy balance between the specimen and its environment, the measurements are generally made in vacuum so that radiation is the only significant heat-transfer mechanism. For test chamber pressures above 10^{-2} torr, convective heat transfer becomes increasingly important and must be accurately accounted for in order to preserve the accuracy of the total hemispherical emittance determination. Convective heat-loss corrections are difficult to determine and change with ambient pressure, surface temperature, specimen size, and specimen orientation; consequently, radiometric measurement methods are generally used for nonvacuum exposure conditions. Calorimetric emittance determinations in flowing-gas

environments are virtually impossible with any suitable degree of accuracy because of large errors associated with the convective heat transfer.

From the energy balance equation for a sample at steady state conditions the total hemispherical emittance is computed from (Ref. 4)

$$\epsilon_{TH} = \frac{P_{in} - P_L}{A_s \, \sigma \left(T_s^{\,4} - T_o^{\,4} \right)}$$

and the accuracy of the calorimetrically determined value is a function of the following parameters:

T_s,   the surface temperature of the test specimen

T_o,   the temperature of the test chamber walls surrounding the test specimen

A_s,   the radiating surface area of the test specimen

σ,   Stefan–Boltzmann constant

P_{in},   the input heating power to the test specimen

P_L,   the nonradiative heat losses from the test specimen

The uncertainty in test area, A_s, is negligible for engineering calculations. For electrical heating methods the error in P_{in} is generally less than 0.25 percent because of the high accuracy of current and potential drop measuring instrumentation and the availability of well regulated power supplies.

The principal sources of error are temperature measurement and the nonradiative losses. The error in emittance due to temperature measurement is expressed as

$$\left[\frac{\Delta \epsilon_s}{\epsilon_s} \right]_T = \left[\frac{4\,T_s^4}{T_s^4 - T_o^4} \right] \frac{\Delta T_s}{T_s} + \left[\frac{4\,T_o^4}{T_s^4 - T_o^4} \right] \frac{\Delta T_o}{T_o}$$

and the emittance error as a function of the $\Delta T_s/T_s$ and T_s/T_o terms as shown in figure 1. The same results are obtained for values of $\Delta T_s/T_o$ as a function of T_o/T_s. Since the temperature of the surrounds represents a source of background energy that must be differentiated from the sample emittance, it is customary to cool the background to levels where $T_s/T_o \geq 3.0$. Measurements performed with $T_s/T_o < 3.0$ require an accurate determination of both T_s and T_o to avoid increasing the basic error due to the sample temperature measurement.

The error due to nonradiative losses from the test area most commonly results from solid conduction through instrumentation leads and to the cooled specimen ends and from convection to an ambient atmosphere or a flowing gas stream. The influence of solid conduction is minimized through the use of small leads and proper selection of specimen geometry. Errors due to convection or gas conduction are generally eliminated by performing the measurements under vacuum conditions (10^{-5} torr or less). In a static or flow environment at pressures in the range of 1 to 760 torr convective losses become significant. The relationship of convective to radiative heat transfer in a static environment is illustrated in figure 2. The error associated with this loss is directly proportional to product of the uncertainty in the convective heat flux and the ratio of convective-to-radiative heat fluxes. Experimental studies of the convective loss term are discussed in Section 3.3.

2.2.2 Radiometric Methods

Radiometric determinations of total or spectral high temperature emittance are accomplished by "viewing" the energy emitted by a sample with a calibrated detector. For total measurements, the detector used can be a thermocouple, thermopile, bolometer, or a similar unit that is responsive to the radiant flux emitted by the specimen. For spectral measurements, the total detector is replaced by a monochromator (prism, grating, or filter), and a sensitive detecting system.

The electrical heating technique is frequently used for conducting samples. Other indirect methods such as radiant heating, induction heating, or electron beam heating
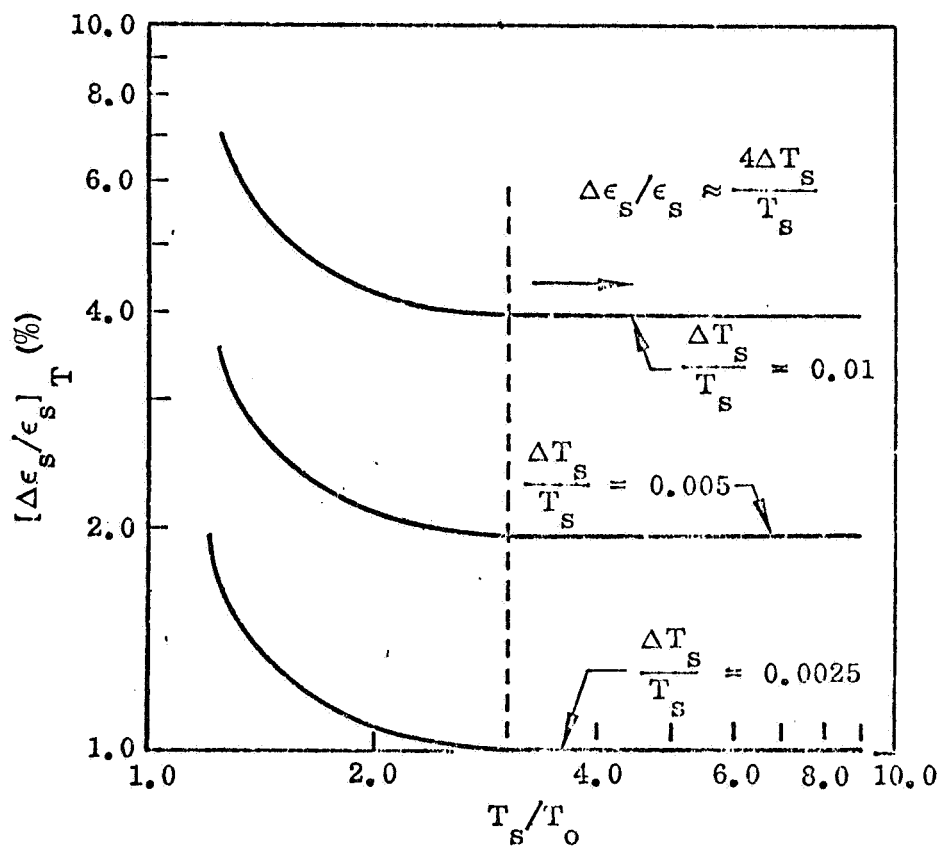
Fig. 1 Error in Emittance Due to Temperature Measurement Error
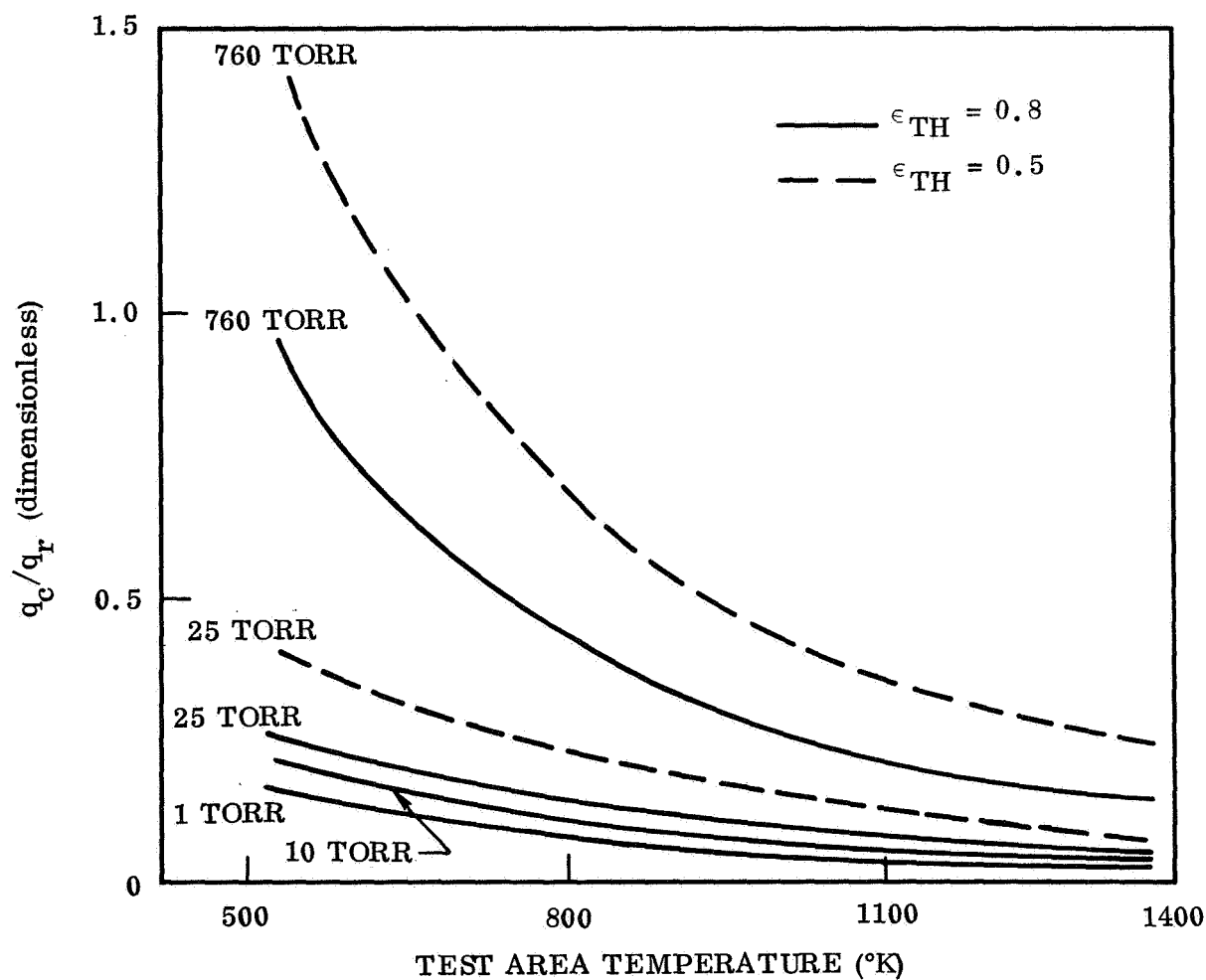
Fig. 2 Ratio of Convective to Radiative Heat Fluxes from Test Area as a Function of Temperature and Ambient Pressure for Surfaces of ϵ_{TH} = 0.8 and 0.5 in a Static Air Environment

2-8

are also commonly used; however, the measurement procedure is basically the same. The heated sample is surrounded by an enclosure at temperature T_o, and the emitted energy is detected by a calibrated detector. An external optical system is normally used to collect and direct the emitted beam to the detecting system, and a beam-chopping system is used to obtain a modulated detector signal suitable for amplification and measurement. The simplified equation for emittance is

$$\epsilon = V/K\sigma \left(T_s^4 - T_o^4 \right)$$

where V is the detector response and K a detection system constant.

From the preceding equation it is seen that temperature measurement errors have the same effect on total emittance error as for the calorimetric method (see figure 1). However, the other uncertainties associated with energy losses from the measuring area by conduction and convection are eliminated in the radiometric method. For this reason such measurements can be made in air as long as the area viewed by the detection system is uniform in both temperature and emittance.

The detector introduces sources of error that are difficult to assess numerically in general terms since numerous types of detectors are in current use. Detector errors are minimized through adherence to the following requirements:

- The detector is gray throughout the energy spectrum of interest (non-gray error).

- Detector response is a linear function of incident energy (nonlinearity error).

- Detector response is uniform for energy incident from all receiving directions (directional sensitivity error).

- Detector sensitivity for all surface area elements is constant (nonuniformity error).

Since no single detector in current use meets all of these requirements, it is necessary to systematically investigate the system performance in terms of the above requirements to minimize errors due to the detection scheme.

Spectral emittance can be determined by focusing the emitted energy on the inlet slits of a calibrated monochromator-detector system and scanning the spectrum of interest, or by using narrow band pass filters in the detection system. For the spectral case, the temperature measurement error is a function of both wavelength and absolute temperature, and can be evaluated by

$$\left(\frac{\Delta\epsilon_{\lambda s}}{\epsilon_{\lambda s}}\right)_{T_s} = \left(e^{c_2/\lambda T_s} - 1\right)^{-1} e^{c_2/\lambda T_s} \frac{c_2}{\lambda T_s}\frac{\Delta T_s}{T_s}$$

The error as a function of wavelength is shown by figure 3 for several temperature measurement errors. Errors due to the monochromatic detection system are similar to those of a total detector with the addition of several sources within the monochromator itself. Scattered energy, wavelength resolution, atmospheric absorption, and the effects of the reflecting and transmitting optics in the transfer system must also be evaluated.

The direct measurement of hemispherical emittance using radiometric procedures can be accomplished by collecting the sample energy emitted over 2π steradians with a parabolic or elliptic reflector and directing the collected energy to a detector. This approach introduces problems due to blockage of the collected beam by the sample, aberrations due to the required high f number system, interreflections between the sample and detector, and in some cases detector heating. Also, large collecting optics may interfere with the gas flow, and contamination of the optics is a serious problem. In the practical application of this concept, it is often found that sample directional effects are a major source of error because the collecting system is sensitive to any nonuniformity of the collected beam.
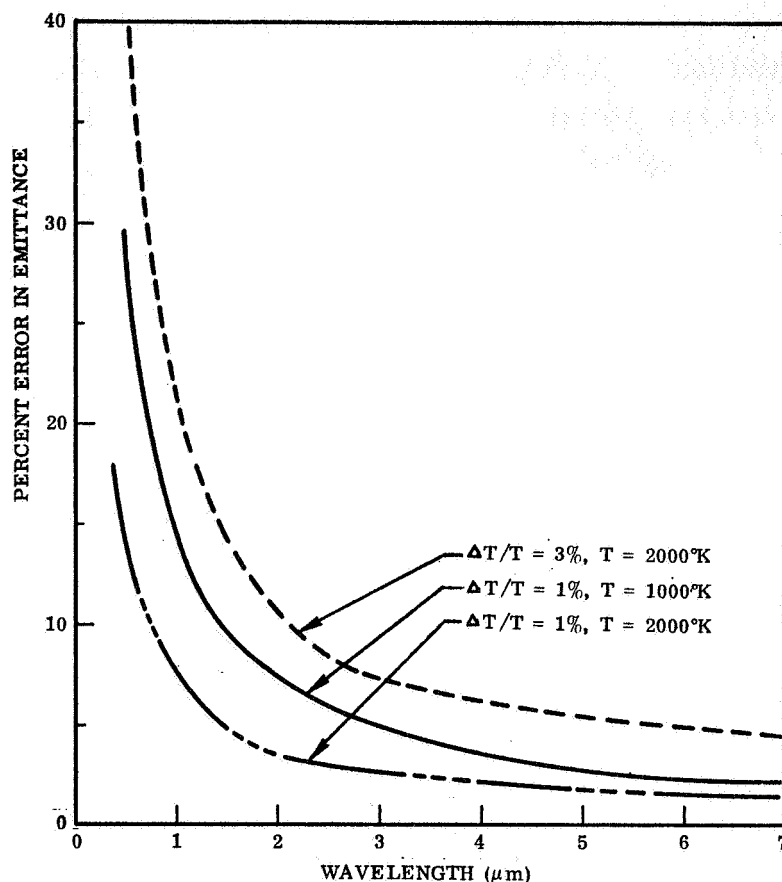
Fig. 3 Spectral Emittance Error as a Function of Wavelength and
Temperature Error

2.3 ENVIRONMENTAL SIMULATION

At high temperatures, the thermal radiative properties of many materials are strongly
dependent upon the environment in which they are heated. Factors such as time of
exposure and the pressure, temperature, and gas species present in the atmosphere
with which the material is in contact may control the composition of the surface layer
which in turn governs the radiative properties of the material. Shearing forces due to
high velocity flow may result in the removal of portions of this surface layer and alter
the radiative characteristics of the body. Also, rapid temperature changes may induce
thermal stresses which singly, or in combination with stresses due to the shear forces
will remove some of the surface material. Finally, as the shuttle is designed for up
to 100 reuse cycles, the effect of repeated exposure to these environments must be
considered.

Other environmental factors such as vibration, strain, water and salt atmospheres, impact, and abrasion may also play an important role in the performance of the surface material. Vibrational loads will occur principally during boost and at low altitudes during entry at which time surface temperatures are low. Also, large strains due to aerodynamic forces will not occur in the high temperature portions of the flight. Similarly, exposure to water and salt atmospheres, erosion, and impact, except orbital meteoroid considerations, will be during the low altitude part of the flight. While these environmental factors are important to the reuse capability, they do not bear directly on emittance stability during a specific entry cycle. As the effects of these environments will not change with time, the period between environmental exposure and testing will not have any significant influence on the emittance properties. Specimens could be exposed to these mechanical and low altitude environments and subsequently tested under the simulated emittance measurement entry conditions to evaluate their effects on the radiative behavior of the candidate materials.

2.3.1 Entry Environment

To establish the simulation capabilities required for the test apparatus, an analysis was performed to develop typical boundary layer flow properties at three locations on an orbiter vehicle. For this purpose a Delta body configuration, figure 4, was selected, and the entry trajectory parameters were for a 2300 km cross range, figure 5. As no specific configuration had been selected by NASA for the orbiter at this point in the program, the Delta body was used because of LMSC's extensive studies on this configuration. Three surface locations representative of maximum temperatures were employed for the analysis; stagnation point, lower surface at mid-body, and leading edge. An approximate analysis was carried out to determine temperature density, and species concentration profiles across the boundary layer. The following assumptions were made for the simplified model:

- Viscous flow field is locally similar in that the boundary layer flow at any point along the vehicle surface approximates a wedge-like local pressure gradient. Consequently, a similarity transformation can be used to reduce the partial differential equations to the ordinary type for numerical analysis.

NOSE RADIUS = 2.32 m
LEADING EDGE RADIUS = 1.22 m
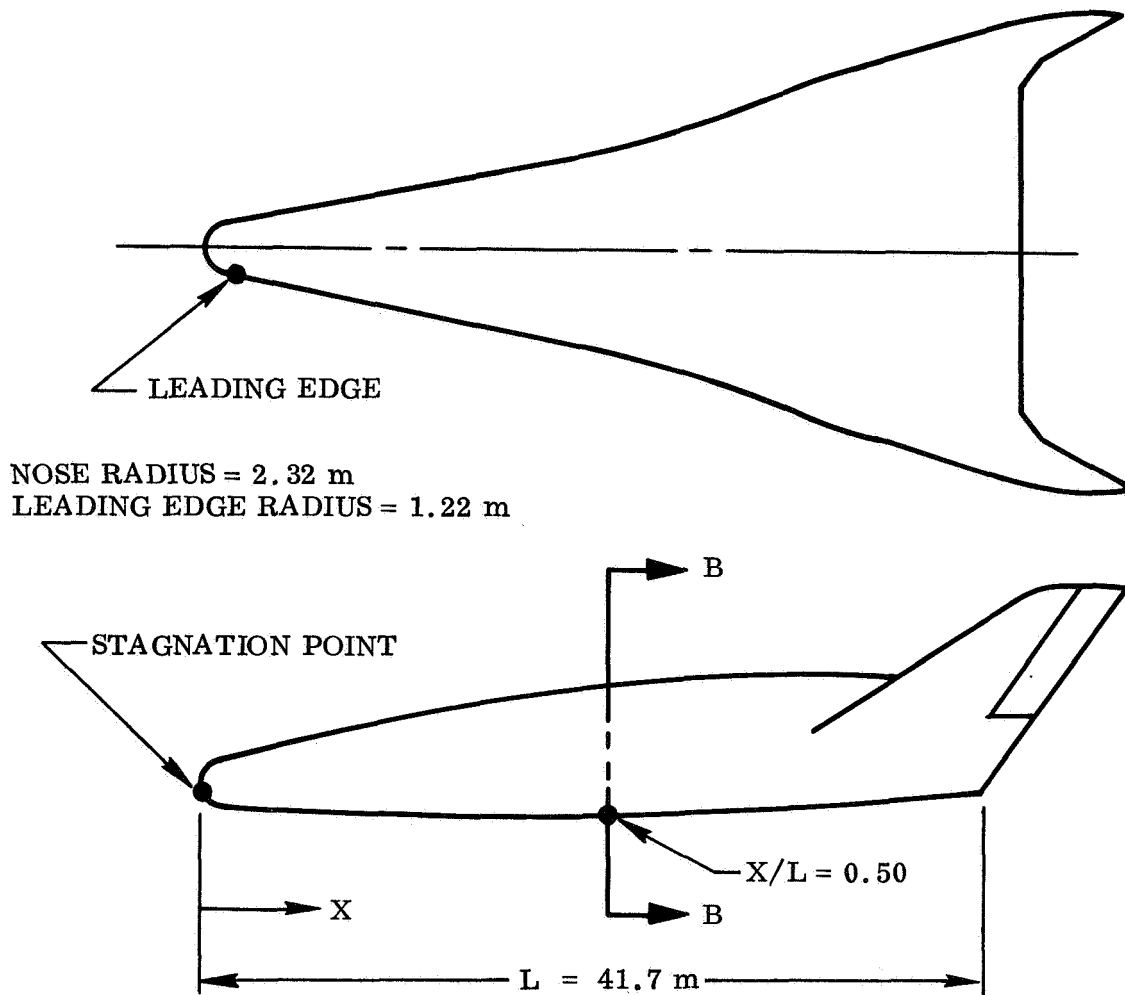
Fig. 4 Delta Body Orbiter Configuration Used for Flow Properties Study

2-13
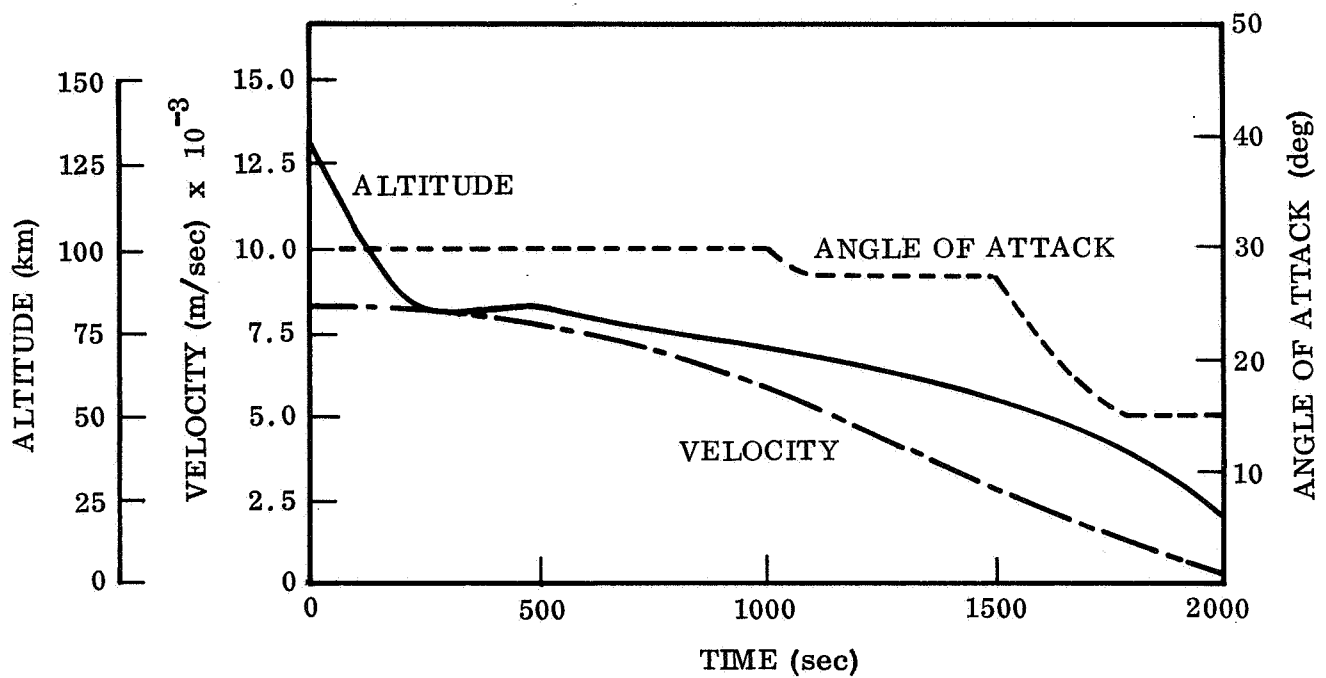
Fig. 5 Typical Delta Body Orbiter Entry Trajectory for a 2300 km
Cross Range

2-14

● Equilibrium air chemistry with no surface ablation or mass injection.

The stagnation-point boundary layer profiles were developed using two functional boundary layer computer programs. Vorticity and boundary layer thickness parameters were determined (Ref. 5), and then temperature and density profiles were constructed (Ref. 6). Finally, equilibrium thermochemical calculations were carried out to obtain species concentration profiles.

The procedure was also used to compute the boundary layer properties at the lower surface location. However, in contrast to the stagnation point case, laminar-to-turbulent transition occurs at this location during entry. Since the programs are valid only for pure laminar or fully developed turbulent flows, the turbulent option was used when transition was encountered. Also, because of vehicle pitching during entry, crossflow boundary layer effects may occur. However, since this location is on the windward plane of symmetry, a small cross flow is anticipated at moderate angles of attack. Thus, it was neglected for this analysis.

At the leading edge, the swept infinite cylinder theory was used as the vehicle configuration has a relatively straight swept leading edge. For the laminar flow regime, assuming thermochemical equilibrium, the swept cylinder boundary layer profiles of Ref. 7 were used to describe the leading edge case. At lower altitudes (< 40 km), the leading edge flow is turbulent and the 1/5-power law of Ref. 8 was used in profile determination.

The computed boundary layer properties are given in Table 1, and it is seen that during the elevated temperature portion of the entry surface temperature will vary from 500° to 1700° K; boundary layer temperatures range from less than 500° to 5,500° K; total pressures at the surface will vary from 5 to nearly 100 torr; and the Mach number range is from 3 to 25. Also, dissociation of oxygen occurs in the boundary layer, but with the exception of a very short time period at the stagnation point, the boundary layer at the surface is essentially undissociated air (N_2 and O_2). Using these results and limited data appearing in the open literature on the behavior of materials in simulated earth entry environments, the flow simulation requirements for the emittance apparatus were established.

2-15

TABLE 1

THERMODYNAMIC ENVIRONMENT DATA

Time (sec)	Altitude (km)	M_∞	$\dot{q}$ (W/m²×10⁻⁴)	U_e (km/sec)	P_e (Torr)	T_e (°K)	T_w (°K)	δ (m)	Flow Conditions	O_2	N_2	O	N	NO	Density at Surface (kg/m³)
						STAGNATION POINT									
300	75	25.4	41	0	19.0	5850	1650	0.025	Laminar	0.21	0.76	0.02	<10⁻⁴	10⁻³	5.3X10⁻³
1000	63.5	17.3	28	0	47.0	5300	1600	0.016	Laminar	0.22	0.76	<10⁻²	<10⁻⁴	10⁻⁴	1.4x10⁻²
1400	53.5	11.4	9	0	66.7	3500	1330	0.010	Laminar	0.23	0.76	<10⁻⁴	<10⁻⁴	10⁻⁴	2.4X10⁻²
1650	45.7	6.4	3	0	69.6	1900	930	0.008	Laminar	0.23	0.76	<10⁻⁴	<10⁻⁴	<10⁻⁴	3.5X10⁻²
1750	39.6	5.1	—	0	77.8	1350	795	0.005	Laminar	0.23	0.76	<10⁻⁴	<10⁻⁴	<10⁻⁴	4.8X10⁻²
1850	31.6	3.9	—	0	84.7	930	650	0.003	Laminar	0.23	0.76	<10⁻⁴	<10⁻⁴	<10⁻⁴	6.4X10⁻²
						LOWER SURFACE AT X/L = 0.5									
300	75	25.4	7	19.9	5.0	3500	1050	0.121	Laminar	0.23	0.76	<10⁻⁴	<10⁻⁴	10⁻³	2.2X10⁻³
1000	62.5	17.3	17	14.6	12.8	3000	1470	1.27	Turbulent	0.23	0.76	10⁻³	<10⁻⁴	10⁻³	4.0X10⁻³
1400	53.5	11.4	6	10.3	14.9	1850	1200	1.05	Turbulent	0.23	0.76	<10⁻⁴	<10⁻⁴	10⁻³	5.8X10⁻³
1650	45.7	6.4	2	6.0	15.7	775	1160	0.35	Turbulent	0.23	0.76	<10⁻⁴	<10⁻⁴	10⁻³	6.3X10⁻³
1750	39.6	5.1	—	4.7	17.7	510	830	0.090	Turbulent	0.23	0.76	<10⁻⁴	<10⁻⁴	10⁻³	9.6X10⁻³
1850	31.6	3.9	—	3.6	22.5	320	620	0.010	Turbulent	0.23	0.76	<10⁻⁴	<10⁻⁴	10⁻³	1.8 10⁻²
						LEADING EDGE									
300	75	25.4	16	20.2	5.8	3500	1320	0.051	Laminar	0.23	0.76	<10⁻⁴	<10⁻⁴	10⁻³	2.1X10⁻³
1000	63.5	17.3	11	15.0	13.3	2250	1270	0.02	Laminar	0.23	0.76	<10⁻⁴	<10⁻⁴	10⁻⁴	4.8X10⁻³
1400	53.5	11.4	3	10.8	15.5	1600	1040	0.018	Laminar	0.23	0.76	<10⁻⁴	<10⁻⁴	10⁻⁴	6.9X10⁻³
1650	45.7	6.4	1	6.2	15.1	695	735	0.014	Laminar	0.23	0.76	<10⁻⁴	<10⁻⁴	10⁻⁴	9.6X10⁻⁸
1750	39.6	5.1	—	4.8	16.0	400	790	0.011	Turbulent	0.23	0.76	<10⁻⁴	<10⁻⁴	10⁻⁴	9.5X10⁻³
1850	31.6	3.9	—	3.6	18.7	340	635	0.008	Turbulent	0.23	0.76	<10⁻⁴	<10⁻⁴	10⁻⁴	1.4X10⁻²

Notes: M_∞ is freestream Mach number.

δ is boundary layer thickness.

Subscripts e and w refer to outer edge and wall conditions, respectively.

2.3.2 Flow Simulation Requirements

The results of a literature survey on the thermal radiative properties of candidate space shuttle materials did not disclose any data as to the influence of velocity, temperature, or composition of the gas stream on emittance. Limited information on oxidation performance of some materials was found, and it was necessary to rely on this information in the formulation of the simulation recommendations. The significant parameters are summarized in the following subsections.

Velocity — Boundary layer velocity conditions may contribute to the radiative performance of the surface material in terms of shear forces and mass transfer. Although no facility exists for exact simulation of the velocity and pressure conditions encountered during the entry trajectory, the requirement of approximating this environment by using supersonic or hypersonic flow conditions was examined. Considering first the mechanical effects of shear stresses at the wall, these may cause the thinning or total removal of a viscous or liquid surface layer or a loosely adhering solid oxide film. As long as a glassy like material is used at a temperature sufficiently below its melting or softening temperature, simulation of shear forces is not necessary as demonstrated by the oxidation performance data of Perkins and Packer (Ref. 9). Exposure of coated TZM (99 Mo-Ti-Zr) specimens in a Mach 3 turbulent duct showed that at temperatures below 1850° K and pressures of 5 and 20 torr there was essentially no difference in useful lifetime from that observed for slowly moving air tests at the same temperatures and pressures. Similar agreement is reported for coated columbium-based alloys and a Sn-Al coating on Ta-10W. Although thinning of the coating occurred for the latter material, oxidation resistance was not significantly altered from low velocity tests.

If the surface layer is homogeneous and has a very large extinction coefficient, such as a metal, emittance at elevated temperatures will generally be independent of thickness as long as the layer is a few thousand Angstroms thick. However, ceramic-like materials typically have a smaller extinction coefficient, and a thinning of the coating may reduce the optical thickness which will decrease the emittance. Therefore, the

stability of radiative properties cannot be quantitatively related to oxidation perform-
ance for all materials. Little data was found in the literature which could be used to
relate emittance to flow conditions. Kaufman et al. (Refs. 10 and 11) reported emit-
tance data from supersonic arc and subsonic test facilities for a number of materials.
However, no conclusions can be drawn regarding velocity effects because low velocity
tests were conducted at nearly atmospheric pressures, whereas supersonic flow
conditions were achieved at much lower pressures. Goldstein and Centalanzi (Ref. 12)
have studied several TD Ni Cr alloys in a supersonic arc tunnel. They observed
differences in visual appearance of the surface between tunnel tests and the pre-
oxidized material (furnace); however, only limited emittance data were obtained
(λ = 0.65 μm), and no comparison was presented regarding different flow conditions.

Another important factor of velocity is its effect on the mass transfer parameter at
the surface. For emittance testing, the conditions should be such that the reactions
in this test environment proceed as they would in the entry environment. If this
condition is met, then the surface composition and radiative properties should be the
same as for flight conditions. If the reaction kinetics are known for a particular
material, the mass transfer at the wall may be related to the heat transfer coefficient,
the velocity and density (evaluated at boundary layer edge conditions) and flow proper-
ties may be adjusted to give a mass transfer which is calculated for the specific
material under flight conditions. Boeing (Ref. 13) conducted a study on the oxidation
of uncoated molybdenum in which they computed the attack rates for the X-20 vehicle
environment for various pressures and temperatures and compared these with exper-
imental data from a series of tests using near sonic flow of low temperature air over
a resistance heated strip of molybdenum. Their results showed that the lower velocity
conditions gave oxidation rates comparable to the values predicted for the flight
environment. In a direct comparison of subsonic and supersonic flow effects Buckley
et al. (Ref. 14) presented recession rate data for ATJ graphite and several graphite
composites from both subsonic and supersonic arc tunnel data. Surface temperatures
were on the order of 2500° K for the former and 3000° K for the latter test conditions.
The ATJ recession rates did not increase significantly with increasing Mach number.
The ATJ composite results did show a large increase in recession rate by going to
supersonic conditions, but the authors indicated that this was probably due to the

2-18

higher temperature, and the velocity effect was small. Data reported by Kaufman et al. (Ref. 10) for a number of materials show that at temperatures of 1900° K or less no significant differences in recession rates were observed between supersonic and high velocity subsonic flows.

Based upon these recession rate studies, supersonic flow conditions are not necessary to achieve the mass transfer rates which will adequately simulate the shuttle vehicle entry conditions. Considering that the candidate materials are selected for long-term stability in order to have a reuse capability of 100 cycles, their reaction rates with the oxidizing atmosphere will be much less than a bare refractory metal or graphite. Consequently, the mass flow associated with the near sonic velocity at the specimen will provide adequate mass transfer for these materials so that reactions will not be diffusion limited by lack of oxygen in the boundary layer. Simulation of shear force is not a realistic parameter in emittance testing. If this effect is an important consideration for specific materials this type of exposure could be carried out in a facility such as a turbulent duct, and then emittance measurements performed in a separate facility.

Pressure — Simulation of the pressure history at the surface of the material is necessary because the partial pressures of the gas species participating in the reaction and the total pressure are major parameters in the reaction and mass transfer rates. The test apparatus, therefore, should have the capability of simulating the pressure cycles at various locations on the vehicle. Also, as the high temperature oxidation performance of some materials degrades at pressures less than 1 torr (Ref. 9), and as some of the interior surfaces of the vehicle will be exposed to these very low static pressures during peak heating, the apparatus should have the capability of achieving pressures as low as 10^{-3} torr.

Composition — As discussed earlier, the composition at the surface is that of air, except in the stagnation region for the initial portion of the trajectory. Although no data were found in the literature regarding reactions with dissociated oxygen, it is believed that the short elevated temperature exposure to atomic oxygen will not have a significant effect on the radiative behavior of the candidate materials (Ref. 9).

Temperature — The principal area in question concerning the requirements for gas temperature simulation is that of the thermal gradients through the surface layer. During entry the exterior surface is at a higher temperature than the bulk of a coating or the substrate. For materials that form thick, relatively low thermal conductivity oxide layers, very large gradients will exist between the substrate and the surface. For hot-gas plasma arc tests, Kaufman et al. (Ref. 11) reported large gradients, on the order of 1100° K/mm, for ZrB_2 in the temperature range of 2500° to 2800° K. Conversely, for cold gas flow conditions at low flow velocity, 15 m/sec, and a substrate temperature of 2150° K, the gradient was on the order of 400° K/mm of oxide thickness (surface temperature lower than substrate). Therefore, under cold gas testing conditions the materials which form thick oxide layers and ceramic coatings will have surface temperatures as much as 100° to 200° K lower than the substrate temperature during the peak temperature portion of the test cycle.

Materials which form a thinner oxide layer, such as on the superalloys or coated refractory metals, will not be subject to large gradients. Estimates of the gradient per mm of coating or oxide thickness have been made for radiative only and convective plus radiative heat transfer (cold gas) as a function of surface temperature. Using a heated substrate technique and assuming a thermal conductivity of 1.7 W/m ° K, which is typical for glass-like materials, with a 1900° K surface temperature and a 0.013 mm thick coating, the substrate temperature would be 1940° K for radiation losses only, and 1970° K for radiative plus convective losses. For the superalloys which form thin oxide layers the temperature gradient through the surface layer is negligible.

For testing of materials which form thick layers of low thermal conductivity material, or ceramic coatings, the use of a cold gas flow may result in temperature differences between substrate and surface which will significantly influence the reactions occurring at the interface and in depth in the surface layer. For these materials it would be desirable to use a hot gas flow so that the gradients may be minimized. In the case of coated refractory metals or superalloys the use of a cold gas flow should not result in temperature gradients which will significantly affect the material behavior.

2.4 FACILITIES

As discussed in Section 2.1, a review was made of existing high temperature test facilities to determine if an apparatus currently existed that would meet the program goals or could be modified to accomplish these objectives. This was done by means of a literature review and a survey of laboratories active in the field of high temperature materials research. The results of this survey are reported in Refs. 1 and 15, and a summary of the facilities reporting a capability for measurement of emittance properties in air is given in Table 2 in terms of the radiative property measured, heating method, and environmental simulation capability. Of these facilities, only the plasma-arc tunnels test under supersonic, hot gas conditions, and none of these tests simulate actual velocity but rather attempt to match stagnation enthalpy and pressure (Ref. 16). The radiative properties measurements, with the exception of AVCO, are limited to spectral data in the visible portion of the spectrum. AVCO's arc tunnel incorporates a total detector (thermopile) for total normal measurements during testing. The Beoing apparatus utilizes near room temperature air flow from a sonic nozzle for entry simulation during temperature and pressure cycling, and it has provisions for determining total normal and spectral (λ = 0.65μm) normal emittance. The test facilities at North American Rockwell and McDonnell-Douglas are equipped to provide for exposure to air but only at very low velocities. Total normal and spectral normal emittances are measured in these facilities. Of those having total hemispherical emittance capability, none are equipped for flow simulation. However, the Boeing apparatus could be easily adapted for total hemispherical emittance measurement under static conditions.

Descriptions of the various types of facilities listed in Table 2 are contained in Ref. 1. Brief summaries for each of the basic types of facilities are given in the following paragraphs.

- Plasma-Arc Tunnel. This type of test facility most nearly simulates entry conditions in that supersonic velocities are achieved (Mach numbers of 2 to 5), and the gas stream temperature is higher than the surface temperature.

Table 2

SUMMARY OF EMITTANCE TEST FACILITIES FOR MEASUREMENTS IN AIR AT ELEVATED TEMPERATURES

	Facility	Radiative Property	Specimen Heating	Pressure Range	Flow Simulation	Comments
(1)	AVCO Corporation Wilmington, Mass.	ϵ_λ(0.65 μm), ϵ_{TN}	Plasma-arc tunnel	Vacuum to 1 atmosphere	Supersonic flow, simulates 90% of stagnation enthalpy and pressure range	Continuous run time of 60 min; hot gas flow; possibility of sample contamination from arc.
(2)	Arthur D. Little, Inc. Cambridge, Mass.	$\rho_\lambda(\theta_\lambda)$	Arc-imaging furnace and induction heated specimen	Atmospheric pressure; Vacuum to 1 atmosphere	Static air or other gases; inert gases	Possibility of specimen contamination of optics.
(3)	Boeing Company Kent, Wash.	ϵ_λ(0.65 μm), ϵ_{TN}	Sample resistance	Vacuum to 1 atmosphere	Air or other gases, sonic nozzle at fixed angle with respect to test surface	Continuous run can duplicate cyclic temperature and pressure requirements; flow reported to be adequate simulation for silicide-coated refractory metal.
(4)	Grumman Aerospace Corporation Bethpage, Long Island, N.Y.	ϵ_λ(0.65 μm), ϵ_{TN}, ϵ_{TH}	Sample resistance	Vacuum to 1 atmosphere	Static air or other gases	No flow simulation capability.
(5)	IIT Research Inst. Chicago, Ill.	ϵ_λ(1 to 14 μm and 0.65 μm), ϵ_{TN}	Furnace	Atmospheric	Static air or other gases	No flow simulation capability.
(6)	LTV Aerospace Corporation Dallas, Tex.	ϵ_{TN}	Gas and plasma torches impinging in specimen faces	Atmospheric	N_2 or N_2/O_2 mixture for plasma torch mixed with ambient air; subsonic velocity	No capability for pressure variation.
(7)	Lockheed Missiles & Space Company Palo Alto, Calif.	ϵ_λ(0.65 μm)	Induction heated	Atmospheric	Static to 250 fps air or other gases	No capability to cover pressure range; low to accelerate flow velocities.
		ϵ_λ(0.4 to 25 μm), ϵ_{TN}, ϵ_{TH} (angular data for ϵ_λ and ϵ_T from 0° to ±98° from normal; also polarizers)	Specimen resistance	Vacuum to 1 atmosphere	Static air or other gases	No flow simulation capability.
(8)	Material Consultants, Inc. Denver, Colo.	ϵ_λ(0.65 μm), ϵ_{TN}, ϵ_{TH}	Sample resistance	Vacuum to 1 atmosphere	Static air or other gases	No flow simulation capability.
(9)	McDonnell Douglas Corporation St. Louis, Mo.	ϵ_λ(1 to 14 μm and 0.65 μm), ϵ_{TN}	Induction heated	Vacuum to 1 atmosphere	Static and very low velocity air or other gases	No moderate to high velocity flow simulation.
(10)	North American Rockwell Los Angeles, Calif.	ϵ_λ(1 to 14 μm and 0.65 μm), ϵ_{TN}	Furnace	Vacuum to 1 atmosphere	Static and very low velocity air or other gases	No moderate to high velocity flow simulation.
(11)	Pratt & Whitney Aircraft East Hartford, Conn.	ϵ_λ, ϵ_{TN}, ϵ_{TH}	Specimen resistance	Vacuum to 1 atmosphere	Static and very low velocity air or other gases	No moderate to high velocity flow simulation.
(12)	Southern Research Inst. Birmingham, Ala.	ϵ_λ(0.65 μm), ϵ_{TN}	Induction heating	Vacuum to 1 atmosphere	Static air or other gases	No flow simulation capability.
(13)	Southern Arc Facilities Tunnels at NASA, LRC and ARC, Martin Marietta/Baltimore, Aerotherm and Plasmadyne	ϵ_λ from optical pyrometer or visible/near IR radiometer	Plasma-arc tunnel	Vacuum to near atmosphere pressure	Supersonic flow; various facilities simulate stagnation enthalpy and pressure from 70% to 100% of desired range.	Facilities not setup for total or spectral (over sufficiently wide-band) for emittance studies; possibility of sample contamination from arc.

However, at pressures corresponding to the entry trajectory, surface shear stresses and velocity are much lower than are obtained in flight. Specimen temperature and pressure profiles can be simulated for time periods corresponding to the range of shuttle vehicle trajectories. Stagnation, inclined plate, wedge, and wall (turbulent duct) flow conditions can be obtained. This type of apparatus could be modified for total and spectral normal or angular emittance measurements. However, uncertainties in the energy balance on the specimen will result in poor accuracy of total hemispherical emittance measurements during flow. Although the specimen is convectively heated, data could possibly be obtained for no-flow conditions from a transient analysis, but again the thermal balance uncertainties will result in poor accuracy for the total emittance determination. Contamination of the specimen surface by condensation of arc electrode materials (copper or tungsten) entrained in the plasma may also be a problem.

- Resistance Heating. The resistance heated strip method used by Boeing for the X-20 program studies was reported (Ref. 17) to satisfy the mass transfer rate criteria for coated refractory metals. This apparatus uses a near sonic velocity free jet of ambient air impinging on the central area of the specimen to achieve the necessary mass transfer. The apparatus can duplicate the pressure and temperature requirements of the shuttle vehicle trajectories and is instrumented for total normal and spectral (0.65 μm) normal emittance measurements during flow. It could be modified for calorimetric measurements with the flow interrupted. Various flow angles may be obtained by moving the nozzle or rotating the specimen plane.

None of the other facilities employing the heated strip or filament heating method are equipped for simulation of flow conditions. However, they could be modified to accomplish the same performance as the Boeing apparatus. Principally, this would entail the addition of a nozzle with a pumping system sized to accommodate the high mass flows at the low pressures.

- Induction Heating. Facilities using induction heating of the specimens could also be modified to incorporate means for high velocity flow, pressure

simulation, and radiometric emittance measurement capabilities similar to those discussed previously. Total hemispherical emittance cannot be measured directly because of the difficulty in evaluating the power input to the sample during heating. For transient test conditions, the problems are similar to those in an arc tunnel. One problem associated with induction heating is the requirement for a susceptor material for nonconductors or thin sheet specimens which will survive the test environment. For high velocity flow tests, the specimen surface should be flush with the face of the suscep-tor, and for thin samples it is difficult to obtain a uniform temperature distribution over the test area.

- Furnace. This type of heating method is not suitable for dynamic test condi-tions because of the poor cyclic temperature response of a furnace and the difficulty in achieving high velocity flow in the furnace hot zone while still maintaining the advantage of near blackbody conditions which minimizes the specimen temperature measurement problem. Also, total hemispherical emittance measurements cannot be obtained under these conditions and, in general, angular measurements cannot be made because of the constructional features of a furnace.

The conclusion obtained from the facility survey activities was that none of the existing high-temperature test facilities meet all of the measurement and flow simulation re-quirements for this program. The two basic types of apparatus which could be modified to meet the majority of the measurement objectives are the plasma arc and the resistance heated strip facilities. The latter type is recommended over the plasma arc for the following reasons:

- Adaptable to direct measurement of total hemispherical emittance
- Pressure simulation from $<10^{-4}$ to 760 torr
- Suitable for low temperature range (450° K to 700° K) material studies
- No problem of contamination of specimen surface by environment; i.e., by arc electrode materials
- Configuration more adaptable to radiometric instrumentation.

Section 3
DEVELOPMENTAL STUDIES

Prior to the design and fabrication of the experimental facility several preliminary studies were conducted to define the gas flow system, temperature measurement errors and effect of convective heat losses on calorimetric emittance data. The basic concept selected for the apparatus is to use a resistively heated specimen mounted in a water cooled chamber in which the total pressure on the specimen can be varied from 10^{-5} to 760 torr. The exposure conditions are for static air or air at free stream velocities to M = 3. Specimen temperature and total pressure are varied with time to simulate the entry conditions. A typical time history of these parameters is illustrated by figure 6. Under flow conditions the radiative proper- ties of total and spectral emittance are measured radiometrically, and calorimetric total hemispherical emittance is measured under static conditions. The system is designed for heating of the air to the flow nozzle using an r-f plasma unit. The results of the developmental studies are summarized in the following subsections.

3.1 FLOW SYSTEM

Two potential problem areas were envisioned in the development of a suitable en- vironmental simulation flow system. These were stability of the flow field at large Mach numbers over the range of pressures desired and a suitable method for heating the gas stream which is controllable over a wide range of temperature and will not contaminate the specimen. Proof tests were conducted to confirm both flow condi- tions and a recommended heating method. The final apparatus design was based upon the results of these investigations.

3.1.1 Supersonic/Hypersonic Flow

Initially, computations were made to determine the pump size required to achieve Mach numbers from 1 to 5 over the total pressure range for the shuttle entry
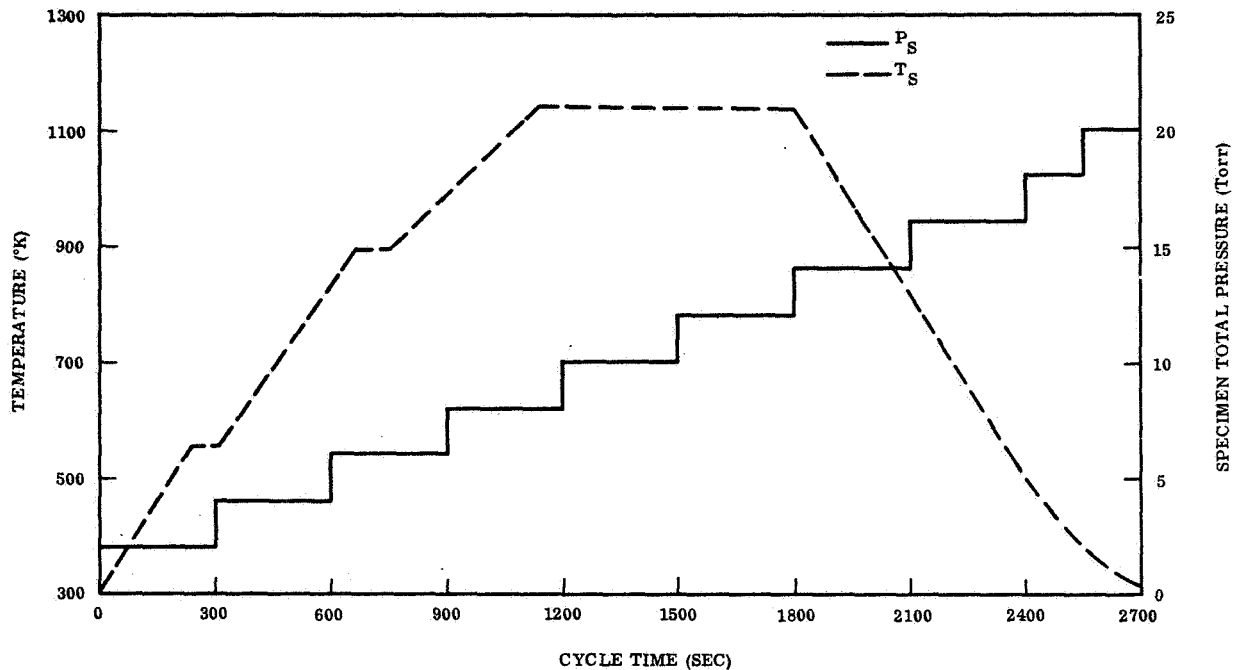
Fig. 6 Typical Cycle of Specimen Test Area Temperature and Total Pressure

environment. For pump sizing it was assumed that for hot flow conditions a heat exchanger at the test chamber exit section would reduce the air temperature to ambient level prior to entry to the main pump duct. Flow field dimensions were sized to accommodate specimen test areas of 1.7-cm and 2.5-cm diameter. Using the isentropic flow and normal shock relationships the nozzle and chamber pressure conditions were computed as a function of Mach number for the specimen total pressure range of the predicted entry environment. Volumetric capacity requirements were then computed as a function of nozzle temperature and chamber pressure assuming that the temperature at the pump inlet is ambient. Required pump capacity as a function of Mach number is shown in figure 7 for three gas temperatures and two test area diameters. As a 1.7-cm diam specimen test area is adequate for emittance measurements two pump sizes were recommended considering cost and Mach number range. These were 0.8 m^3/sec (1700 cfm) and 0.4 m^2/sec (850 cfm). The larger pump is adequate to M = 5 for both cold and hot flow conditions, and the smaller pump will accommodate M = 3 for cold flow and M = 5 for hot flow conditions.

3-2
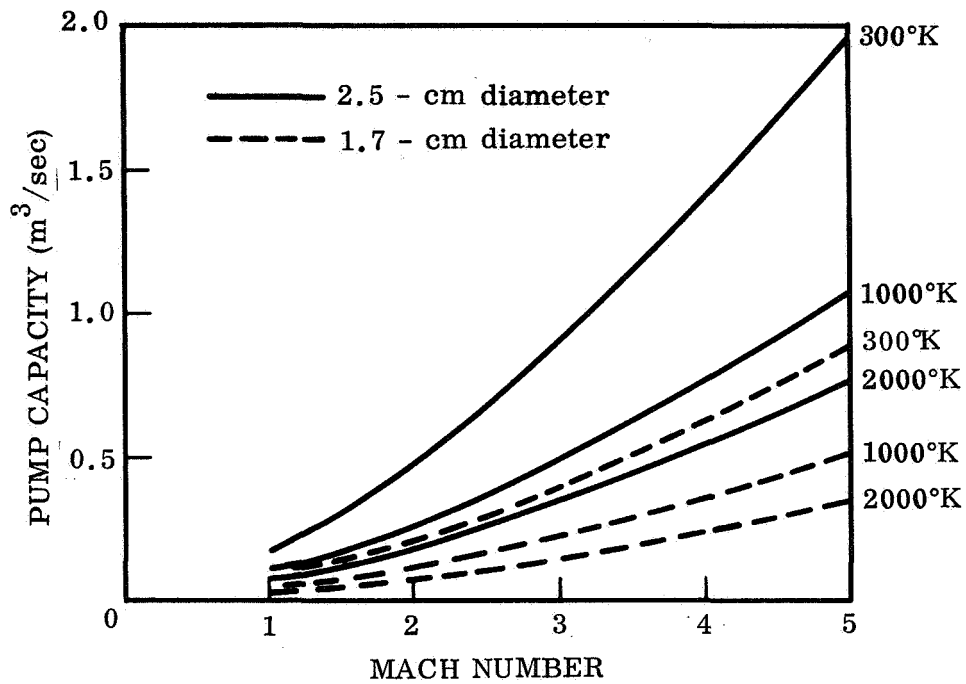
Fig. 7 Required Pumping Capacity as a Function of Free Stream
Mach Number and Temperature
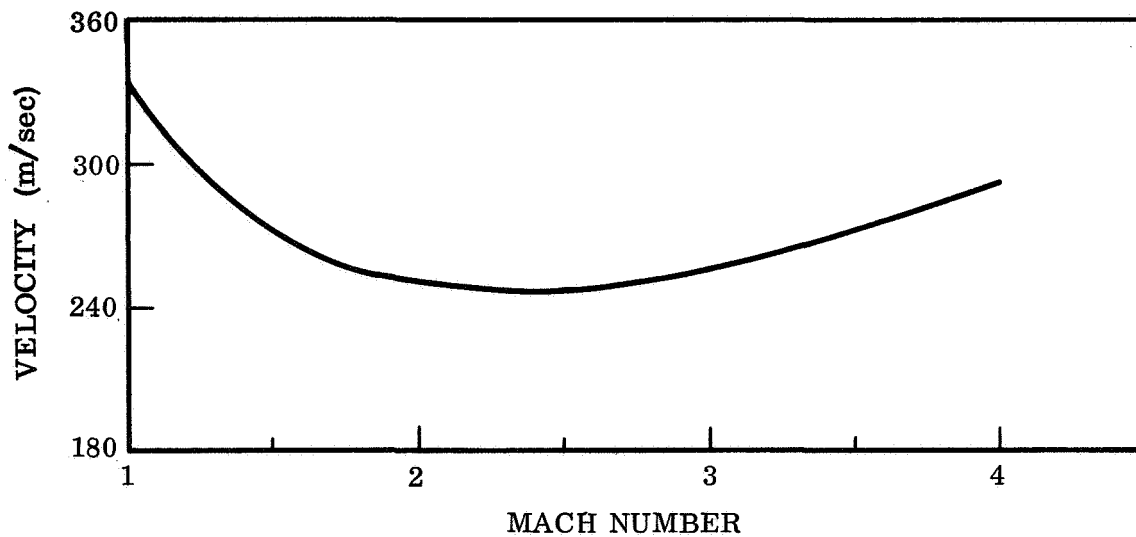
Fig. 8 Velocity Behind Normal Shock as a Function of Free Stream
Mach Number

3–3

The next phase was to evaluate the uniformity of flow conditions in the supersonic regime over the range of entry pressures. This was done experimentally using converging-diverging nozzles in a chamber having a pumping capacity of 0.56 m^2/sec. Free stream Mach numbers ranged from 2.5 to 4.0. At M > 3 large pressure fluctuations (on the order fo 50 percent) were observed across the surface of a 1.6 cm diameter flat plate test area as total pressure was increased. The plate was instrumented with five total pressure positions and was located normal to the flow. At M = 3 and M = 2.5, the pressure was uniform to within 10 percent and steady over the desired total pressure range.

The problems encountered in the operation of a supersonic nozzle such as unsteady flow and nonisentropic effects are directly related to high Mach numbers. Thus, it is possible to obtain a larger flow field with a given pump size and steadier flow by operating the apparatus at a lower Mach number (3 or less). Another consideration is that for this test geometry (specimen normal to flow) the supersonic shock wave in front of the specimen recovers very little of the upstream total pressure. Therefore, high upstream total pressures must be used to obtain the desired sample total pressure, and for a reasonable pump size the flow field size becomes smaller with increasing Mach number. Finally, the velocity behind the normal shock in front of the specimen is relatively insensitive to upstream Mach number, as shown in figure 8, and therefore, by specifying total pressure on the specimen the exact value of free stream Mach number is not significant. On the basis of this study it was decided to use a 0.4 m^3/sec pump and design flow nozzles for Mach number of 1 and 3.

3.1.2 Air Heating

Two concepts were evaluated for heating of the flow stream; these were resistance and r-f plasma. An arc-plasma was not considered because of possible specimen contamination by products from the electrodes. A preliminary design was prepared for a resistance heating unit using an alumina parallel tubular heat exchanger bundle heated by molybdenum windings connected to a variable, high current power supply. The materials choices were selected on the basis of temperature requirements. The specific design employed a low pressure N_2 purged winding chamber. The purge gas

was discharged into the specimen stream (resulting in 3 to 4 percent N_2 rich air) so that the purge chamber would not have to support a large pressure difference across the high temperature elements. This type of heater becomes very complex because of the requirement of an inert atmosphere for the heater windings, and the thermal stresses encountered during the cyclic temperature would place severe limitations on the life of this type of unit.

From a preliminary study the r-f plasma concept appeared to be a promising solution to the hot gas problem. Initial contacts were made with personnel at Stanford Research Institute and the University of California, Berkeley, who were working with these devices. At the latter institution an r-f plasma unit was being used in a heated wind tunnel facility. This unit was a 50 kw output TAFA torch operated at 3.5 mhz. Their experience with this unit was very good, and contacts were then made with the manufacturer (TAFFA) regarding the emittance apparatus application. Although TAFFA did not have specific experience with the operation of their units on air at low pressures (100 torr or less) the approach appeared feasible, and a test series was conducted at their facility, under contract funding, to prove the concept.

Although the TAFA test facility was limited by vacuum pumping capacity to mass flow rates approximately one-third of the maximum rate projected for the emittance apparatus, system performance could be verified for operation at the desired total pressures and over the percentage output range. The specifications for the test were: operation of a standard Model 56 torch with a 15 kw r-f power supply at pressures from 10 to 100 torr and at mass flow rates from 1×10^{-3} to 3×10^{-3} kg/sec of air. These conditions were selected as being representative of the cyclic emittance test parameters. The test equipment consisted of a 0.15 m^3/sec vacuum pump, drawing through a heat exchanger coupled to a cylindrical, cross-shaped, water cooled vacuum chamber 30-cm diameter by 60-cm long. A Model 56 torch was mounted exterior to the chamber on the end of one cross arm, and it was provided with a 1.27-cm diameter throat leading into the chamber. The torch was started on pure argon at a pressure of 10 torr, then air was injected both tangentially and radially as the argon was cut off.

Operation was initially accomplished at 50 torr vacuum chamber pressure and 160 torr in the torch. The minimum sustaining power was 28 kw (4A, 7050V) plate power. Subsequent changes in current, mass flow rate and ratio of tangential to radial gas injection did not significantly change the minimum operating power level. A larger throat nozzle was then installed at the torch exit, and operation was attempted at lower torch total pressures. The minimum torch pressure at which stable plasma operation could be sustained was 130 torr, and the corresponding power level was 38 kw. As torch pressure was decreased input power increased, and operation was only marginally stable.

A review of the test data with the manufacturer led to the conclusion that r-f coil design would have to be changed, and further work would have to be done on the torch air injection schemes. As this would entail a substantial amount of research an alternate concept for using a standard unit was considered. This method is to operate the torch at near atmospheric pressure, high enthalpy and power (50 kw), and to discharge this flow into a large chamber so that pressure would be dissipated across a shock in this chamber. This low pressure flow would then be mixed with room-temperature air, and the combined flow directed to the primary nozzle. Under these conditions the flow nozzle can be operated at design pressure ratio over the range of test total pressures. Preliminary calculations showed that for a 1700°K stream, 28 percent of the total flow would be from the hot jet which would require a 0.4-cm throat nozzle. Because of the increased costs due to the requirements of a larger plasma unit and the auxiliary equipment the hot gas feature was not implemented.

3.2 TEMPERATURE MEASUREMENT

The most significant problem associated with emittance measurements is that of accurately determining the absolute temperature of the emitting surface. Thermocouples cannot be used with some materials at elevated temperatures because of problems of compatibility of the instrumentation with the test material. Also, at elevated temperatures, large thermal gradients may exist across some coatings so that in-depth or substrate temperature measurements cannot be accurately related to the true surface temperature. Radiation methods are useful for measuring surface temperature, but their accuracy is related to the accuracy of the knowledge of the

emittance properties of the surface. The relationship between measured brightness temperature and true temperature is a function of the spectral emittance of the surface at the pyrometer mean effective wavelength. In an attempt to eliminate the emittance term from the temperature equation, multiple spectral band pyrometers have been developed on the principal that if the material emits as a gray body, i.e., emittance is not dependent upon wavelength, the temperature measurement is independent of emittance. Total radiation pyrometers have also been used, principally at lower temperatures, but again, a value of emittance must be used in the temperature calculation. Figure 9 illustrates the temperature error as a function of assumed emittance for this type of device. Two-temperature pyrometer methods have also been used with limited success as discussed in Ref. 18 which reviews pyrometry techniques.

Single-color optical pyrometers have been used extensively for high temperature measurements of materials having a wide range of spectral emittance. Temperature errors for a pyrometer operating at 0.65μm are shown in figures 10 and 11 for surfaces having assumed emittance values at 0.65μm of 0.5 and 0.8, respectively. To achieve a 1 percent maximum temperature error at 2000°K, the true emittance of a surface for which ϵ_λ is assumed to be 0.5 must be between 0.45 and 0.55. If the surface emittance at 0.65μm is assumed to be 0.8 and the real spectral emittance is between 0.7 and 0.9, a 1 percent temperature accuracy will be attained. For materials having a low emittance at 0.65μm, a more accurate knowledge of the true emittance is required to give a small error. With polished metals, for example, the emittance at 0.65μm may be 10 times the total emittance which can result in extremely large temperature errors if spectral data are not available and the 0.65μm value is estimated from a total emittance value.

Two color pyrometer errors are shown in figure 12 for a 0.50μm and 0.65μm band instrument. This technique does not improve the temperature measurement accuracy unless bands can be selected at which the emittance values are very nearly equal. Consider a surface which appears dark gray in the visible spectrum, and assume $\epsilon_1 = 0.8$ and $\epsilon_2 = 0.75$. At 2000°K this would introduce a 1 percent temperature error. However, if ϵ_2 was 0.70, the error would increase to nearly 2.5 percent.
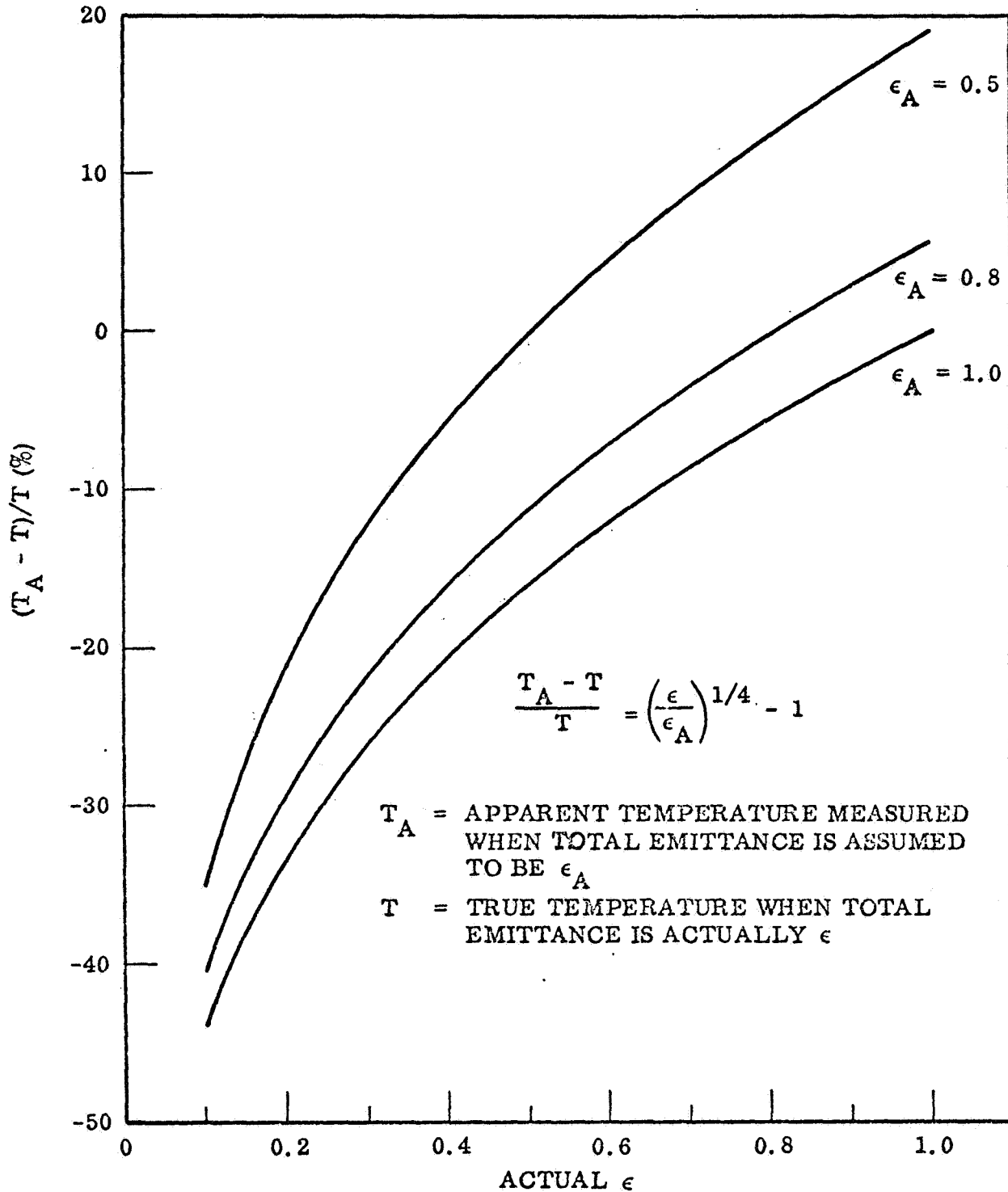
Fig. 9 Temperature Error Versus Emittance Error for a Total Radiation
Thermopile for Three Assumed Emittance Values
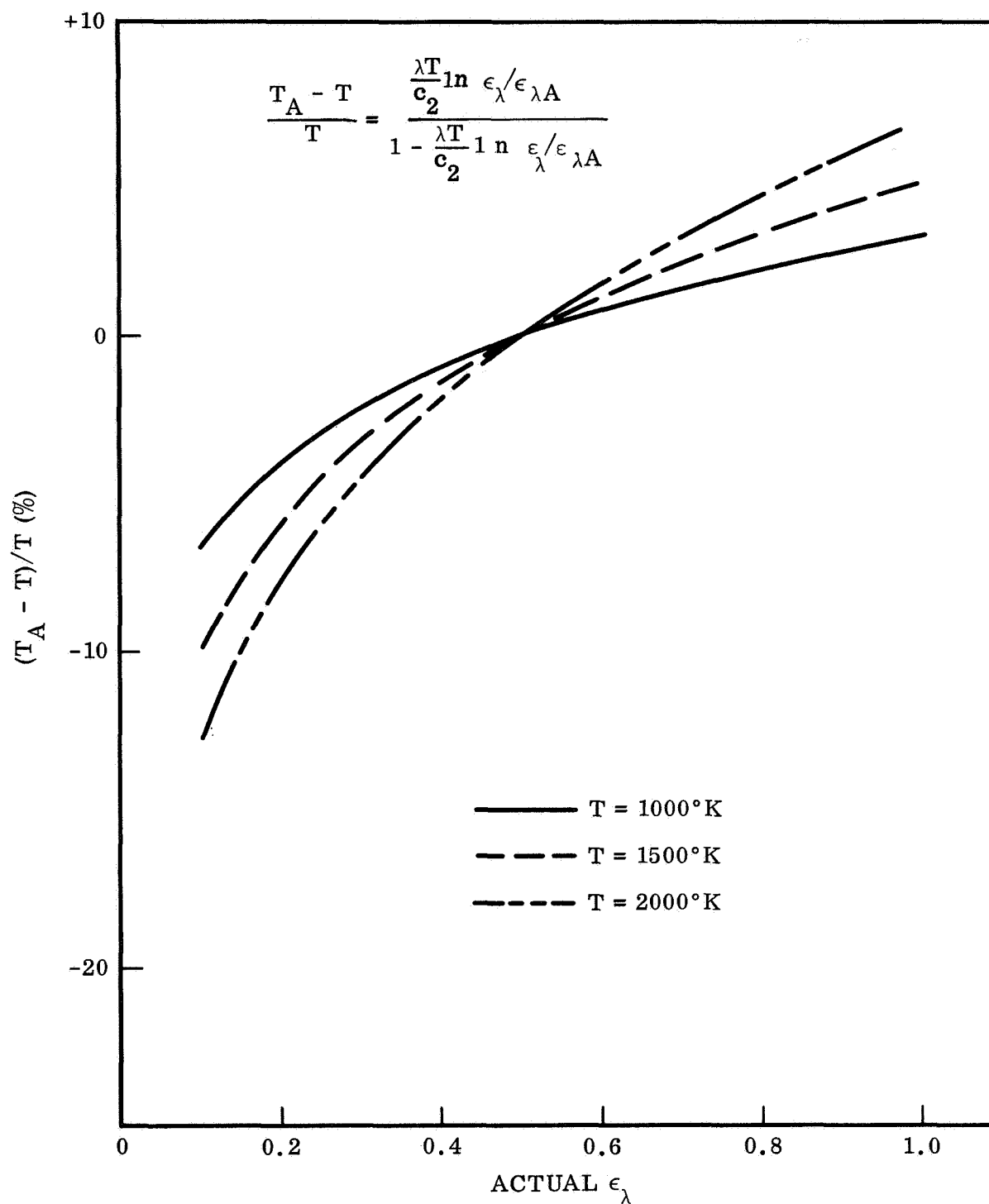
3-8

$$\frac{T_A - T}{T} = \frac{\frac{\lambda T}{c_2} \ln \epsilon_\lambda / \epsilon_{\lambda A}}{1 - \frac{\lambda T}{c_2} \ln \epsilon_\lambda / \epsilon_{\lambda A}}$$

Fig. 10 Temperature Error Versus Emittance Error of an Optical Pyrom-
eter, for Three Temperatures, when the Assumed Spectral Emittance
at 0.65 μm is $\epsilon_{\lambda A}$ = 0.5

$$\frac{T_A - T}{T} = \frac{\frac{\lambda T}{c_2} 1 \, n \, \epsilon_\lambda / \epsilon_{\lambda A}}{1 - \frac{\lambda T}{c_2} 1 \, n \, \epsilon_\lambda / \epsilon_{\lambda A}}$$

T = 1000°K

T = 1500°K

T = 2000°K

Fig. 11 Temperature Error Versus Emittance Error of an Optical Pyrometer, for Three Temperatures, when the Assumed Spectral Emittance at 0.65 μm is $\epsilon_{\lambda A}$ = 0.8

3-10

$$\frac{T_A - T}{T} = \frac{c_2\left(\frac{1}{\lambda_1} - \frac{1}{\lambda_2}\right)}{T\ln(\epsilon_2/\epsilon_1) + c_2\left(\frac{1}{\lambda_1} - \frac{1}{\lambda_2}\right)} - 1$$

T_A = APPARENT TEMPERATURE MEASURED WHEN IT IS ASSUMED THAT $\epsilon_{\lambda_1} = \epsilon_{\lambda_2}$

T = TRUE TEMPERATURE WHEN REAL EMITTANCE VALUES ARE IN THE RATIO ϵ_1/ϵ_2

——— $T = 1000°K$

— — — $T = 1500°K$

— ·· — $T = 2000°K$
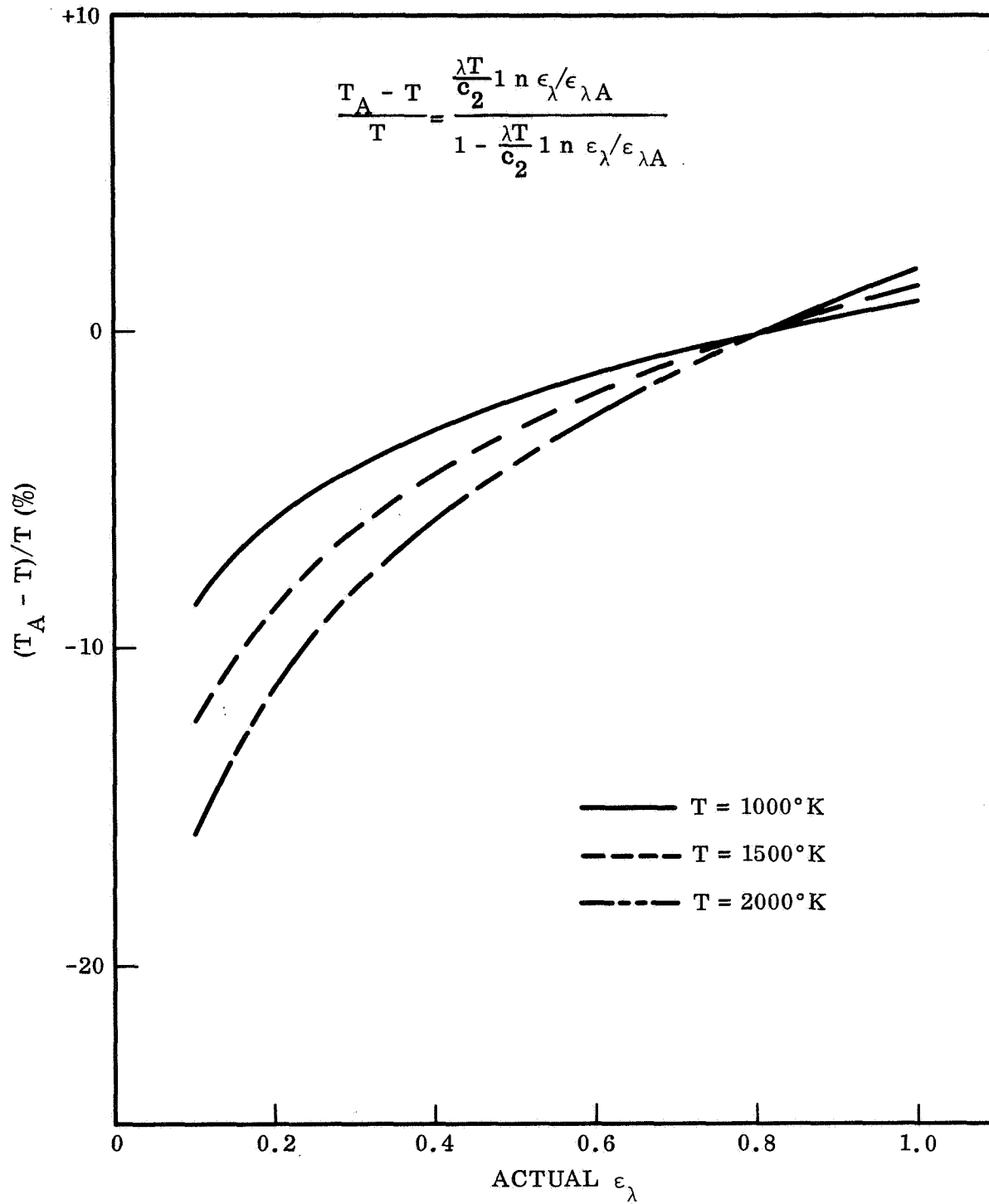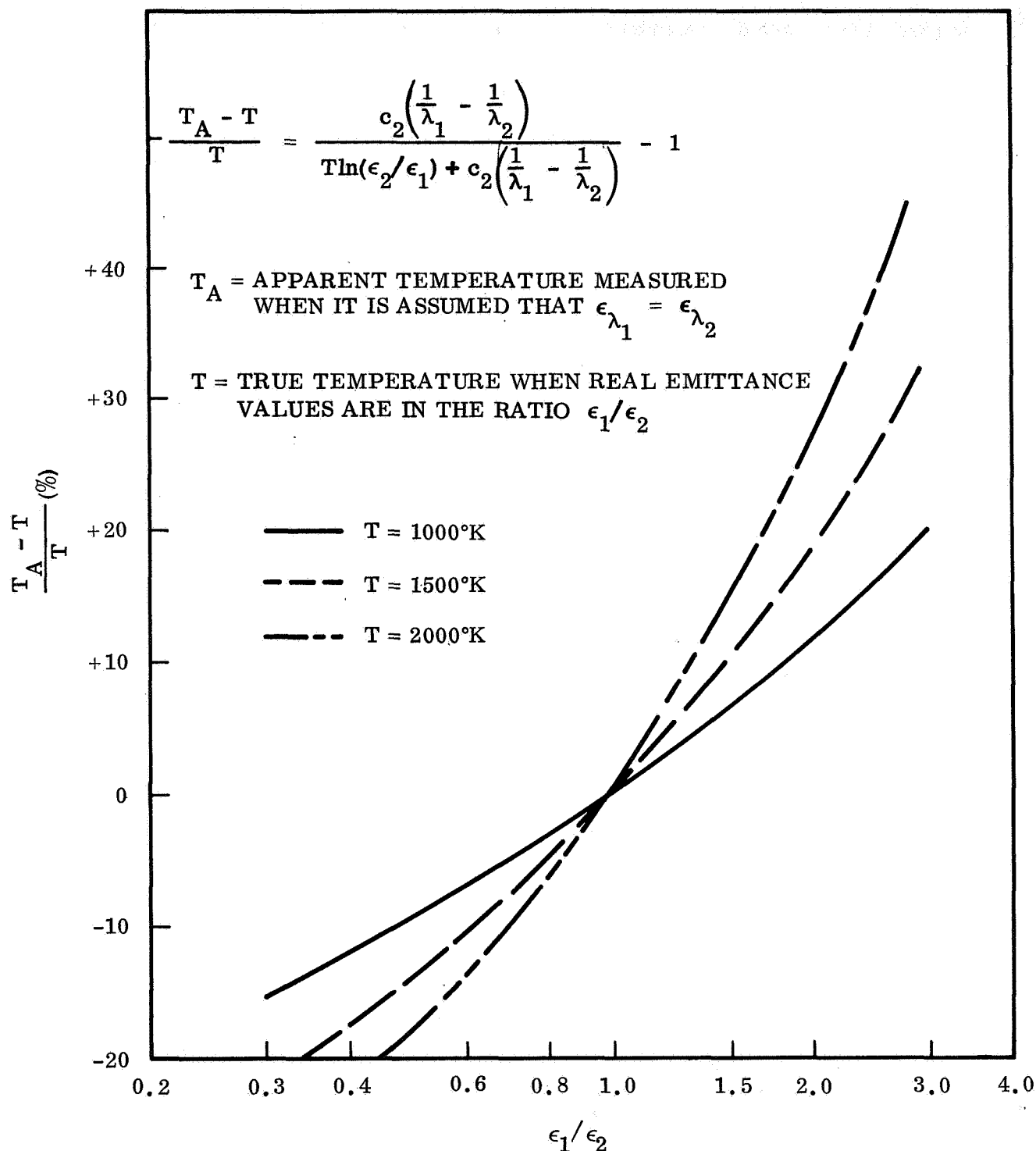
Fig. 12 Temperature Error Versus Error in Graybody Assumption for a Two-Color Pyrometer Operating at Wavelengths $\lambda_1 = 0.50\ \mu m$ and $\lambda_2 = 0.65\ \mu m$

3-11

Clayton (Ref. 19) reported a technique for using an optical pyrometer and a total radiation pyrometer to compute total normal emittance. The emittance accuracy is within 5 percent if the ratio of ϵ_λ to ϵ_{TN} is within 0.8 to 1.2.

A comparison of experimentally measured temperatures using both thermocouples and an optical pyrometer for low and high emittance surfaces is presented in Table 3. The materials are 99.99 percent pure platinum, annealed for 4-1/2 hours at 1615°K and oxidized L605 alloy, respectively. The true temperatures are taken as those measured with the optical pyrometer from a small cavity (L/D = 4) drilled into the edge of a vertical strip specimen. A Pyrometer Instrument Company "Micro Optical" pyrometer was used for brightness temperature measurements. The effective emittance of the cavity was assumed to be equal to unity. Thermocouples were 3 mil diameter Pt/Pt 13 percent Rh (1/2 percent accuracy) with their junctions peened into holes drilled into the edge of the strip opposite the cavity. Surface brightness temperatures were measured at the center of the strip.

Table 3

COMPARISON OF TEMPERATURE MEASUREMENT METHODS

Chamber Pressure (Torr)	Measured Temperature (°K)		
	By Thermocouple	By Optical Pyrometer, (Cavity)	By Optical Pyrometer, (Surface)
PLATINUM			
10^{-5}	1081	1080	1084
10^{-5}	1370	1368	1366
10^{-5}	1645	1639	1639
1	1107	1103	1109
1	1372	1363	1365
10	1091	1094	1095
10	1385	1379	1377
50	1098	1097	1103
50	1370	1365	1366
OXIDIZED L605			
10^{-5}	1103	1112	1112
1	1105	1121	1121
760	1090	1116	1116
1	1341	1355	1361

Agreement between the thermocouple and pyrometer temperatures and the assumed true temperatures (cavity) was within 1 percent for all of the platinum data. The value of ϵ_λ at $0.65\mu m$ was taken as 0.32 (Ref. 20), and the surface temperatures computed from measured brightness temperatures using this value were generally within 1/2 percent of the cavity temperature. For the oxidized L605 material the data indicated consistently good agreement between cavity temperatures and the surface temperatures computed from brightness temperatures using a value of $\epsilon_\lambda = 0.85$ at $0.65\mu m$ (from room temperature spectral reflectance data). Temperatures measured by thermocouples were 1 to 2-1/2 percent lower than cavity temperatures, the larger deviations occurring at higher chamber pressures. This apparent thermocouple error is attributed to poor contact between the oxidized low thermal conductivity material and the thermocouple junction, the junction temperature being slightly depressed by lead losses. This explanation is supported by the observed increase in temperature deviation with increased chamber pressure.

3.3 CONVECTIVE HEAT LOSS

The effect of convection heat losses on calorimetric emittance measurements was considered for both a flow environment and a static atmosphere. The strip specimen configuration was used, and for flow conditions the measuring area was oriented normal to the stream centerline. An accurate evaluation of the total convective heat loss under flow conditions is not feasible because of the uncertainty in the heat transfer at the rear uninsulated surface of the strip. However, for a static atmosphere the convective heat transfer can be determined with reasonable accuracy and calorimetric measurements are a possibility for high emittance materials at elevated temperatures.

In examining natural convection effects both vertical and horizontal orientations of the strip were considered. For the horizontal case the width dimension of the strip may be placed in a vertical or a horizontal plane. The latter position presents some radiometer positioning difficulties as it is necessary to view the test area from above or below the test chamber. Also, the upper and lower surfaces have different heat transfer coefficients and unacceptable temperature gradients in the measuring area

may exist for low thermal conductivity materials. Vertical positioning of the width dimension will result in the same heat transfer coefficient for both surfaces. However, with short vertical heights the local heat transfer coefficient is strongly dependent upon the distance above the lower edge, and again temperature gradients may be present in the test area. The long vertical strip has a larger heat transfer coefficient than the short vertical width orientation, and there is also some non-uniformity in the local heat transfer coefficient across its width due to the thinning of the boundary layer at the edges.

The effect of convection on calorimetric emittance determinations is considered in two parts; one, the heat loss which must be accounted for in the energy balance equation (Section 2) and two, the temperature gradient effect. The influence of convection on emittance accuracy can be evaluated once the heat transfer coefficient is established for a particular specimen geometry. The thermal gradient effects are related to the establishment of an effective test area radiation temperature based upon a local surface temperature measurement. For example with a vertical strip the temperature at the edge will be lower than at the center because of the higher convective heat transfer at the edge. The magnitude of this temperature difference will be a function of the convective and radiation heat transfer and the thermal conductivity of the material. For very high thermal conductivity materials having a high emittance the temperature gradient effect will be negligible at elevated temperatures because heat transfer by convection is very small compared to that by conduction and radiation. For low thermal conductivity materials the effect becomes significant and must be accounted for in the emittance computation. This can be done by determining the temperature distribution over the test area and then evaluating a mean effective radiation temperature.

Convective heat transfer coefficients were experimentally determined for the vertical strip case as no data were found in the literature for this geometry with a large temperature gradient along the vertical axis. The free convection heat transfer from the central portion of the vertical strip was computed from the measured difference in total power required to maintain a 1.27-cm by 1.27-cm test area at a fixed temperature in both elevated pressure and vacuum environments. Heat transfer by natural

convection was determined in this manner for a series of strip temperatures and ambient pressures using a platinum strip, and the data are shown in figures 13 and 14. A comparison between vertical and horizontal strip heat transfer coefficients is shown in figure 15. The data of King (Ref. 21) were used to compute the latter case.

The vertical strip heat transfer coefficient results were used to compute total hemispherical emittance values from the total electrical power input data for an oxidized L605 specimen. Good agreement was achieved between vacuum data and measurements at 1 and 760 torr as shown in Table 4. It is estimated that the uncertainty due to convective heat transfer is a maximum of 10 percent at the lower temperatures decreasing to 5 percent at 1100°K.

Table 4

COMPARISON OF CALORIMETRIC DETERMINATIONS OF TOTAL
HEMISPHERICAL EMITTANCE OF OXIDIZED L605

Temperature (°K)	Ambient Pressure (Torr)	ϵ_{TH}
1130	10^{-5}	0.64
1120	1	0.65
1110	760	0.63
840	10^{-5}	0.62
800	1	0.63
800	760	0.59

In summary, calorimetric emittance measurements can be made with reasonable accuracy in a static atmosphere once the convective heat transfer coefficient has been established for the specimen geometry. This measurement method has been verified experimentally for moderate to high emittance materials at temperatures about 800°K. Temperature distribution across the measuring area should be determined to evaluate a mean effective radiation temperature for computation of emittance of low thermal conductivity materials.
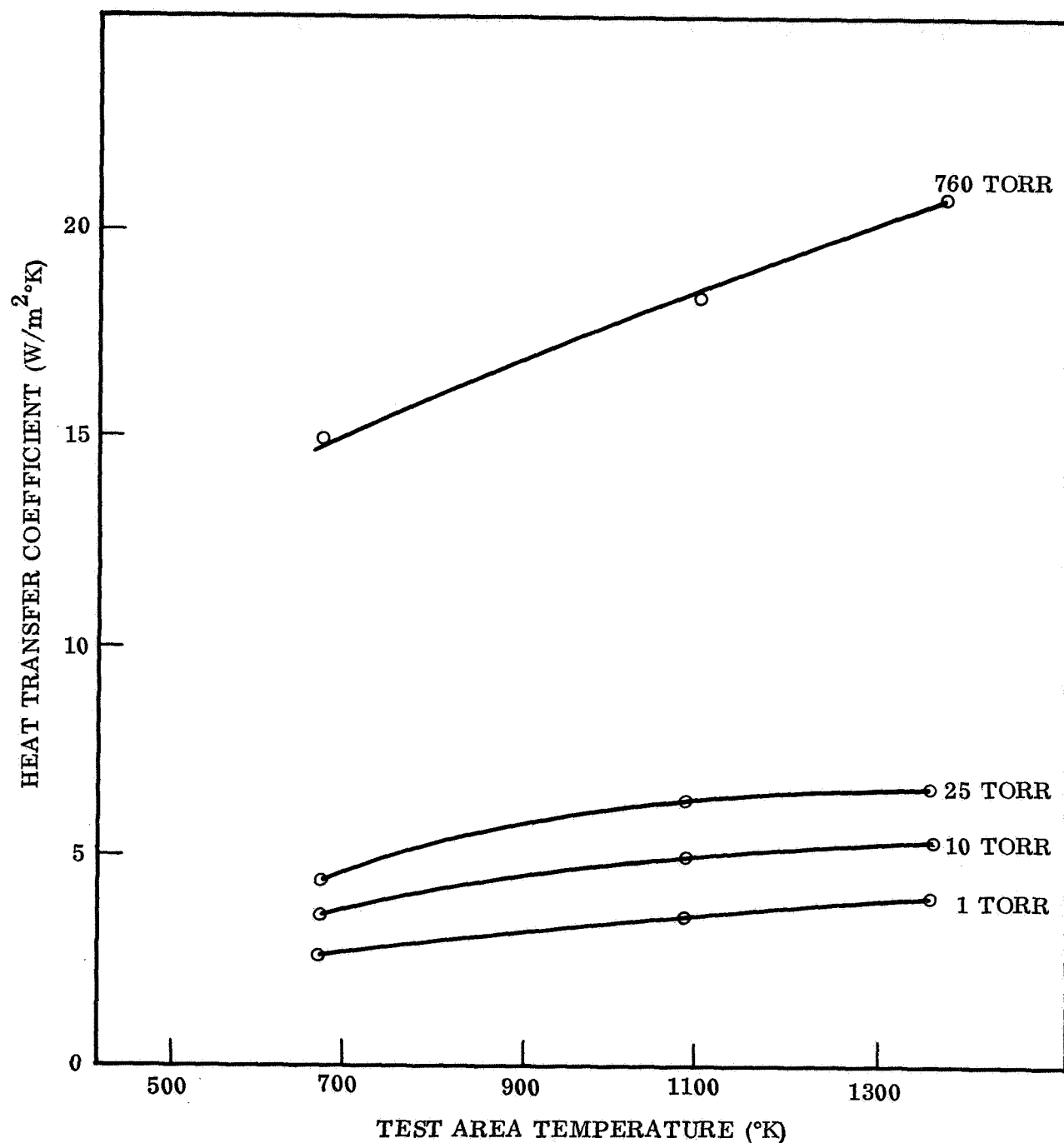
Fig. 13 Test Area Convective Heat Transfer Coefficients for Platinum Vertical
Strip (1.25-cm wide by 20-cm long) as a Function of Surface Tempera-
ture and Ambient Air Pressure
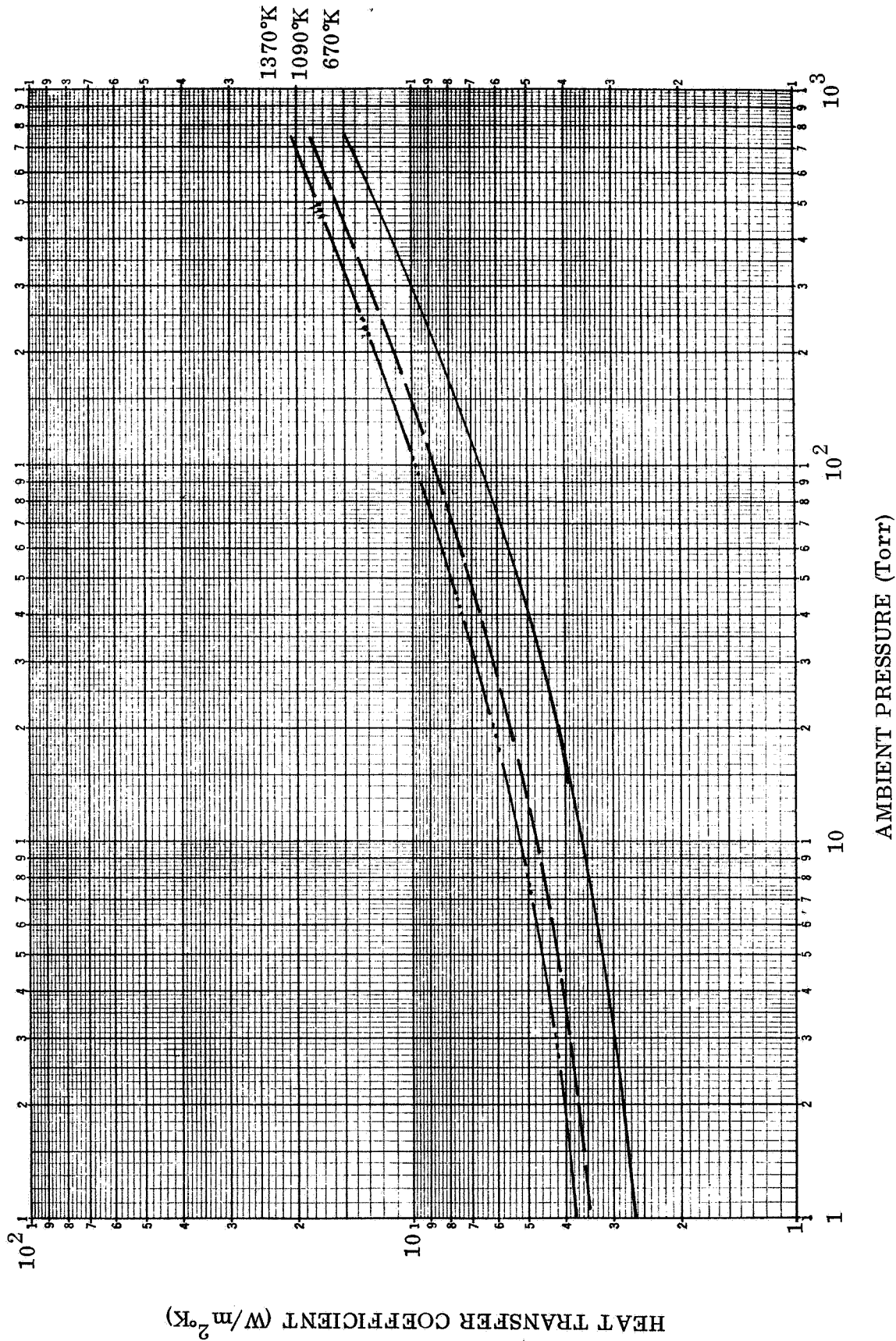
Fig. 14 Variation of Test Area Convective Heat Transfer Coefficient with
Air Pressure for Three Temperatures

3-17
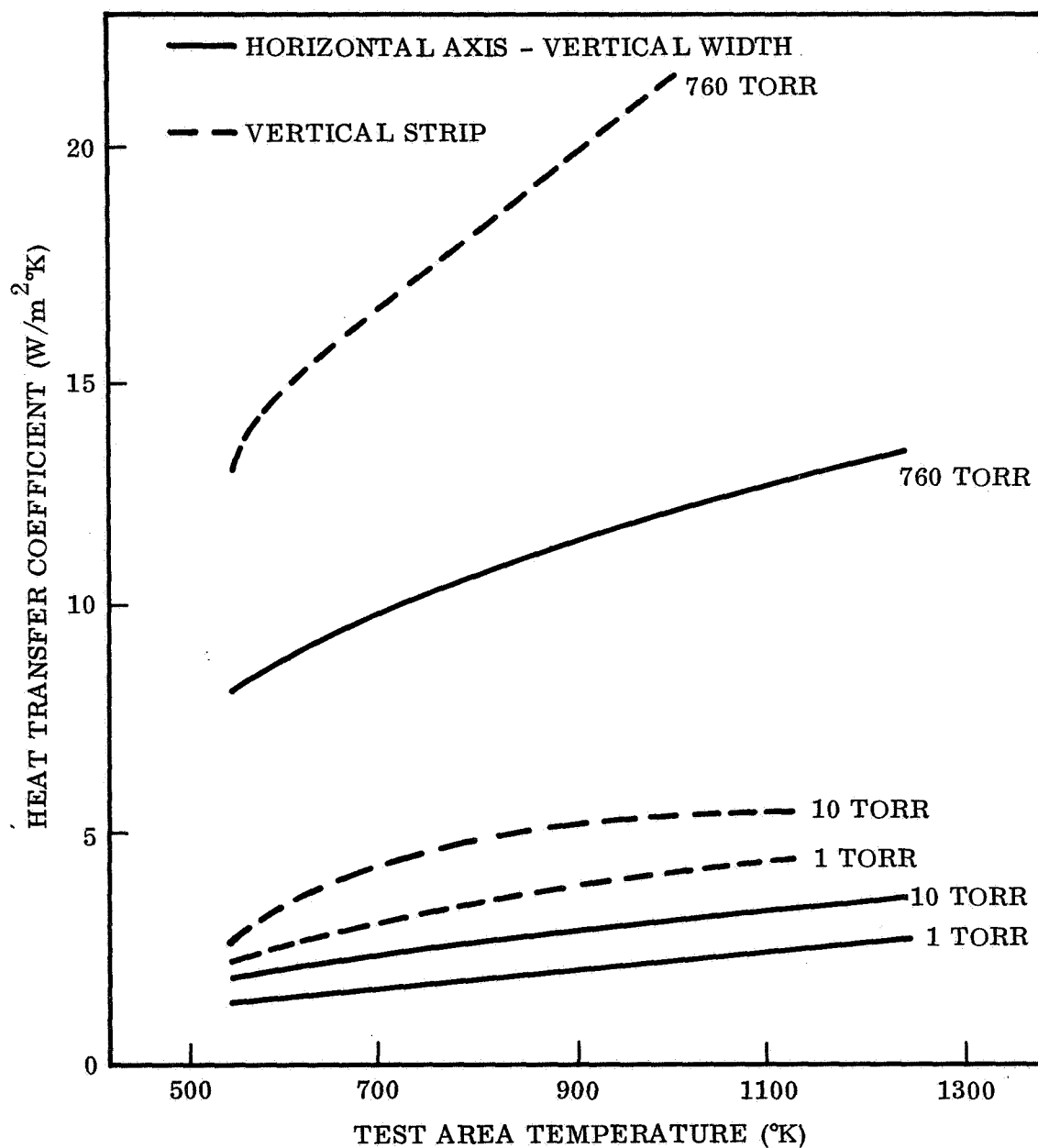
Fig. 15 Variation of Test Area Convective Heat Transfer Coefficient with
Temperature and Pressure for Two Sample Orientations

3-18

Section 4

EXPERIMENTAL APPARATUS

The design concept selected for the experimental apparatus is to use a resistivity-heated specimen mounted in a water-cooled chamber in which the ambient pressure may be varied from 10^{-5} to 760 Torr. A flow of air from sonic and supersonic nozzles is directed onto the specimen at fixed angles of incidence to simulate the entry environment. Specimen temperature and total pressure are varied with time to simulate those occurring during entry at various locations on the vehicle surface. Instrumentation is provided for measurement of total and spectral normal and directional emittance during cyclic tests with flow directed onto the specimen. Capability for calorimetric total hemispherical emittance measurement under static conditions is also included. For electrically conducting substrates, the specimen is in the form of a strip, 15 to 30-cm long and 1.27 to 2.54-cm wide. Thickness is sized so as not to exceed the voltage and current limitations of the power supply at maximum test temperature. The nominal 1.27-cm wide test area is used for supersonic flow testing. Non-electrical conducting specimens are heated by attaching them to a conductive substrate such as platinum. The flow system is designed for subsonic to $M = 3$ capability with specimen total pressures of 2 to 760 Torr. The overall layout of the facility is shown schematically in figure 16. The test chamber, power supplies, instrumentation, etc. are located in a 10-ft by 13-ft laboratory room with compressed air, electrical power (30 kw, 440 V and 120 V) and cooling water services (10 gpm at 290°K). Air-operated vacuum valves are provided in both vacuum system lines for rapid switch-over between pumps. The services for the large vacuum pump, located exterior to the laboratory building are 40 hp, 440 V, 3 phase and 5 gpm cooling water at 290°K. Details of the major facility components are discussed in the following subsection.

4.1 TEST CHAMBER

The chamber, figure 17, is of a cylindrical configuration with domed ends having feed-throughs for specimen mounting. Cooling is accomplished by a water-jacket on the

1 KINNEY NO. KT-850 VACUUM PUMP

2 BELLOWS CONNECTOR

3 TRAP

4 AIR-OPERATED VACUUM VALVE, 8-IN.

5 6-IN. OIL DIFFUSION PUMP SYSTEM

6 WATER – HOT AIR HEAT EXCHANGER

7 TEST CHAMBER

8 AIR FLOW NOZZLE ASSEMBLY

9 RADIOMETER, SPECTRAL AND TOTAL
   (0.5 μm to 35 μm)

10 INSTRUMENTATION CONSOLE

11 SPECIMEN HEATING POWER SUPPLY
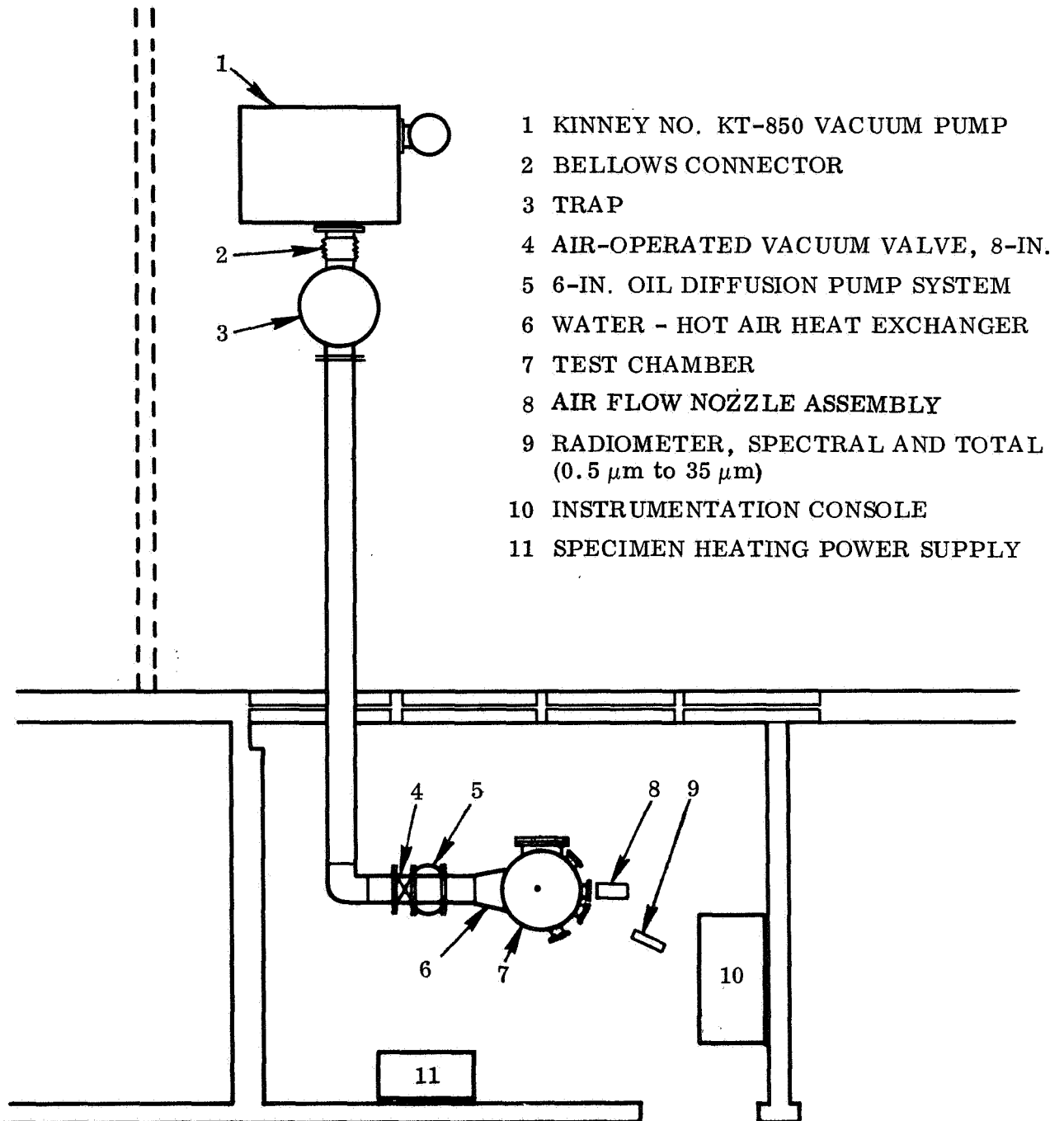
Fig. 16 Test Facility Layout

1 UPPER WATER-COOLED SAMPLE MOUNT
   AND ELECTRODE WITH CONSTANT
   TENSION ASSEMBLY

2 TEST CHAMBER, WATER-COOLED

3 LOWER WATER-COOLED SAMPLE MOUNT
   AND ELECTRODE

4 FLOW NOZZLE ASSEMBLY ENTRANCE
   PORT

5 PYROMETER VIEW PORT

6 WATER-HEATED AIR HEAT EXCHANGER

7 AIR-OPERATED VACUUM VALVE, 8-IN.

8 AIR-OPERATED VACUUM VALVE, 6-IN.

9 LN_2 TRAP

10 OIL-DIFFUSION PUMP, 6-IN.

11 CHAMBER SUPPORT FRAME

12 RADIOMETER PORTS, KBr WINDOW
   WITH WATER-COOLED SHUTTER

13 SAMPLE ACCESS PORT, 10-IN. CLEAR
   OPENING

Fig. 17 Test Chamber Schematic

4-3

cylindrical section and brazed tubing on the dome sections. Type 304-L stainless steel was used for fabrication of the chamber, and the interior is painted with a flat black paint, Cat-a-lac Black*. A 25-cm diameter clear opening is provided in one side of the chamber for access to the specimen mounting/electrode assemblies and for instrumentation connections. The lower water-cooled specimen mounting electrode is fixed, and the upper one has a pneumatic cylinder for maintaining a constant axial load on the specimen to accommodate for length changes due to thermal expansion. The vertical axis of these mounting electrodes is 2.5-cm off the chamber centerline which together with the diffuse black paint on the chamber interior eliminates reflected energy considerations in emittance measurements. A water cooled heat exchanger is located in the water-cooled exit duct from the chamber to cool the air before passage to the vacuum system.

Four 7.6-cm diameter ports are provided in the chamber wall at positions normal to and at 25°, 40° and 60° from a normal to the test surface. One port accommodates the air-nozzle duct assembly which is designed so that it may be moved to change the distance between the nozzle exit plane and the specimen plane without degrading the chamber pressure. The other three ports are fitted with KBr windows for radiometric measurements. Water-cooled externally operated shutters are located on the chamber side of each window to reduce contamination of these optical elements during testing.

The test chamber is mounted on a frame, figure 18, so that the windows are located approximately 1.5 m above floor level for ease of specimen viewing through the radiometer and optical pyrometer. The main power transformer (15 KVA, 220 V, single phase primary, variable secondary to 20 V) is also mounted in this frame and its secondary is electrically connected to the electrode assemblies through insulated water-cooled copper tubing configured so as to not place a significant axial force on the constant tension electrode assembly.

---

*Finch Paint and Chemical Company
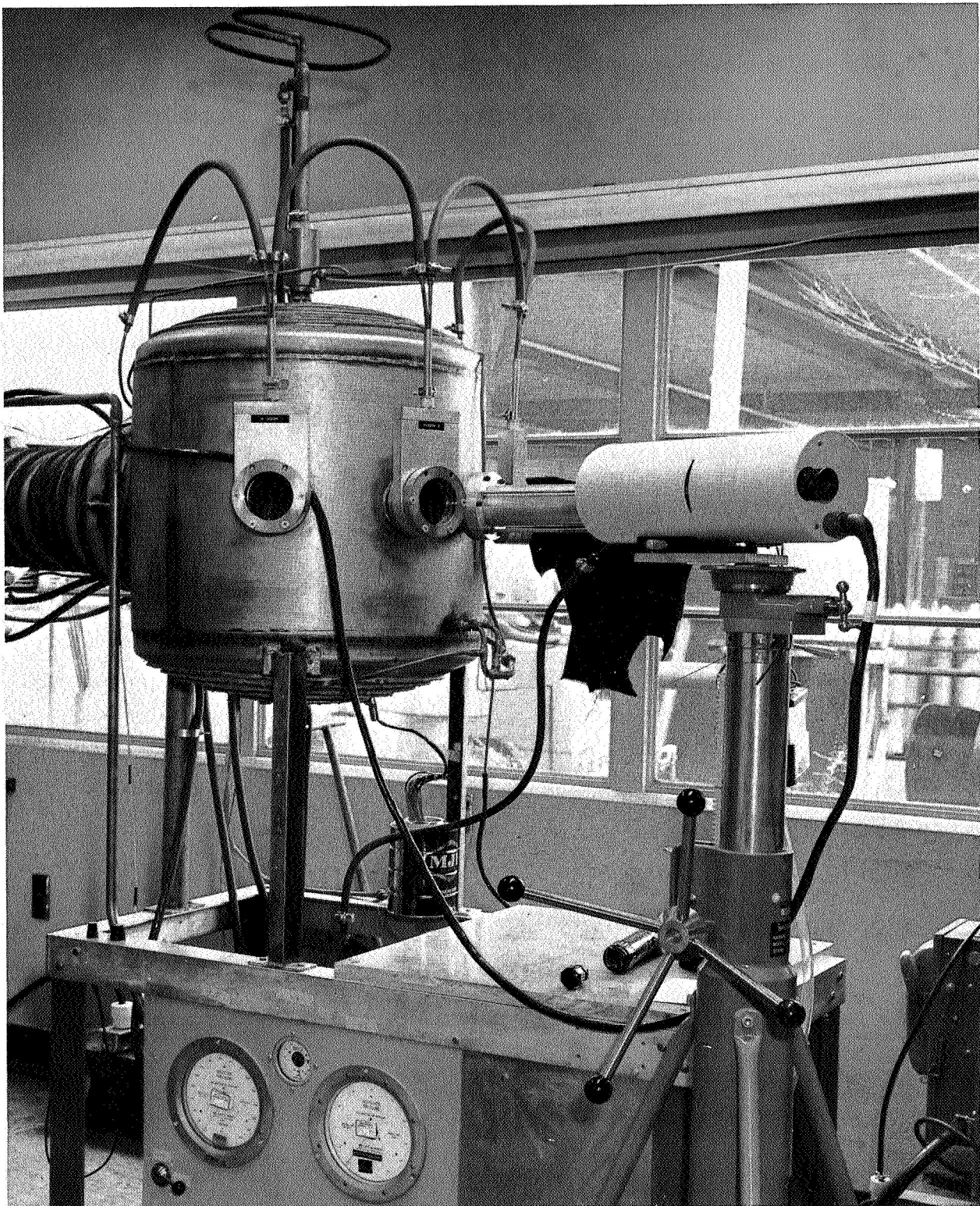
Fig. 18 Test Chamber and Radiometer

4–5

4.2 VACUUM SYSTEM

The facility has two separate vacuum systems for high vacuum and for flow operations. The latter uses an 850 cfm (0.5 m^3/sec) mechanical pump (Kinney KT-850) connected to the chamber exit directly through 20-cm diameter aluminum piping, flanged at lengths suitable for shipping to MSFC. The general arrangement of pumps, valves, bellows and piping are shown by figures 19 and 20. The mechanical pump is mounted on a concrete pad exterior to the building to reduce noise and vibration in the test area. A water-cooled trap is located at the pump inlet, and a cylindrical oil eliminator is connected to the vacuum exhaust, figure 20. During high vacuum operation, the large pump system is isolated from the chamber with a pneumatically operated vacuum valve. For flow testing the diffusion pump system is valved off from the chamber in a similar manner. During flow testing the chamber pressure is controlled by bleeding room air into the pump duct through a ball-type vacuum valve located on the chamber support frame.

High vacuum capability is provided with a LN$_2$ trapped 15-cm diameter oil diffusion pump backed by a 15 cfm mechanical pump, figure 19, with a molecular sieve fore-line trap. Pump switching is accomplished through pneumatic values. For high vacuum operation the large pump is operated to reduce chamber pressure to 1 Torr. This system is then valved-off and pumpdown continued with the 15 cfm pump. At approximately 0.05 Torr the diffusion pump valves are opened and the chamber evacuated to 10^{-5} Torr.

4.3 RADIOMETER

A Barnes Model 12-511A Research Radiometer is used to make total and spectral emittance measurements. The instrument consists of two separate components; an optical head which collects and transduces the target radiation into an electrical signal, and an electronics unit for signal processing.

The optical head is a cylindrically-shaped container that houses the energy collecting and detector-transducing systems. These include a Cassegrain reflecting system
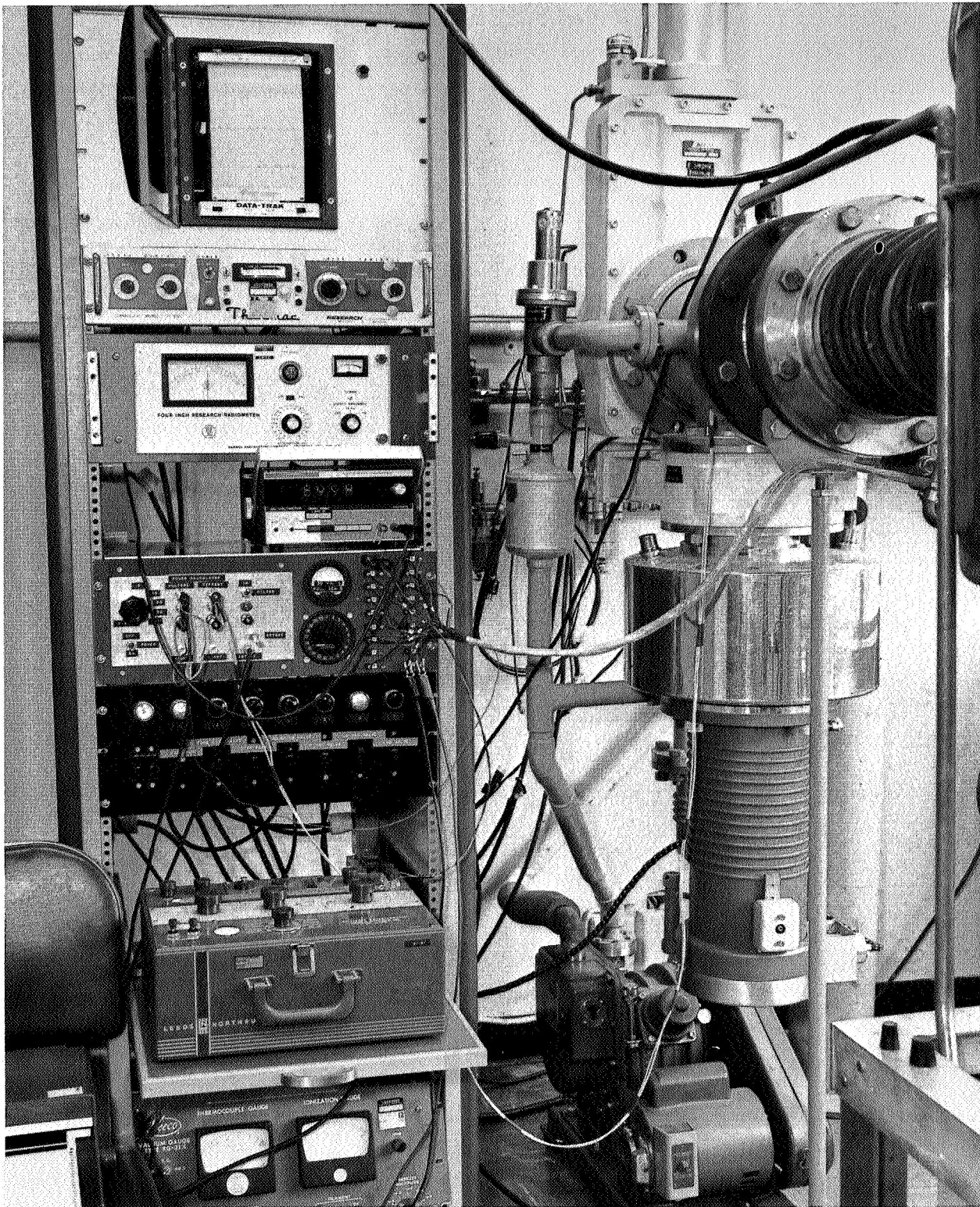
Fig. 19 Vacuum System and Instrumentation

4-7
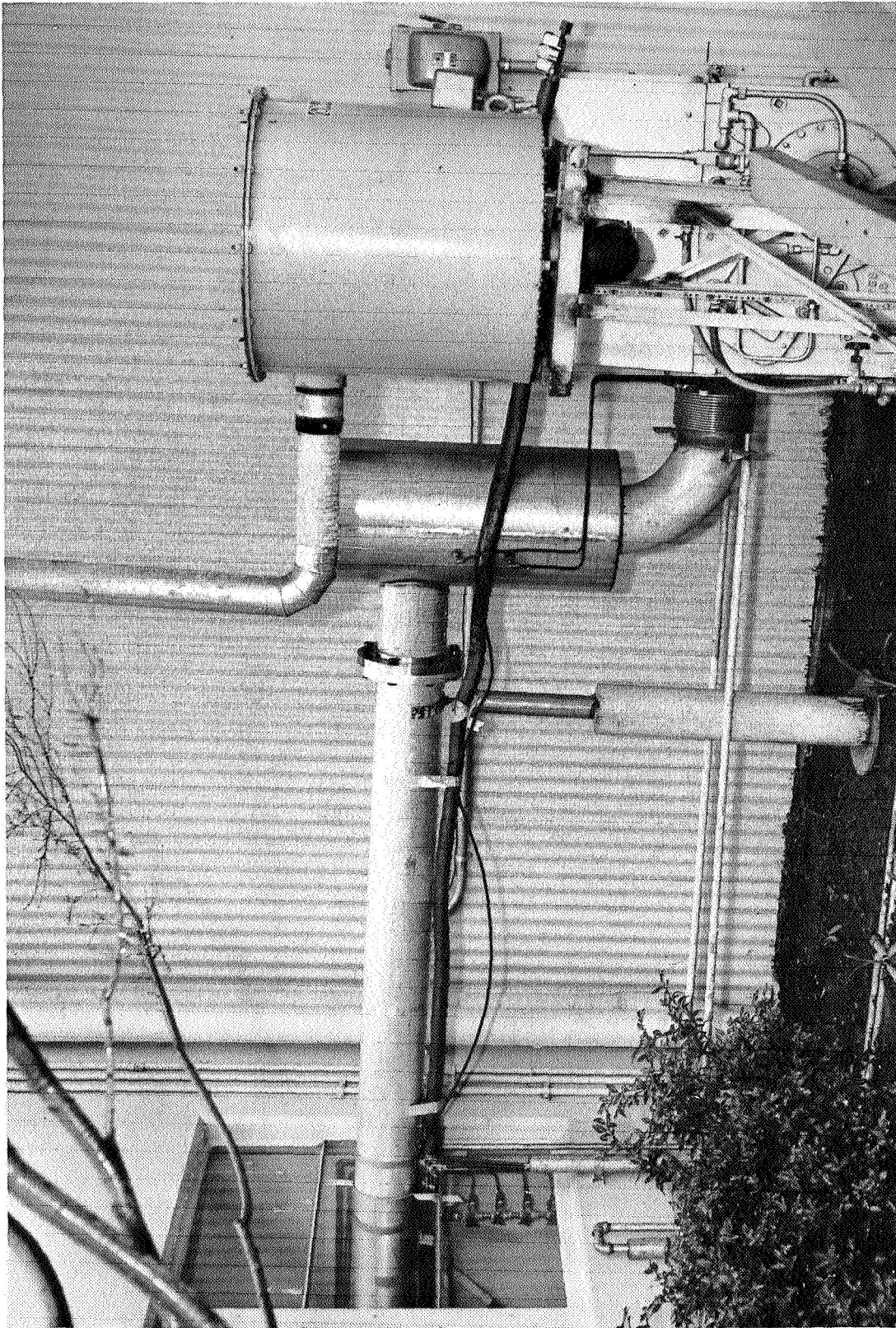
Fig. 20 Vacuum Pump for Flow Testing

with an adjustable secondary (focusing) mirror; a visual sighting system which permits parallax-free focusing; a motor driven optical chopper; a temperature-controlled reference cavity; field and aperture stops; a set of image-transfer mirrors; and a thermistor-bolometer detector package which converts the incident radiant energy into an electrical signal. A pair of rotatable filter wheels is located in the optical path between the transfer mirrors and the detector. Each wheel can accommodate up to eight separate filters to permit spectral studies of the target radiation. A photoelectric pickup is also located in the optical head which develops a signal synchronous with the radiation chopping rate for phase referencing in the radiation-signal demodulation. The primary collecting mirror is a ten-cm diameter, twenty-cm focal length mirror which collects and focuses the incoming radiation onto a five-cm adjustable secondary mirror. Radiation from the secondary mirror is directed into a temperature-controlled cavity and through the aperture stops and transfer optics to the detector. All mirrors are first-surface aluminized reflectors.

The optical chopper consists of four highly polished reflecting blades which rotate at a 240-cps rate between the secondary mirror and the heated reference cavity. During those periods when the chopper blocks the incoming target radiation, the reference cavity is presented to the detector as a blackbody radiating at a constant $331°$ K. The detector alternately "sees", therefore, the incoming target radiation and then the blackbody reference radiation.

A thermistor-bolometer detector package was selected for use with this radiometer. The 0.5 mm x 0.5 mm detector flake is hermetically sealed behind a 6.35 mm diameter KRS-5 window. The time constant for this detector is 1.7 msec., and the overall system responsivity is reported as 1.11×10^3 volts/watt/cm^2-ster. The relative spectral response of the detector over the wave-length range from 0.4 μm to 35 μm is shown in figure 21. Since the spectral response of this detector is not flat, corrections are required for total or broad-band emittance determinations for materials which are spectrally selective.

The electronics unit for the radiometer contains the processing circuits which amplify, filter and demodulate signals received from the optical head as well as the circuits and
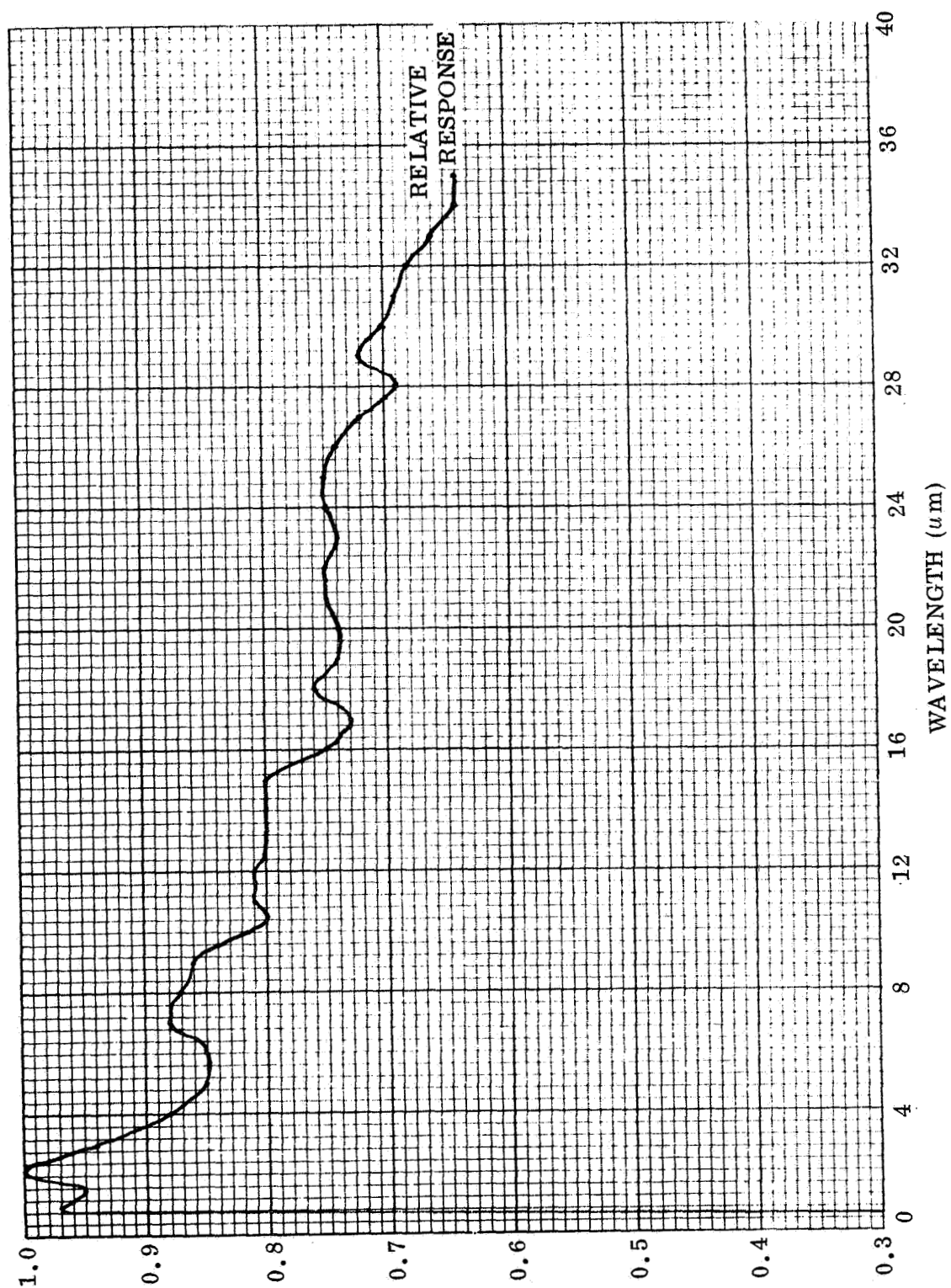
Fig. 21 Relative Spectral Response of Radiometer Detector

controls to supply the temperature controllers, detector bias, photoelectric pickup and chopper drive motor. All of the electronic system operating controls and indicators are mounted to the front panel of the unit. These include a three-position rotary bandwidth selector switch which is used to apply input power to the radiometer and to select one of two output signal bandwidths (dc-to-55 Hz or dc-to-1 Hz); a 21-position rotary signal-attenuator switch which permits attenuation of the preamplifier output signal in 3 db increments from 0 to 57 db; an electronic temperature offset switch and control by which common components in the reference and target radiation signals may be cancelled so that small variations in target radiation may be observed more readily; a wide-view meter which gives a relative indication of the target irradiance; and a control meter which gives a qualitative indication of the reference cavity temperature and detector housing temperature. The output meter is a center-zero dc voltmeter for which a full scale deflection corresponds to a 10 volt signal at the output recorder jack.

Eight narrow bandpass and one broad bandpass filter are installed in the two filter wheels in the radiometer head. Descriptions of the bandpass characteristics for each filter are shown in Table 5.

4.4 FLOW SYSTEM

The test apparatus is equipped with a cold gas flow system for exposure of the specimens to either a near sonic or a supersonic free jet during emittance testing. Room air is passed through a throttling valve into a 6.4-cm diameter by 51-cm long settling chamber upstream of the nozzle throat. Pressure level in this chamber is measured through a static pressure tap located in the end wall. The nozzle exit plane is 13.5-cm from the specimen to permit near normal emittance measurements, and provisions are included for alignment of the nozzle so that the specimen measuring area is centrally located in the flow field.

Two interchangeable nozzle blocks were fabricated for free stream Mach numbers of 1.0 and 2.25. The former is a simple converging nozzle having a 3.02-cm diameter sharp edged sonic throat and no supersonic section. The M = 2.25 nozzle has a

Table 5

BANDPASS CHARACTERISTICS OF IR FILTERS FOR
THE BARNES MODEL 12-511A RADIOMETER

Filter No.	Bandpass Wavelength (μm)	Bandwidth at 50% τ Cutoff Wavelengths (μm)	Average Transmittance (%)	Transmittance Outside Bandpass (%)
1	1.420	0.580	75	≤ 0.1
2	2.171	0.204	65	≤ 0.1
3	2.704	0.207	78	≤ 0.1
4	3.388	0.124	75	≤ 0.1 below ≤ 0.1 above to 5.0 μm
5	4.259	0.266	75	≤ 0.1
6	4.851	0.324	73	≤ 0.1
7	5.464	0.186	58	≤ 0.1 below ≤ 0.1 above to 11.4 μm
8	7.958	0.218	60	≤ 0.1 below ≤ 0.1 above to 13.8
9	7.84 to 16.6	broad bandpass	85	≤ 0.1 below

1.17-cm diameter throat followed by a 5° taper conical supersonic section with an exit diameter of 1.70-cm. Both nozzle blocks are of an easily interchanged cylindrical design using "O" ring seals to the settling chamber section.

4.5 INSTRUMENTATION AND CONTROLS

In addition to the Barnes radiometer instrumentation is provided for temperature, pressure, and electrical power measurements. Twelve channels are included for temperature measurement by thermocouples, and pressure instrumentation is provided for chamber and nozzle pressures during flow conditions. For vacuum operation, chamber pressure is measured with thermocouple and ionization gauges. Specimen power for calorimetric data is measured using a precision current shunt and the

voltage drop across the central measuring section length of the specimen (voltage probes are one leg of edge thermoscouples). The shunt and probe voltages are connected to a variable gain differential integrating multiplier, the output of which is directly proportional to the test area power. A Pyrometer Instrument Company Micro Optical pyrometer is used for brightness temperature measurements. Thermocouple output measurement is with a precision potentiometer, and a digital multirange voltmeter is used to measure power meter and radiometer output voltages. Typical instrumentation is shown pictorially in figure 19.

The two principal control functions are for the cyclic temperatures and total pressures during flow testing. Specimen time-temperature control is derived from a program controller unit which compares specimen temperature with a preselected temperature-time profile and uses the error signal to drive a SCR to control the primary voltage to the main power transformer. Pressure control is accomplished by simultaneous manual operation of the nozzle settling chamber throttling and pump bleed air valves to obtain the correct nozzle-to-chamber pressure ratio and nozzle pressure for a desired value of specimen total pressure. These valve settings are varied throughout the cycle to give a step-wise change in specimen total pressure following the desired time-pressure cycle for the simulated entry environment, as shown in figure 6.

4-13

Section 5

EXPERIMENTAL PROCEDURES

5.1 RADIOMETRIC DETERMINATION OF SPECTRAL AND TOTAL EMITTANCE

For the radiometer-specimen arrangement shown in figure 22 the radiometer signal is proportional to the difference in monochromatic or total radiant flux incident on the detector from the sample and from the reference cavity. When viewing the sample the detector output is:

$$S_s = K_s \left[(\epsilon_s N_s + \epsilon_s N_s \rho_s \rho_c \frac{A_s^2}{A_c^2} + \epsilon_c \rho_s N_c) \tau_w + \rho_w N_o + \epsilon_w N_w \right] \quad (1)$$

where the first term inside the brackets is the sample energy emitted into the solid angle collected by the radiometer; the second term accounts for sample energy that is reflected off the test chamber walls back to the sample and then reflected into the same solid viewing angle; and the third term accounts for energy emitted by the test chamber walls that is reflected by the sample into the radiometer viewing angle. (Note: the subscripts s, b, c, w, ch, r and o are used in this section to designate properties of the sample, blackbody, chamber walls, window, chopper, reference cavity and ambient surrounds, respectively). All the energy originating from the aforementioned sources is attenuated by the window transmittance (τ_w), before reaching the radiometer. The final two terms of equation (1) account for those portions of reflected ambient room energy and emitted energy from the window that fall into the viewing angle of the radiometer; and K_s is the instrument constant, including optical and electronic amplification, for the total amount of radiant flux detected in this case. Taking the window, chamber walls and room to be at essentially the same temperature, and neglecting the second term because of the large chamber-wall area relative to the

5-1
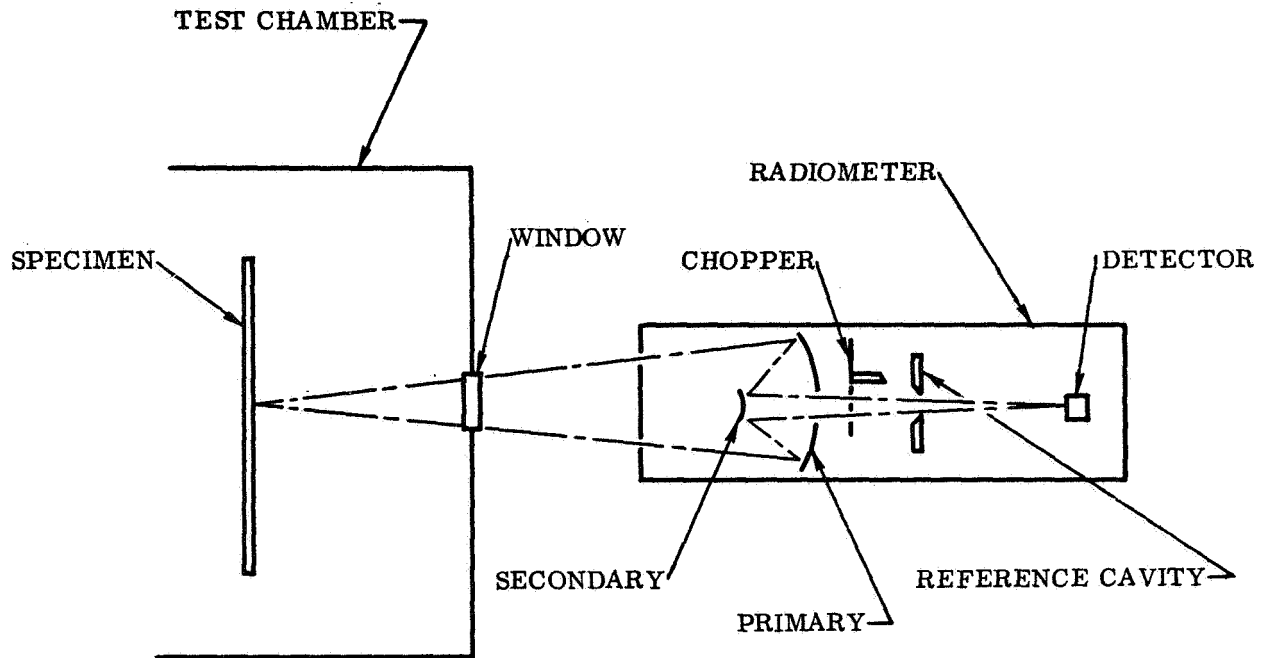
Fig. 22 Schematic of Specimen — Radiometer Arrangement for Emittance Measurements

sample area in combination with the low reflectance of the chamber walls, then equation (1) simplifies to:

$$S_s = K_s \left[(\epsilon_s N_s + \epsilon_c \rho_s N_o) \tau_w + N_o (\rho_w + \epsilon_w) \right] \qquad (2)$$

When viewing the chopper and reference cavity, the detector output is:

$$S_r = K_r (\epsilon_{ch} N_o + \rho_{ch} N_r) \qquad (3)$$

assuming the chopper to be at room temperature. The radiometer output when viewing the sample is then:

$$V_s = (S_s - S_r) = \overline{K}_s \left[(\epsilon_s N_s + \epsilon_c \rho_s N_o) \tau_w + N_o (\rho_w + \epsilon_w) - \epsilon_{ch} N_o - \rho_{ch} N_r \right] (4)$$

5–2

where $\bar{K}_s$ is the effective responsivity of the radiometer when viewing a sample at some temperature T_s. (Note: For monochromatic energy, $K_s = K_r = \bar{K}_s$; but for total or broad-band energy $K_s \neq K_r$ because the detector response is not perfectly grey, see figure 21).

Now by assuming that 1) $\alpha_w = \epsilon_w$ and $\alpha_w + \rho_w + \tau_w = 1$; 2) $\epsilon_s = \alpha_s = 1-\rho_s$; 3) $\epsilon_{ch} = 1-\rho_{ch}$ and; 4) $\epsilon_c = 1$, equation (4) reduces to:

$$V_s = \bar{K}_s \left[\epsilon_s \tau_w (N_s - N_o) - \rho_{ch} (N_r - N_o) \right] \tag{5}$$

In a similar manner the radiometer output when viewing the calibrating blackbody, (no window), is derived as:

$$V_b = \bar{K}_b \left[(N_b - N_o) - \rho_{ch} (N_r - N_o) \right] \tag{6}$$

If the temperature of the backbody is the same as that of the sample then $\bar{K}_b$ will be the same as $\bar{K}_s$, and the ratio of the radiometer signals is:

$$\frac{V_s}{V_b} = \frac{\epsilon_s \tau_w (N_s - N_o) - \rho_{ch} (N_r - N_o)}{(N_b - N_o) - \rho_{ch} (N_r - N_o)} \tag{7}$$

By rearranging terms, ϵ_s in equation (7) is found to be:

$$\epsilon_s = \frac{V_s/V_b \left[(N_b - N_o) - \rho_{ch} (N_r - N_o) \right] + \rho_{ch} (N_r - N_o)}{\tau_w (N_s - N_o)} \tag{8}$$

and since $N_s = N_b$ when $T_s = T_b$, equation (8) reduces to:

$$\epsilon_s = \frac{1}{\tau_w} \left[\frac{V_s}{V_b} + \rho_{ch} (1 - V_s/V_b) \left(\frac{N_r - N_o}{N_s - N_o} \right) \right] \tag{9}$$

Equation (9) is the basic form used to compute sample emittance from the measured radiometer signal and sample temperature, and the blackbody calibration data. For the total energy case τ_w is the transmittance of the window for the blackbody energy spectrum at τ_s. Also, the assumptions that $\epsilon_s = \alpha_s$ and $\epsilon_w = \alpha_w$ must be verified for the appropriate energy spectrum. The latter assumption is correct because the KBr window transmittance is essentially flat, (0.92 ± 0.01), from 0.60 to $20\,\mu m$ and ϵ_w is negligible in this region. The former assumption does not significantly effect the accuracy of the total measurement because of the very low value of $\rho_s N_o$ compared to $\epsilon_s N_s$ for elevated temperature measurements on moderate to high emittance surfaces.

The emittance computations are performed using the blackbody calibration data for the radiometer which is described in the next section. Curves of radiometer signal versus blackbody temperature were constructed for total radiation and for each spectral filter. A radiometer signal is taken from the curves for a blackbody temperature corresponding to the sample temperature. The ratio $(N_r - N_o)/(N_s - N_o)$ is then obtained from a set of curves of this ratio versus specimen temperature for either the total or the appropriate filter. These curves were computed for each particular bandpass using reference cavity and ambient temperature values of $331°$ and $300°\,K$, respectively. Using the measured radiometer signal, V_s, and the corresponding blackbody signal and radiance ratio the specimen emittance is computed from equation (9) with ρ_{ch} being taken as 0.98.

5.2 CALORIMETRIC DETERMINATION OF TOTAL HEMISPHERICAL EMITTANCE

The basic method for determining ϵ_{TH} is as described in Section 2. To determine the input heating power the power meter is connected to the voltage probes from the measuring area of the specimen and to the current shunt voltage taps. Total emittance is computed from

$$\epsilon_{TH} = \frac{P_{in} - P_L}{A_s \sigma (T_s^4 - T_c^4)} \tag{10}$$

where P_{in} is the electrical power dissipation in the test area and P_L is the loss term accounting for thermal conduction losses at each end of the test area of the specimen (and for convection losses if not in vacuum). A_s is the total radiating surface area of the test section between the voltage probes, and T_s and T_c are the absolute temperatures of the specimen and chamber walls, respectively. The loss term, P_L for the conduction case is determined from estimates of the temperature gradient at the ends of the test section, published values of material thermal conductivity, and the specimen cross sectional area. Estimates of the temperature gradients are obtained from plots of the measured temperature distribution along the length of the strip. If measurements are made in other than vacuum conditions convection losses are computed from the data of Section 3. The surface and cross sectional areas are determined from micrometer measurements and corrected for thermal expansion using published values for the test material. For vacuum testing of low thermal conductivity high emittance materials, such as the superalloys, the P_L term becomes negligibly small at test temperatures above 800° K.

5.3 TEST PROCEDURE

Each test specimen is instrumented with four to six thermocouples attached to the edge and rear surface in the vicinity of the test area. Chromel-alumel, Pt/Pt 13% Rh and Pt 6% Rh/Pt 30% Rh thermocouples, 3- or 5-mil diameter, are used, the selection of thermocouple type being made on the basis of material and test temperatures. More details of the specific instrumentation for each specimen tested in this program are given in Section 8. Method of thermocouple attachment is also dependent upon the material being investigated. Generally the junctions are spotwelded to the material, but in some cases they are simply inserted into small diameter holes drilled into the specimen edge and secured by peening or by wedging with a small length of thermocouple wire.

The instrumented sample is mounted in the test chamber and clamped to the water-cooled electrodes. After connection of the instrumentation leads to the appropriate chamber feed-throughs, the test chamber is evacuated. Radiometric spectral and

total normal and calorimetric total hemispherical emittance measurements are made in vacuum, starting at the lowest desired test temperature and working up to the maximum desired temperature level. The specimen is then cooled to ambient temperature and a time-pressure and-temperature cyclic test conducted in static air. Total normal emittance measurements are made during each cycle which is repeated five times. This procedure is repeated for M = 1.1 and M = 2.15 flow conditions.

Specimen temperature data from thermocouples are recorded continuously during the cyclic testing. Pressure measurements are typically recorded at two minute intervals. Optical pyrometer temperature measurements are made at the steady-state temperature portions of the cycle. Total and spectral data are also obtained at these points. A typical time-temperature and pressure profile for a test cycle is shown by figure 6.

Section 6

APPARATUS CALIBRATION

A series of calibration tests were conducted to verify performance of three apparatus components, after which an overall apparatus checkout was performed using two NBS emittance standards. Component tests were for flow characterization, power meter accuracy and radiometer operation. The following subsections summarize the results of these tests.

6.1 FLOW CHARACTERIZATION

Cold flow calibration tests were conducted using both the sonic and M = 2.25 nozzles. First, a pitot-static pressure survey was made of the flow field at the specimen position using a 1.5-mm diameter pitot-static probe. The ratio of nozzle upstream (settling chamber) pressure, P_t , to test chamber pressure, P_c , was varied, and a plot was made of Mach number versus this ratio. The Mach number and other flow field properties are a function of this pressure ratio because of the appearance of compression and expansion waves in the free jet. These phenomena are a result of over or under expansion and are therefore, dependent upon the pressure ratio P_t/P_c. From the data an optimum operating point was found for each nozzle. Using this pressure ratio, P_t was then varied to determine if a constant Mach number was achieved for the cyclic pressure range desired for emittance testing.

A pitot static traverse was made across the sample position plane to define the flow field as a function of chamber pressure while operating at the optimum nozzle pressure ratio. An instrumented 2.54-cm wide flat-plate test specimen was then placed in the emittance sample position. This plate was provided with five 0.5-mm dia pressure taps located at the plate center, 5.1-mm to each side of and below the center and 10.2-mm to one side of the center. These taps were individually connected to a Texas Instruments quartz tube pressure gauge. The nozzle was aligned with the plate by

balancing the pressure at the taps located 5.1-mm about the center tap. Plate pressures were then measured as a function of P_t/P_c .

The optimum pressure ratio, P_t/P_c , determined from the pitot-static survey was found to be 12.7 for the $M = 2.25$ nozzle. At this ratio the measured free stream Mach number was 2.15, and the Mach number was constant to within 5 percent as P_t was varied. After alignment of the flat plate specimen the measured pressures at the 5.1-mm positions were 3 percent below the center tap pressure, and the 10.1-mm tap measured 8 percent low. Variation of P_t/P_c about the optimum point, 12.7, resulted in rapidly fluctuating plate pressure due to the formation of expansion and compression waves in the free jet. However, at $P_t/P_c = 12.7$ plate pressures were quite steady. The ratio of nozzle pressure to plate pressure, P_t/P_m , was next determined as P_t was varied while P_t/P_c was held constant at the 12.7 value. The P_t/P_m ratio was found to be a function of P_t . This dependence is probably caused by nonisentropic and non-steady effects. The ratio of P_t/P_m is theoretically quite sensitive to these effects and the effects contributing to the measured 5 percent variation in Mach number fully account for the measured changes in P_t/P_m . The change in P_t/P_m with P_t was plotted and this graphical relationship used to calculate the value of P_t corresponding to a desired specimen total pressure. This then defines the operating parameters, P_t and P_m , to be used to simulate the entry total pressure profile. Figure 23 shows this relationship for the $M = 2.25$ nozzle.

The sonic nozzle was operated at a pressure ratio, P_t/P_c , of 2.0 so that there was a slight supersonic expansion in the free jet. For this condition, the free stream Mach number was 1.1 and the flow field was very steady. The flat-plate calibration specimen was then installed and aligned with the flow. Measurements were made of P_t/P_m as a function of P_t , and for this nozzle no variation was observed in the plate-to-nozzle pressure ratio over a nozzle pressure range of 1 to 100 Torr. Operating conditions for the sonic nozzle are $P_t/P_c = 2.0$ and $P_m = 0.91 \, P_t$. During testing the nozzle pressure is adjusted to 1.1 times the desired specimen pressure and the chamber pressure is maintained at one-half of the nozzle pressure.
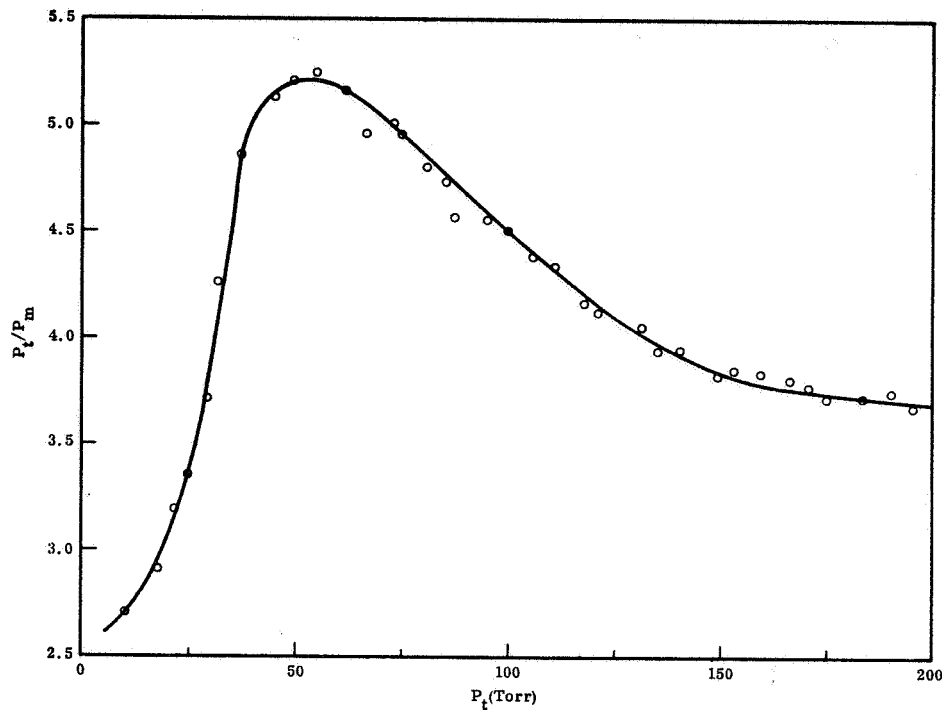
Fig. 23 Ratio of Nozzle to Specimen Total Pressure as a Function of
Nozzle Total Pressure for Mach 2.15 Nozzle

6.2 POWER METER

Calibration of the power meter was obtained from a comparison of meter output
voltage with precision power measurements (0.25 percent) made using a resistively
heated tantalum strip under vacuum conditions. The tantalum strip was 20-cm long
by 1.27-cm wide, and the central 2.54-cm section was instrumented with potential
leads spotwelded to the strip at its edge. A precision current shunt was connected
in series with the strip and a variable output, 60 cycle power supply having a unity
power factor. Shunt and potential lead voltages were read with a precision ac milli-
volt meter (0.15 percent).

Power was applied to the strip, and after its temperature stabilized the potential drop
and current shunt voltages were measured. These leads were then connected to the
power meter and its output voltage measured. This procedure was repeated several
times for each of the four meter gain settings over a power range of 1.3 to 150 watts.

For a given power level repeated meter readings were averaged and a calibration factor computed from the output voltage divided by the measured power. The results are given in Table 6. The estimated accuracy of the power determined from the meter output signal is 1 percent. This meter may be used with power supplies having power factors less than unity or waveforms other than sinusoidal because it simultaneously integrates the current and voltage over a fixed time interval.

Table 6

POWER METER
CALIBRATION CONSTANT

Meter Gain Setting	Constant (w/mv)
5	0.393
10	0.0982
20	0.0253
50	0.00389

6.3 RADIOMETER

The Barnes radiometer was subjected to calibration testing to determine range-of-focus, effective field-of-view, system response characteristics and the near-range focal plane loss factor. The results of these tests are summarized in this sub-section.

Measurements at target distances between 0.3 and 1.5 m of target sizes from 0.32 to 15.33 mm indicated that the effective field-of-view of the radiometer is 4 milliradians. This parameter determines the target area that is "viewed" by the detector at a given target distance. As the target distance increases from 0.3 to 1.5 m, the target diameter increases proportionally from 1.2 to 6.0 mm. In the test facility the radiometer is located 0.76 m from the test specimen plane, and therefore, the area of the specimen viewed by the radiometer is 3.0 mm in diameter.

The range of focus of the radiometer is from 0.3 m to infinity. At target distances less than approximately 0.9 m, however, Barnes reports that the constant focal loss feature of the radiometer is not maintained, and the relative responsivity of the

system may change. Laboratory tests of the radiometer response to full-field targets at distances between 0.3 and 1.5 m and at three different target temperatures, demonstrated that the relative response of the system remains essentially constant for target distances down to 0.6 m, then drops off to approximately 67 percent of maximum at a distance of 0.3 m.

Response calibration data for the Barnes radiometer was obtained for the unfiltered (total) operating mode and for the nine filtered (spectral) operating modes. The data consists of relative radiometer signal outputs for each operating mode (filter wheel position) vs. blackbody target temperature. The data was obtained at temperatures between 375°K and 1280°K using an Infrared Industries Inc. Model 404 Blackbody with a 10-mm diameter aperture, and the blackbody-to-radiometer distance was 0.76 m. The relative response range of the radiometer for each operating mode is given in Table 7. The total response range for the radiometer is from 0 to 9400 output units, i.e., radiometer detector output times amplifier attenuation units. A response of zero corresponds to the irradiance level (total) obtained from a 331° K blackbody target. This is the operating temperature of the radiometer's reference cavity against which all incoming radiation levels are referenced. The maximum response, 9400, corresponds to the total irradiance obtained from a 1600°K blackbody target.

6.4 APPARATUS CHECKOUT

To verify the accuracy of the radiometric measurements of total and spectral near normal emittance in the completed test apparatus, data were obtained on two NBS Standard Reference Material spectral emittance specimens. These specimens were installed in the test chamber in the configuration for entry testing, however, measurements were made only under static air or vacuum (lower temperatures) conditions to avoid possible damage to the standard specimens. The two standards were Platinum-13 percent Rhodium (NBS SRM No. 1409) and oxidized Kanthal (NBS SRM No. 1427) purchased from NBS in the form of 1.9-cm wide by 25-cm long strips. The majority of testing was conducted in air in accordance with the NBS recommendations for these materials. However, several lower temperature vacuum runs were made on the Kanthal strip to evaluate possible convection effects on thermocouple temperature measurements.

Table 7

TOTAL AND SPECTRAL CALIBRATION DATA FOR THE BARNES MODEL 12-511A RADIOMETER FOR BLACKBODY SOURCE TEMPERATURES BETWEEN 400 AND 1400°K AT A DISTANCE OF 0.76 METERS

Black-Body Temp. (°K)	Relative Response as a Function of Filter-Wheel Position									
	1-1 (Total)	1-2 (1.42 μm)	1-3 (2.17 μm)	1-4 (2.70 μm)	1-5 (3.39 μm)	1-6 (4.26 μm)	1-7 (4.85 μm)	1-8 (5.46 μm)	2-1 (7.96 μm)	3-1 (7.8-16.6 μm)
400	18.0	0	0	0	0	0.17	0.22	0.19	0.78	7.65
500	68.0	0	0	0.23	0.42	1.00	1.87	1.04	2.50	25.0
600	160	0.10	0.56	1.65	2.25	3.20	5.10	2.53	4.65	46.5
700	320	0.67	2.76	5.50	6.00	7.00	10.5	4.45	7.00	70.0
800	555	3.75	8.50	14.0	12.5	13.0	17.8	6.90	9.40	97.0
900	900	12.6	21.3	29.8	23.0	20.8	27.5	10.0	12.1	124
1000	1380	36.0	46.8	53.5	38.0	30.2	39.0	13.4	15.0	154
1100	2000	93.0	88.0	86.5	56.0	43.0	53.0	17.3	18.0	183
1200	2870	170	141	131	78.0	57.5	68.0	21.3	21.6	220
1300	4370	313	208	180	103	72.0	83.5	25.5	24.8	243
1400	6000	550	289	249	130	84.0	97.5	29.3	27.6	267

Three Pt 6% Rh/Pt 30% Rh thermocouples, 3 mil diameter, were spotwelded to the Platinum-13 percent Rhodium specimen on the vertical edge; one at the center of the strip and one each 1.3-cm below and above the center thermocouple. The edge location was chosen to avoid damage to the central area of the strip which was viewed by the radiometer. Chromel-alumel thermocouples, 3 mil diameter, were spotwelded to the edge of the Kanthal strip in a similar fashion to the Platinum Rhodium alloy strip with the addition of a thermocouple on the rear surface opposite the central viewing area. This latter thermocouple was used because of relatively large center-to-edge temperature gradients which might exist with this lower thermal conductivity, high emittance material in a convective environment.

Each standard was installed in the apparatus and the ends were clamped to the water-cooled electrode assemblies. Tension on the strip was regulated by the pneumatic cylinder which positioned the upper moveable electrode unit. Electrical power for specimen heating was supplied from a silicon controlled rectifier (SCR) unit operated by a variable set-point, proportional band controller using one specimen thermocouple for the controller set-point deviation input. Radiometer output voltage and attenuator switch position were recorded for each temperature level together with all thermocouple outputs (including control) and electrical power across the test area. Additionally, optical pyrometer brightness temperatures were measured for temperatures of 1100°K and higher.

6.4.1 Platinum — 13 Percent Rhodium Results

A total of nineteen sets of emittance data were obtained for this material. Measurements were made at four temperatures (800°, 1100°, 1400° and 1600°K) corresponding to those for the NBS spectral data supplied with the standard. Both total and spectral near normal emittance measurements were obtained, the latter through the use of the nine spectral filters in the radiometer filter wheel. The measured values of ϵ as a function of filter band center wavelength for the four temperatures are shown in figures 24 through 27. The solid curves represent the NBS spectral data at each temperature, and these are based upon the arithmetic average of twenty-one measured values at each wavelength. Standard deviations of the average value for each of seven
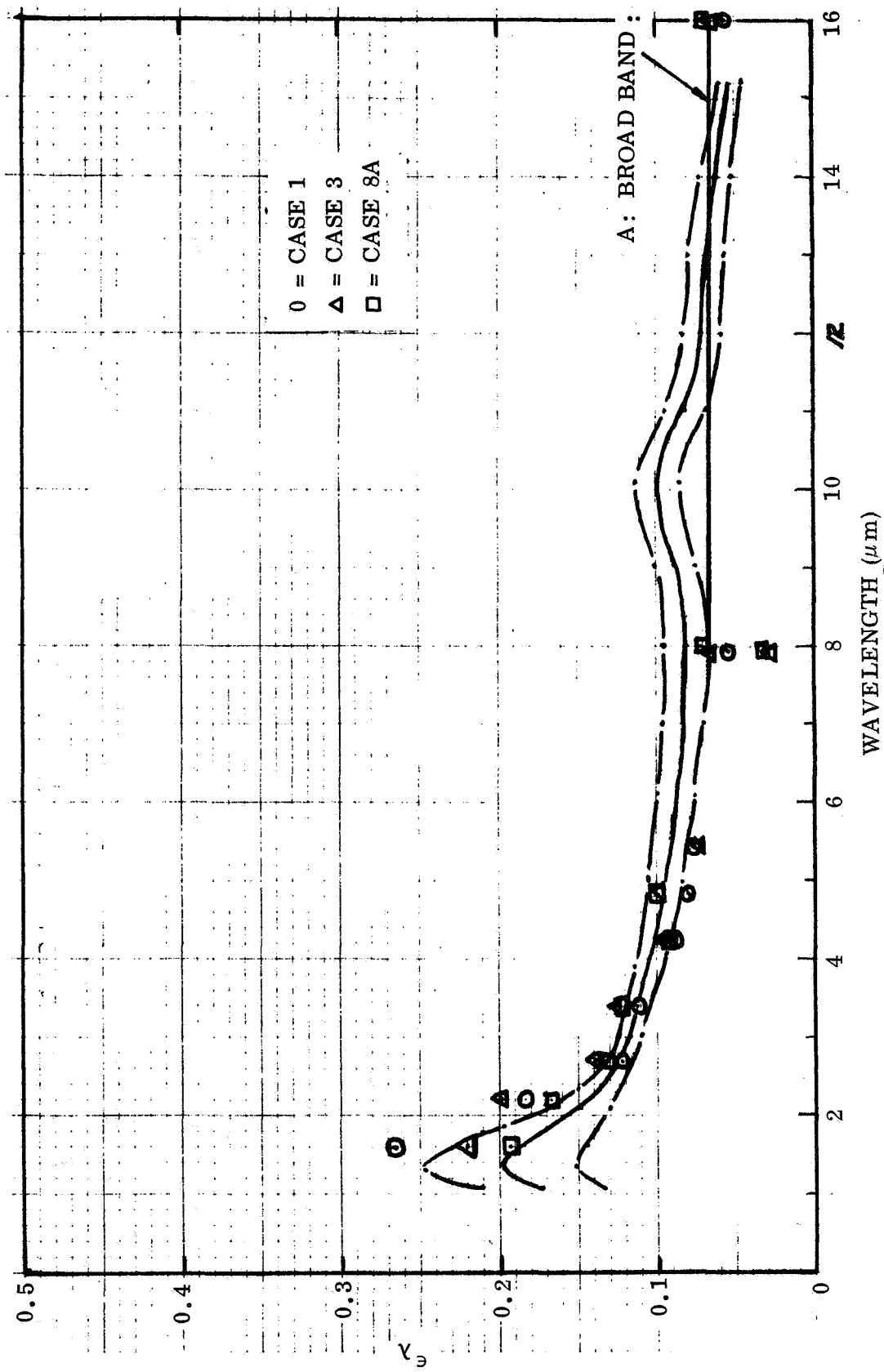
Fig. 24 Spectral Emittance Data for NBS Platinum – 13% Rhodium
Emittance Standard Measured in Air, T = 800°K
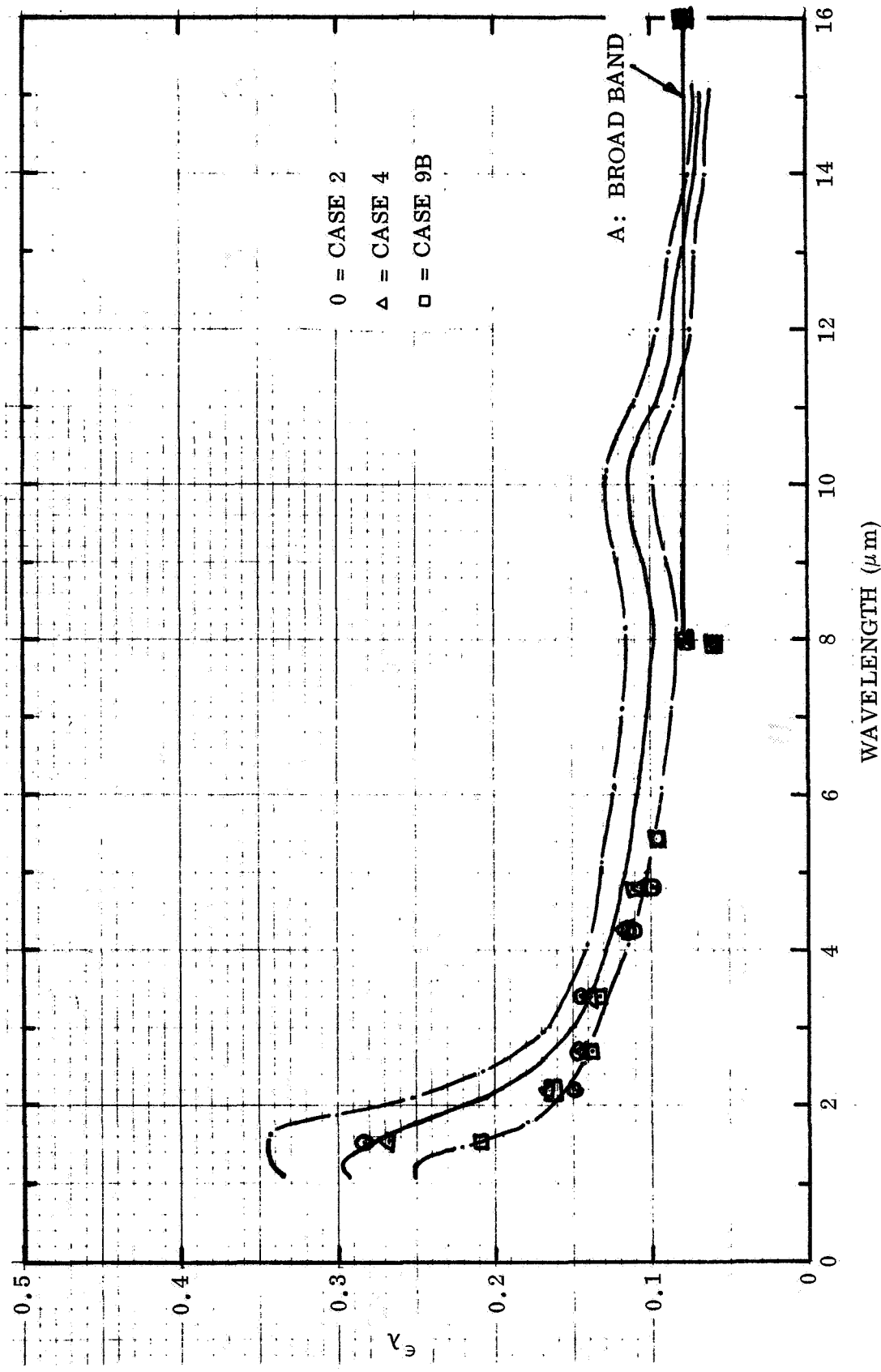
Fig. 25 Spectral Emittance Data for NBS Platinum – 13% Rhodium Emittance Standard Measured in Air, T = 1100°K
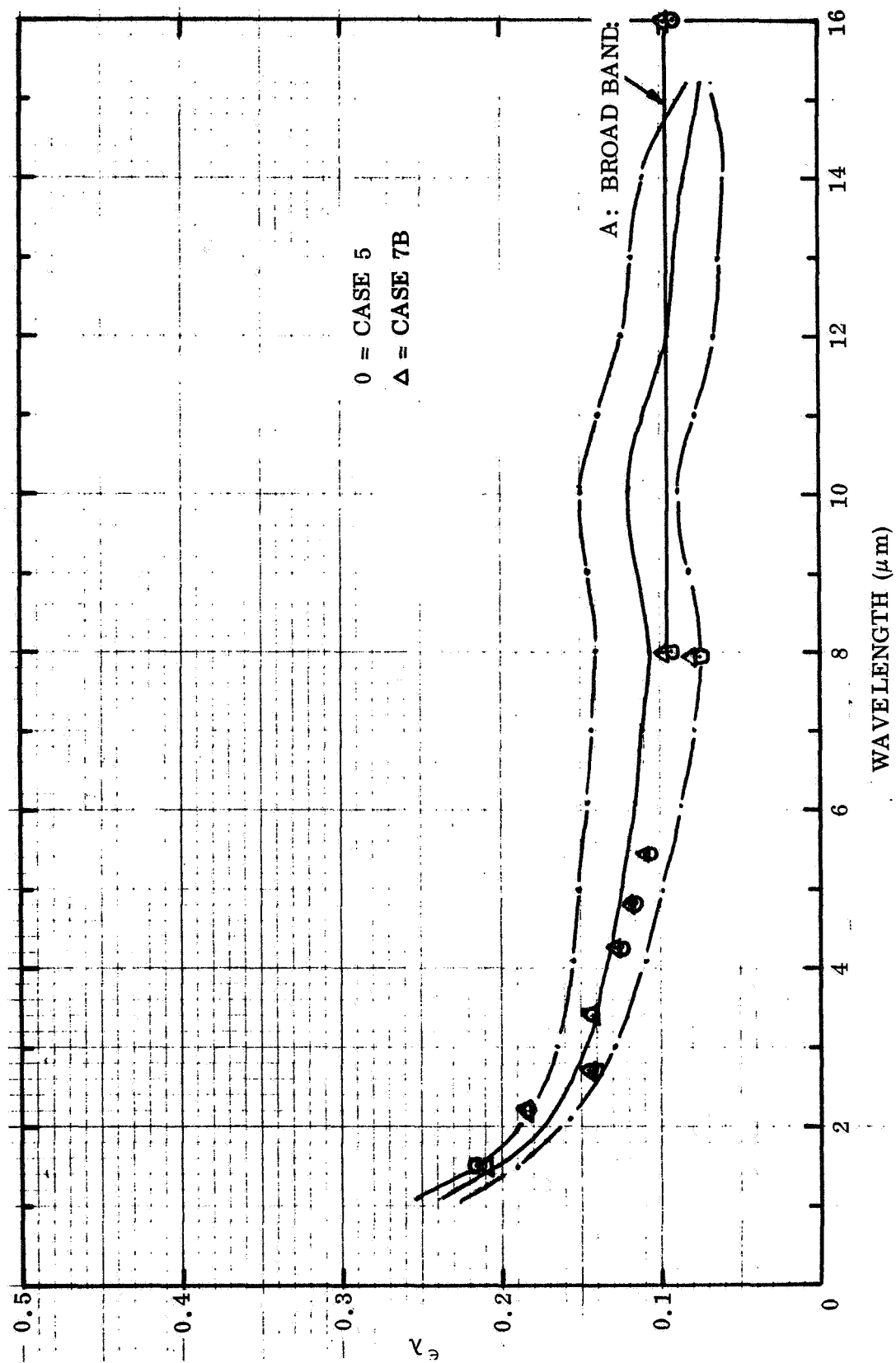
Fig. 26 Spectral Emittance Data for NBS Platinum – 13% Rhodium
Emittance Standard Measured in Air, T = 1400°K
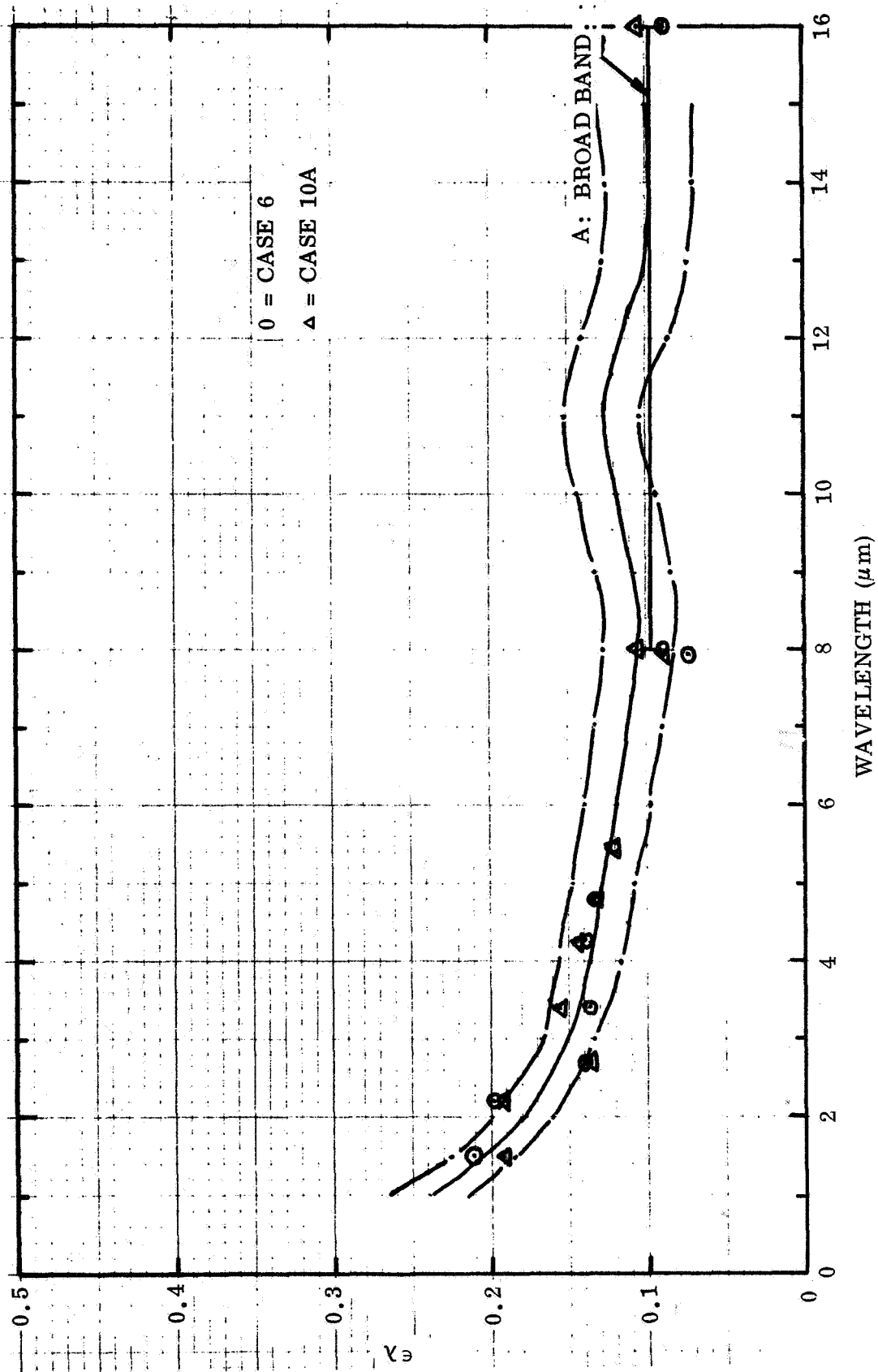
Fig. 27 Spectral Emittance Data for NBS Platinum – 13% Rhodium
Emittance Standard Measured in Air, T = 1600°K

LOCKHEED PALO ALTO RESEARCH LABORATORY

LOCKHEED   MISSILES   &   SPACE   COMPANY,   INC.
A   SUBSIDIARY   OF   LOCKHEED   AIRCRAFT   CORPORATION

samples measured by NBS are shown by the broken lines of each figure (ref. 22).   In
general, the spectral data are in good agreement with the NBS values with the excep-
tion of the 800°K data at 1.42, 2.17 and 7.96 μm.   The errors in these data points are
attributed to the very low radiometer signal levels resulting from the low specimen
spectral radiances and narrow filter band passes.   These resulted in signal uncertain-
ties of from 10 to 20 percent because of noise at the very high instrument gain settings
required at these wavelengths.   The reproducibility of successive measurements at a
given wavelength and temperature, with the exceptions noted earlier, was within 0.02.

Measured total near-normal emittance values are compared in Table 8 with those cal-
culated from the NBS spectral data by numerical integration of the spectral emittance
curves for the appropriate blackbody energy distributions at each temperature.   Spec-
tral standard deviations were used to determine a deviation for ϵ_{TN} assuming that a
high or low standard is consistently high or low at all wavelengths.   The measured
values of ϵ_{TN} agree with the integrated NBS data to within 0.012 which is within the
standard deviation.

Table 8

TOTAL NORMAL EMITTANCE OF NBS PLATINUM-13% RHODIUM STANDARD
(SRM 1409) AS A FUNCTION OF TEMPERATURE

Nominal Test Temperature (°K)	Number of Measurements	Measured ϵ_{TN}	Calculated ϵ_{TN} From NBS Spectral Data
800	4	0.0965 $^{+0.00135}_{-0.0015}$	0.097 $\pm$ 0.013
1100	5	0.142 $^{+0.013}_{-0.010}$	0.146 $\pm$ 0.015
1400	6	0.159 $^{+0.004}_{-0.003}$	0.153 $\pm$ 0.020
1600	4	0.174 $^{+0.005}_{-0.009}$	0.165 $\pm$ 0.020

Values of ϵ_{TN} computed from thermocouple temperature data are 0.003 higher than those computed on the basis of optical pyrometer temperature values at 1100° K, 0.006 higher at 1400° K and 0.013 higher at 1600° K. True temperatures were calculated from pyrometer brightness temperature readings using ϵ_λ = 0.32 for the sample emittance and τ = 0.92 for the window (KBr) transmittance at 0.65 μm. From these data it appears that the temperatures measured by edge thermocouples are 10° to 20° K low. This may be attributed to small gradients at the edge and losses from the leads, both being due to convection.

6.4.2 Oxidized Kanthal Results

During the initial measurements on this specimen a temperature controller malfunction caused a momentary (2 to 3 sec) overshoot of power to the strip resulting in overheating, and a fracture of the strip occurred approximately 4-cm from the upper electrode. As there was no visual change in specimen surface appearance, the strip was cut to a 18-cm length and reinstrumented with thermocouples for a new central measuring area.

Measured values of ϵ_λ at temperatures of 1100° and 1300° K are shown in figures 28 and 29 in comparison with the NBS spectral data for these temperatures. Solid and broken curves represent average and standard deviation values supplied by NBS. The measured values of ϵ_λ are typically 0.03 to 0.05 higher than the upper deviation limit. Temperature measurement error must be considered as one possibility for this behavior; i.e., temperature data from both thermocouple and optical pyrometer readings are lower than the true temperature. A comparison of thermocouple and pyrometer brightness temperature yields values of ϵ_λ at 0.65 μm of between 0.86 and 0.89 for the 1100° and 1300° K temperatures. These values are consistent with room temperature values of 0.84 computed from spectral reflectance measurements made on the strip prior to testing. The spectral emittance data of figures 28 and 29 were computed from pyrometer readings assuming ϵ_λ = 0.84 at 0.65 μm, and the use of the higher value of ϵ_λ would result in a slightly lower temperature and higher emittance.
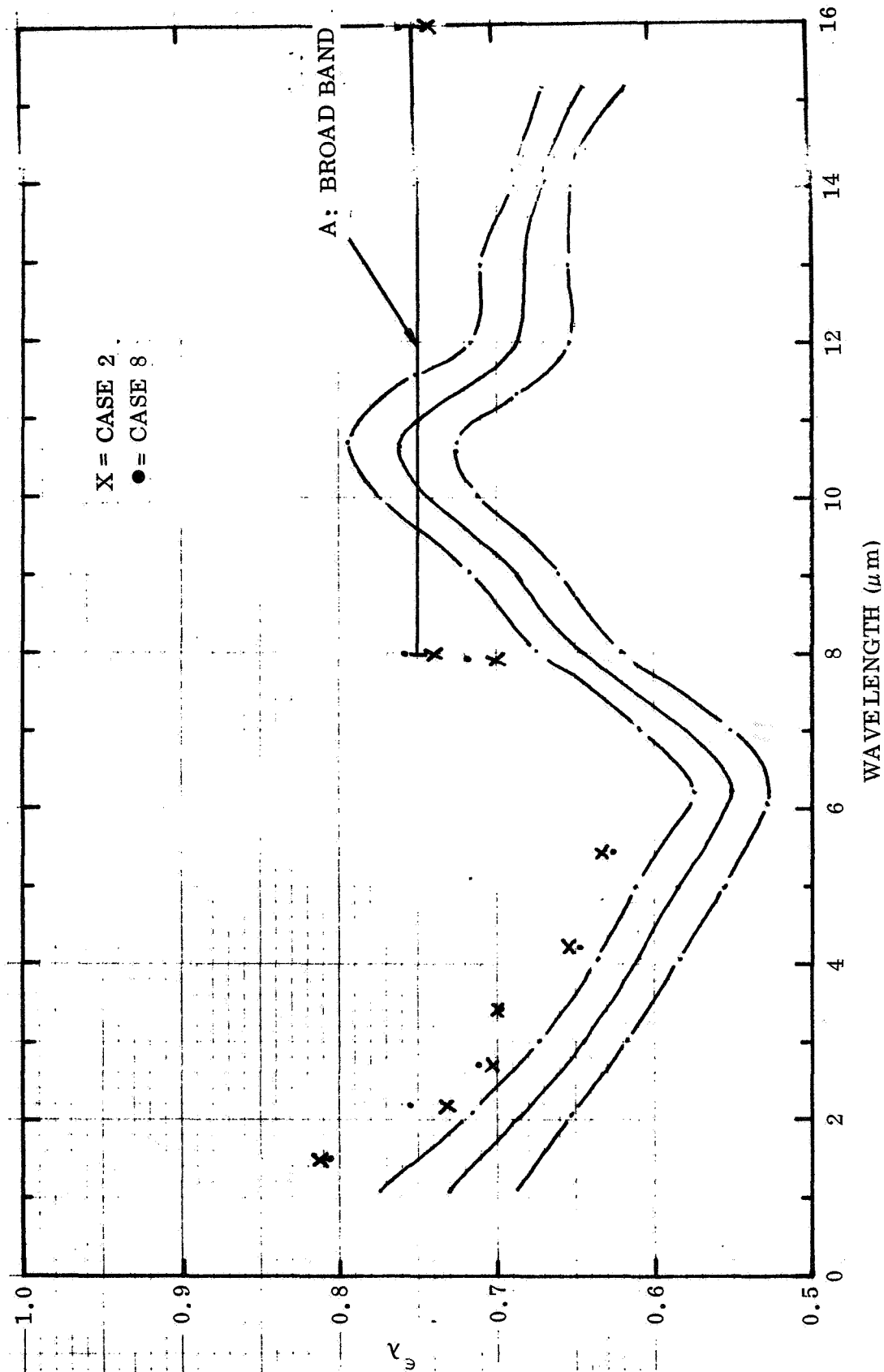
Fig. 28 Spectral Emittance Data for NBS Oxidized Kanthal Emittance
Standard Measured in Air, T = 1100°K
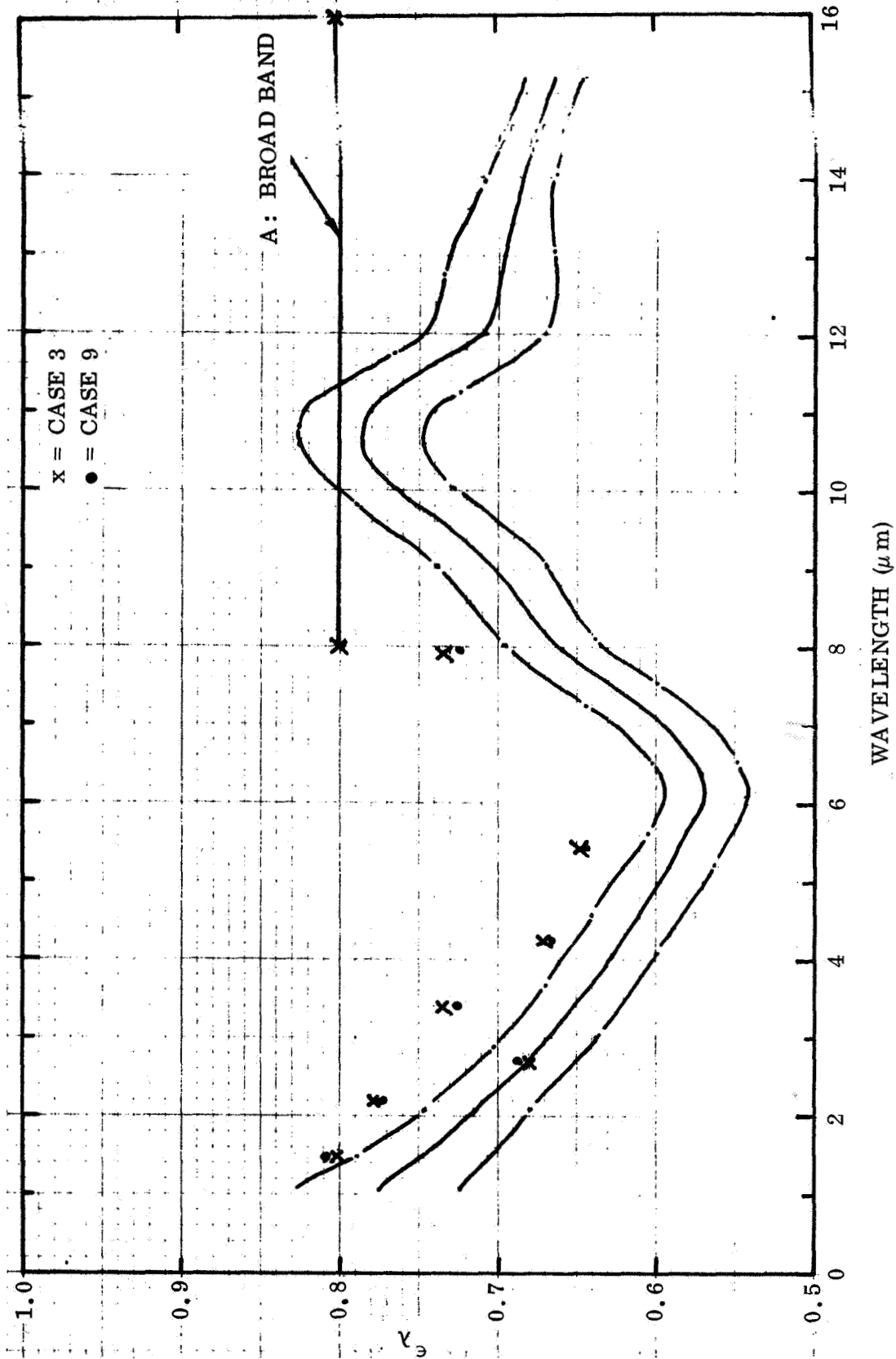
Fig. 29 Spectral Emittance Data for NBS Oxidized Kanthal Emittance Standard Measured in Air, T = 1300°K

A second consideration regarding temperature measurement error is to determine the temperature that would be required to adjust the measured values to agree with the NBS data. For example, at 2.2 μm and 1100°K it would be necessary to use a temperature of 1105°K to obtain the NBS value from the radiometer signal, whereas, the temperature used to reduce the signal data to ϵ_λ was 1086°K. This difference of 19°K between brightness and true temperature would require ϵ_λ = 0.56 at 0.65 μm which seems to be an unreasonably low value for a temperature of 1100°K. In a further attempt to resolve the differences in spectral emittance room temperature spectral reflectance measurements were performed on a 1.9-cm square segment taken from one end of the standard strip. Spectral emittance data computed from the reflectance values are shown in figure 30 together with the NBS data. The NBS values show a slight increase in ϵ_λ with increasing temperature and yet the room temperature reflectance measurements give ϵ_λ values greater than the elevated temperature NBS data in the 2 to 6.5 μm region. The 300°K reflectance data also is in good agreement with the data measured in this program. Considering the possible temperature measurement errors and the spectral reflectance data it appears that the spectral emittance of the standard strip specimen is in fact higher than the NBS values. The possibility of contamination of the surface during instrumentation and installation in the apparatus must, of course, be considered, but no evidence to support this was found.

Total normal emittance values calculated from the radiometer data at four temperatures, are shown in Table 9 together with total values computed from the NBS spectral data using average values. The standard deviations would add ±0.02 to 0.03 to these values. Total hemispherical emittances were determined calorimetrically at three lower temperatures under vacuum conditions, and these values are in reasonable agreement with the total normal data. The higher measured emittances again do not appear to be due to temperature measurement errors but rather are representative of the actual specimen which was measured in this program, ϵ_{TN} being 0.05 to 0.07 greater than computed from the NBS spectral data.

On the basis of the results obtained on the Platinum-Rhodium specimen the values of ϵ_λ and ϵ_{TN} determined in the test apparatus should be within 0.02 to 0.03 of the true surface properties.

6-16
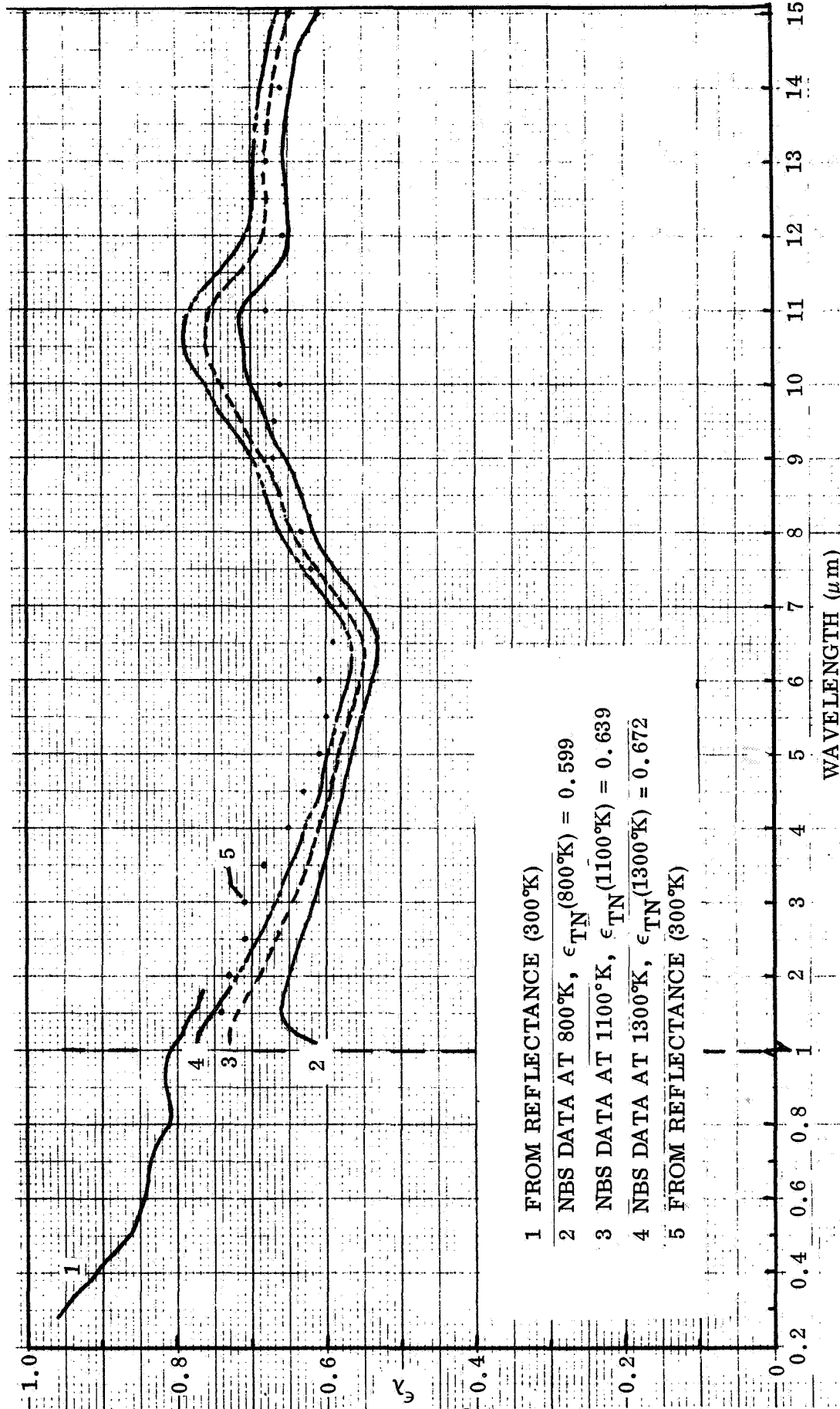
Fig. 30 Spectral Emittance of NBS Oxidized Kanthal Standard

1 FROM REFLECTANCE (300°K)

2 NBS DATA AT 800°K, $\epsilon_{TN}(800°K) = 0.599$

3 NBS DATA AT 1100°K, $\epsilon_{TN}(1100°K) = 0.639$

4 NBS DATA AT 1300°K, $\epsilon_{TN}(1300°K) = 0.672$

5 FROM REFLECTANCE (300°K)

WAVELENGTH (μm)

LOCKHEED PALO ALTO RESEARCH LABORATORY

L O C K H E E D   M I S S I L E S   &   S P A C E   C O M P A N Y,   I N C.

A   S U B S I D I A R Y   O F   L O C K H E E D   A I R C R A F T   C O R P O R A T I O N

Table 9

TOTAL EMITTANCE OF NBS OXIDIZED KANTHAL STANDARD (SRM 1427)
AS A FUNCTION OF TEMPERATURE

Test Temperature (°K)	Measured Emittance		Total Normal Emittance Calculated from NBS Spectral Data	Remarks
	Total Normal	Total Hemispherical		
645	0.648	0.667	–	In vacuum
805	0.661	0.636	$\left\{ 0.60 \right.$	In vacuum
797	0.697	–		Air
1100	0.731	–	$\left\{ 0.64 \right.$	Air
1086	0.728	0.711		Vacuum
1093	0.723	–		Air
1320	0.724	–	$\left\{ 0.67 \right.$	Air
1296	0.723	–		Air

Section 7

SAMPLE PREPARATION AND CHARACTERIZATION

The high-temperature/high-strength alloys selected for testing in this program are listed in Table 10 along with pertinent information provided by the supplier on the as-received condition of each alloy. Samples of the two columbium alloys were coated with commercial, oxidation-resistant coatings. Oxidation procedures for the René 41, HS-188 and TD Ni Cr alloys were selected, and oxidized test strips were prepared for the emittance-stability tests performed in this program. The samples of these alloys were oxidized in the laboratory using a high temperature tubular furnace in conjunction with an airdrying system. A description of the furnace and of the oxidation exposures and results for each alloy is given in the following subsections.

7.1 OXIDATION APPARATUS

A schematic of the high temperature furnace and air-drying system is shown in figure 31. Pressurized air was regulated to a nominal flow rate of 7 CFH through the system as indicated by a gas flow meter. Excess moisture was removed from the air by passing it first through a cooled (dry-ice/alcohol) flask and then through a 30-cm column of molecular-sieve drying agent. The dry air was then introduced into a 92-cm long by 4.15-cm I.D. quartz tube which ran through the center of the furnace and extended 15-cm from both ends of the furnace. This tube served as a clean housing for each sample during its oxidation exposure and was plugged at each end with unfired lava plugs with air feed-through tubes. A wad of glass wood was placed in the air-entry end of the tube to aid in diffusing the air flow through the tube.

Samples in the form of strips or disks (for control evaluations were introduced into the tube by removing the air vent plug, sliding the samples to the hot central region of the furnace with a quartz rod, and then replacing the vent plug. Disk samples were supported horizontally on a small boat fabricated of quartz, high purity alumina and

7-1

Table 10

HIGH TEMPERATURE ALLOYS FOR EMITTANCE TESTS

Alloy	Supplier	Heat No.	Strip Dimensions	As Received Condition
Haynes Alloy R–41 (René 41)	Stellite Division Cabot Corp.	2490–1–8218	30.5x2.74x0.102 cm	Smooth dull grey surface.
Haynes Alloy No. 188 (HS–188)	Stellite Division Cabot Corp.	1880–0–0159	30.5x2.62x0.104 cm	Smooth bright surface. Annealed and cooled in dry hydrogen atmosphere.
TD Ni Cr Alloy (Ni–20% Cr–2% ThO_2)	Fansteel Inc.	TC 3277	30.5x2.70x0.109 cm	Bright clean surface. Rolling direction $\perp$ to length of strips. Stress relieved.
Columbium Alloy Cb–752 (Cb–9.5% W–2.6% Zr)	Teledyne Wah Chang Albany	770036	30.5x2.56x0.104 cm	Smooth clean surface. Annealed. 100% recrystallized. Avg. ASTM. Grain size No. 8
Columbium Alloy Cb–129Y (Cb–9% W–10% Hf–0.1%Y)	Teledyne Wah Chang Albany	572068	30.5x2.56x0.104 cm	Smooth, clean surface. Annealed. 100% recrystallized. Avg. ASTM. Grain size No. 9
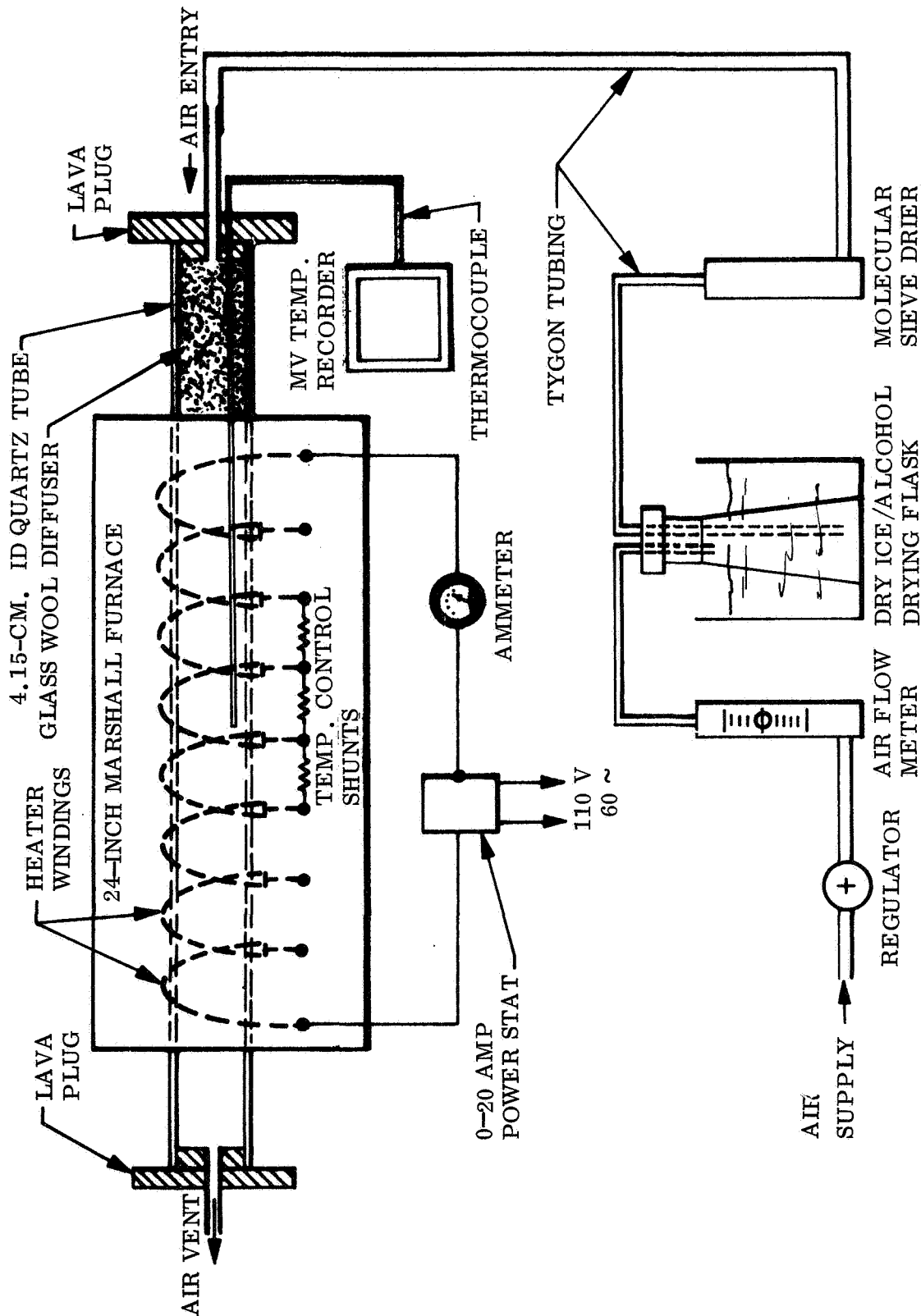
Fig. 31 Schematic of Sample Oxidation Apparatus

platinum. Strip samples were supported horizontally by tying each end of the strip to a small quartz boat with platinum wire. These supports were of such size as to position the top surface of each sample near the longitudinal center-line of the furnace. At the end of each oxidation exposure, the air-vent plug was removed and the samples were withdrawn from the furnace, and allowed to cool in ambient room air.

The alumina tube furnace had heater windings of Kanthal A-1 with a maximum temperature rating of 1590° K. External shunt posts along the length of the furnace winding were used for control of the temperature gradient along the length of the furnace tube. Electrical power to the furnace was controlled manually with a 0 to 20 ampere Powerstat and an ammeter in series with the heater windings. Furnace temperatures were monitored with an Pt/Pt-13% Rh thermocouple which could be positioned anywhere along the length of the furnace inside the quartz support tube. The thermocouple leads were protected with alumina tubing to facilitate sliding the thermocouple through a small hole in the lava plug at the air-entry end of the furnace. The normal location of the thermocouple was at the center of the furnace, and the temperature at this point was controlled to the nominal oxidation temperature used for each sample. This thermocouple was also used to measure gradients along the furnace tube length. Temperature-time records for each sample exposure were recorded with a calibrated millivolt strip chart recorder.

7.2 OXIDATION PROCEDURES

For each operational temperature the furnace was brought to steady state and maintained there for at least 1 hour before starting a sample oxidation exposure. During this period the proper input power (i.e., current) level was determined and only minor adjustments were required thereafter to maintain a constant furnace temperature. The introduction of a strip sample into the furnace resulted in a short-duration temperature drop of from 25° to 50° K at the center of the furnace, but the steady-state condition was recovered within a 3 to 5 minute period.

The 30.5 cm long strip samples were oxidized one at a time due to the limited working volume within the furnace, but the 2.54-cm diameter disk samples were oxidized in

batches of four or five. Disk samples were used to evaluate different exposure-time effects on emittance and to determine the sample-to-sample emittance variations for a particular exposure condition. The disks were punched from the same sheet of material that the strips were cut from, and after oxidation are assumed to be representative of the center 15 to 20-cm region of each strip sample with the same oxidation exposure.

Exposure temperatures, time durations, and atmosphere conditions for each alloy were selected on the basis of recommendations from MSFC which were as follows:

- For René 41: a) Resolution heat treat at 1393° K (2050° F) for 1/2 hr. in a controlled atmosphere of argon or vacuum, then cool rapidly. b) Age at 1170° K (1650° F) for 2 hrs. in a controlled argon or vacuum atmosphere, then c) Oxidize at 1170° K for 2 hours in air.

- For HS-188: Oxidize at 1310° K (1900° F) for a short time in dry air.

- For Td Ni Cr: Oxidize at 1477° K (2200° F) for 1/2 to 1 hr. in air.

Since specific oxidation exposure times were not specified by MSFC for the HS-188 and TD Ni Cr alloys, times of 1, 2 and 3 hours were evaluated for the HS-188 alloy and times of 1/2, 1 and 1-1/2 hrs were evaluated for the TD Ni Cr alloy. On the basis of spectral reflectance results for disk samples with these exposures, the 3 hr. exposure time was selected for the HS-188 alloy and a 1 hr. exposure time was selected for the TD Ni Cr alloy.

Prior to oxidization the samples were cleaned using a procedure which would not alter the surface condition so the samples would be representative of the as-received condition of each alloy. The use of strong pickling acids or caustic washes was avoided so as to not alter the surface chemistry of the materials. Also, the use of surface roughening methods to improve the initial emittance characteristics of the materials was not investigated. Before oxidation, each sample was lightly scrubbed with steel wool, Boraxo and warm water, rinsed, and then washed with ethyl alcohol. This procedure resulted in a visually clean uniform surface for each sample.

Resolution heat treatment of the René 41 samples at 1393° K was accomplished using the same system as described in figure 31 with the exception that argon instead of air was connected to the inlet regulator. The argon flow rate was maintained at 5 CHF during this treatment and after 1/2 hr., the samples were 'quick-cooled' in air by rapidly removing them from the furnace. This treatment resulted in the formation of a light oxide film on the surface of the samples which was strongly adherent to the substrate. No attempt was made to reclean the surface before the aging and oxidation exposure. No pre-oxidation heat treatments were given to the HS-188 and TD Ni Cr alloys except those performed by the suppliers and noted in Table 10.

Typical temperature gradients along the length of the furnace for each oxidation exposure temperature are shown in figure 32. These temperature differences were determined from thermocouple readings of the temperature distribution inside the quartz support tube during actual sample oxidation exposures. Sample locations within the furnace are also shown on this figure. The sample strips were positioned 2.5 to 5.0 cm towards the air-vent end of the furnace because the air flow shifted the maximum temperature region inside the quartz support tube towards that end. The figure shows that temperatures were uniform to within ±150° K of the nominal control temperature over the central 15-cm region of each strip sample. The circled numbers for each sample location indicate areas where total reflectance measurements were made after the sample was oxidized to indicate the uniformity of the oxide coating from end-to-end and on both sides of each sample.

7.3 RESULTS

Five test strip samples and three witness disk samples of each alloy were prepared by the methods described in the preceding subsection. The disk samples were used to obtain spectral reflectance measurements indicative of the initial emittance characteristics of each sample. The visual appearances of the oxidized strip samples were as follows:

- René 41: Uniform smooth, dull-slate-grey colored oxide on both sides and from end-to-end with a slight blush of lighter, cream-colored oxide at each end.

7-6
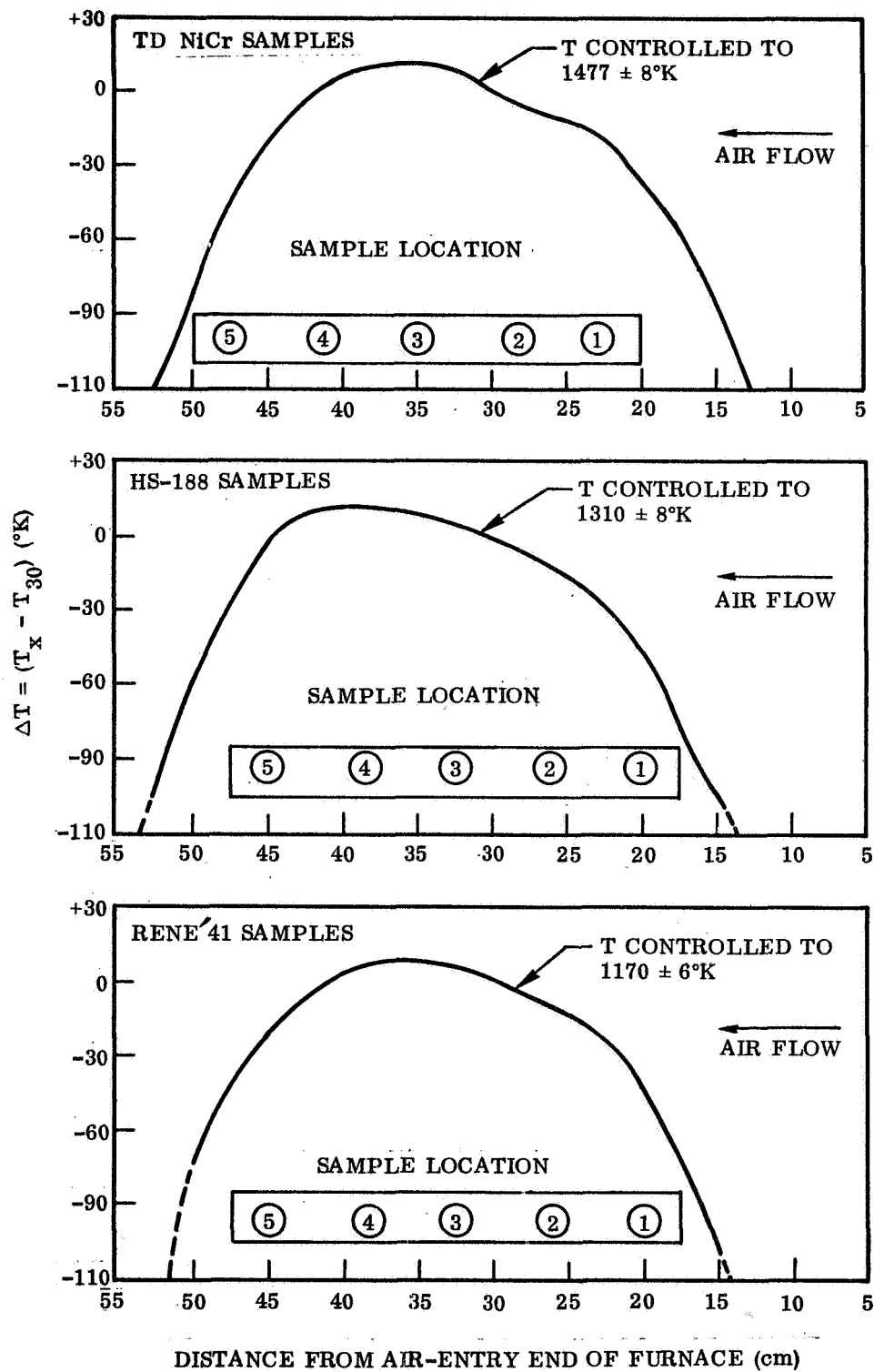
Fig. 32 Furnace Temperature Gradients During Oxidation of Test-Strip Samples

7-7

- HS-188: Uniform smooth, dark-blue-grey colored oxide on both sides and from end-to-end

- TD Ni Cr: Uniform smooth, dark-blue-grey colored oxide on both sides and from end-to-end with a few, randomly scattered black specks on the order of 0.5 mm in diameter.

All of the oxides appear to be tough (i.e., abrasion resistant) and strongly adherent to the substrate metal.

Total room-temperature emittance values for the oxidized strip samples at the five location points indicated previously in figure 32 are shown in Table 11. These values were determined from total reflectance measurements with a Gier-Dunkle Model DB-100 reflectometer. The emittance values are the average at each location for the five oxidized sample strips of each alloy. The variability values indicate the range between maximum and minimum readings obtained at that location for each set of five samples. These measurements show that the TD Ni Cr samples had the most uniform and least variable emittance, and the emittance of the René 41 samples was the least uniform with the highest variability between samples.

Results of room temperature spectral reflectance measurements for the oxidized disk samples are shown in figures 33 through 37. These measurements were made with a Cary Model 14 spectroreflectometer at wavelengths between 0.28 and 1.8 μm; and with a Gier-Dunkle Model HC-300 heated cavity reflectometer at wavelengths between 2 and 24 μm. Predicted values of total normal emittance at five temperatures up to 1350° K, determined by numerical integration of the room temperature spectral curves shown in the figures, are listed in Table 12. These predicted values are based on the assumption that the spectral emittance characteristics of the sample surface do not change with temperature. For these materials this assumption should be approximately correct up to the temperatures at which the oxides were formed, and the values are probably somewhat low since ϵ_λ values for most oxides tend to increase slightly with increasing temperature. The above remarks apply only to the initial characteristics of the samples and become invalid as soon as changes in the thickness or chemical composition of the surface oxide occur.

7-8

Table 11

VARIATIONS IN ROOM TEMPERATURE TOTAL EMITTANCE
FOR OXIDIZED SAMPLE STRIPS

Sample/Side	Location Point Along Strip*				
	①	②	③	④	⑤
René 41					
Top	0.58 ± .08	0.59 ± .04	0.62 ± .03	0.56 ± .05	0.54 ± .04
Bottom	0.54 ± .05	0.56 ± .04	0.57 ± .04	0.56 ± .04	0.53 ± .05
HS-188					
Top	0.37 ± .03	0.45 ± .02	0.47 ± .01	0.47 ± .02	0.44 ± .02
Bottom	0.38 ± .02	0.45 ± .02	0.47 ± .01	0.47 ± .01	0.44 ± .03
TD Ni Cr					
Top	0.43 ± .03	0.42 ± .01	0.42 ± .01	0.42 ± .01	0.43 ± .01
Bottom	0.43 ± .01	0.43 ± .01	0.43 ± .01	0.43 ± .01	0.44 ± .01

*See Figure 32

Table 12

PREDICTED* TOTAL NORMAL EMITTANCE VALUES AT
FIVE TEMPERATURES FOR OXIDIZED RENÉ 41,
HS-188 AND TD Ni Cr SAMPLES

Alloy	Oxidation Exposure	ϵ_{TN}*				
		T = 300° K	T = 533° K	T = 810° K	T = 1090° K	T = 1350° K
René 41	As Received	0.26	0.30	0.34	0.36	0.39
''	1170° K/2 hrs	0.54	0.64	0.70	0.74	0.77
HS-188	As Received	0.10	0.13	0.16	0.18	0.20
''	1310° K/1 hr	0.30	0.42	0.49	0.53	0.57
''	1310° K/2 hrs	0.46	0.49	0.55	0.60	0.65
''	1310° K/3 hrs	0.54	0.55	0.60	0.64	0.68
TD Ni Cr	As Received	0.13	0.16	0.19	0.21	0.23
''	1477° K/1/2 hr	0.46	0.45	0.51	0.58	0.63
''	1477° K/1 hr	0.48	0.47	0.54	0.61	0.67
''	1477° K/1.5 hrs	0.49	0.48	0.55	0.62	0.67

*Calculated from room temperature spectral reflectance data.
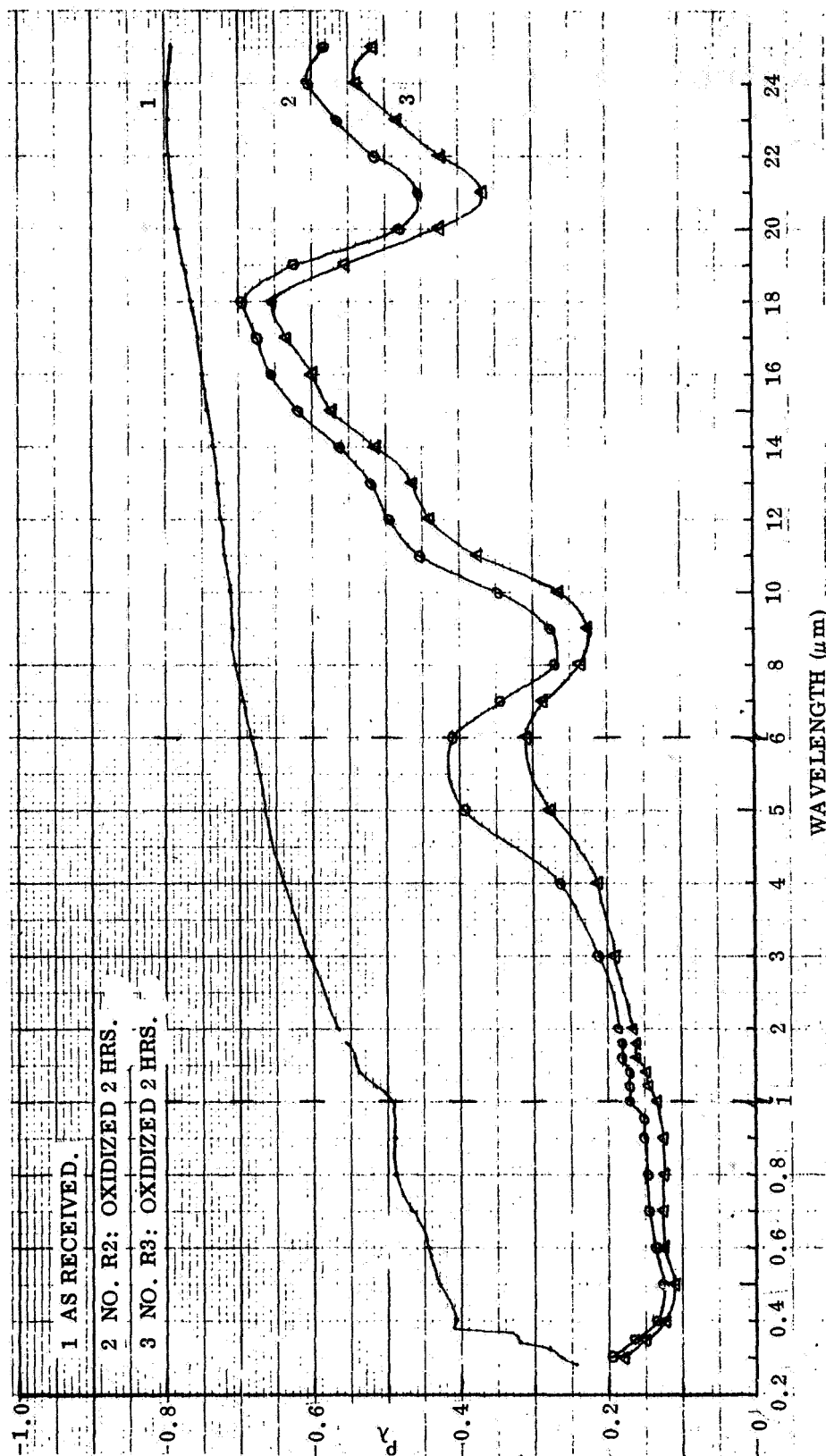
Fig. 33 Room Temperature Spectral Reflectance of as Received and Oxidized (1170°K) Rene´ 41 Samples

LOCKHEED PALO ALTO RESEARCH LABORATORY

LOCKHEED   MISSILES   &   SPACE   COMPANY,   INC.
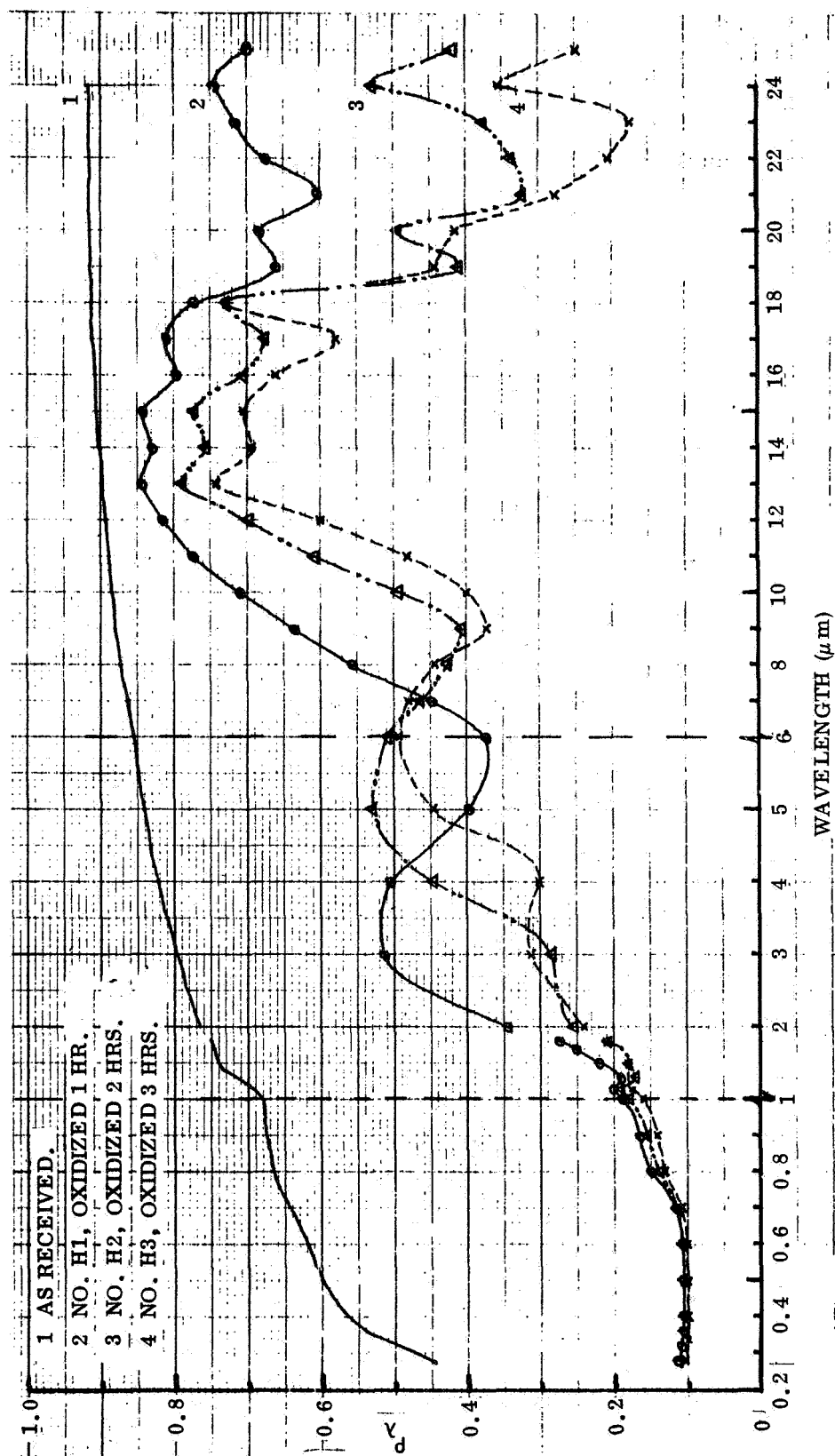
Fig. 34 Room Temperature Spectral Reflectance of as Received and
Oxidized (1310°K) HS–188 Samples
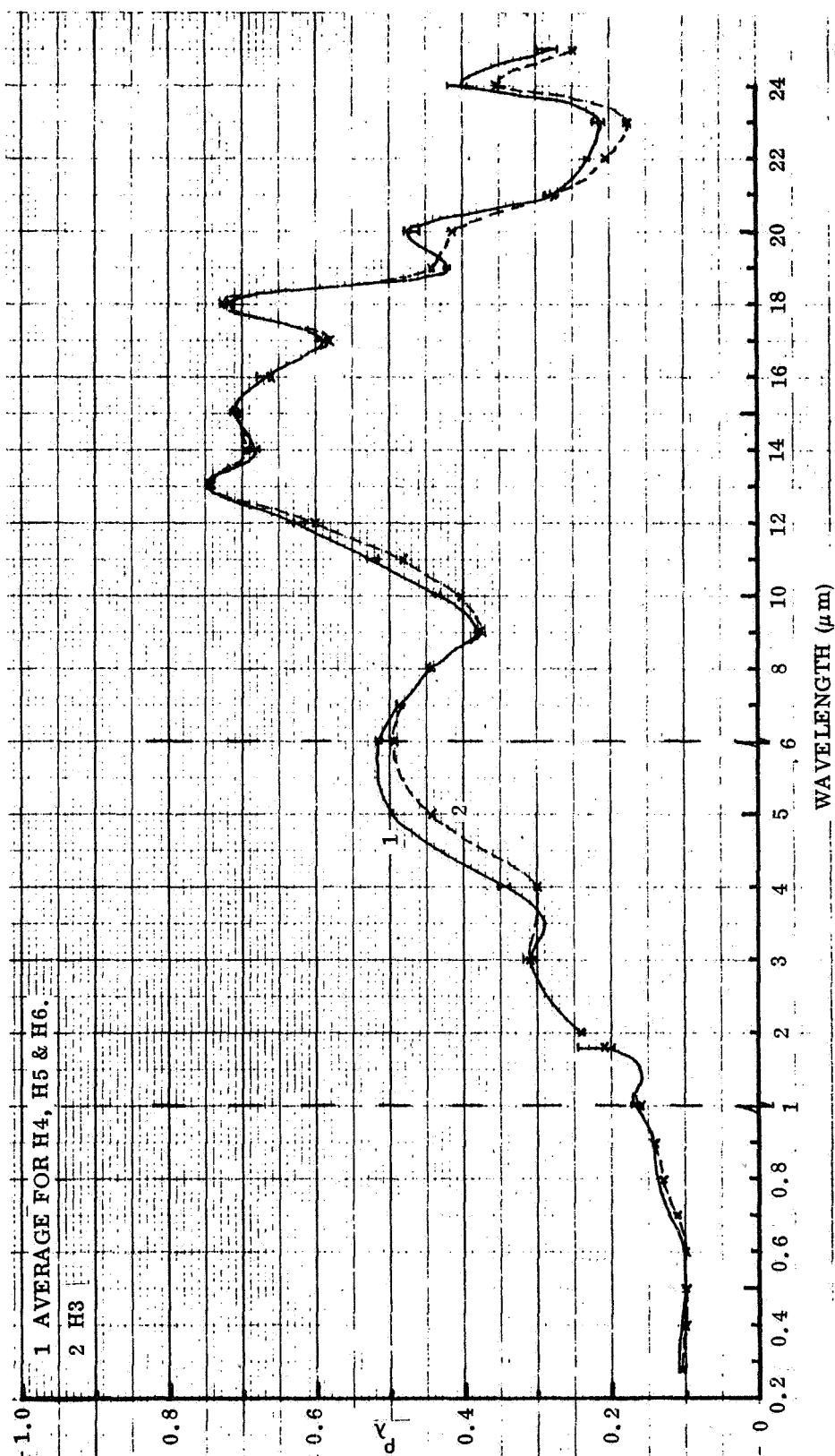
Fig. 35 Variations in Spectral Reflectance for Four HS-188 Samples Oxidized for 3 Hours at 1310°K
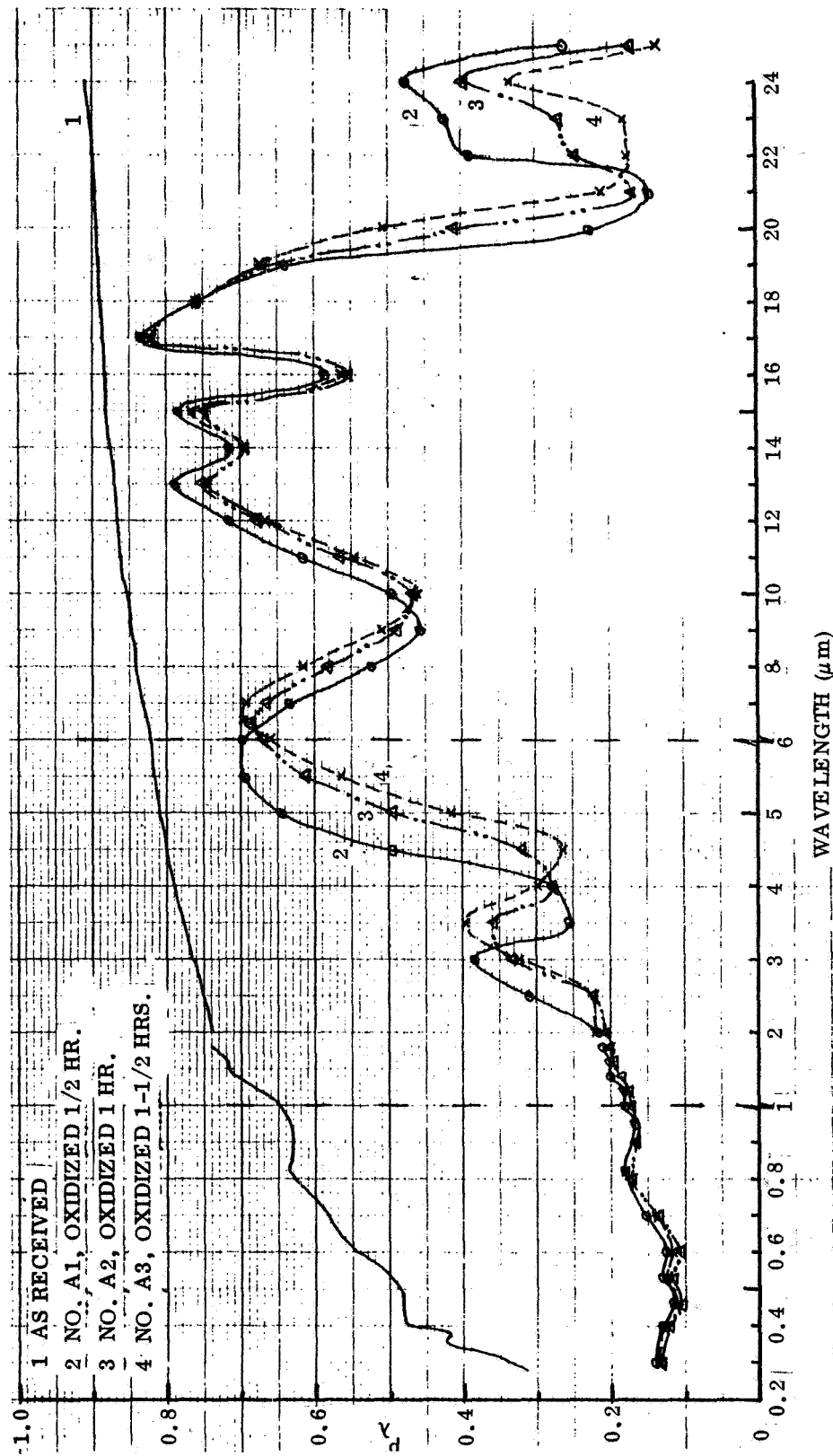
Fig. 36 Room Temperature Spectral Reflectance of as Received and Oxidized TD Ni Cr Samples (1477°K)

1 AS RECEIVED
2 NO. A1, OXIDIZED 1/2 HR.
3 NO. A2, OXIDIZED 1 HR.
4 NO. A3, OXIDIZED 1-1/2 HRS.

WAVELENGTH (μm)

7-13
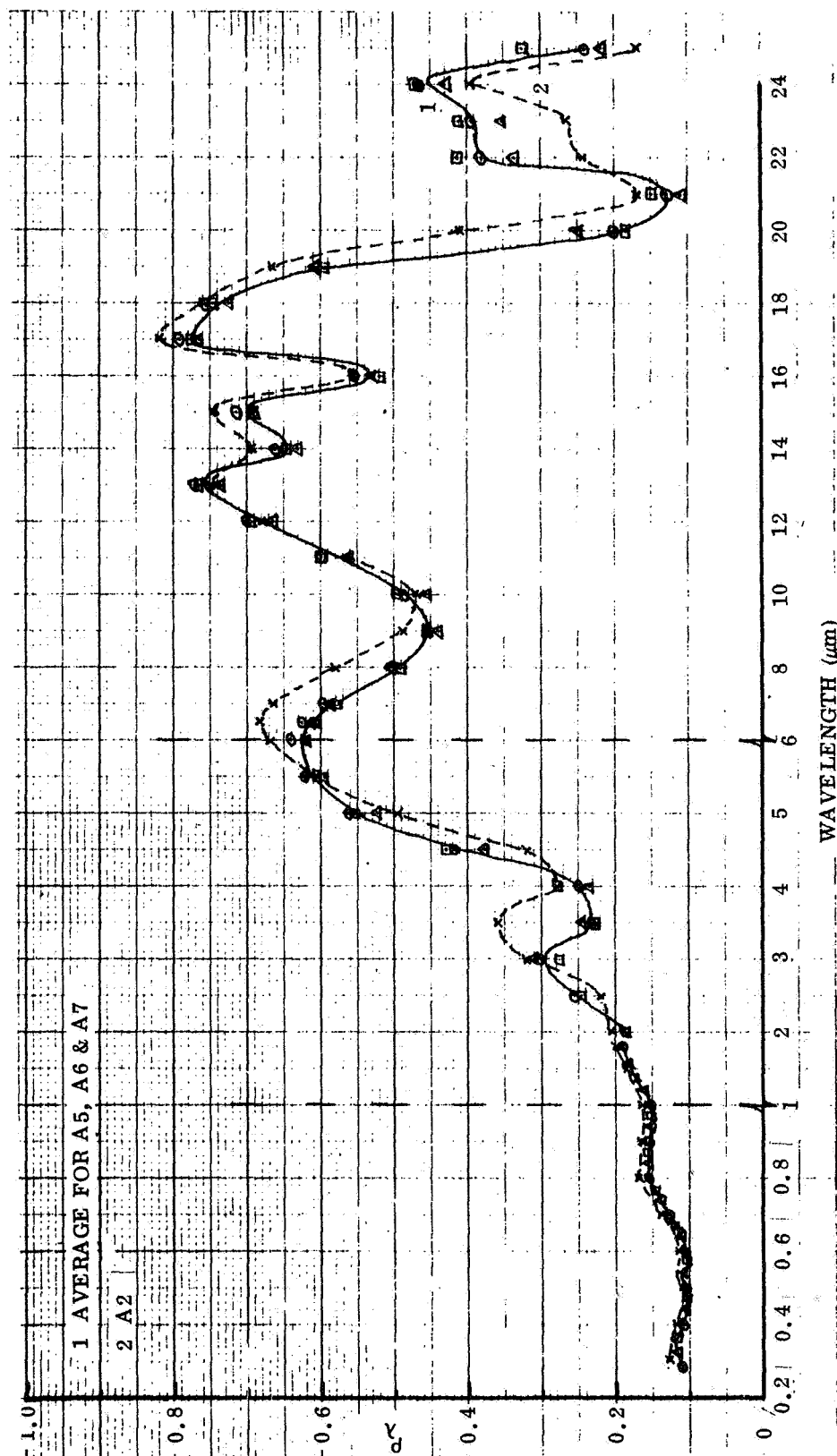
Fig. 37 Variations in Spectral Reflectance for Four TD Ni Cr Samples Oxidized for 1 Hour at 1477°K

Figure 33 shows the variations in spectral emittance obtained for two of the heat treated, aged and oxidized René 41 disk samples. The emittance characteristics of the unoxidized as received material is also shown for comparison. The total normal emittance values given in Table 12 for the oxidizied René 41 samples are average values for the two curves shown in figure 33. With these spectral characteristics, the total emittance of the oxidized René 41 samples should increase with temperature from about 0.56 at room temperature to about 0.75 at 1150° K.

Figure 34 shows the spectral reflectance characteristics of the HS-188 disk samples that were oxidized for 1, 2 and 3 hours, and of the as received material. The progression of the reflectance peak that occurs between 3.5 μm and 6 μm towards longer wavelength with increasing exposure time indicates that the oxide coatings are probably not thick enough to be optically opaque at these wavelengths. On the basis of these measurements, the oxidation exposure time of 3 hrs. was selected for this alloy in order to obtain maximum initial emittance characteristics along with a more stable, optically thick oxide layer.

The curves in figure 35 are for four individual HS-188 disk samples oxidized for 3 hrs. at 1310° K and indicate the good repeatability of emittance characteristics that was obtained for these samples. The solid curve is a plot of the average ϵ_λ values for three samples oxidized on the same day, and the vertical bars through this curve indicate the maximum and minimum values obtained. The dashed curve is for the first disk sample oxidized for 3 hrs. which was prepared several weeks earlier. The differences are minor and can be attributed to slightly different furnace conditions. On the basis of these spectral characteristics, the total emittance of the oxidized HS-188 strip samples should increase with temperature from 0.48 at room temperature to 0.68 at 1350° K.

Figure 36 shows the spectral reflectance characteristics of the TD Ni Cr disk samples that were oxidized for 1/2, 1 and 1-1/2 hrs., and of the as-received material. The change in location of the major reflectance peak occurring around 6 μm again suggests that these oxide film thicknesses are not optically opaque at this wavelength; but the

effect of increased exposure from 1 to 1-1/2 hrs. on the total emittance character-
istics of the samples (see Table 12) is small, therefore an oxidation exposure time
of 1 hr. was selected for this alloy.

The curves in figure 37 are for four separate TD Ni Cr disk samples oxidized for 1 hr.
at 1477° K and indicate the good repeatability of emittance characteristics that was
obtained for these samples. The solid curves are for three samples that were oxidized
on the same day and the dashed curve is for the first sample oxidized for 1 hr. which
was prepared several days earlier. As with the HS-188 samples, the differences are
small and can be attributed to slightly different furnace conditions for the oxidation
exposures. With these spectral characteristics, the total emittance of the oxidized
TD Ni Cr samples should increase with temperature from 0.44 at room temperature
to about 0.70 at 1480° K.

7.4 COATED Cb ALLOYS

Samples of the two columbium alloys listed in Table 10 were coated with two com-
mercially available, oxidation resistant coatings, (specified by MSFC), for the
exposure tests conducted in this study. The Cb-752 alloy samples were coated by the
HiTemCo Company, Hicksville, N.Y. with a standard R512E coating; and the Cb-129Y
alloy samples were coated by the VacHyde Processing Corp., Los Angeles, Calif.,
with a VH-101 (formerly VH-109) silicide coating.

Before coating, some of the as-received strips of each alloy, which were 30.5 cm
long by 2.56-cm wide, were cut in half (lengthwise) and machined to obtain a narrow
test-section area at the center, nominally 1.0-cm wide by 1.8-cm long. These
narrow test strips were used for the M1.1 and M2.1 flow exposure tests. Disk
samples, 2.5-cm in diameter, were also machined from one strip of each alloy so
that room-temperature spectral reflectance measurements for each coating could be
obtained. Holes were drilled in each end and into one edge of each of the strip samples,
as described in Section 8, to facilitate clamping of the samples to the test chamber
electrodes and for attaching thermocouples. After coating, no further machining or
drilling was done which would disturb the integrity of the protective coatings.

7-16

Room-temperature spectral reflectance data for the as-received samples, before and after coating, are shown in figures 38 and 39. The coated-sample measurements were obtained from the disk samples that were coated along with the strip samples. Both coatings are seen to have similar reflectance characteristics in the region $0.3\,\mu m \leq \lambda \leq 25\,\mu m$ and both were observed to have about the same visual appearance, namely a dull, metallic grey color. The room-temperature ϵ_{TN} values indicated by these curves are 0.38 for the Cb-752/R512E samples and 0.27 for the Cb-129Y/VH-101 samples; and ϵ_{TN} for both coatings should increase with increasing temperature. As discussed in Sections 8.4 and 8.5, the total emittance properties for both coatings were observed to increase significantly during the first high-temperature test cycle in air, and considerable changes in the visual appearance of the coatings occurred. Post-exposure test reflectance measurements with the DB-100 Reflectometer indicated the long wavelength ($\lambda > 5\,\mu m$) IR reflectance of both coatings to be significantly lower, (higher emittance), than the initial reflectance characteristics shown in these figures.

7.5 RSI COATINGS

Two different reusable surface insulation (RSI) coatings were tested in this study: a grey coating developed by LMSC for their LI-1500 and LI-900 insulation materials which is designated in this report as LMSC/0042 coating; and a black coating developed by the McDonnell-Douglas Corp. for their HCF insulation material which is designated as MDAC/HCF coating. Samples of the LMSC/0042 coating were obtained from the LMSC RSI-Program division and samples of the MDAC/HCF coating were supplied by MSFC.

The room-temperature spectral reflectance characteristics of the two coatings are shown in figure 40 along with a tabulation of 'predicted' total normal emittance values for temperatures up to 1644° K (2500° F). The predicted ϵ_{TN} values are obtained by integration of the two reflectance curves over the appropriate wavelength region for each temperature. These values should be valid provided that the room-temperature ρ_λ values shown in the figure do not change with temperature, and that the coating materials remain opaque, i.e., that the assumption that $\epsilon_\lambda = 1 - \rho_\lambda$ remains valid.

Details of the sample preparation and testing procedures are discussed in Section 8.6.

7-17
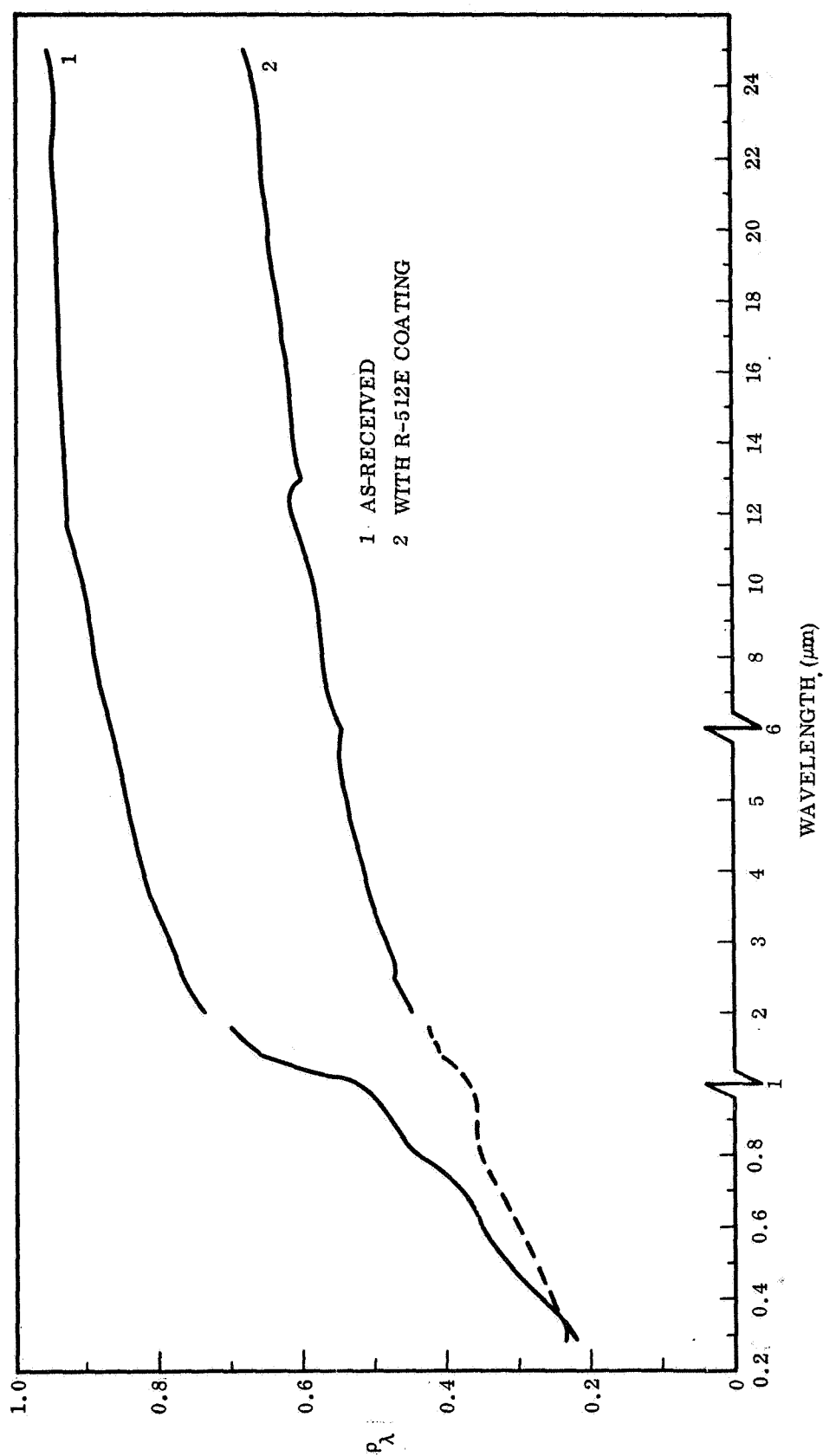
Fig 38 Spectral Reflectance of As–Received and Coated, (R512E), Cb 752

7–18
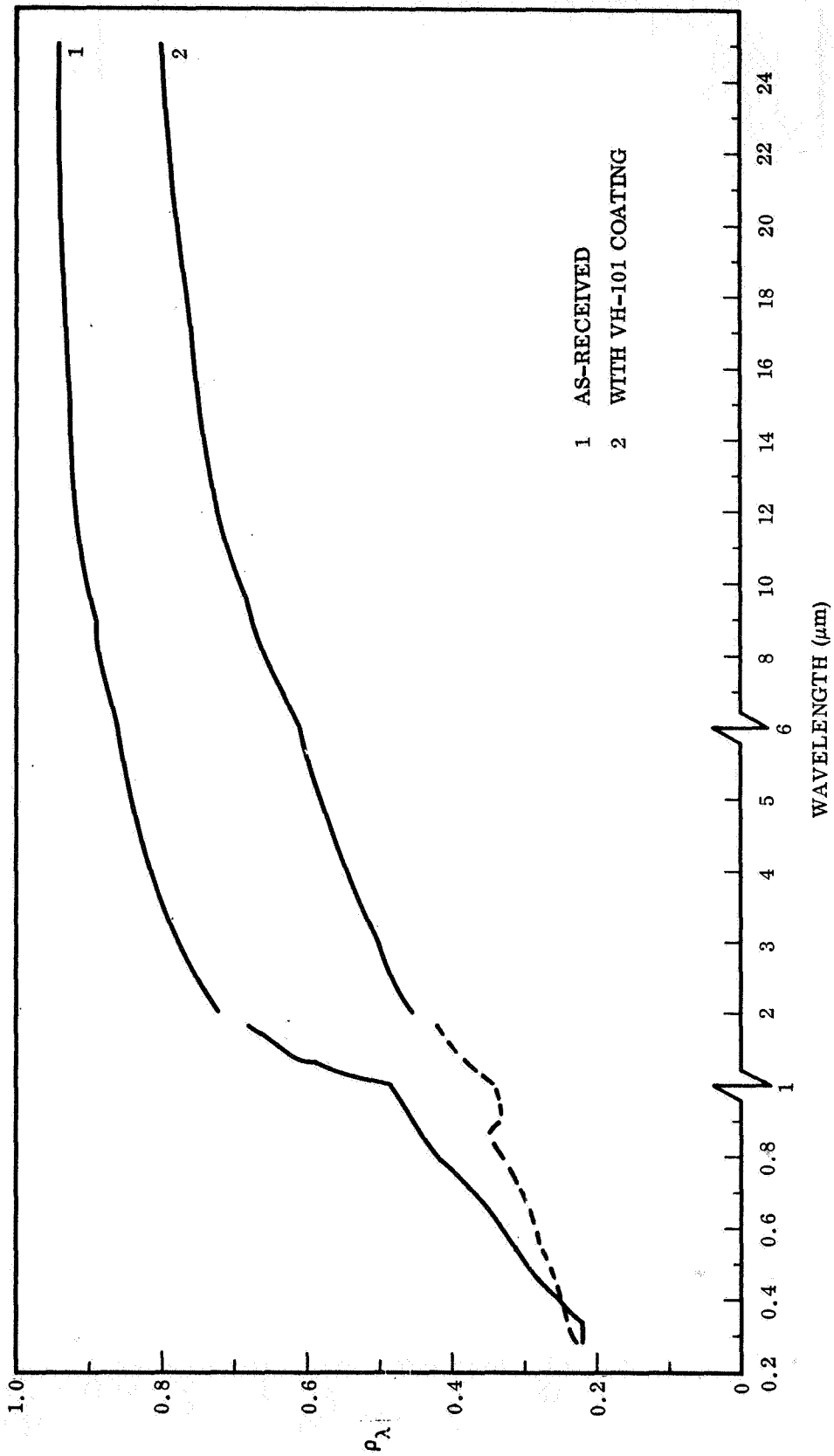
Fig. 39 Spectral Reflectance of As–Received and Coated, (VH–101), Cb 129Y
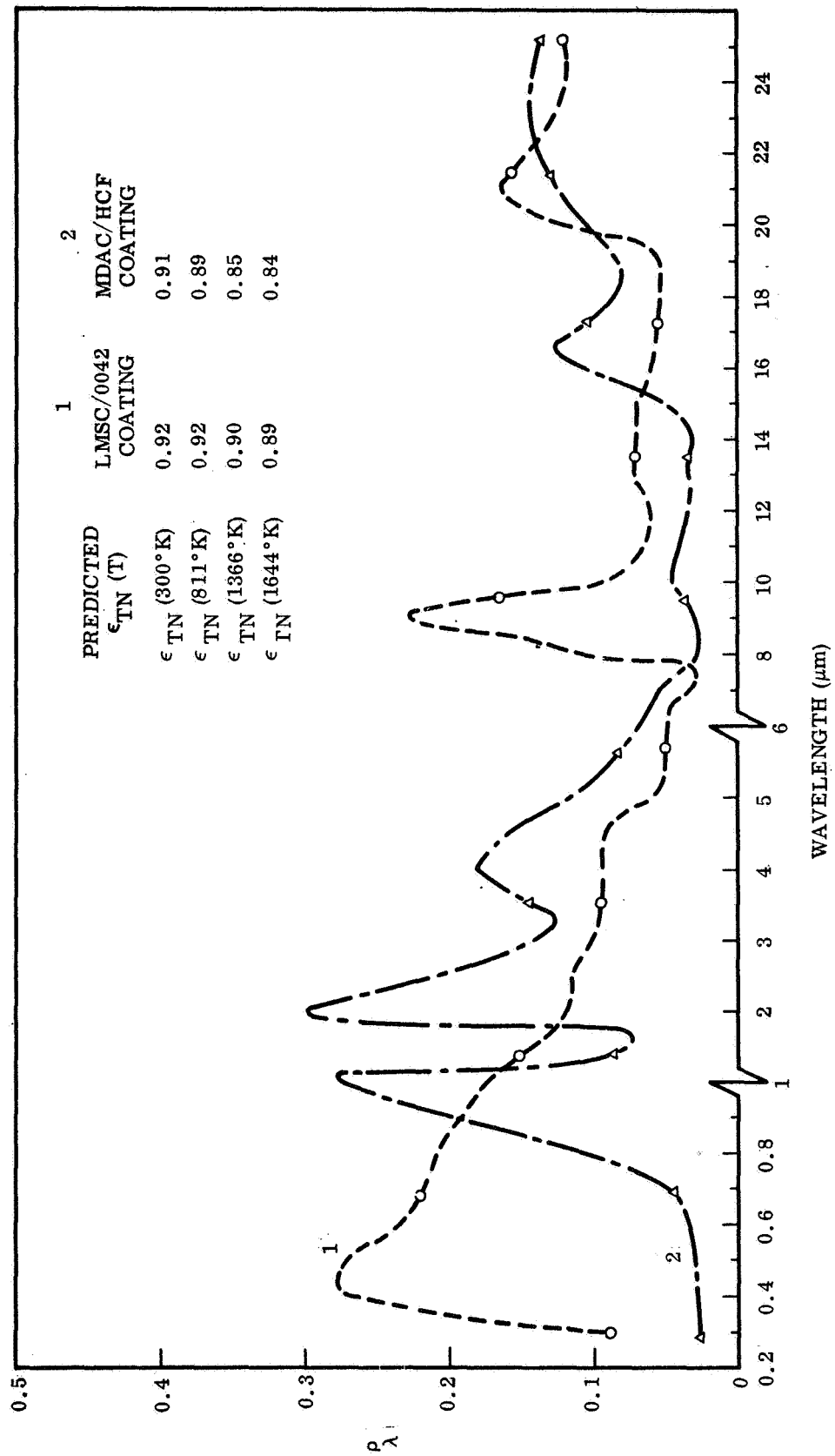
Fig. 40 Spectral Reflectance of As Received RSI Coatings

	1 LMSC/0042 COATING	2 MDAC/HCF COATING
PREDICTED ϵ_{TN} (T)		
ϵ_{TN} (300°K)	0.92	0.91
ϵ_{TN} (811°K)	0.92	0.89
ϵ_{TN} (1366°K)	0.90	0.85
ϵ_{TN} (1644°K)	0.89	0.84

WAVELENGTH (μm)

ρ_λ

Section 8
EXPERIMENTAL RESULTS

8.1 OXIDIZED RENÉ 41

Two series of tests were conducted on oxidized samples of this alloy to determine the emittance characteristics and stability of the material at temperatures up to 1170° K (1650° F) in the static air and Mach 1.1 and 2.1 flow test environments. The purpose of the first series of tests was primarily to evaluate the effects of the different flow-test environments on the temperature of a heated strip sample (No. C2), and the suitability of thermocouple instrumentation for sample temperature measurement and control. The second series of tests consisted of five static air and five Mach 1.1 flow test cycles to evaluate the emittance stability of this material under these test con-ditions. Emittance properties were determined in vacuum before and after each set of cyclic tests, and since no significant changes were observed after the first or second sets of exposures, the Mach 2.1 flow tests were made on the same sample (No. C4).

The initial room-temperature spectral and total emittance characteristics for these samples were inferred from room temperature reflectance measurements of the strip samples and of 2.54-cm diameter witness-disk samples which were prepared under the same conditions as the strip samples (See Section 7.2). Reflectance measurements of the strip samples were also made after testing to determine the changes in sample properties resulting from the test exposures.

A description of each sample and of the instrumentation and test procedures used is given in the following paragraphs before discussing the results.

8.1.1 Sample C2

This sample was 30.5-cm long by 2.64-cm wide by 0.102-cm thick. The center 2.54-cm length of the strip was machined to have a narrowed test-section width of 2.16-cm.

Instrumentation for the sample consisted of five thermocouples, (3-mil bare wire chromel/alumel with a spherical-bead junction formed in an argon-purged arc welder), which were spot welded to the bare metal substrate of the strip at the following locations:

(A) Back surface, on the vertical centerline and 0.25-cm above the horizontal centerline

(B) Same as above, but 0.25-cm below the horizontal centerline.

(1) Right edge (facing the front surface), on the horizontal centerline.

(2) Right edge, 0.63-cm below (1).

(3) Right edge, 1.9-cm above (1), and 0.63-cm above the top of the narrowed test section.

During the tests of this sample, thermocouple (A) served as the control thermocouple to the Temperature Controller and the remaining thermocouples served to measure the center and edge temperatures of the sample during the various test exposures.

The first set of tests involved measurements of the temperature gradients and the total normal emittance at four steady-state temperatures, maintained by the temperature controller, during three different Mach 1.1 flow test conditions. The nominal test temperatures were 645° K, 810° K, 980° K and 1140° K. The three flow-test conditions investigated at each temperature were for test chamber pressures (P_c) of 5, 10 and 20 Torr. These conditions correspond to total pressures at the sample surface (P_s) of about 9, 18 and 36 Torr (see discussion of flow calibration in Section 6.1), over a circular area about 3.8-cm in diameter at the sample location; and are somewhat higher than the range of P_s values planned for the regular Mach 1.1 flow test cycles, i.e. 0 to 20 Torr. The steady-state sample emittance characteristics were also measured in vacuum (10^{-2} Torr) at each test-temperature before investigating the flow-test conditions.

Following these tests, a similar set of measurements were made at the same temperatures using the Mach 2.1 flow test nozzle. These tests were made for six different flow-test conditions with test-chamber pressures between 1.3 and 16 Torr. These pressures correspond to total pressures on the sample surface of about 6 to

80 Torr over a circular area about 1.9-cm in diameter at the sample location. The higher P_s test conditions were run to determine the pumping capability limit for the KT-850 pump and are not representative of the normal M2.1 flow test cycle pressures used in this program. For the normal test cycles, the maximum chamber pressure was controlled to 7.2 Torr, corresponding to a total sample pressure of 20 Torr. As before, the steady-state sample emittance characteristics were measured in vacuum at each test temperature before investigating the flow-test conditions.

8.1.2 Sample C4

This sample was 30.5-cm long by 2.64-cm wide by 0.102-cm thick, and was uniform in width from top to bottom. The sample was used to evaluate the emittance stability of the oxidized René 41 surface for five static-air test cycles to a maximum temperature of 1165° K, and subsequently was exposed to five Mach 1.1 flow test cycles and five Mach 2.1 flow test cycles since no apparent changes in emittance were observed.

Initially the sample was tested in vacuum at temperatures of 710° K, 940° K and 1165° K to determine the total hemispherical, total normal and spectral normal emittance characteristics of the sample before the air-exposure tests. For these tests, the center test area of the sample strip was instrumented with six thermocouples which were spot-welded to the bare-metal substrate of the strip at the following locations:

(1) Back surface, on the vertical centerline and 1.27-cm above the horizontal centerline

(2) Same as above but on the horizontal centerline

(3) Same as above, but a 1.27-cm below the horizontal centerline

(4) Back surface, 1.27-cm below the horizontal centerline and halfway between (3) above and the right-hand edge of the strip.

(5) Right hand edge of strip, 1.27-cm above horizontal centerline.

(6) Right hand edge of strip, 1.27-cm below horizontal centerline.

The first four thermocouples were 3-mil diameter, bare wire Pt 6% Rh/Pt 30% Rh and the two edge-located thermocouples were Pt/Pt 13% Rh.

The sample was installed in the test chamber in the same manner as Sample C2 and, for the tests in vacuum, was heated in the same manner using the Temperature Controller with a Pt/Pt 13% Rh control unit in place of the Chromel/Alumel control unit, and the manual ("Set-Point") control mode. For the cyclic tests, a Data-Trak Program Unit with an appropriate program control card was used in conjunction with the temperature control unit to drive the controller to the pre-planned temperature control settings for these test cycles. These instrumentation and test procedures proved to be suitable for all the sample tests except for the second Mach 2.1 test cycle when the control thermocouple open-circuited, (one of the leads separated from the sample), and prematurely shut off the sample heating power. The remaining test cycles were completed using the other Pt/Pt 13% Rh thermocouple as the control.

8.1.3 Results

A photograph of Samples C2 and C4 along with an untested (Reference) strip is shown in figure 41 to illustrate the small changes in visual appearance that occurred as a result of the exposure tests for each sample. The initial appearance of the sample oxide coating was a uniform, smooth, dull-slate-grey color. No change in the appearance of Sample C4 was observed until after the five Mach 2.1 flow test cycles were completed, at which time it was observed that the oxide color was changed slightly in some areas to a light yellow-green, and also that a few small, dark spots had formed on and around the test area region. Similarly, no change in the appearance of Sample C2 was observed after the Mach 1.1 flow test exposures, but the test area appeared slightly lighter grey in color after the Mach 2.1 flow tests. Lighter grey areas also developed on the upper half of both test strips, outside the calibrated-flow test region. Post-test reflectance measurements of the sample test areas showed that ρ_λ in the region 0.3 μm $\lambda \leq$ 1.8 μm did not change by more than 0.02 units from the initial ρ_λ curve for these samples, i.e. the differences were small and about the same as the initial sample-to-sample variations.

8-4
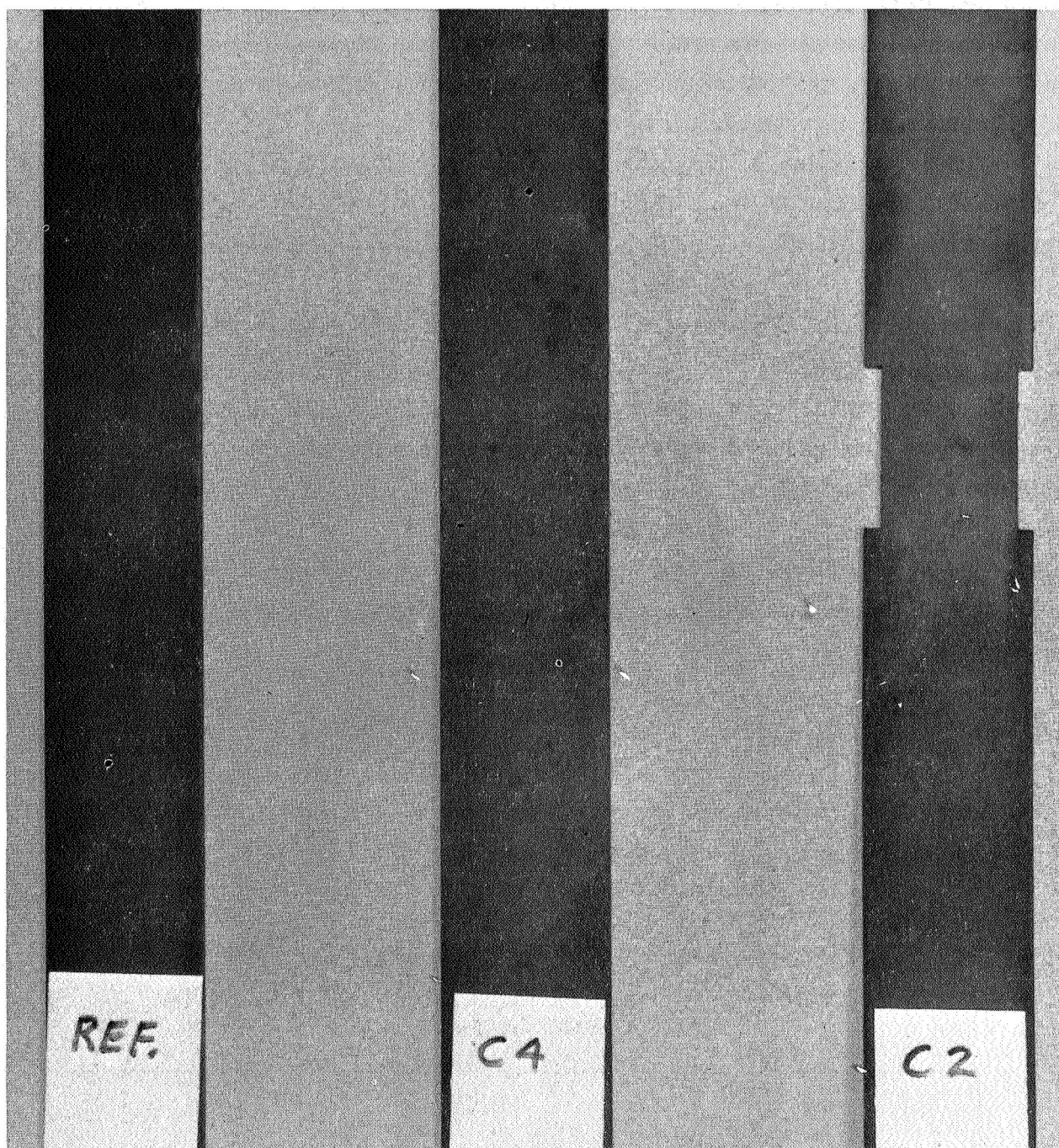
Fig. 41 Visual Appearance of Three Oxidized Rene 41 Samples

8-5

Initial and final room temperature properties determined from the reflectance meas-
urements for these samples are shown in Table 13. Little or no change in α_s or ϵ_λ
at $\lambda = 0.65\,\mu m$, (the optical pyrometer wavelength),,was observed, which agrees
with the visual observation of little change. A small increase in ϵ_{TN} was indicated
by the DB-100 readings, implying that ϵ_λ increased slightly in the long wavelength,
($\lambda > 7\,\mu m$), spectral region. The initial room temperature ϵ_λ characteristics for
this material are shown in figures 43 and 44, but post-test measurements of ρ_λ at
$\lambda > 1.8\,\mu m$ were not made; therefore the nature of the changes in ϵ_λ at these longer
IR wavelengths was not determined.

Results of the two flow effects tests on Sample C2 are summarized in Tables 14 and
15. Table 14 shows some of the sample temperature measurement data that was
obtained at the four different test temperatures. This data illustrates the maximum
effect of the two flow-test environments on the sample temperature gradients from
center-to-edge and from the center-to-upper edge. Data obtained at lower mass-flow
rates (i.e. at lower chamber pressures), showed proportionally less severe tempera-
ture gradients.

The upper set of data obtained in vacuum indicates the actual temperature gradients
that existed in the test section area of this sample with no convective effects on either
the sample surface or on the thermocouple lead wires. The validity of the
thermocouple-indicated gradients was supported by optical pyrometer measurements

Table 13

INITIAL AND FINAL ROOM TEMPERATURE PROPERTIES OF
OXIDIZED RENÉ 41 SAMPLES

	αs	ϵ_λ(Pyrom) $\lambda=0.65\,\mu m$	ϵ_{TN} (DB 100)	ϵ_λ (0.3 $\mu m \leq \lambda \leq 1.8\,\mu m$)	ϵ_λ (2 $\mu m \leq \lambda \leq 16\,\mu m$)
Initial	0.86	0.87	0.59	See Figures 42 and 43	See Figures 42 and 43
Final					
C2	0.86	0.88	0.64	See Figure 42	Not Measured
C4	0.87	0.88	0.62	See Figure 43	Not Measured

Table 14

EFFECT OF MACH 1.1 AND MACH 2.1 FLOW ENVIRONMENTS ON TEMPERATURE GRADIENTS IN THE TEST AREA FOR SAMPLE C2

Test Conditions	Location Point, (x)	Temperature Difference, $\Delta T = T_B - T_x$			
		At $T_B = 645°$ K ($°$ K)	At $T_B = 810°$ K ($°$ K)	At $T_B = 980°$ K ($°$ K)	At $T_B = 1140°$ K ($°$ K)
No Flow $P_c = .05$ Torr	(1)	-3	-4	-6	-11 (-11)
	(2)	-5	-7	-10	-14
	(3)	-30	-48	-70	-94 (-82)
Mach 1.1 Flow $P_c = 20$ Torr	(1)	-13	-17	-21	-30 (-18)
	(2)	-6	-8	-13	-21
	(3)	-53	-80	-102	-130 (-103)
Mach 2.1 Flow $P_c = 16$ Torr	(1)	-5	0	+4	+6 (+60)
	(2)	+28	+37	+40	+37
	(3)	+1	-7	-22	-42

Location Point Indicator

(A) Temperature control thermocouple - 0.25 cm above HC_L

(B) Temperature measurement thermocouple - 0.25 cm below VC_L

(1) Edge thermocouple - at HC_L, 1.08 cm from VC_L

(2) Edge thermocouple - 0.63 cm below (1)

(3) Edge thermocouple - 1.9 cm above (1) and 0.63 cm above upper end of test section

Notes:

(1) All thermocouples were 3-mil, bare wire Chromel/Alumel.
(2) ΔT values in parenthesis are these measured with an optical pyrometer.
(3) ΔT values for flow tests are not corrected for convection effects on thermocouple readings.

Table 15

TOTAL NORMAL EMITTANCE RECORD FOR OXIDIZED RENÉ 41 SAMPLE C2
DURING MACH 1.1 AND MACH 2.1 FLOW TESTS AT FOUR TEMPERATURES

Test Chamber Pressure, P_c (Torr)	ϵ_{TN} Values Determined at:			
	T = 645°K	T = 810°K	T = 980°K	T = 1140°K
For Mach 1.1 Flow				
.05 (No Flow)	0.75	0.79	0.83	0.86
5	0.77	0.82	0.84	0.85
10	0.77	0.82	0.84	0.85
20	0.78	0.82	0.84	0.85
For Mach 2.1 Flow				
.05 (No Flow)	0.74	0.78	0.81	0.88
1.3	0.75	0.79	0.83	0.86
4.0	0.73	0.78	0.83	0.87
7.9	0.74	0.79	0.85	0.86
10	0.76	0.80	0.88	0.85
12	0.75	0.81	0.89	0.84
16	0.74	0.82	0.90	0.83

Notes:

(1) Apparent changes in ϵ_{TN} during flow tests are attributed to convection effects on the thermocouple temperature readings. (See Discussion.)

(2) Mach 2.1 flow-test cycles do not normally involve test chamber pressures greater than 8 Torr. See Section 6.1 for calibrated relationships between P_c, P_t and P_s.

that were made during the 1140° K test. The gradients to points 1 and 2 were repeatable to within ±2° K of the values shown for each set of vacuum environment test conditions. Data for the Mach 1.1 flow environment indicates that the edges of the sample test area were convectively cooled to a greater extent than the center of the test area which was maintained at approximately a constant temperature by control thermocouple (A) located directly behind the test area. Cooler edges were also indicated by the optical pyrometer readings at 1140° K; however, the pyrometer readings also indicate that the gradients were not as large as indicated by the thermocouples. The reason for this is attributed to additional convective cooling effects on the thermocouple lead wires which caused low temperature readings at the sample edges. This latter effect was observed to be much more severe for the exposed edge-located thermocouples than for the 'sheltered' thermocouples located on the back surface of the sample.

Data for the Mach 2.1 flow environment indicates that the center of the test area tended to be cooled to a greater extent than the edges of the test section, particularly at the higher test temperatures and test chamber pressures. However upper edge location point (3), which was outside the calibrated flow field for the Mach 2.1 nozzle, still ran cooler than the center area at all test temperatures. Optical pyrometer readings obtained for the 1140° K test also indicated the test section edge temperature to be higher than the center temperature; and indicated the convective cooling effect on thermocouple (1) to be on the order of 54° K, considerably greater than the effect observed in the Mach 1.1 flow environment.

In contrast to the cooling error for the edge-located thermocouples, a comparison of optical pyrometer temperature readings at the center of the sample with the back-surface thermocouple readings indicated errors of opposite sign for these thermocouples. While pyrometer readings indicated that the center temperature dropped slightly with increasing mass flow, thermocouple (B) indicated a slight increase in temperature. The reason for this behavior is not obvious, however two possible answers are suggested: 1) Thermocouples in this region may be convectively heated by hot air from the warmer adjacent areas of the back surface, or 2) the difference may be due to real temperature gradients between the front and back surface of the sample. In either case, the effect on ϵ_{TN} determinations that are based on the higher

(thermocouple) indicated temperatures is that low ϵ_{TN} values are obtained. This is the tendency that was observed for the ϵ_{TN} determinations at 1140° K in this flow environment which are shown in Table 15. Before leaving Table 14 it should be recalled that the effects shown for these two flow environments are maximum, to indicate trends, and are not normally encountered until the end of the normal flow-test cycle when sample temperatures are low and measurements are not being made.

Table 15 is a record of the ϵ_{TN} determinations that were obtained for Sample C2 during the two flow-test investigations when the sample temperature gradients were changing as indicated in Table 14. All of the ϵ_{TN} values in this table were determined on the basis of the sample temperature measurements from thermocouple (B) which was located directly behind the 0.3-cm diameter target area for the radiometer. The initial values (in vacuum) indicate the 'true' emittance of the sample at each temperature, and subsequent values show the effect of the sample temperature perturbations associated with each flow condition on the emittance determination. ϵ_{TN} values for both flow environments at the three lower test temperatures are generally higher than the 'true' values at these temperatures, indicating that the effective temperature of the target area viewed by the radiometer was higher than was indicated by thermocouple (B). For the Mach 1.1 flow tests the explanation for this is that convective cooling of the thermocouple leads must occur and the effect must be greater than the temperature drop, if any, of the target area due to the cooler adjacent areas. For the Mach 2.1 flow tests there is the additional possibility that the effective temperature of the target area is higher than indicated due to heating by the hotter, surrounding sample area. At low chamber pressures, ($P_c <$ 7 Torr), maximum sample temperatures with Mach 2.1 flow occur at the center of the sample. At higher chamber pressures, the center of the sample is cooled more effectively and the region of maximum temperature moves toward the top, bottom and edges of the test section area.

ϵ_{TN} determinations at 1140° K for both flow environments tended to be lower than the 'true' values, indicating that thermocouple (B) was reading too high. Possible explanations for this occurrence have already been mentioned — either convective heating of the thermocouple lead wires to a higher temperature than the junction, or a real temperature gradient between the front and back surface of the sample, or both.

8-10

The results of this study on Sample C2 indicate that ϵ_{TN} for a heated-strip sample can be satisfactorily monitored during flow-test exposures by the methods described. At low test temperatures the accuracy of thermocouple measurements at the back center surface appears to be on the order of 1%, and the error tends towards a low temperature reading. The error in ϵ_{TN} determinations corresponding to this temperature error is about 4%, normally high. At higher test temperatures, the temperature errors may reverse direction and result in low ϵ_{TN} determinations. In the latter cases, optical pyrometer temperature determinations are more reliable for determining sample temperature gradients, and will be more reliable for absolute temperature determinations also provided that ϵ_{λ} at the pyrometer wavelength is known and does not change too greatly with temperature or exposure time.

Total and spectral emittance data obtained during the vacuum tests of Sample C2 are shown in figures 42 and 44 to indicate the temperature dependency of these properties. These results are essentially the same as obtained for Sample C4 and will be discussed after the flow-test results for this latter sample have been presented.

Total normal emittance determinations made before, during and after each of the sets of five exposure test cycles that were made on Sample C4 are shown in Table 16. As before, the ϵ_{TN} determinations made in vacuum are assumed to be most representative of the 'true' ϵ_{TN} values for this material, and the variations obtained during the various test cycles are attributed primarily to the convective effects described earlier. ϵ_{TN} values during the five static air test cycles tended to be slightly low, particularly at the lowest temperature, indicating that the backface thermocouple readings were between 1 and 2 percent too high.

After these five test cycles, the sample was retested in vacuum and no significant change in emittance properties was detected; therefore the sample was used to evaluate the effects of five Mach 1.1 flow-test cycles. During these tests the ϵ_{TN} determinations tended to be high, similar to the results obtained for Sample C2 in this type of flow-test environment, indicating that the backface thermocouple readings were between 1 and 2 percent too low.

Table 16

TOTAL NORMAL EMITTANCE VALUES FOR OXIDIZED RENÉ 41 SAMPLE NO. C4 BEFORE, DURING AND AFTER STATIC AIR, MACH 1.1 AND MACH 2.1 FLOW TEST CYCLES

Test Cycle No.	Static Air Test Cycles		Mach 1.1 Flow Test Cycles		Mach 2.1 Flow Test Cycles	
	T_S (° K)	ϵ_{TN}	T_S (° K)	ϵ_{TN}	T_S (° K)	ϵ_{TN}
Preliminary Tests in Vacuum	710	0.76	711	0.76	710	0.77
	940	0.79	944	0.77	940	0.79
	1167	0.85	1173	0.83	1161	0.85
#1	661	N.R.	641	N.R.	650	0.84
	888	0.78	896	N.R.	901	0.84
	1131	0.83	1143	0.88	1136	0.91
#2	640	0.71	636	0.78	650	N.R.
	893	0.77	887	0.84	900	N.R.
	1138	0.83	1136	0.88	----	(3) --
#3	640	0.71	637	0.78	647	0.76
	891	0.78	887	0.84	892	0.81
	1138	0.83	1135	0.88	1127	0.90
#4	647	0.75	637	0.79	641	0.78
	896	0.80	891	0.83	886	0.84
	1142	0.85	1137	0.88	1112	0.95
#5	642	0.72	643	0.80	645	0.79
	893	0.78	894	0.86	887	0.82
	1140	0.83	1137	0.89	1134	0.87
Post-Cyclic Tests in Vacuum	(Same as preliminary test data in vacuum for Mach 1.1 Flow Tests)		(Same as preliminary test data in vacuum for Mach 2.1 Flow Tests)		710	0.77
					939	0.79
					1161	0.83

Notes:

(1) N.R. indicates no radiometer reading obtained.

(2) All T_S values are those determined from thermocouple readings at the center, backface of the sample.

(3) The back-surface temperature control thermocouple failed at this time. The remaining test cycles were made using an edge-located thermocouple for control.

Post-test measurements in vacuum again indicated no significant change in the emittance properties of the sample; therefore, the sample was used again to evaluate the effects of five Mach 2.1 flow test cycles. Sample temperatures and ϵ_{TN} determinations were more variable during these last test cycles, apparently because of the more severe vibration and flutter of the thermocouple lead wires in this test environment. During the second M2.1 test cycle, one of the control thermocouple leads separated from the sample causing a power shut-down and early termination of the cycle. The remaining test cycles were completed using one of the edge-located thermocouples for the temperature controller. Post-test measurements in vacuum again indicated no significant change from the initial sample emittance properties.

Calorimetric determinations of total hemispherical emittance are shown in Table 17 along with each corresponding ϵ_{TN} value. These determinations are based on the applied power and sample temperature measurements that were made during each of the tests in vacuum. ϵ_{TH} values at the two lower test temperatures were from 1 to 3 percent lower than the corresponding ϵ_{TN} values. At the highest test temperature, the difference increased to about 5%. These differences appear to be consistent with $\epsilon_{TH}/\epsilon_{TN}$ ratios that are usually reported for metallic oxides of this type. A summary of the total emittance data for oxidized René 41 as a function of temperature is shown in figure 42.

Spectral emittance measurements made during the vacuum tests of Samples C2 and C4 are summarized in figures 43, 44 and 45. The initial and final spectral emittance characteristics determined from room temperature reflectance measurements are also included in figures 43 and 44 for comparison. At wavelengths between 1 and 5 μm, neither sample displays much change in ϵ_λ with temperature although all of the elevated temperature determinations are somewhat higher than the initial room temperature determinations. At wavelengths longer than 5 μm a definite and consistent increase in ϵ_λ with increasing temperature is evident. One exception is noted for the 7.95 μm narrow-band measurements which all are lower than the initial room temperature value of ϵ_λ at that wavelength. These spectral emittance characteristics are in good agreement with the total emittance determinations for these samples and they indicate that the observed increase in total emittance with temperature is due primarily to the nongrey emittance characteristics of the samples rather than to any marked

Table 17

TOTAL HEMISPHERICAL AND TOTAL NORMAL EMITTANCE VALUES FOR OXIDIZED RENÉ 41 SAMPLE NO. C4 BEFORE AND AFTER STATIC AIR, MACH 1.1 AND MACH 2.1 FLOW TEST CYCLES

Measurement	At 710° K		At 940° K		At 1165° K	
	T_s (° K)	$\epsilon_{TH}/\epsilon_{TN}$	T_s (° K)	$\epsilon_{TH}/\epsilon_{TN}$	T_s	$\epsilon_{TH}/\epsilon_{TN}$
Before Static Air Tests	710	0.75/0.76	940	0.77/0.79	1167	0.80/0.85
After Five Static Air Test Cycles and Before M1.1 Flow Tests	711	(N.R.)/0.76	944	0.77/0.77	1173	0.80/0.83
After Five M1.1 Flow Test Cycles Before M2.1 Flow Tests	710	(N.R.)/0.77	940	0.78/0.79	1161	0.80/0.85
After Five M2.1 Flow Test Cycles	710	0.75/0.77	939	0.77/0.79	1161	0.79/0.83

(1) N.R. Indicates that power-measurement readings were not obtained for these tests.

8-14
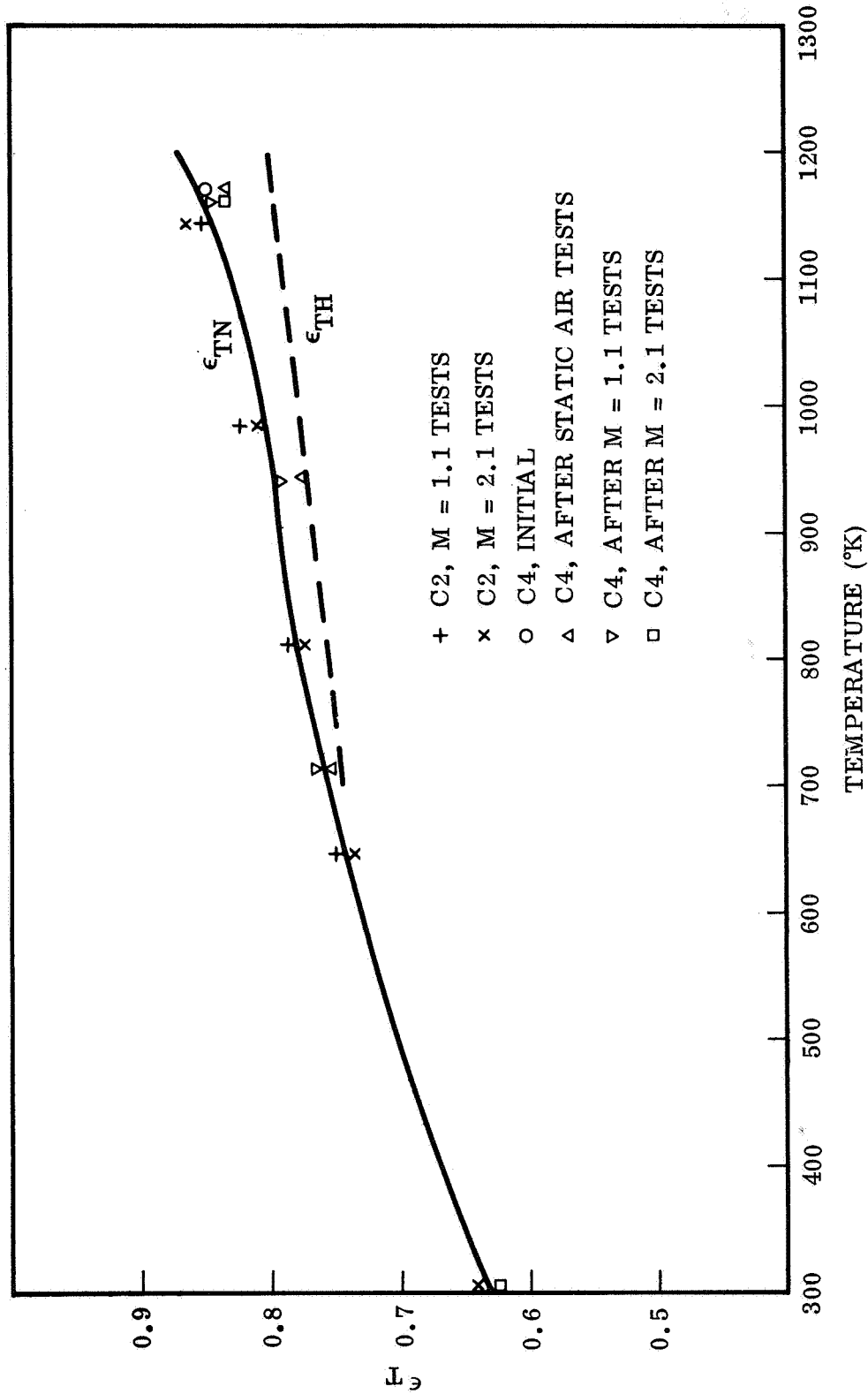
Fig. 42 Total Emittance as a Function of Temperature for Oxidized
Rene' 41 Samples
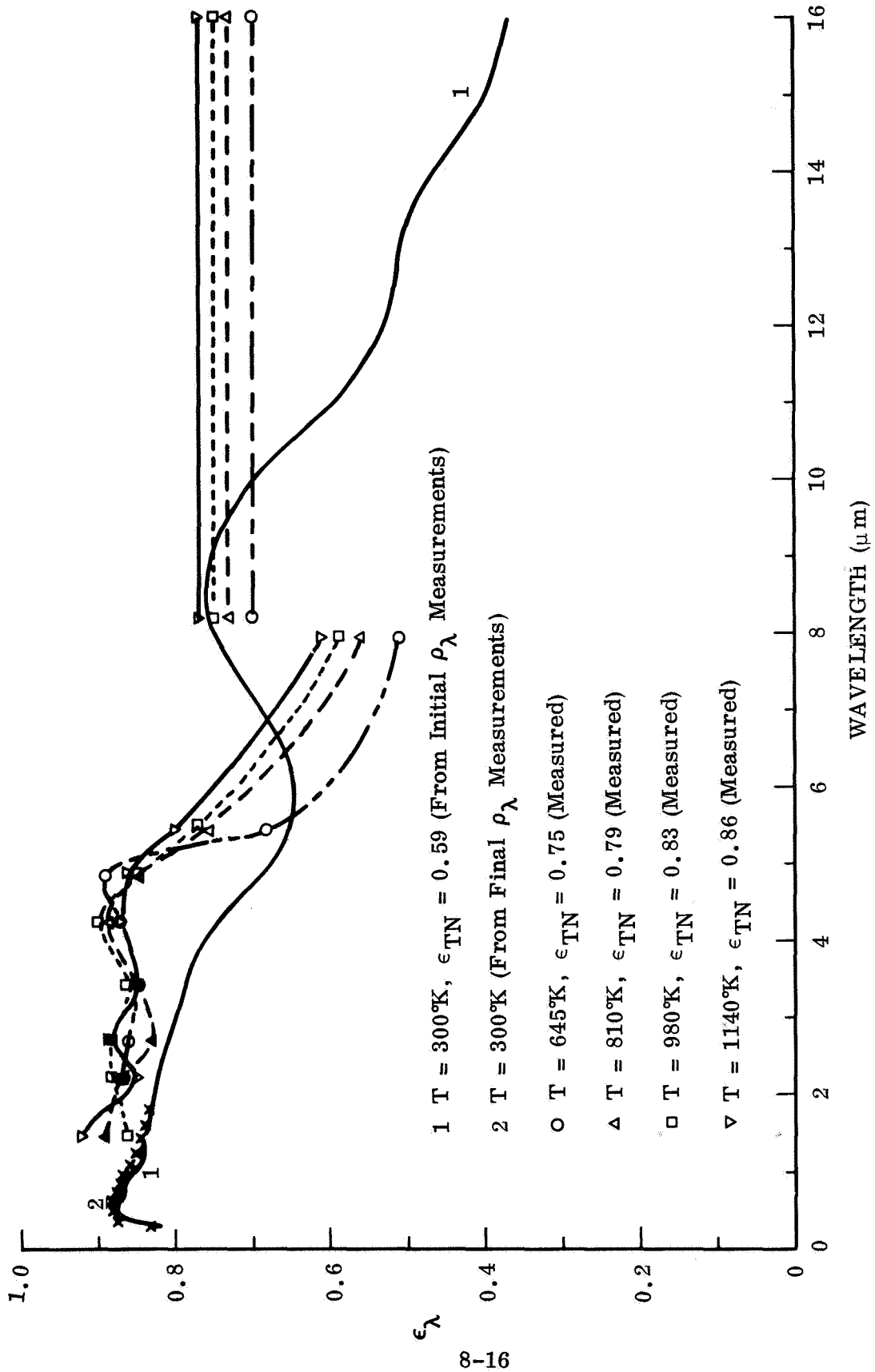
Fig. 43 Temperature Dependence of Spectral Emittance of Oxidized Rene´ 41 Sample C2

1 T = 300°K, ϵ_{TN} = 0.59 (From Initial ρ_λ Measurements)

2 T = 300°K (From Final ρ_λ Measurements)

O T = 645°K, ϵ_{TN} = 0.75 (Measured)

△ T = 810°K, ϵ_{TN} = 0.79 (Measured)

□ T = 980°K, ϵ_{TN} = 0.83 (Measured)

▽ T = 1140°K, ϵ_{TN} = 0.86 (Measured)
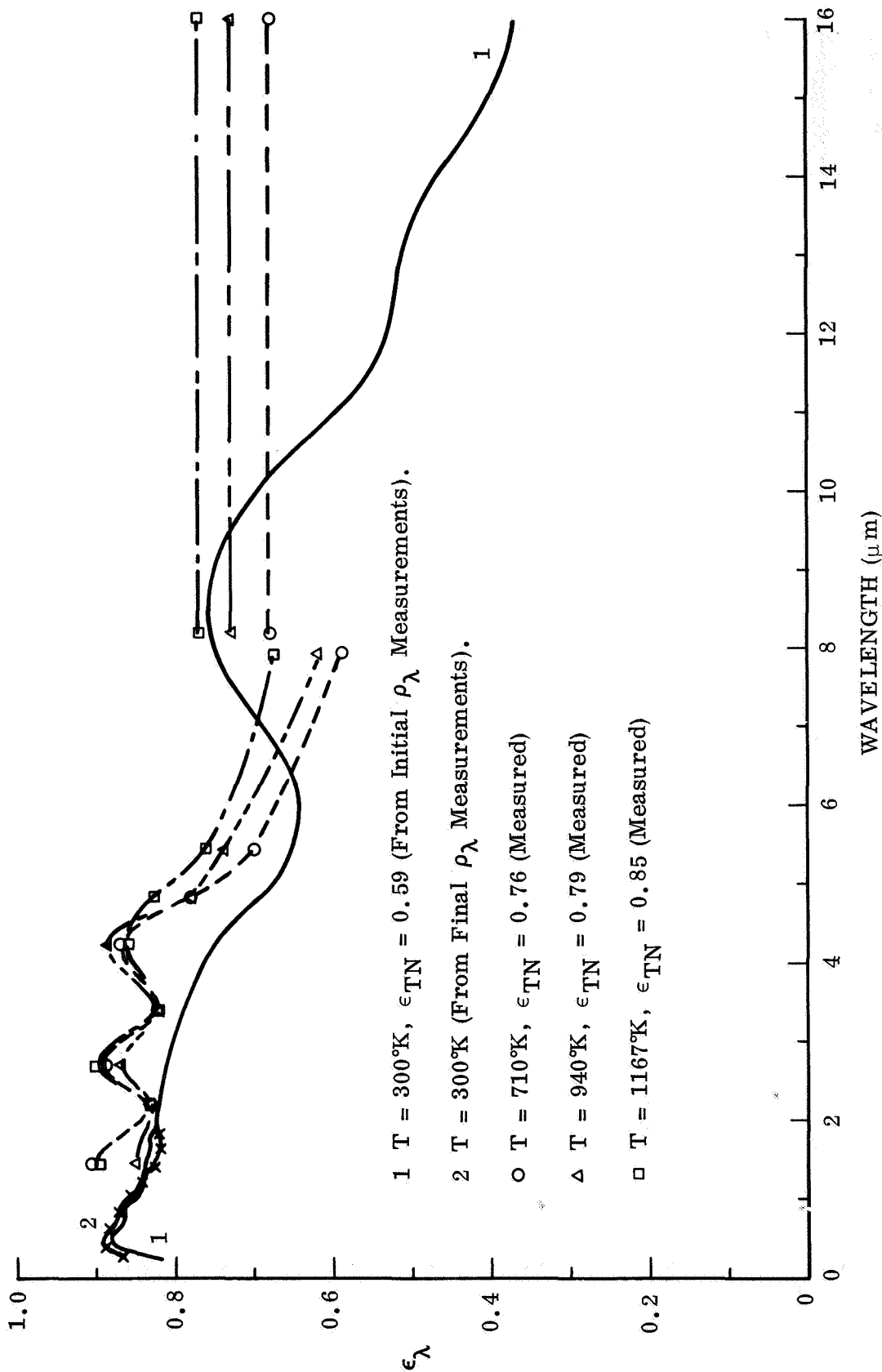
Fig. 44 Temperature Dependence of Spectral Emittance of Oxidized Rene' 41 Sample C4

1 $T = 300°K$, $\epsilon_{TN} = 0.59$ (From Initial ρ_λ Measurements).

2 $T = 300°K$ (From Final ρ_λ Measurements).

○ $T = 710°K$, $\epsilon_{TN} = 0.76$ (Measured)

△ $T = 940°K$, $\epsilon_{TN} = 0.79$ (Measured)

□ $T = 1167°K$, $\epsilon_{TN} = 0.85$ (Measured)

8-17
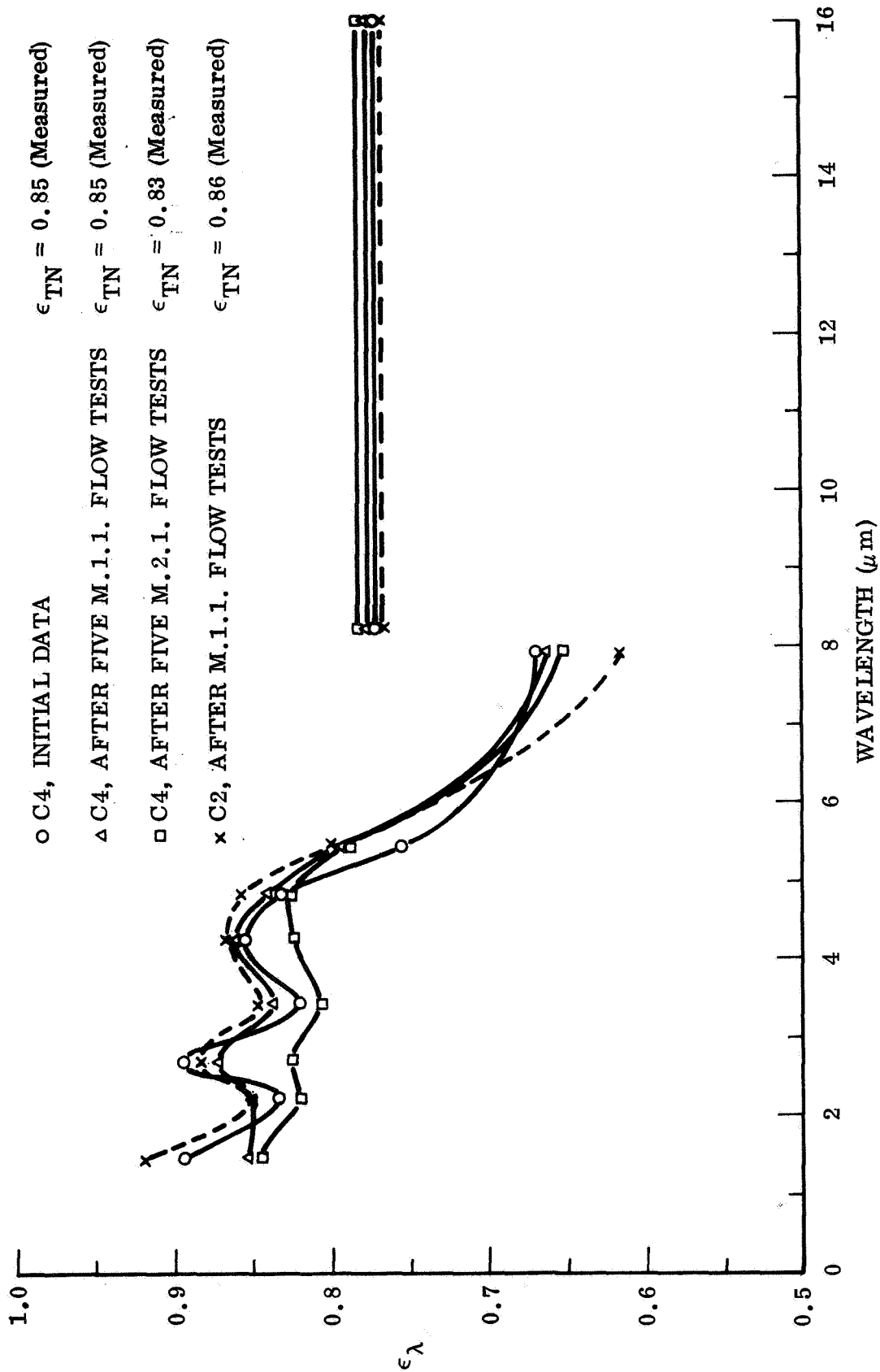
Fig. 45 Initial and Final Spectral Emittance Characteristics of Oxidized René 41 at 1165°K

change in spectral emittance characteristics with temperature. The relative impor-
tance of the shorter wavelengths to total emittance is shown in Table 18. This table
shows the percentages of total blackbody energy radiated in three different spectral
bands for three typical test temperatures for the oxidized René 41 samples. At
temperatures between 700° K and 1150° K, 70 to 87 percent of the total energy radiated
by a blackbody lies in the 1.45 to 8 μm spectral region.

Table 18

SUMMARY OF BLACKBODY ENERGY DISTRIBUTION IN THE SPECTRAL BANDS
MEASURED BY THE RADIOMETER AT THREE TYPICAL TEST TEMPERATURES
FOR THE OXIDIZED RENÉ 41 SAMPLES

Temperature (° K)	Percentage of E_b at $\lambda < 1.45\,\mu$m	Percentage of E_b at $1.45\,\mu$m $\leq \lambda \leq 8\,\mu$m	Percentage of E_b at $\lambda > 8\,\mu$m
700° K	0	70	30
950° K	1	83	16
1150° K	3	87	10

Figure 45 shows a comparison of the spectral emittance data obtained (in vacuum)
from Samples C2 and C4 at the highest test temperature after each of the flow-test
exposures. The data indicates that little or no change in the initial characteristics
occurred as a result of the Mach 1.1 flow test cycles; however, a slight drop of ϵ_λ
in the 1.45 μm to 4.25 μm region is indicated for Sample C4 after the Mach 2.1 flow
tests. This correlates with the slightly lower (about 2%) ϵ_{TN} determination for this
sample after these tests. Additional tests are needed to verify if this change is
caused by this more severe flow exposure; and if so, whether the emittance will con-
tinue to drop as the material is subjected to a greater number of test cycles.

8.2 OXIDIZED HS-188

Static and flowing air exposure cycles were performed on two samples of oxidized
HS-188 alloy at temperatures to 1310° K (1900° F). The static air and Mach 1.1 flow
test exposures were evaluated using Sample No. D1; the Mach 2.1 flow test exposures
were made using Sample No. D2. The initial room-temperature spectral and total

emittance characteristics of the samples were inferred from reflectance measurements of the sample strips and of 2.54-cm diameter witness-disk samples which were oxidized in the same manner as the strip samples, (see Section 7). Post-test reflectance measurements of the sample strips were also made to determine the effect of the various exposures on the room-temperature properties. The spectral and total emittance properties of both samples were also determined in vacuum at three temperatures, (nominally 810° K, 1140° K and 1310° K), before and after each set of exposure cycles to determine the effects of the exposures on the high-temperature emittance properties of the samples.

A description of each sample and of the instrumentation and test procedures used is presented in the following paragraphs before discussing the results.

8.2.1 Sample D1

The dimensions of this sample strip, before oxidation, were: 30.5-cm long by 2.61-cm wide by 0.103-cm thick. The width and thickness of the strip were uniform from top to bottom. This sample was used to evaluate the emittance stability of the oxidized HS-188 surface during five static-air test cycles to temperatures of 1310° K and was then exposed to five Mach 1.1 flow-test cycles at the same nominal test temperatures. Before and after each set of exposure-test cycles the sample was tested at three steady-state temperatures in vacuum to determine the total hemispherical, total normal and spectral normal emittance characteristics of the sample.

The central test-section region of the sample strip was instrumented with several thermocouples attached at various locations on the back surface and at one edge of the strip to indicate the temperature variations in the test region during each exposure condition. These thermocouples also served as temperature control sensors during the exposure-test cycles, and as voltage-drop measurement leads for the calorimetric ϵ_{TH} determinations in vacuum. All of the thermocouples were fabricated from 3-mil diameter wires and their junctions were spot-welded to small, clean areas of bare substrate metal where the surface oxide had been removed with a small grinder. After attaching the thermocouples, the sample was clamped into the test-chamber electrodes

8-20

and positioned so that the radiometer viewed the center, approximately 0.3-cm diameter, area of the sample test zone.

For the tests in vacuum, sample temperatures were controlled using the Temperature Control unit in conjunction with one of the back-face sample thermocouples and the SCR Power Unit, and using the "Set-Point" control mode of operation. For the cyclic exposure tests, the Data-Trak unit was used in conjunction with the control units above and was programmed to give approximately the same steady-state temperature steps as were obtained in the vacuum tests. Sample temperatures for the first three static-air test cycles were about 50° K lower than desired; therefore, a new control card was made and used thereafter to bring T_{max} up to approximately 1310° K. These instrumentation and control methods resulted in consistent sample temperatures from cycle-to-cycle and proved satisfactory for all the tests conducted with this sample.

At the 1140° K and 1310° K test temperatures, optical pyrometer measurements of sample temperature were also made. As discussed later with the results, these temperature readings were generally in good agreement with the thermocouple-indicated temperatures — indicating that the sample emittance at the pyrometer wavelength did not change appreciably between 300° K and 1310° K.

8.2.2 Sample D2

The Mach 2.1 flow exposure-tests were made using Sample Strip No. D2 which was machined to have a narrowed test section region at the center to prevent overheating of the sample regions above and below the test section during the high-temperature portion of the exposure cycles. The strip dimensions were 30.5-cm long by 1.42-cm wide, and the narrowed test section at the center of the strip was 1.85-cm long by 1.17-cm wide. The thickness of the strip, before oxidation, was 0.103-cm.

Sample instrumentation consisted of three thermocouples which were attached to the back surface of the strip at the center, top and bottom of the narrow test section, and four additional thermocouples which were attached at points 2.5, 5, 7.5 and 10-cm below the test section. The test temperatures were programmed and controlled in the same manner as described for Sample D1.

8-21

As with Sample D1, the emittance properties of Sample D2 were also determined in vacuum before and after the five exposure test cycles to indicate if any change occurred as a result of the exposures. Calorimetrically determined ϵ_{TH} values for this sample are less certain than for Sample D1 because of the larger temperature gradients which necessitated estimations of the average temperature of the test section surface area. The effect of the temperature gradients on the ϵ_{TN} and ϵ_λ determinations, however, was assumed to be small because of the small area viewed by the radiometer.

8.2.3 Results

A photograph of Samples D1 and D2 along with an untested (Reference) strip is shown in figure 46 to illustrate that no significant change in the visual appearance of either sample occurred as a result of the sample exposure tests. The initial appearance of the oxide coating was uniform, smooth, and dark-blue-grey color on both sides and from end-to-end. The oxide coating was strongly adherent to the substrate metal. After testing, the appearance of Sample D1 was slightly darker than that of Sample D2, but neither sample appeared much different than initially. Post-test reflectance measurements of the sample test areas showed that changes in ρ_λ were not more than ± 0.02 in the region $0.3 \, \mu m \leq 1.8 \, \mu m$. (See figure 49.)

Initial and final room-temperature properties for these samples, determined from the reflectance measurements, are listed in Table 19. The changes observed in α_s and ϵ_λ at $\lambda = 0.65 \, \mu m$ were small and in agreement with the visual observations. The total IR-reflectance measurements for Sample D1 indicated a slight increase in ϵ_{TN}, from 0.47 to 0.50. ϵ_{TN} values for Sample D2 could not be determined because the strip was too narrow for measurement with the DB-100 reflectometer. The initial room-temperature ϵ_λ characteristics of the oxidized HS-188 samples for the region $0.30 \, \mu m \leq \lambda \leq 16 \, \mu m$ are shown in figures 47 and 48 for comparison with the high temperature ϵ_λ data that is discussed later. Post-test measurements of ϵ_λ at $\lambda > 1.8 \, \mu m$ were not made, but measurements at the shorter wavelengths were obtained and are shown in figure 47.
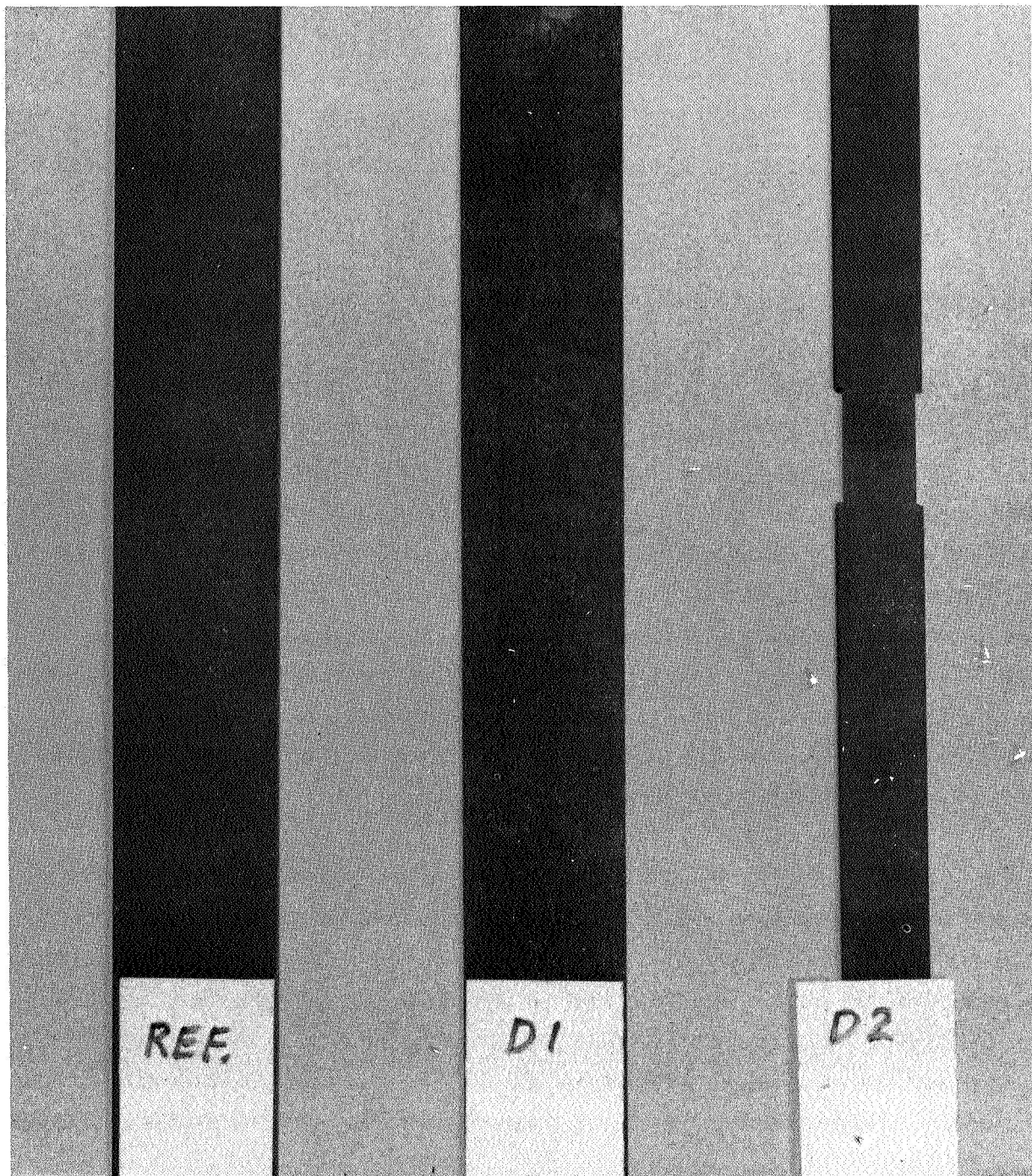
Fig. 46 Visual Appearance of Three Oxidized HS-188 Samples

Table 19

INITIAL AND FINAL ROOM TEMPERATURE PROPERTIES OF
OXIDIZED HS-188 SAMPLES

	αs	ϵ_λ(Pyrom) $\lambda = 0.65\,\mu m$	ϵ_{TN} (DB-100)	ϵ_λ ($0.3\,\mu m \leq \lambda \leq 1.8\,\mu m$)	ϵ_λ ($2\,\mu m \leq \lambda \leq 16\,\mu m$)
Initial	0.87	0.89	0.47	See Figures 47 and 48	See Figures 47 and 48
Final					
D1	0.88	0.90	0.50	See Figure 49	Not Measured
D2	0.85	0.89	N.R.	See Figure 49	Not Measured

A summary of the radiometer-determined values of ϵ_{TN} for both samples before, during and after each set of exposure test cycles is shown in Table 20. During the static-air test cycles of Sample D1, ϵ_{TN} determinations were from 5 to 10 percent higher at each temperature than those obtained during the initial tests in vacuum. Higher ϵ_{TN} values were also obtained from the tests in vacuum after this series of exposures, indicating that a real increase in ϵ_{TN} occurred as a result of these exposures. Subsequent tests of the sample in the Mach 1.1 flow environment did not appear to have any significant affect on emittance.

Total normal emittance values for Sample D2 before, during and after five Mach 2.1 flow-test exposures are shown in the right-hand column of Table 20. The ϵ_{TN} values for this sample were consistently about 10 percent lower than the values obtained for Sample D1. These differences could be real sample-to-sample variations in the thickness and/or composition of the oxidized surface, or could be the result of temperature determination errors for the sample area viewed by the radiometer. In either case, no significant change in ϵ_{TN} was observed to occur as a result of these test exposures.

The sample temperatures listed in Table 20 for the first set of tests of Sample D1 are those that were indicated by the back-face thermocouples attached to this sample. During the tests in vacuum and in the static air pressure environment, the thermocouple readings indicated the temperature of the test-section area of this sample to be

Table 20

TOTAL NORMAL EMITTANCE VALUES FOR OXIDIZED HS-188 SAMPLES BEFORE, DURING AND AFTER FLOW TEST CYCLES

Test Cycle No.	Static Air Test Cycles, (Sample D1)		Mach 1.1 Flow Test Cycles, (Sample D1)		Mach 2.1 Flow Test Cycles, (Sample D2)	
	T_S (°K)	ϵ_{TN}	T_S (°K)	ϵ_{TN}	T_S (°K)	ϵ_{TN}
Preliminary Tests in Vacuum	810	0.64	810	0.70	812	0.62
	1149	0.78	1140	0.82	1142	0.74
	1310	0.76	1305	0.81	1325	0.72
#1	756	0.67	744	0.67	765	0.61
	1097	0.80	1090	0.81	1105	0.75
	1259	0.82	1311	0.83	1331	0.74
#2	757	0.67	747	0.68	766	0.61
	1091	0.81	1093	0.79	1100	0.75
	1276	0.84	1310	0.82	1332	0.75
#3	756	0.67	744	0.67	769	0.62
	1091	0.80	1090	0.79	1111	0.74
	1272	0.84	1308	0.82	1336	0.74
#4	757	0.70	749	0.68	748	N.R.
	1101	0.84	1094	0.81	1113	N.R.
	1323	0.87	1309	0.83	1335	0.73
#5	754	0.68	754	0.68	744	0.66
	1099	0.82	1095	0.79	1111	0.72
	1320	0.86	1296	0.83	1332	0.75
Post Exposure Tests in Vacuum	Same as preliminary Data in Vacuum Before M1.1 Flow Tests		804	0.67	812	0.62
			1140	0.81	1142	0.73
			1312	0.80	1317	0.75

Notes:

(1) T_S values at 1100° K and 1310° K during the Flow-Test Cycles were determined from optical pyrometer readings. All others are thermocouple-indicated temperatures.

(2) N.R. indicates that radiometer readings were not obtained.

8-25

uniform to within 10° K, from top-to-bottom; and indicated center-to-edge differences of about 10° K at T_S = 810° K, to about 30° K at T_S = 1310° K. Similar temperature gradients were indicated by optical pyrometer readings at the 1310° K test temperatures. Absolute sample temperatures determined from the optical pyrometer readings at 1310° K also agreed with the thermocouple temperature readings to within ±5° K, which indicates that the emittance of the oxidized surface at 0.65 μm (the pyrometer wavelength) did not change appreciably from the value indicated by the room-temperature reflectance readings, i.e. 0.90 ±0.02. Most of the temperature drop at the edges of this sample appeared to occur in the region immediately adjacent to the edges and should have no effect on the temperature of the central test area viewed by the radiometer. For the calorimetrically determined values of ϵ_{TH}, corrections of -3° K, -6° K and -8° K at each of the respective test temperatures were used to obtain an average temperature value for the total test-section area.

During the Mach 1.1 Flow-Test exposures for Sample D1, optical pyrometer readings indicated that the center of the test section area was cooled 15 to 20° K below the temperatures at the top and bottom of the test area at T_S = 1310° K, but was about 20° K higher than the edges of the sample. These gradients increased as the test chamber/flow nozzle pressures were increased during the high-temperature portion of each test cycle. The sample thermocouple readings under these test conditions indicated similar temperature gradients, but the absolute temperature indications were from 5 to 10° K lower than those indicated by the pyrometer. The optical pyrometer temperature readings are believed to be more reliable than the thermocouple readings under these test conditions and are the ones listed in Table 20 for all but the 750° K tests.

The T_S values for Sample D2 in Table 20 are those indicated by the center, back-face thermocouple for the initial tests at 812° K and 1142° K in vacuum and for the low-temperature portions of the Mach 2.1 flow test cycles. All the other T_S values were determined from optical pyrometer readings. For the tests in vacuum, temperatures at the center of the narrowed test section were observed to be higher than the temperatures at the top and bottom of the test-section area by the following amounts: 9° K at 812° K, 22° K at 1142° K, and 37° K at 1320° K. Center-to-edge temperature gradients of 2° K and 9° K at 1142° K and 1320° K, respectively, were indicated by the

8-26

optical pyrometer. For the calorimetric ϵ_{TH} determinations for this sample, corrections of -4° K, -11° K and -15° K were used at each respective test-temperature level to obtain an estimate of the average temperature for the test section area.

During the Mach 2.1 flow-test cycles of Sample D2, the test section temperature gradients appeared to be about the same as for the tests in vacuum, but the absolute temperatures indicated by the thermocouples were from 20 to 25° K lower than indicated by the optical pyrometer at 1330° K. The reason for this difference is attributed to convective cooling of the thermocouple lead wires in this environment, therefore the pyrometer-indicated temperatures are believed to be more reliable.

Total hemispherical and total normal emittance values for Samples D1 and D2, determined during the tests in vacuum before and after each set of exposure-test cycles, are shown in Table 21. ϵ_{TH} values for Sample D1 before and after the five static-air test cycles show about the same percentage increase as was observed for the ϵ_{TN} values. This further supports the belief that the increase observed in the emittance of this sample was real, and probably due to additional oxidation of the sample surface. No significant change in either ϵ_{TH} or ϵ_{TN} was observed after the five Mach 1.1 flow-test exposures for this sample. The hemispherical-to-normal emittance ratios for this sample appeared to vary from about 1.0 at 810° K to about 0.96 at the two higher test temperatures, both before and after the static air and Mach 1.1 flow-test exposures.

The ϵ_{TH} values for Sample D2 in Table 21 are shown in parenthesis to indicate that they are less reliable than the values determined from Sample D1, due to greater uncertainties in the applied power and sample temperature determinations. On the basis of the $\epsilon_{TH}/\epsilon_{TN}$ ratios obtained for Sample D1, the ϵ_{TH} values for Sample D2 appear to be from 10 to 15 percent too high; however, their consistency serves as an additional indication that no significant change in the emittance of the sample occurred as a result of the five Mach 2.1 flow-test exposure cycles.

Table 21

TOTAL HEMISPHERICAL AND TOTAL NORMAL EMITTANCE VALUES
FOR OXIDIZED HS-188 SAMPLES

Sample No.	Before Testing		After Testing	
	T_s (° K)	$\epsilon_{TH}/\epsilon_{TN}$	T_s (° K)	$\epsilon_{TH}/\epsilon_{TN}$
D1 (Static Air Tests)	810	0.65/0.64	810	0.70/0.70
	1149	0.73/0.78	1140	0.77/0.82
	1310	0.73/0.76	1305	0.77/0.81
D1 (M1.1 Flow Tests)	810	0.70/0.70	804	0.70/0.67
	1140	0.77/0.82	1140	0.77/0.81
	1305	0.77/0.81	1312	0.77/0.80
D2 (M2.1 Flow Tests)	812	(0.72)/0.62	812	(0.74)/0.62
	1142	(0.78)/0.74	1142	(0.78)/0.73
	1325	(0.77)/0.72	1317	(0.78)/0.75

Note:

(1) ϵ_{TH} values for Sample D2 are less reliable than for Sample D1 due to greater uncertainties in the applied power and sample temperature determinations.

Spectral emittance data for the two oxidized HS-188 samples are shown in figures 47, 48, 49. Figure 47 shows the initial ϵ_λ characteristics obtained for Sample D1 during the first set of tests in vacuum and for comparison, shows the room-temperature emittance characteristics that were derived from spectral reflectance measurements on an oxidized disk sample. Figure 48 shows a similar set of data for Sample D2; and figure 49 compares the initial and final ϵ_λ curves obtained at 1320° K (nominal) for both samples along with the post-test reflectance measurement results for the samples at $0.3 \mu m \leq \lambda \leq 1.8 \mu m$.

The data in figures 47 and 48 indicates that the spectral emittance characteristics for both samples were essentially the same although the ϵ_λ values for Sample D1 were slightly higher than for Sample D2 at all wavelengths. The higher ϵ_λ values for Sample D1 correlate with the higher ϵ_{TN} values obtained for this sample and, as discussed earlier, may be due to real sample-to-sample differences and/or to sample temperature measurement errors. The latter error would be more likely for Sample D2. At wavelengths less than $8 \mu m$, ϵ_λ values for this oxidized alloy do not change

8-28
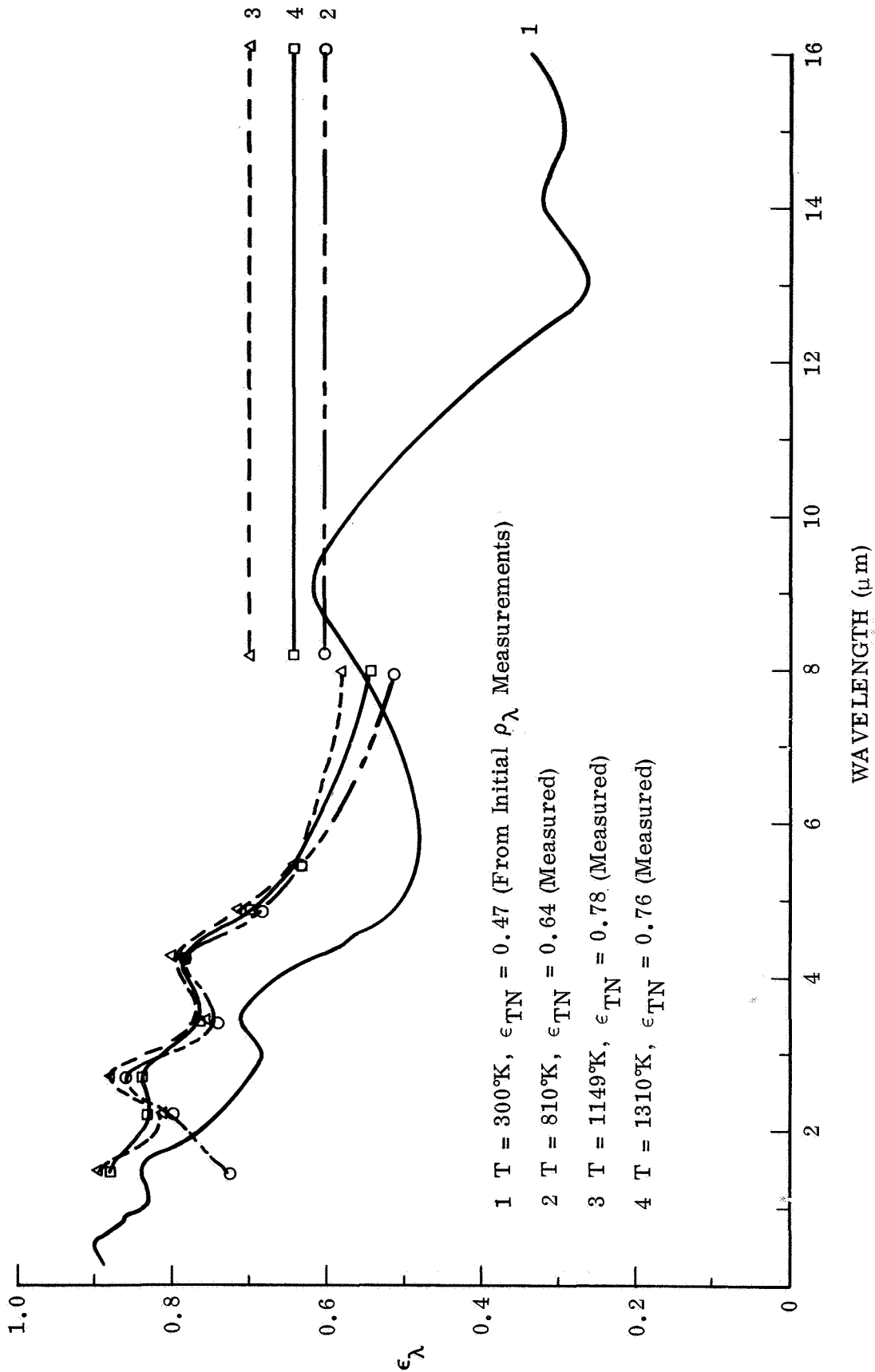
Fig. 47 Spectral Emittance of Oxidized HS-188 Sample No. D1 at Four Temperatures

1 T = 300°K, ϵ_{TN} = 0.47 (From Initial ρ_λ Measurements)

2 T = 810°K, ϵ_{TN} = 0.64 (Measured)

3 T = 1149°K, ϵ_{TN} = 0.78 (Measured)

4 T = 1310°K, ϵ_{TN} = 0.76 (Measured)

1 T = 300°K, ϵ_{TN} = 0.47 (From Initial ρ_λ Measurements)

2 T = 812°K, ϵ_{TN} = 0.62 (Measured)

3 T = 1142°K, ϵ_{TN} = 0.74 (Measured)

4 T = 1325°K, ϵ_{TN} = 0.72 (Measured)
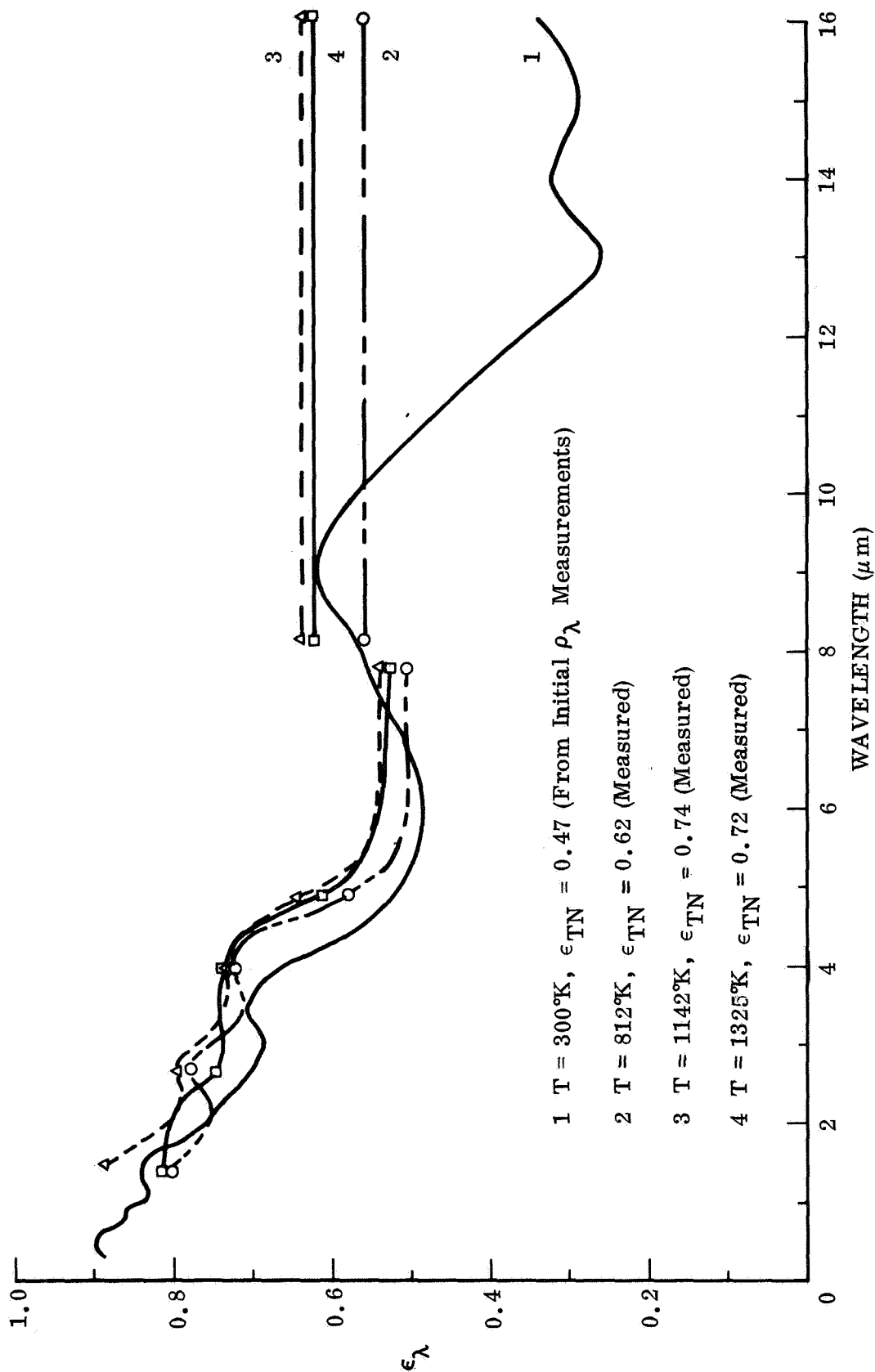
Fig. 48 Spectral Emittance of Oxidized HS-188 Sample No. D2 at Four Temperatures
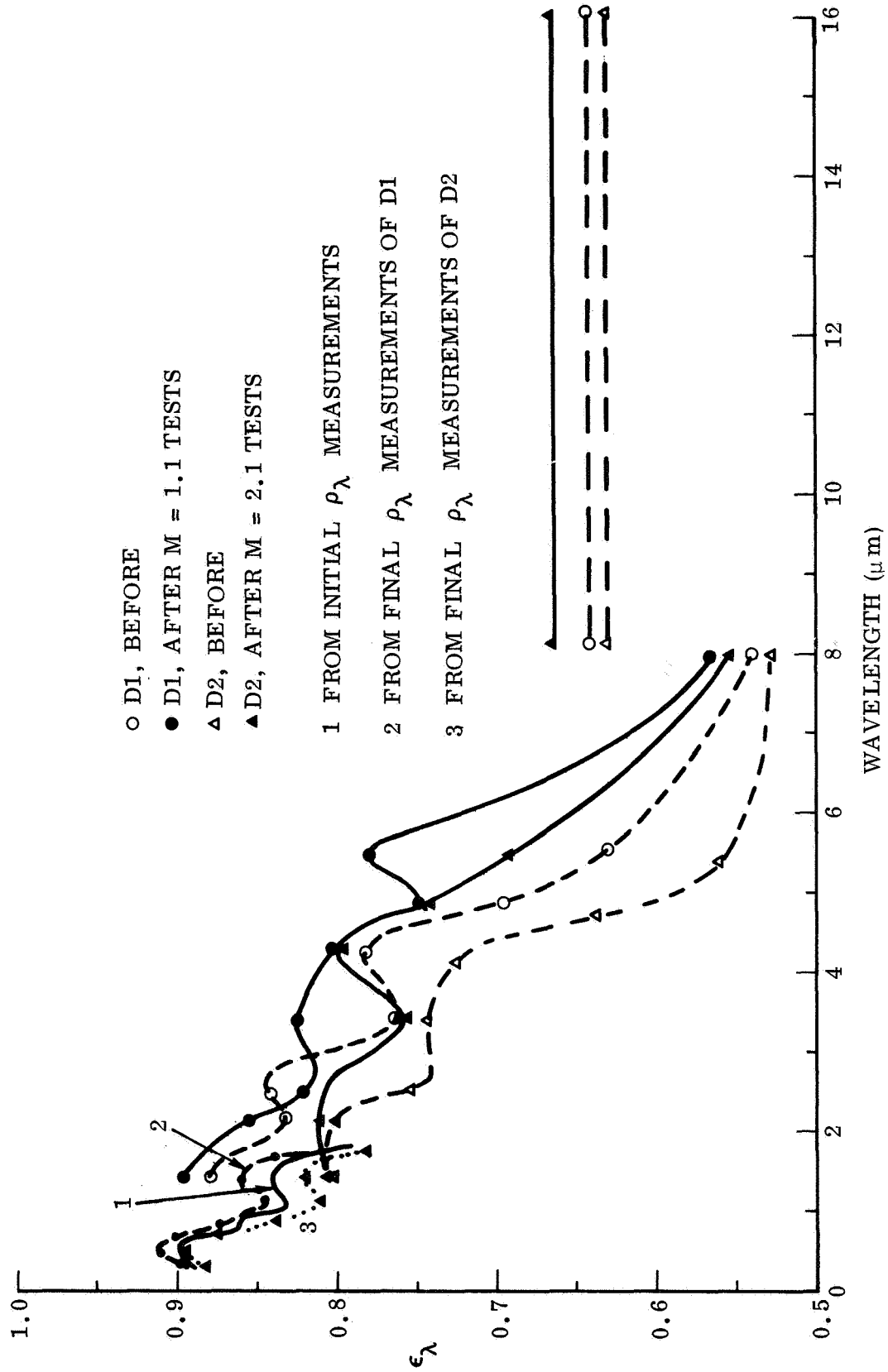
Fig. 49 Initial and Final Spectral Emittance of Oxidized HS–188 Samples at 1320°K

○ D1, BEFORE

● D1, AFTER M = 1.1 TESTS

△ D2, BEFORE

▲ D2, AFTER M = 2.1 TESTS

1 FROM INITIAL ρ_λ MEASUREMENTS

2 FROM FINAL ρ_λ MEASUREMENTS OF D1

3 FROM FINAL ρ_λ MEASUREMENTS OF D2

WAVELENGTH (μm)

ϵ_λ

appreciably with temperature between 810° K and 1320° K, but most of the elevated temperature values are from 5 to 15 percent higher than the corresponding room-temperature values indicated by the reflectance measurements. In the 8 to 16 μm band, a greater temperature dependence is noted, and both samples show maximum ϵ_λ values in this band at 1145° K and then a slight drop at 1320° K. This tendency towards decreasing ϵ_λ with increasing temperature between 1145° K and 1320° K correlates with the 2 to 3 percent drop that was observed in the ϵ_{TN} determinations at these temperatures. The increase in ϵ_{TN} with temperature between 300° K and 1140° K is clearly due to the non-grey ϵ_λ characteristics of the samples, i.e. increases at the shorter wavelengths. The relative importance to ϵ_{TN} of the spectral bands below, in and beyond the 1.45 μm to 8 μm band region covered by the radiometer filters is shown in Table 22 for the three nominal test temperatures used for this material.

Changes in the spectral emittance characteristics of Samples D1 and D2 as a result of their exposure tests are shown by the data in figure 49. This data is from the initial and final vacuum test measurements made on these samples at 1320° K. The post-test reflectance data for each sample in the region 0.3 μm $\leq \lambda \leq$ 1.8 μm is also shown on this figure to indicate the small changes that occurred in this spectral region. For both samples ϵ_λ values obtained after the exposure tests were higher than before at all wavelengths except for Sample D1 at $\lambda = 2.7 \mu$m. The largest increases occurred at $\lambda = 4.85 \mu$m and $\lambda = 5.45 \mu$m and these changes would account for most of the observed increase in ϵ_{TN} for these samples. Note that the higher reflectance, (lower emittance), measurements for Sample D2, as compared with Sample D1, correlates with the lower emittance values obtained for this sample at the longer wavelengths. This lends support to the belief that the observed differences in emittance for these two samples was due to real sample-to-sample variations rather than to temperature measurement errors.

8-32

Table 22

BLACKBODY ENERGY DISTRIBUTION IN THE SPECTRAL BANDS MEASURED
BY THE RADIOMETER AT THREE TYPICAL TEST TEMPERATURES FOR THE
OXIDIZED HS-188 SAMPLES

Temperature (°K)	Percentage of E_b at $\lambda < 1.45\,\mu m$	Percentage of E_b at $1.45\,\mu m \leq \lambda \leq 8\,\mu m$	Percentage of E_b at $\lambda > 8\,\mu m$
810	0	77	23
1140	2	87	11
1310	5	87	8

8.3 OXIDIZED TD Ni Cr

The emittance stability of two samples of this oxidized alloy was evaluated in static
and flowing-air environments at temperatures up to 1480° K. The effects of the static-
air and Mach 1.1 flow-test exposures were evaluated using Sample A1. The effects
of the Mach 2.1 flow-test exposure cycles were evaluated with Sample A2. The initial
room-temperature spectral and total emittance characteristics of the samples were
inferred from reflectance measurements of the strip samples and of 1-inch diameter
witness-disk samples which were oxidized in the same manner (see Section 7). Changes
in the room-temperature properties resulting from the various exposure tests were
determined from post-test reflectance measurements. Total and spectral emittance
properties of the strip samples were also determined at four temperatures, (nominally
815° K, 1144° K, 1310° K and 1477° K), in vacuum before and after each set of exposure
test cycles.

One exception was made for Sample A1 which was not tested in vacuum after the
Mach 1.1 flow-test exposures because the sample accidently overheated and was
damaged during the third exposure test cycle. As discussed later with the test
results, total normal emittance values for Sample A1 appeared to remain stable up
until this time, therefore no additional testing was attempted.

A description of the samples and of the instrumentation and test procedures used is
given in the following paragraphs before discussing the results.

8.3.1 Sample A1

The dimensions of this strip sample before oxidation were: 30.5-cm long by 2.70-cm wide by 0.101-cm thick. The width and thickness of the strip were uniform from top to bottom. Sample instrumentation consisted of eight thermocouples attached to the sample as follows: Four Pt 6% Rh/Pt 30% Rh thermocouples spot welded to the back surface of the central test section; two Pt/Pt 13% Rh thermocouples spot welded to one edge of the test section; and two Chromel/Alumel thermocouples spot welded to the back surface of the test section between the Pt 6% Rh/Pt 30% Rh locations. All of the thermocouples were made from 3-mil diameter lead wire and were spot welded to clean, bare-metal areas on the sample where the surface oxide had been removed with a small grinder. These thermocouples served to indicate temperature variations in the test-section region of the sample and as temperature control sensors for the temperature controller. The similar-metal legs of the thermocouples also served as voltage measurement leads for the applied power measurements used to determine total hemispherical emittance values for the sample. After attaching the thermo- couples the sample was clamped between the test-chamber electrodes and was verti- cally positioned so the radiometer and optical pyrometer viewed the center area of the sample test zone.

Sample temperatures were controlled using the same methods as described in the preceeding section for HS-188 Sample D1; i.e., the steady-state tests in vacuum were controlled manually and the cyclic static-air and Mach 1.1 flow test temperatures were controlled by the programmed Data-Trak unit. These methods provided stable sample temperatures and consistent temperature readings for all the tests in vacuum and in the static-air environment, but proved to be unreliable during the Mach 1.1 flow-test exposures. During these later test cycles, excessive vibration and fluttering of the thermocouple leads occurred which caused them to either separate from the sample or to cross over one another and thereby 'short-out' the true temperature reading. Midway through the third test cycle the control thermocouple leads 'shorted' against one another, and due to an inadequate power-limit setting on the controller, this caused the sample to overheat and separate in the region about 5-cm below the top electrode clamp. No further tests on this sample were attempted after this occurrence.

Sample temperature measurements were also made with the optical pyrometer at the higher test temperatures and were generally in good agreement with the thermocouple-indicated temperatures during the tests in vacuum and in the static-air environment. During the Mach 1.1 flow-test cycles, sample temperatures were determined primarily by the pyrometer method because of the erratic thermocouple readings that were obtained in this test-environment.

8.3.2 Sample A2

Five Mach 2.1 flow-test cycles were made using strip Sample A2 which was machined to have a narrowed test section at the center, similar to that for HS-188 Sample D2. The dimensions of this strip, before oxidation, were 30.5-cm long by 1.20-cm wide by 0.109-cm thick, and the narrowed test section was 1.91-cm long by 0.89-cm wide. Five thermocouples, (three Pt 6% Rh/Pt 30% Rh and two Chromel/Alumel), were spot-welded to the back surface of the sample in the usual manner. By moving the thermocouple lead-wire support stand which was located about 15-cm behind the sample in closer to the sample, much of the vibration and flutter problem with the thermocouple leads was eliminated and satisfactory temperature measurement and control was obtained throughout these tests.

Tests in vacuum were made before and after the five Mach 2.1 flow-test cycles to determine the effect of the exposures on the high temperature emittance properties of the sample. Due to the non-uniform temperatures in the narrowed test-section region, the calorimetrically-determined ϵ_{TH} values are less certain than those for Sample A1 but they serve to indicate the emittance stability of the sample. The effect of temperature gradients on the ϵ_{TN} and ϵ_{λ} determinations was assumed to be small because of the small area viewed by the radiometer, therefore no corrections were attempted.

8.3.3 Results

A photograph of Samples A1 and A2 along with an untested (Reference) sample strip is shown in figure 50 to illustrate the initial and final appearance of each sample. The initial appearance of the oxidized surface of these samples was uniform, smooth, and
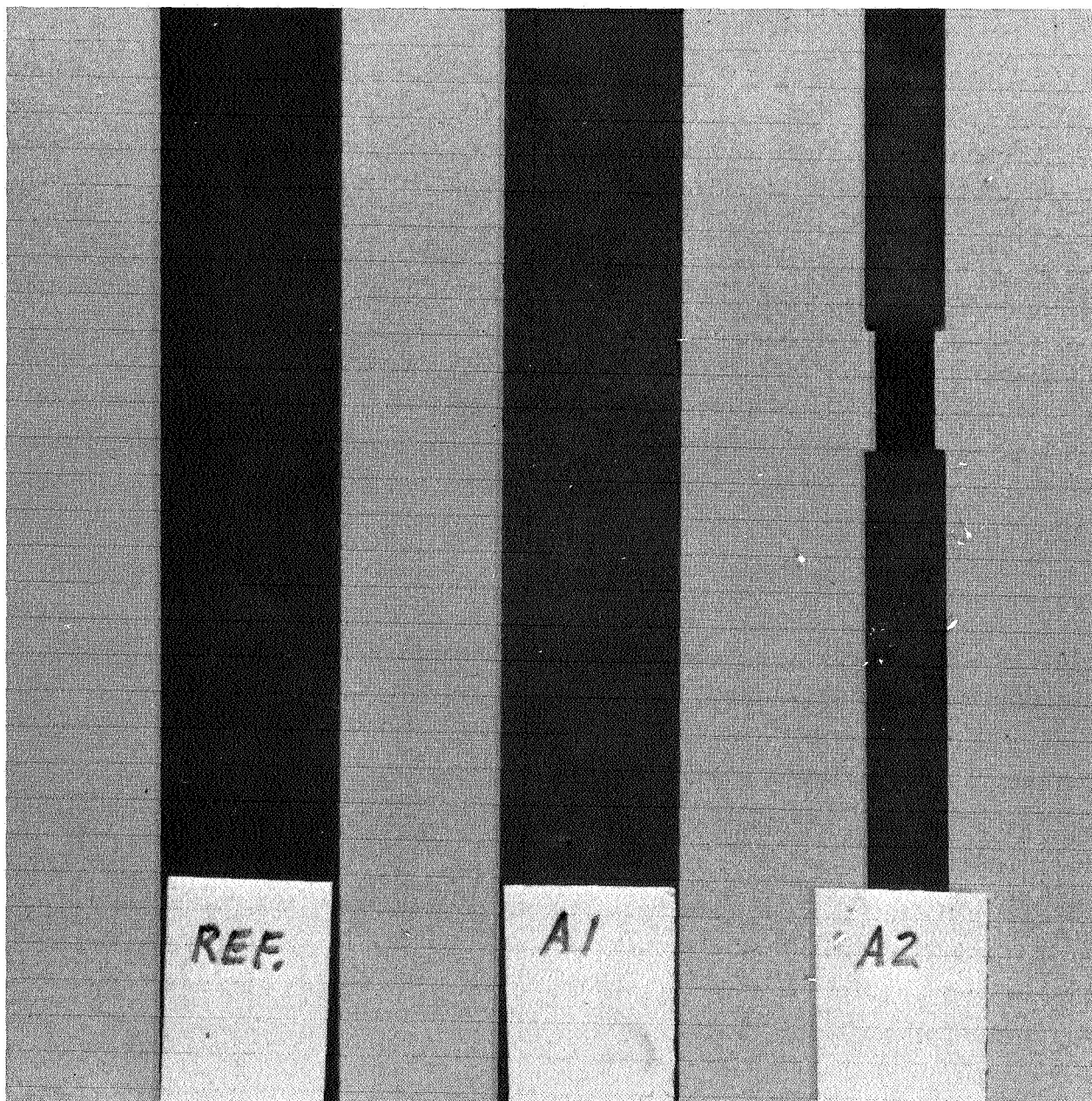
Fig. 50 Visual Appearance of Three Oxidized TD Ni Cr Samples

dark blue-grey in color. A few randomly scattered specks of dark black oxide were also observed which were on the order of 0.2 to 0.5 mm in diameter. The appearance of Sample A1 after five static-air exposure cycles and three Mach 1.1 flow-test cycles was slightly lighter grey in color and the surface texture was somewhat coarser. This latter characteristic appeared to be related to the formation of more black specks on the surface which were observed to form primarily during the 25-minute period of initial testing in vacuum at 1483° K. The appearance of Sample A2 after five Mach 2.1 flow-test cycles was similar to that of Sample A1 in the regions above and below the narrowed test section, but the test section area changed to a dark-green color, and appeared less uniform with a coarser texture.

Changes in the sample properties indicated by the room-temperature reflectance measurements are shown in Table 23. The solar absorptance of Sample A1 changed from 0.87 to 0.84, which correlates with the slightly lighter appearance of the sample after the test exposures. No change in α_s for Sample A2 was observed. The reflectance data for Sample A2 (see figure 54) indicated a slightly higher absorptance after testing in the region $0.3 \mu m \leq \lambda \leq 0.6 \mu m$ and a lower absorptance in the region $0.8 \mu m \leq \lambda \leq 1.8 \mu m$. No significant change in the reflectance (or emittance) of either sample at the pyrometer wavelength was observed; and the DB-100 reflectance measurements indicated that ϵ_{TN} for Sample A1 did not change appreciably. Sample A2 was too narrow to measure with the DB-100. The initial ϵ_λ characteristics of the oxidized TD Ni Cr samples for the region $0.30 \mu m \leq \lambda \leq 16 \mu m$ are shown in figures 51 and 52 for comparison with the high temperature ϵ_λ data that is discussed later. Post-test ϵ_λ data for the two samples in the region $0.30 \mu m \leq \lambda \leq 1.8 \mu m$ are shown in figure 54.

A record of the ϵ_{TN} data obtained for the two TD Ni Cr samples before, during and after the static-air and flow-test exposure cycles is shown in Table 24. No significant change in the emittance of Sample A1 was observed during or after the five static-air test cycles. During the first three Mach 1.1 flow-test cycles, the ϵ_{TN} determinations were slightly lower than the initial values. This may have been due to a slight mis-alignment of the radiometer or to the effect of the sample temperature gradients that occurred during these test cycles. Post-exposure tests of Sample A1 in vacuum were not made because of the sample failure that occurred during the third Mach 1.1 test

Table 23

INITIAL AND FINAL ROOM TEMPERATURE PROPERTIES OF OXIDIZED
TD Ni Cr SAMPLES

	α_s	ϵ_λ(Pyrom) $\lambda = 0.65\,\mu m$	ϵ_{TN} (DB-100)	ϵ_λ $0.3\,\mu m \le \lambda \le 1.8\,\mu m$	ϵ_λ $2\,\mu m \le \lambda \le 16\,\mu m$
Initial	0.87	0.89	0.42	See Figures 51 and 52	See Figures 51 and 52
Final					
A1	0.84	0.88	0.43	See Figure 53	Not measured
A2	0.87	0.90	Not measured	See Figure 54	Not measured

cycle; however, the data obtained up until this time indicated that the emittance of the sample was stable. ϵ_{TN} determinations for Sample A2 were generally the same as for Sample A1 and indicated that no significant change occurred during the five Mach 2.1 Flow-Test exposures for this sample.

Except for the low-temperature tests in vacuum, all the T_s values listed in Table 24 are those determined from optical pyrometer readings at the center of the test sections, where it was assumed that ϵ_λ at $\lambda = 0.65\,\mu m$ did not change from 0.89 with temperature. During the tests in vacuum the temperatures indicated by the optical pyrometer agreed with the back face thermocouple readings at 1145° K, but were about 1/2% higher (+7° K) at 1310° K and about 1% higher (+14° K) at 1485° K. At these higher test temperatures, and during all of the flow-exposure tests, more confidence was put into the pyrometer temperature determinations. The sample temperature gradients that were observed during these tests were similar to those observed for the HS-188 samples under the same test conditions, and similar corrections were made to obtain the average test-section temperature values used for the calorimetric ϵ_{TH} determinations. At the four nominal test temperatures in vacuum these corrections were: -2° K, -3° K, -4° K and -6° K for Sample A1, to correct for the center-to-edge gradients; and -3° K, -6° K, -9° K and -12° K for Sample A2, to correct for the vertical gradients that occurred in the narrowed test-section of this sample.

8-38

LMSC-D352380

Table 24

TOTAL NORMAL EMITTANCE VALUES FOR OXIDIZED TD Ni Cr SAMPLES
BEFORE, DURING AND AFTER EXPOSURE TEST CYCLES

Test Cycle No.	Sample A1 (Static Air Tests)		Sample A1 (M1.1 Flow Tests)		Sample A2 (M2.1 Flow Tests)	
	T_s (°K)	ϵ_{TN}	T_s (°K)	ϵ_{TN}	T_s (°K)	ϵ_{TN}
Preliminary Tests in Vacuum	812	0.61	814	0.61	830	0.63
	1145	0.71	1147	0.71	1144	0.71
	1309	0.73	1313	0.74	1300	0.72
	1483	0.70	1485	0.72	1473	0.69
#1	1127	0.67	1089	0.63	1122	0.65
	1286	0.70	1262	0.68	1253	0.63
	1444	0.71	1450	0.65	1396	0.64
#2	1128	0.70	1095	0.68	1106	0.68
	1287	0.70	1283	0.67	1291	0.71
	1444	0.71	1468	0.68	1472	0.68
#3	1128	0.69	1089	0.69	1106	0.70
	1286	0.70	1279	0.68	1289	0.74
	1444	0.71	1470	0.69	1473	0.73
#4	1128	0.70			1101	0.69
	1286	0.71	(See Note 2)		1265	0.72
	1443	0.71			1447	0.72
#5	1129	0.70			1106	0.70
	1287	0.71			1280	0.71
	1439	0.73			1445	0.72
Post-Cyclic Tests in Vacuum	(Same as Preliminary Test Data for Next Column)				841	0.60
					1140	0.71
					1309	0.71
					1479	0.72

Notes:

(1) All T_s values determined from optical pyrometer readings except for lowest temperature tests in vacuum.

(2) Tests of Sample A1 were terminated after the sample failed (overheated) midway through the third Mach 1.1 flow-test cycle.

8-39

LOCKHEED PALO ALTO RESEARCH LABORATORY
LOCKHEED   MISSILES   &   SPACE   COMPANY,   INC.
A   SUBSIDIARY   OF   LOCKHEED   AIRCRAFT   CORPORATION

Total hemispherical emittance values for Sample A1 and A2 which were determined along with the total normal values during the tests in vacuum before and after the static-air and Mach 2.1 flow-test exposures are shown in Table 25. No significant change in either of these properties for either sample was detected. The ϵ_{TH} values for Sample A2 are obviously too high, due either to errors in the average temperature determination for the narrowed test-section area or to errors in the applied power measurements for this sample, or both. Their consistency however, serves as an additional indication that no significant change in the total emittance properties of the sample occurred. The more reliable ϵ_{TH} determinations obtained for Sample A1 indicate that the $\epsilon_{TH}/\epsilon_{TN}$ ratio for this oxidized alloy is close to unity. Both sets of data indicate that there is little or no increase in total emittance with temperature above 1145° K.

Results of the initial spectral emittance determinations for Samples A1 and A2 are shown in figures 51 and 52, respectively, along with the room temperature emittance curve (inferred from ρ_λ measurements) for comparison. The characteristics for

Table 25

TOTAL HEMISPHERICAL AND TOTAL NORMAL EMITTANCE VALUES FOR
OXIDIZED TD Ni Cr SAMPLES BEFORE AND AFTER EXPOSURE TEST CYCLES

Sample No.	Before Testing		After Testing	
	T_s (° K)	$\epsilon_{TH}/\epsilon_{TN}$	T_s (° K)	$\epsilon_{TH}/\epsilon_{TN}$
A1	812	0.63/0.61	814	0.63/0.61
	1145	0.71/0.71	1147	0.70/0.71
	1309	0.73/0.73	1313	0.73/0.74
	1483	0.71/0.70	1485	0.72/0.72
A2	830	(0.76)/0.63	841	(0.79)/0.60
	1144	(0.78)/0.71	1140	(0.80)/0.71
	1300	(0.78)/0.72	1309	(0.80)/0.71
	1473	(0.75)/0.69	1479	(0.77)/0.72

Note: ϵ_{TH} values for Sample A2 are less certain than for Sample A1 because of greater uncertainties in the applied power and sample temperature determinations.

Fig. 51 Initial Spectral Emittance Characteristics for Oxidized TD Ni Cr Sample A1
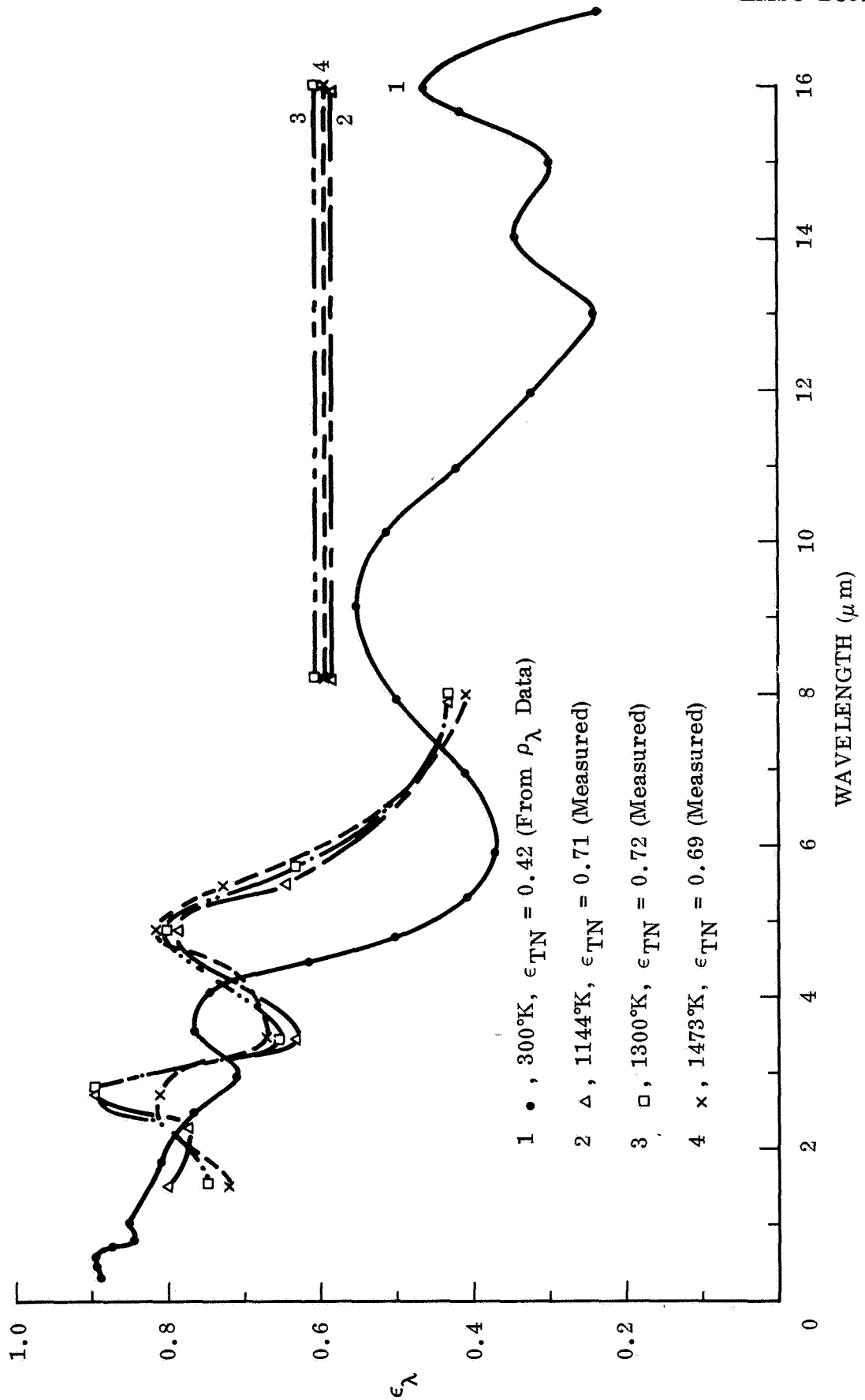
1 , • 300°K, $\epsilon_{TN} = 0.42$ (FROM REFLECTANCE MEASUREMENTS)

2 , ○ 812°K, $\epsilon_{TN} = 0.61$ (MEASURED)

3 , △ 1145°K, $\epsilon_{TN} = 0.71$ (MEASURED)

4 , □ 1309°K, $\epsilon_{TN} = 0.73$ (MEASURED)

5 , × 1483°K, $\epsilon_{TN} = 0.70$ (MEASURED)

WAVELENGTH (μm)

ϵ_λ

Fig. 52 Initial Spectral Emittance Characteristics for Oxidized TD Ni Cr Sample A2

1 • , 300°K, ϵ_{TN} = 0.42 (From ρ_λ Data)

2 △ , 1144°K, ϵ_{TN} = 0.71 (Measured)

3 □ , 1300°K, ϵ_{TN} = 0.72 (Measured)

4 × , 1473°K, ϵ_{TN} = 0.69 (Measured)

WAVELENGTH (μm)

ϵ_λ

both samples are essentially the same and show very little change with temperature between 810° K and 1480° K. Between room temperature and 810° K the locations of the emittance peaks and valleys appear to shift so that ϵ_λ values at 2.7 μm, 4.85 μm and 5.45 μm are higher, but at 3.4 μm and 7.95 μm the ϵ_λ values are lower than were indicated by the 300° K ρ_λ measurements. The average emittance for the 8–16 μm band appears to increase with temperature up to 1145° K and then does not change appreciable thereafter.

The spectral emittance characteristics of Sample A1 after the five static-air test cycles, and of Sample A2 after the five Mach 2.1 flow-test cycles are shown in figures 53 and 54, respectively, to illustrate the changes in ϵ_λ that occurred as a result of these exposures. The principal change noted in figure 53 for Sample A1 is the shift of the ϵ_λ minimum from 3.4 μm to 4.25 μm and the shift of the ϵ_λ peak from 4.25 μm to 5.45 μm. The change in position of these peaks and valleys appears to be related to the thickness of the oxide layer and is probably due to additional oxidation of the sample during the static-air exposures. In any case, the effect of the changes in ϵ_λ on the high temperature ϵ_{TN} values appears to be negligible, as was shown earlier by the results in Tables 24 and 25. Also shown in figure 53 are the results of the initial and final room temperature ϵ_λ determinations between λ = 0.30 μm and λ = 1.8 μm. The principal change noted in this spectral region was a 2 to 3 percent drop in ϵ_λ at wavelengths between 0.70 and 1.8 μm.

Changes in the spectral emittance characteristics of Sample A2 are seen by comparing the curves in figure 54 with the initial curves in figure 52. The effect of the five Mach 2.1 flow-test exposures on this sample was to 'smooth-out' all the original peaks and valleys so that a somewhat higher average emittance is obtained at wavelengths shorter than 4 μm, and a lower average emittance is obtained between 4.5 and 7.0 μm. These changes are also presumed to be due primarily to further oxidation of the sample; however, the observed change in color of the oxide suggests that the composition of the surface oxide may also have changed. As with Sample A1, the effect of the changes in ϵ_λ for Sample A2 on the high temperature total emittance values seem to be self-cancelling so that little or no change in either ϵ_{TN} or ϵ_{TH} was detected. The relative importance of ϵ_λ to ϵ_{TN} in the spectral region covered
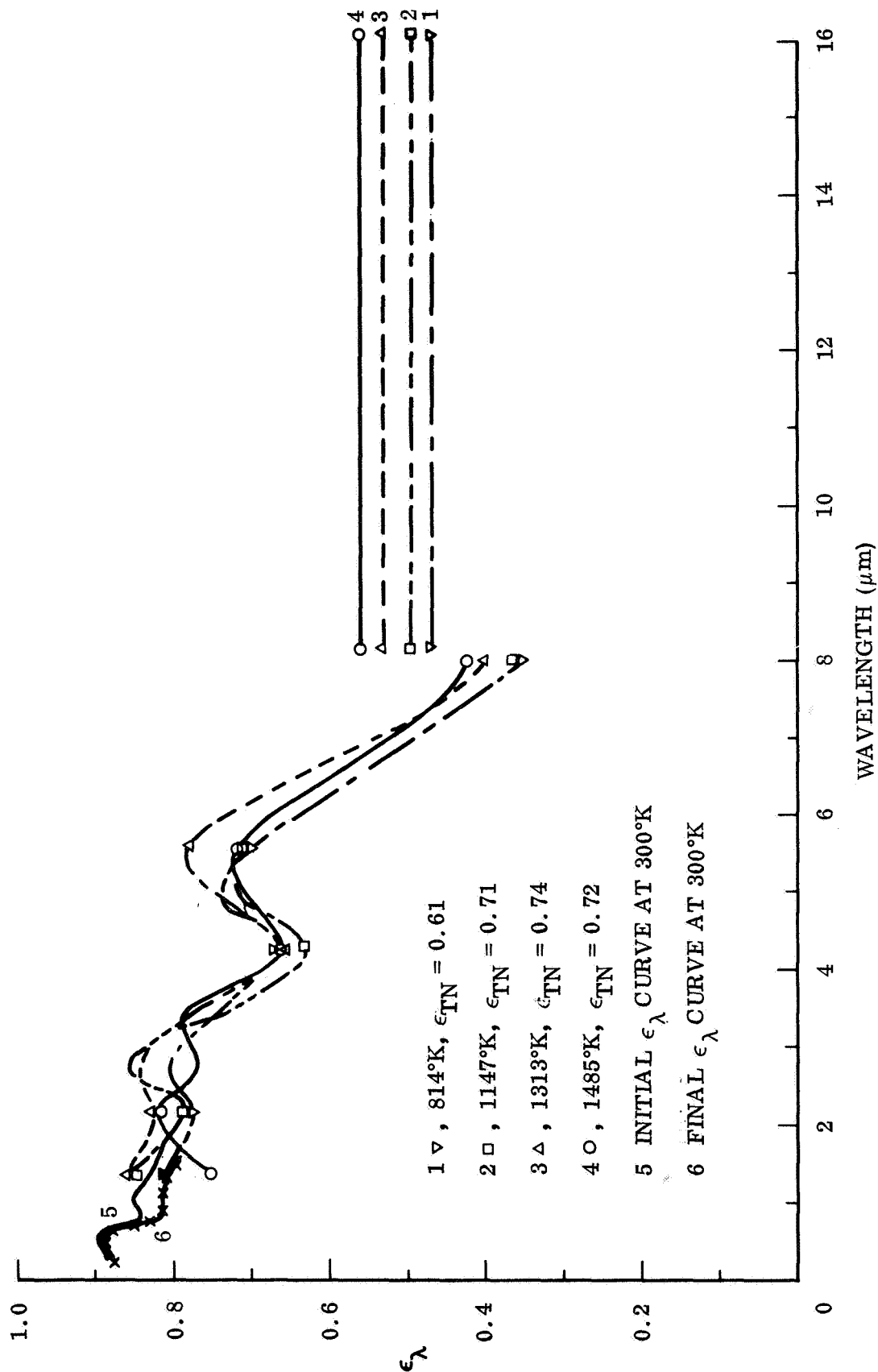
Fig. 53 Spectral Emittance Characteristics of Oxidized TD Ni Cr Sample
A1 after 5 Static Air Test Cycles

1 ▽ , 814°K, ϵ_{TN} = 0.61

2 □ , 1147°K, ϵ_{TN} = 0.71

3 △ , 1313°K, ϵ_{TN} = 0.74

4 ○ , 1485°K, ϵ_{TN} = 0.72

5 INITIAL ϵ_λ CURVE AT 300°K

6 FINAL ϵ_λ CURVE AT 300°K

WAVELENGTH (μm)

ϵ_λ
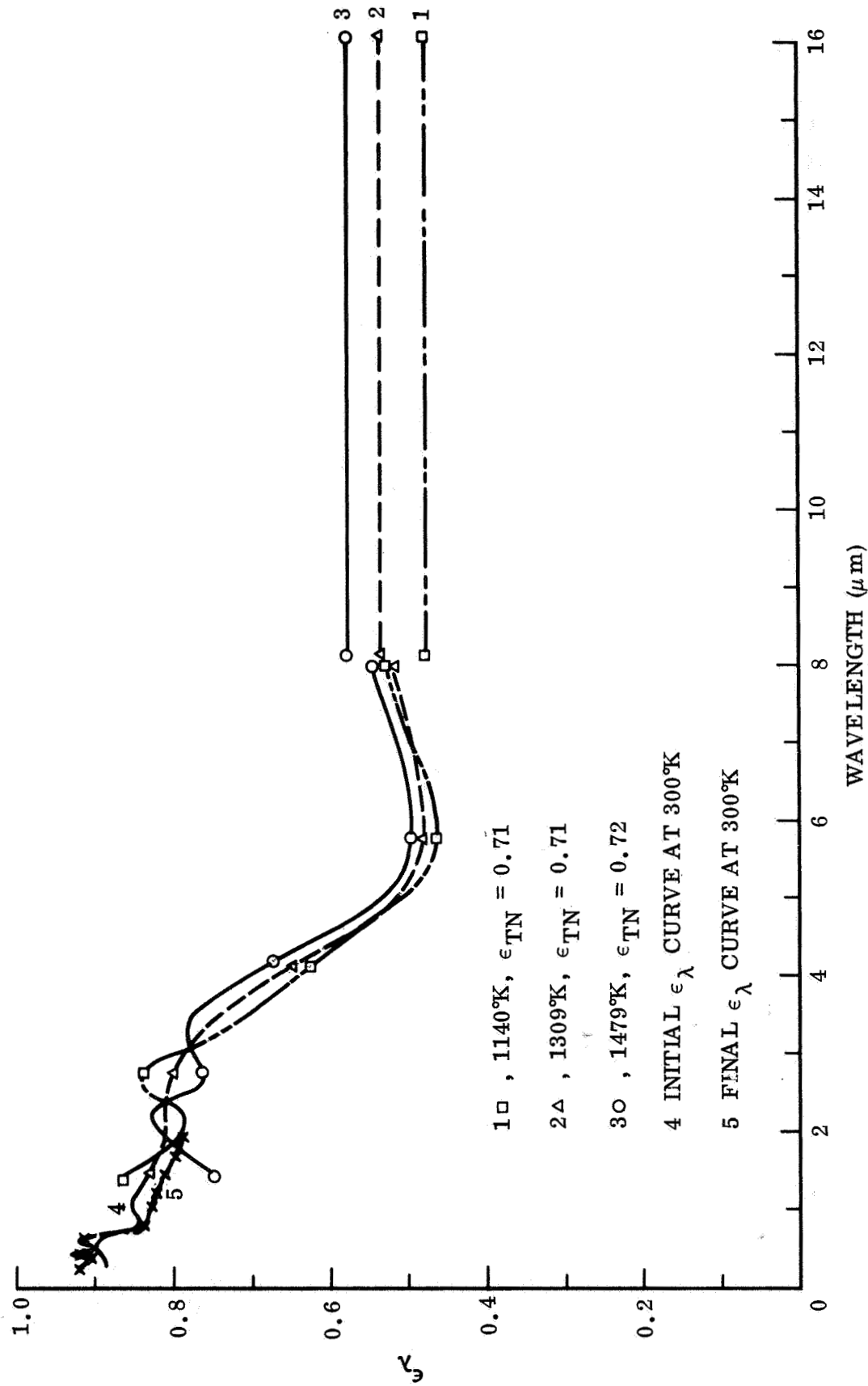
Fig. 54 Spectral Emittance Characteristics of Oxidized TD Ni Cr Sample
A2 after 5 Mach 2.1 Flow Test Cycles

1□ , 1140°K, ϵ_{TN} = 0.71

2△ , 1309°K, ϵ_{TN} = 0.71

3○ , 1479°K, ϵ_{TN} = 0.72

4 INITIAL ϵ_λ CURVE AT 300°K

5 FINAL ϵ_λ CURVE AT 300°K

by the radiometer filters is shown in Table 26 for the four nominal temperatures that these samples were tested at in vacuum.

Table 26

BLACKBODY ENERGY DISTRIBUTION IN THE SPECTRAL BANDS MEASURED
BY THE RADIOMETER AT FOUR TYPICAL TEST TEMPERATURES FOR THE
OXIDIZED TD Ni Cr SAMPLES

Temperature (°K)	Percentage of E_b at $\lambda < 1.45\,\mu$m	Percentage of E_b at $1.45\,\mu$m $\leq \lambda \leq 8\,\mu$m	Percentage of E_b at $\lambda > 8\,\mu$m
810	0	77	23
1145	3	87	10
1310	5	87	8
1480	10	84	6

8.4 CB 129Y/ALLOY WITH VH101 COATING

Three separate samples of this coated alloy were tested in the static air, Mach 1.1 and 2.1 air-flow environments. The static air test cycles were made on Sample No. E1 at temperatures up to 1680° K. The Mach 1.1 and 2.1 flow tests were conducted on Samples E7 and E8, respectively, at temperatures up to 1648° K. Preliminary tests in vacuum were made on all three samples to calorimetrically determine their total hemispherical emittance at temperatures of approximately 870° K and 1080° K. Similar tests were made on Samples E1 and E7 after the cycling tests were completed to determine the changes in emittance as a result of the cycling tests. Total and spectral emittance data were also obtained from these pre- and post-exposure tests in vacuum. Higher test temperatures in vacuum were not attempted in order to avoid changing the normal composition of the coating-substrate interface.

The initial room-temperature spectral and total emittance characteristics of these samples were inferred from room temperature reflectance measurements which were made on 2.54-cm diameter witness-sample disks that were coated along with the strip samples. With the exception of the infrared $\rho\lambda$ measurements, all these measurements were repeated on the strip samples after their cyclic exposure tests to determine

the changes in sample properties for each different flow-environment exposure. Photographs of the test strip samples along with one untested strip were also taken to show the changes in visual appearance that occurred as a result of the test exposures.

A description of each sample and of the instrumentation used to conduct the tests is given in the following paragraphs before discussing the results.

8.4.1 Sample E1

This sample was 30.5-cm long by 2.56-cm wide by 0.114-cm thick, (after coating), and thickness measurements made before and after the coating was applied indicated the coating thickness to be between 2 and 3 mils. Two 0.318-cm diameter holes were drilled through each end of the strip to facilitate clamping the sample to the power electrodes of the test apparatus. Three small holes, approximately 0.064-cm diameter by 0.254-cm deep, were also drilled into one edge of the strip, prior to coating, to facilitate the attachment of thermocouples to the sample without exposing any bare, unprotected substrate metal. These holes were located at the center of the strip and 0.98-cm above and below the centerline hole.

For the initial tests in vacuum, the sample was instrumented as follows. Two Pt-6%/Rh/Pt-30% Rh thermocouples, (3-mil bare wires with a spherical bead junction), were embedded in the edge holes above and below the centerline hole and held in place by wedging each junction in its hole with short lengths (approximately 0.25-cm) of 10-mil diameter platinum wire. These thermocouple locations served to define the center test area of the sample and the Pt-6% Rh lead wires served as voltage-drop measuring leads for determining the applied power to the test section. The centerline hole of the sample was instrumented with a BLH Inc. Micro-Miniature Sheathed thermocouple, (Pt/Pt-13% Rh inside a 0.035-cm diameter by 2.54-cm long Tantalum sheath), which also was held in place by wedging with platinum wires. This latter thermocouple was utilized as the control thermocouple to the temperature controller during the initial tests in vacuum but open-circuited during the sample heating phase of Cycle 1 at approximately T_S = 1550° K. An examination of the thermocouple indicated that the failure was due to rapid oxidation of the Tantalum sheath in combination with sample

8-47

vibration which caused the tip (junction end) to shear off at the edge of the test strip. By the time this failure occurred, which shut down the sample power and terminated the test cycle, both of the adjacent thermocouples had also open-circuited due to one or both leads falling off the sample. Therefore, neither of these techniques proved useful for the high temperature cyclic tests.

For the tests in vacuum, although the instrumentation survived and provided adequate temperature control and power-measurement data, reliable sample temperature measurement was not obtained. For the 1080° K-test in vacuum, (determined by the optical pyrometer method), the small platinum thermocouples were noted to read from 13° K to 40° K lower than the pyrometer determined temperature at the edge of the sample adjacent to the thermocouple, and the sheathed thermocouple reading was on the order of 100° K lower. As a result of these observations at 1080° K, the preceding 845° K test temperature was obtained by adding a 10° K estimated correction to the highest thermocouple temperature reading.

After the first static air test cycle, the sample was removed from the test chamber and a fixture was added to hold two spring-loaded thermocouples against the back, center surface of the sample. These thermocouples were Pt/Pt-13% Rh fabricated from 10-mil diameter bare wires with the beaded-junction located at the tip of a small diameter, 7.6-cm long, two-hole alumina tube. The alumina tube passed through a stainless steel spring-loaded holder which was located approximately 5-cm behind the back surface of the sample. The thermocouples were first located with their junction tips at the back surface of the sample by adjusting the assembly in the threaded holder, then the spring loading was adjusted so that the junctions pressed firmly against the sample surface and would "follow" deflections of the sample surface up to ±0.25-cm in either direction.

After some preliminary testing to determine the thermocouple output for various sample temperatures, a Data Trak temperature control card was prepared to give the proper temperature-time program cycle and this method was used to make a rerun of Cycle #1 and for the remaining four static air test cycles. This method proved adequate for these tests and was also used for the cyclic tests of samples E7 and E8.

Another problem which occurred during the static air tests of sample E1 involved an electrical overload to the laboratory power supply (60 Amp, 220V) for the primary side of the sample power transformer. This problem occurred twice during the first and second test cycles while the sample was operating at 1645° K. To prevent reoccurrence, the power limit setting on the temperature controller was lowered, thereby limiting the maximum power applied to the sample and as a result, the maximum sample temperature attained for the last three test cycles was reduced to 1520° K.

After completing the five static air test cycles, the sample was removed from the test chamber, re-instrumented with three new thermocouples, as originally described, and re-installed for two post-test measurements in vacuum at 863° K and 1091° K.

8.4.2 Sample E7

This sample was 30.5-cm long by 1.28-cm wide by 0.118-cm thick (after coating) with a narrowed test section at the center which was 1.02-cm wide by 1.801-cm long. A single 0.318-cm diameter hole was drilled through each end to facilitate clamping the strip to the power electrodes of the test apparatus. Three thermocouple holes, as described for Sample E1, were located at the centerline of the test section and 1.3-cm above and below the centerline hole. This arrangement placed the upper and lower thermocouples about 0.32-cm above and below the narrowed test section; consequently, a correction to the applied power measurements for this sample was required during the tests in vacuum in order to determine the applied power to the test section alone. This was done by multiplying the total applied power measurement by the ratio of the test section area to the total area of the strip (including the notched out areas) between the thermocouples. This empirical method resulted in ϵ_{TH} determinations for these narrow test strips that were in good agreement with the values determined by the conventional method for Sample E1.

Preliminary tests of this sample in vacuum were made at 868° K and 1076° K to determine the initial emittance characteristics of the sample. For these tests the sample was instrumented with three Pt 6% Rh/Pt 30% Rh thermocouples (3-mil), as described for Sample E1, and the two spring-loaded thermocouples were left in place to obtain a

calibration of their output vs. sample temperature. For the test at 1076° K, the center thermocouple temperature reading was observed to be about 28° K lower than the optical pyrometer-determined temperature at the thermocouple location, presumably due to poor thermal contact between the thermocouple junction and the sample. On the basis of this observation an estimated correction of +20° K was made to the thermo-couple readings obtained during the preceeding test to obtain a T_s value of 868° K for that test.

Following the preliminary vacuum tests, the sample was exposed to five Mach 1.1 flow test cycles at temperatures up to 1645° K. The sample temperature for all five cycles was controlled with a Data Trak Program Control Card in conjunction with the spring loaded control thermocouple and temperature controller. No power overload problems were experienced with this smaller sample. All of the sample thermocouples located at the edge of the sample remained attached to this sample, however, due to the convective cooling effects and to shorting of the lead wires, their temperature readings were from 200 to 500° K lower than the optical pyrometer temperature determinations. Consequently, all the sample test temperatures were determined by the pyrometer method.

After completing the five Mach 1.1 test cycles, the test chamber was opened up to straighten out the thermocouple leads, then pumped out and retested in vacuum at 797° K and 1091° K to determine the post test values of ϵ_{TH}. Corrections similar to those made in the preliminary vacuum tests for the thermocouple readings, but larger, were required to match the pyrometer temperature.

8.4.3 Sample E8

This sample was similar to Sample E7, 30.5-cm long by 1.272-cm wide by 0.118-cm thick (after coating). The narrowed test section at the center was 1.012-cm wide by 1.830-cm long. Preliminary tests in vacuum were made at 875° K and 1077° K to determine the initial emittance characteristics of the sample. The sample was instrumented in the same manner as described for Sample E7 and the same methods were used to determine the applied power to the test section and to determine the

average temperature of the test section. At 1077° K the thermocouple temperature readings were approximately 15° K lower than the pyrometer determined temperatures at the thermocouple locations, therefore an estimated correction of +10° K was made to the thermocouple readings at the lower test temperature to obtain the T_s value of 875° K.

Following the preliminary vacuum tests, the sample was subjected to five Mach 2.1 flow test cycles at temperatures up to 1648° K. The sample temperature for all five cycles was programmed and controlled in the same manner as for Sample E7. Sample temperatures were considerably less stable than for the static air and Mach 1.1 flow tests, consequently the temperature and radiometer readings were more variable and subject to error. The reason for this "noise" is attributed to more severe vibrations of the sample and test chamber during these test conditions which in turn affected the thermal contact between the back surface of the sample and the junction of the spring-loaded temperature control thermocouple.

No post-exposure tests in vacuum were obtained for this sample because the original edge-located thermocouples all separated from the sample and left the attachment holes filled with a hard, glassy material that was difficult to remove.

8.4.4 Results

The visual appearance of all three Cb 129Y/VH101 samples changed considerably as a result of their test exposures. These changes can be seen in the photograph of the three samples along with an untested (Reference) sample strip which is shown in figure 55. The initial appearance of the samples was the same as that of the reference strip in the photo, a uniform dull, metallic gray color. The color of Sample E1 after five static air test cycles changed from top to bottom to light brown, with some areas lighter than others, particularly a narrow horizontal band located at the center of the strip. The test-section area of Sample E7, after five Mach 1.1 flow test cycles, was similar in appearance to the darker brown areas of Sample E1. Above and below the test section, the appearance was mottled with some areas lighter in color and some areas, particularly the upper third of the strip, a darker dull gray similar to the original color. The test-section area of Sample E8, after five Mach 2.1 flow test
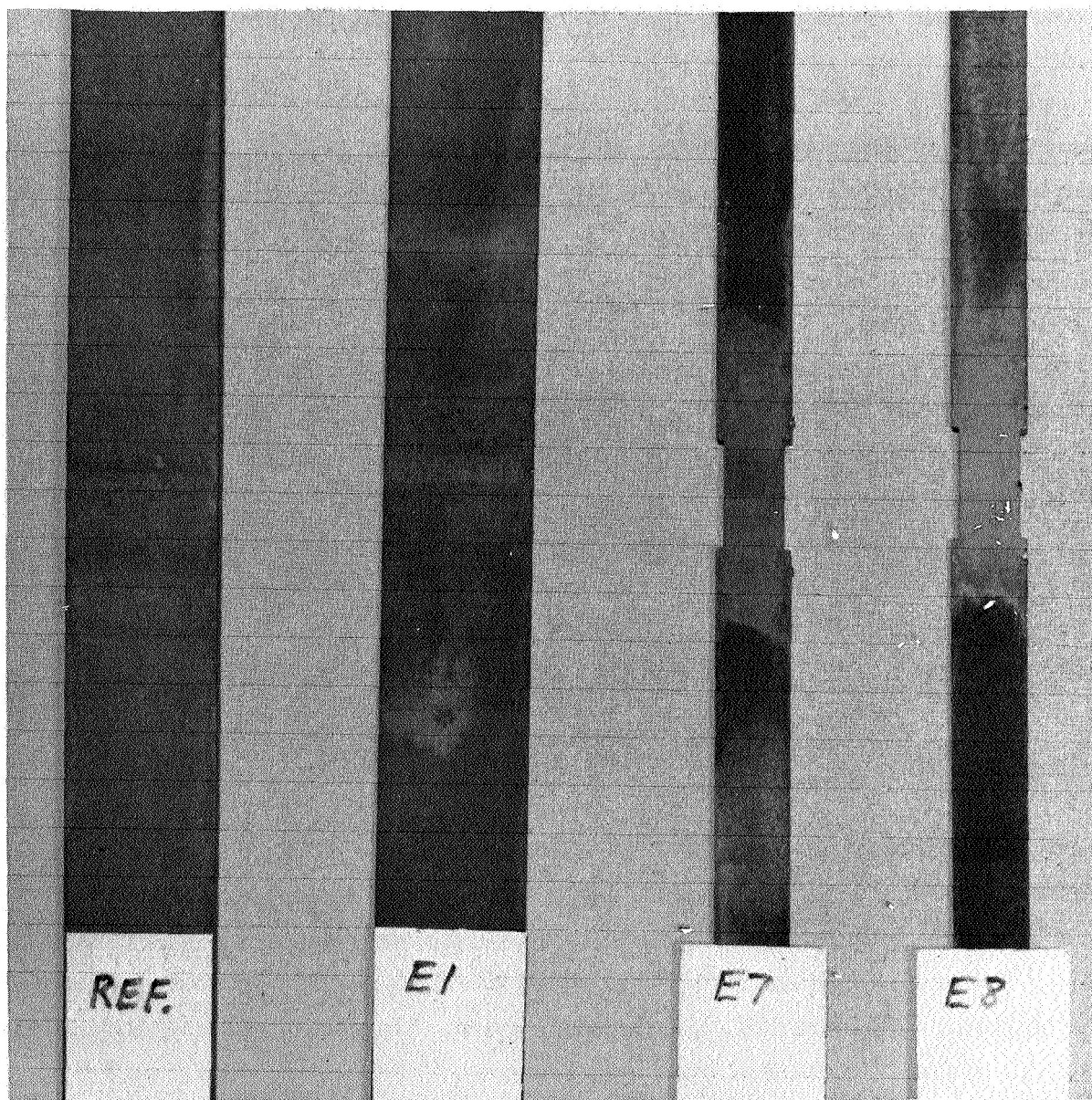
Fig. 55 Visual Appearance of Cb129Y Samples with VH-101 Coating

cycles was significantly lighter in color than either Sample E1 or E7. Above and below the test area, the appearance was similar to that of Sample E7, i.e. mottled gray and light brown areas. These changes in visual appearance correlate with the changes in emittance that were observed to occur during the preliminary vacuum tests and the first exposure test cycles. The color variations indicate that the color changes were flow dependent; however, the emittance data discussed next indicates that the total emittance values of the samples were not significantly different from one another.

Initial and final emittance values for the Cb 129Y/VH101 samples at approximately 870° K and 1080° K in vacuum are shown in Table 27 and the total normal emittance values measured during each of the five test cycles for each sample are listed in Table 28. As noted at the bottom of Table 27 ϵ_{TH} determinations for Samples E7 and E8 are not as reliable as for Sample E1 because of the temperature and power approximations that were required for these samples. Since these approximations were made in a consistent manner, however, the values are useful for indicating the relative change in ϵ_{TH} for these samples. Except for the 870° K tests, the temperatures listed in these two tables are the temperatures determined at the center of the test sections by the pyrometer method either just before or just after (or both), the radiometer and/or power measurements were made.

The initial ϵ_{TN} values in vacuum are seen in Table 27 to range between 0.46 and 0.55 at the nominal 860° K test temperature and between 0.80 and 0.86 at 1080° K. The corresponding ϵ_{TH} values averaged 0.55 at the lower temperature and ranged between 0.79 and 0.88 at the higher temperature. This data confirms the initially low total emittance of the samples and shows that the total emittance of the samples was rapidly increasing as these tests were being made. The total time involved in making the vacuum tests was approximately 1 hour for each sample.

The post-exposure vacuum test results for Sample E1 and E7 indicate that the total emittance values for these two samples were approximately the same, (discounting the approximate ϵ_{TH} values for Sample E7). The ϵ_{TN} value for Sample E7 at 1091° K is about 5% higher than for Sample E1, but at the lower temperature both are about the same. The results for Sample E1 indicate the total hemispherical emittance

Table 27

TOTAL NORMAL AND TOTAL HEMISPHERICAL EMITTANCE VALUES FOR
Cb 129Y/VH101 SAMPLES BEFORE AND AFTER CYCLING TESTS

Sample No.	Before Testing		After Testing	
	T_s (° K)	$\epsilon_{TH}/\epsilon_{TN}$	T_s (° K)	$\epsilon_{TH}/\epsilon_{TN}$
E1 (Static Air Tests)	845	0.54/0.46	863	0.78/0.75
	1084	0.88/0.86	1091	0.72/0.72
E7 (M1.1 Flow Tests)	868	(0.57)/0.51	1091	(0.81)/0.76
	1076	(0.82)/0.80	1169	(0.80)/0.76
E8 (M2.1 Flow Tests)	875	(0.57)/0.55	--	--
	1077	(0.79)/0.82	--	--

Note: ϵ_{TH} values for Samples E7 and E8 (in parentheses) are based on average T_s
and applied power estimates for the narrowed test section area and are less
certain than the values obtained for Sample E1.

to be between 0 and 4 percent higher than the corresponding total normal emittance at
these temperatures.

Table 28 shows that after the first test cycle, ϵ_{TN} for each sample was essentially
independent of temperature between 1060° K and 1650° K and was constant for the last
four test cycles to within ±3% of the average ϵ_{TN} value. The total normal emittance
values for Samples E7 and E8 indicate that this property was essentially the same for
these two samples and therefore was not significantly affected by the differences in
flow velocity. Total normal emittance values for Sample E1 during the last three static
air test cycles were from 10 to 15 percent lower than for Samples E7 and E8, but the
values obtained in the post-exposure vacuum tests were about the same as for Sample
E7. Whether the total emittance of this sample was really lower during these last
three test cycles, and then increased during the post-exposure vacuum test, was not
determined. The spectral emittance determinations discussed next, appear to con-
firm both the low ϵ_{TN} value at 1520° K during the last test cycle, and the higher ϵ_{TN}
values during the post-exposure vacuum tests. One possible explanation is that when
the sample strip was re-mounted in the test chamber for the final vacuum tests, its

Table 28

TOTAL NORMAL EMITTANCE VALUES FOR Cb 129Y/VH101 SAMPLES
BEFORE, DURING AND AFTER CYCLING TESTS

Cycle No.	Sample E1 (Static Air Tests)		Sample E7 (M1.1 Flow Tests)		Sample E8 (M2.1 Flow Tests)	
	T_s (°K)	ϵ_{TN}	T_s (°K)	ϵ_{TN}	T_s (°K)	ϵ_{TN}
Preliminary Tests in Vacuum	845[1]	0.46	868[1]	0.51	875[1]	0.55
	1084	0.86	1076	0.80	1077	0.82
#1	—	—	—	—	—	—
	1221	0.85	1452	0.67	—	—
	1680	0.75	1645	0.67	1630	0.76
#2	1099	0.70	1228	0.73	1185	0.73
	1381	0.65	—	—	1467	0.69
	1641	0.71	1627	0.70	1648	0.73
#3	1073	0.67	1217	0.72	1194	0.74
	1335	0.66	1479	0.69	1459	0.71
	1520	0.66	1612	0.74	1647	0.72
#4	1061	0.66	1196	0.74	—	—
	1327	0.65	1423	0.68	1465	0.69
	1505	0.65	1642	0.73	1641	0.73
#5	1065	0.66	1160	0.75	1170	0.73
	1355	0.63	1416	0.72	1463	0.69
	1520	0.66	1613	0.75	1643	0.71
Post-Cyclic Tests in Vacuum	863[1]	0.75	—	—	— [2]	—
	1091	0.72	1091	0.76	—	—
	—	—	1169	0.76	—	—

Notes:

(1) These temperatures were determined from thermocouple readings at the edges of the sample strips and are less certain than the remaining T_s values which were determined from optical pyrometer readings at the centers of the sample strips.

(2) No post-test data in vacuum obtained for Sample E8.

centerline may have been raised or lowered with respect to its original position so that the radiometer was viewing the darker area on either side of the narrow light colored band that formed at the center of this sample.

Vertical temperature gradients for Sample E1 were essentially negligible at all test temperatures, and the horizontal (center-to-edge) gradients appeared to average about 5° K at T_s = 1090° K and about 20° K at T_s = 1640° K. Most of this drop occurred in the region immediately adjacent to the edge so that approximately 80% of the central sample test area was uniform and equal to T_s . Therefore no corrections were made to the temperature readings for this sample.

For the narrow test-section samples (E7 and E8), edge temperatures at the horizontal centerline of the test section were from 4° K (at 1075° K) to 10° K (at 1640° K) cooler than the center temperatures. The vertical gradients were much larger and variable, and depended both on the sample temperature and on the test-flow conditions. At temperatures of 1090° K in vacuum, the top and bottom temperatures of the test section, (measured along the vertical centerline) averaged 16° K lower than the center temperature. At the low, medium and high cyclic test temperatures for Sample E7, the vertical gradient increased to approximately 40° K, 65° K and 75° K, respectively, and for Sample E8 were approximately 25° K, 45° K and 60° K. These gradients were also steepest in the region immediately adjacent to the upper and lower ends of the test sections so that the center area viewed by the radiometer was essentially uniform and equal to T_s .

To determine the true temperature (T_s) values for these samples from the optical pyrometer brightness temperature (T_B) readings, the initial room-temperature ϵ_λ value at λ = 0.65 μm was used. For these samples this value was 0.70. In addition, the transmittance of the glass window through which all the pyrometer readings were made was taken as 0.92. Since post-test reflectance measurements of the samples indicated that significant changes in ϵ_λ at 0.65 μm had occurred during the tests, T_s values were redetermined on the basis of the latter ϵ_λ values. These changes are shown in Table 29 along with the changes in the other room temperature properties of the samples. The property changes are assumed to have occurred during the initial

Table 29

INITIAL AND FINAL ROOM TEMPERATURE PROPERTIES OF
Cb 129Y/VH101 SAMPLES

	α_s	ϵ_λ (Pyrom) $\lambda=0.65\mu m$	ϵ_{TN} (DB-100)	ϵ_λ $(0.3\,\mu m \leq \lambda \leq 1.8\,\mu m)$	ϵ_λ $(2\,\mu m \leq \lambda \leq 16\,\mu m)$
Initial	0.68	0.70	0.37	See Figure 56	See Figure 56
Final					
E1	0.66	0.69	0.83	See Figure 56	Not Measured
E7	0.72	0.74	—	See Figure 56	Not Measured
E8	0.63	0.61	—	See Figure 56	Not Measured

vacuum and first exposure cycle tests, therefore the redetermined T_s values were used for the measurements made during and after the second test cycle for each sample.

For Sample E1, the change in ϵ_λ at $0.65\,\mu m$ was from 0.70 to 0.69. The effect of this change on T_s and on the total emittance determinations is negligible, therefore no corrections were made. For Sample E7, ϵ_λ at $0.65\,\mu m$ appeared to increase from 0.70 to 0.74. The effect of this change was to lower the original T_s values by 4° K at 1200° K, by 6° K at 1430° K, and by 8° K at 1650° K. These temperature corrections in turn resulted in changes for the total emittance of Sample E7 at +0.01, +0.015 and +0.02, respectively. For Sample E8, ϵ_λ at $0.65\,\mu m$ appeared to drop from 0.70 to 0.61. The effect of this change was to increase the original T_s values by 9° K at 1160° K, by 14° K at 1450° K, and by 17° K at 1640° K. These temperature changes resulted in total emittance changes of -0.02, -0.025 and -0.03 respectively. All of these changes have been incorporated into Tables 27 and 28.

Initial and final spectral emittance results for the three Cb 129Y/VH101 samples at their nominal test temperatures of 870° K, 1090° K and 1630° K (1520° K for Sample E1), are shown in figures 56, 57, and 58. For comparison the room temperature emittance characteristics of the samples before and after their exposure-test cycles are also ·shown on each figure. These room-temperature characteristics were determined

Fig. 56 Spectral Emittance of Cb129Y/VH-101 Samples at 870°K Before and After Five Test Cycles

AFTER

BEFORE

O–E1– ●
Δ–E7– ▲
□–E8– ◻

1 FROM INITIAL ρ_λ DATA AT 300°K

2 FROM FINAL ρ_λ DATA FOR E1

3 FROM FINAL ρ_λ DATA FOR E7

4 FROM FINAL ρ_λ DATA FOR E8
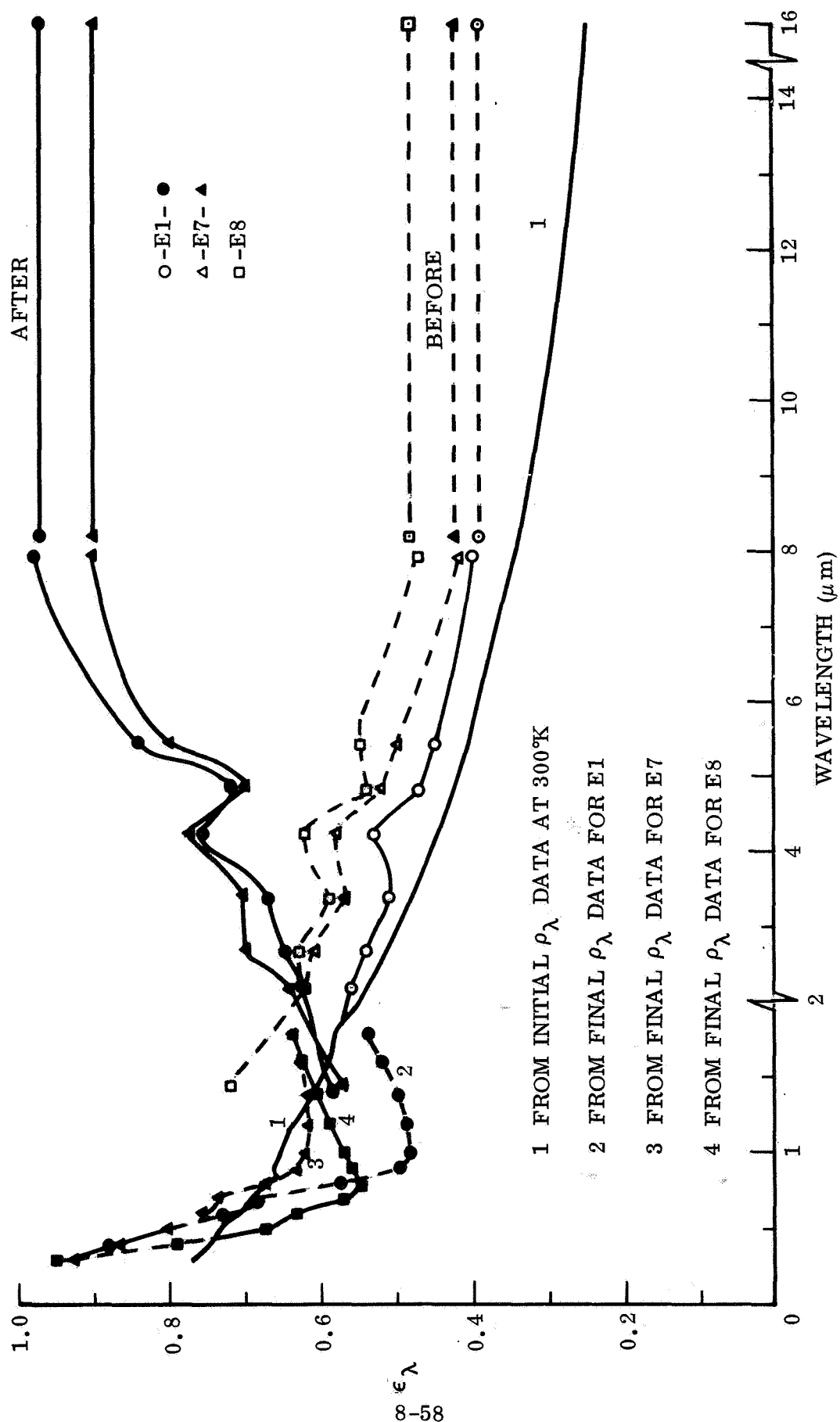
WAVELENGTH (μm)

ϵ_λ
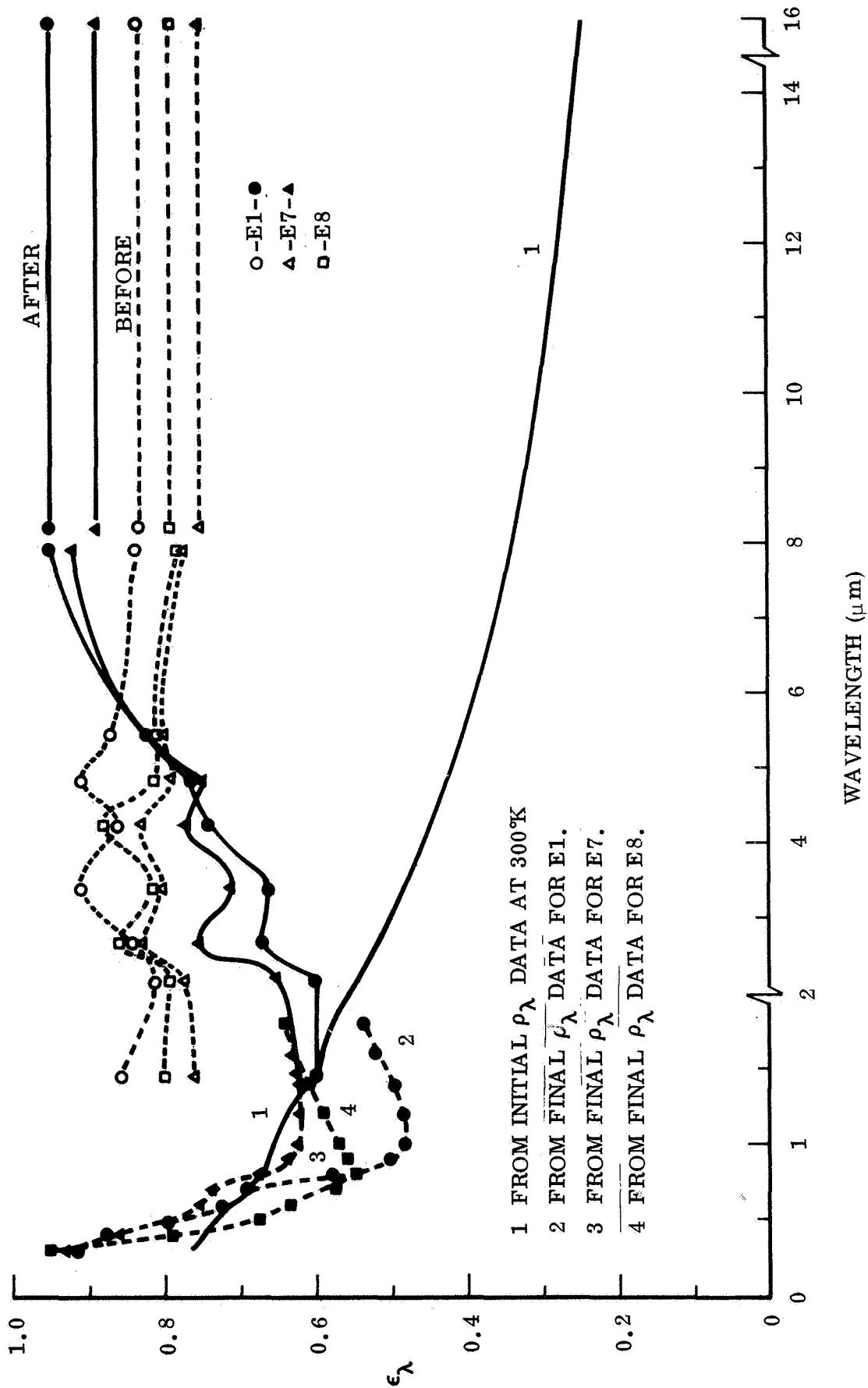
Fig. 57 Spectral Emittance of Cb129Y/VH-101 Samples at 1090°K Before and After Five Test Cycles
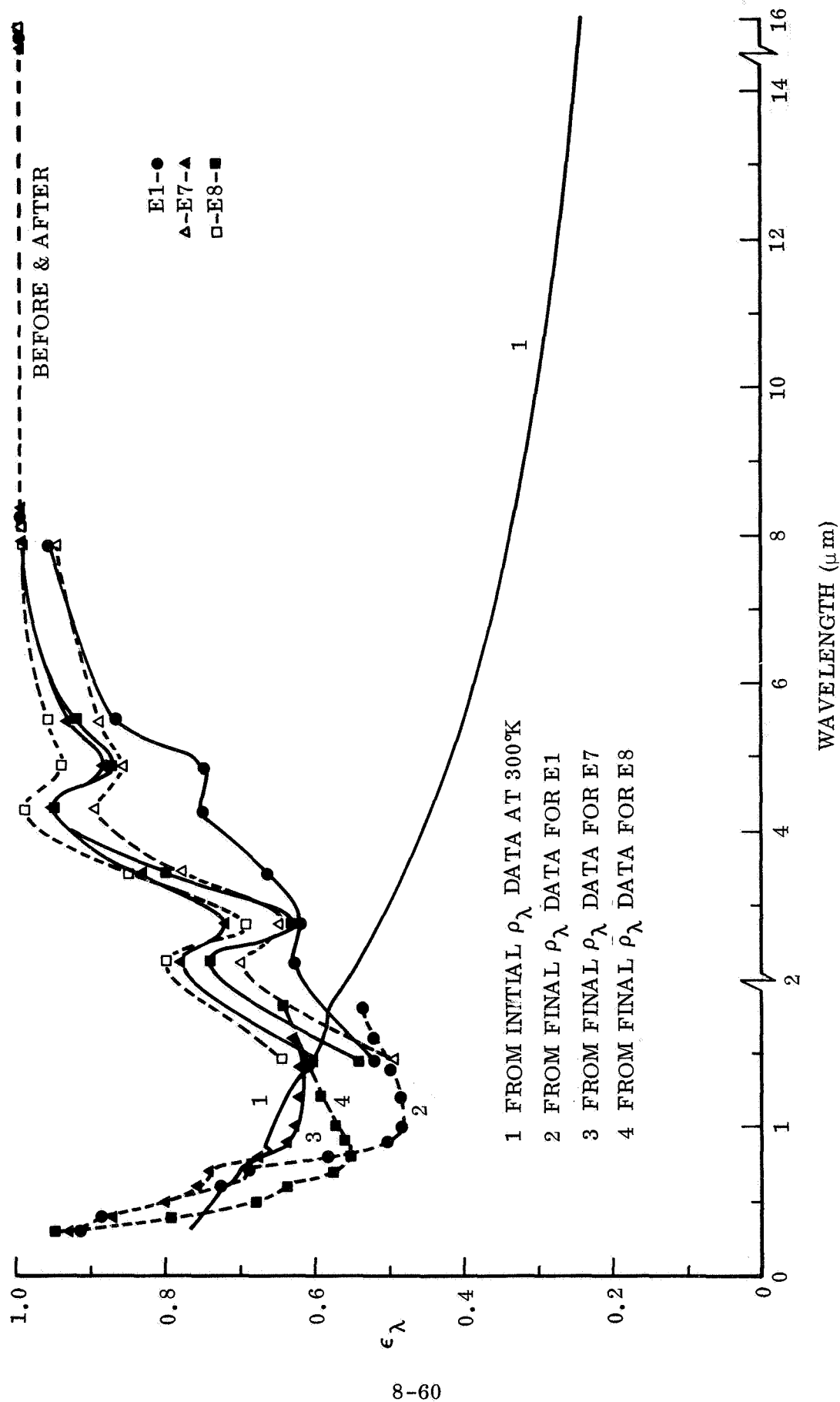
Fig. 58 Spectral Emittance of Cb129Y/VH-101 Samples at 1630°K Before and After Five Test Cycles

from the pre- and post-test reflectance measurements. The elevated-temperature data points were determined with the radiometer during the initial vacuum tests and the first test cycles, and then again during the final test cycles and post-exposure vacuum tests. Post test reflectance measurements for the spectral region beyond $\lambda = 1.8\,\mu$m were not obtained. Measurements in the region $0.3\,\mu$m $\leq \lambda \leq 1.8\,\mu$m show significant changes for each sample after testing, corresponding with the changes in visual appearance.

Figure 56 shows that the initial ϵ_λ characteristics for all three samples at 870° K in vacuum were similar to each other and not greatly different from the initial room temperature characteristics. The spread of the ϵ_λ values for the three samples is attributed to the larger uncertainty in the T_s determinations at this temperature and to the fact that the ϵ_λ characteristics of the samples were rapidly changing during these initial vacuum tests. Post test measurements at this temperature for Samples E1 and E7 and show the final emittance characteristics of these two samples to be similar to each other and the ϵ_λ values at wavelengths longer than $3\,\mu$m to be significantly higher than initially. The ϵ_{TN} values indicated by these curves are in good agreement with the measured ϵ_{TN} values at these temperatures both before and after the exposure test cycles.

Figure 57 shows the initial and final ϵ_λ determinations for these samples at approximately 1090° K in vacuum. The initial set of data at this temperature indicates that the emittance of all three samples had already changed considerably from the "as-received" emittance characteristics and, at this stage of testing, were higher in the $1.45\,\mu$m $\leq \lambda \leq 5\,\mu$m region than the final emittance characteristics for this region. These high spectral emittance values are consistent with the high ϵ_{TN} measurements that were obtained for these samples at this time. The final set of data, from Samples E1 and E7, indicates that the spectral emittance at $\lambda < 5\,\mu$m dropped while the emittance at $\lambda > 6\,\mu$m continued to rise during the exposure-test cycles of these samples. The net effect on the total emittance of the samples was a drop of between 5 to 15 percent.

Figure 58 shows the initial and final ϵ_λ data for these samples during the first and last test cycles at approximately 1630° K. The similarity of the two sets indicates that the sample emittance values were essentially stabilized by the time this temperature was attained in the first test cycle, and that they did not change appreciably during the subsequent test cycles except possibly for static-air tested sample (E1). The final ϵ_λ data for sample E1 was determined at 1520° K, i.e., about 100° K lower than for Samples E7 and E8, consequently the lower ϵ_λ values for Sample E1 may be due to a real temperature dependency of ϵ_λ rather than to a difference in the sample emittance characteristics. This explanation tends to be supported by the temperature dependency data which is presented in Figure 59.

Figure 59 shows the apparent temperature dependency of ϵ_λ for Sample E7 after its five Mach 1.1 flow-test cycles, and since the emittance characteristics of the other two samples were similar, their temperature dependency is assumed to be similar also. The figure shows that ϵ_λ generally increases with increasing temperature, particularly between 1100° K and 1600° K. At the higher temperatures, emittance bands appear to develop in the 1 to 5 μm region and apparently shift towards shorter wavelengths as the temperature increases. The net effect of these changes in spectral characteristics is to maintain ϵ_{TN} at approximately a constant value of 0.75 over the temperature range from 800° K to 1600° K.

The relative importance of the spectral range covered by the radiometer data in these figures to the total emittance of the samples at four typical test temperatures is summarized in Table 30. This table shows the percentages of total energy radiated by a black body at each temperature in the spectral region below $\lambda = 1.45 \mu$m; between $\lambda = 1.45 \mu$m and $\lambda = 8 \mu$m, the region covered by the eight narrow-band radiometer filters; and beyond $\lambda = 8 \mu$m, the region covered by the 8 to 16 μm broadband filter. The table shows that even through ϵ_λ values approaching 1.0 were obtained for these samples with the 7.95 μm narrow-band filter and with the 8 to 16 μm broad-band filter, the influence of high emittance in this spectral region on the high temperature total emittance of the samples is relatively small. At 870° K, less than 20% of the total black body energy is radiated at these wavelengths, and at 1640° K less than 5% of the total energy is radiated at wavelengths longer than 8 μm.
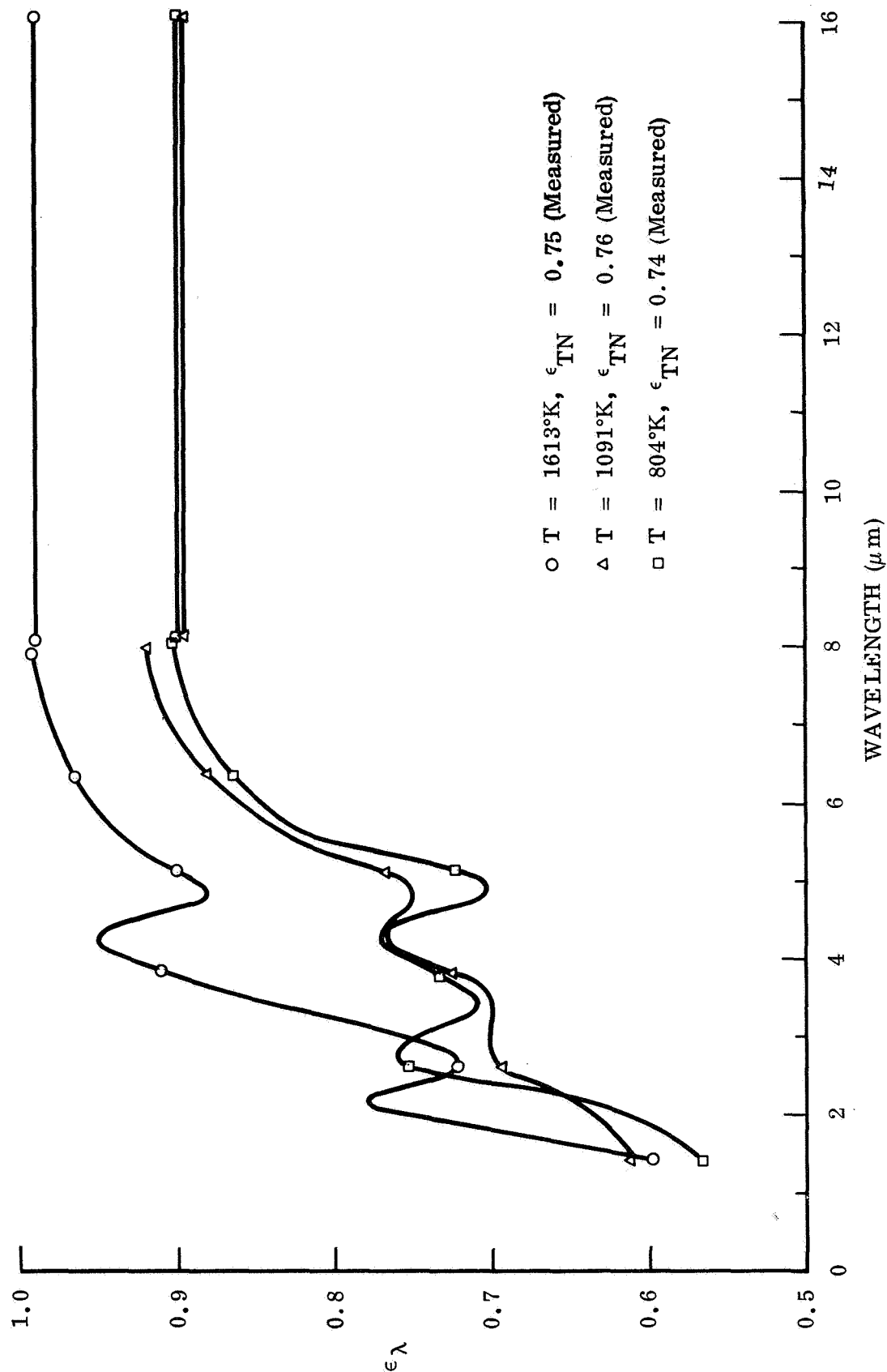
Fig. 59 Temperature Dependence of Spectral Emittance of Cb129Y/VH-101 Sample E7 After Five Mach 1.1 Flow Test Cycles

Table 30

SUMMARY OF BLACKBODY ENERGY DISTRIBUTION IN THE SPECTRAL BANDS
MEASURED BY THE RADIOMETER AT TYPICAL TEST TEMPERATURES
FOR THE Cb 129Y/VH101 SAMPLES

Temperature (°K)	Percentage of E_b at $\lambda < 1.45\,\mu m$	Percentage of E_b at $1.45\,\mu m \leq \lambda \leq 8\,\mu m$	Percentage of E_b at $\lambda > 8\,\mu m$
870	0.3	80.6	19.1
1090	1.8	86.4	11.8
1460	8.6	85.5	5.9
1640	13.6	82.0	4.4

8.5 CB 752 ALLOY WITH R512E COATING

Static air and air-flow exposure tests were conducted on three separate samples of this coated alloy. The static air test cycles were conducted on Sample No. B3 at temperatures up to 1600° K, and the Mach 1.1 and 2.1 flow tests were conducted on Samples B8 and B7, respectively, at temperatures up to 1650° K. Before the cycling tests, preliminary steady-state temperature tests in vacuum were made on Samples B3 and B7 to calorimetrically determine the total hemispherical emittance of these samples at 875° K and 1080° K. Similar tests were made on Samples B3 and B8 after the cycling tests were completed to indicate the changes in ϵ_{TH} at these two temperatures as a result of the cycling tests.

The initial room temperature spectral and total emittance characteristics of these samples were inferred from room temperature reflectance measurements made on 2.54-cm diameter witness-disk samples that were coated along with the strip samples. Some of these room-temperature reflectance measurements were also made on the strip samples after the cycling tests to verify the changes that were observed to occur. Photographs of the tested strip samples along with one untested strip were also taken to show the changes in visual appearance that occurred as a result of the test exposures.

8-64

A description of each sample and of the instrumentation used to conduct the tests is given in the following paragraphs before discussing the results.

8.5.1 Sample B3

This sample was 30.5-cm long by 2.757-cm wide by 0.117-cm thick (after coating), and thickness measurements made before and after coating indicated that the coating thickness was approximately 0.0064-cm. For the initial tests in vacuum, the sample was instrumented with three Pt 6% Rh/Pt 30% Rh, (3-mil wire), thermocouples which were embedded in three 0.064-cm diameter holes, approximately 0.25-cm deep, that were drilled into the edge of the strip prior to coating. The holes were located at the center of the strip and 1-cm above and below the centerline hole. The thermocouples were held in place by wedging each junction into its hole with a small bead of platinum, taking care to insure that the lead wires were not shorted together outside the hole. This method of instrumentation proved sufficient for obtaining the initial temperature and power measurements needed for the ϵ_{TH} determinations in vacuum at temperature up to 1100° K; however, the leads fell off the sample during the first and second static air test cycles, presumably because of reactions with the silica-type coating at temperatures above 1400° K.

For the first static air test cycle, an attempt was made to control the temperature of the sample using a Data Trak Control Card in conjunction with the temperature controller and a Pt/Pt-13% Rh spring-loaded thermocouple which pressed against the back center surface of the sample. Although this method worked satisfactorily for some of the other samples, erratic control was obtained for this sample, apparently because of test chamber vibrations and varying contact pressure between the thermocouple junction and the sample. Consequently, sample temperatures during the final four test cycles were controlled manually by varying the sample power to obtain approximately the same heating and cooling rates and steady-state temperatures as would have been obtained using the Data-Trak Program Card.

The maximum temperatures obtained during the five static-air cycles were between 1563° K and 1599° K. These temperatures were from 45° K to 80° K lower than the desired 1644° K for these tests because higher sample power levels could not be

obtained without overloading the laboratory's primary power supply to the power transformer for the test apparatus.

After completing the five static air test cycles, the sample was removed from the test chamber, re-instrumented with three new thermocouples, and then re-installed for post-test measurements in vacuum.

8.5.2 Sample B8

This sample was 30.5-cm long by 1.283-cm wide by 0.117-cm thick (after coating) with a narrowed test-section area at the center which was 0.990-cm wide by 1.810-cm long. Preliminary tests in vacuum were not performed on this sample and no instrumentation was attached to it until after the five Mach 1.1 flow-test cycles had been completed.

Sample temperatures during the five flow-test cycles were controlled manually, as described for Sample B3, using optical pyrometer readings of brightness temperature to indicate the true sample test temperatures. Subsequent analysis of this data indicated that the sample temperatures obtained were generally within 10° K of the 1089° K, 1366° K and 1644° K temperature levels desired for these tests.

After completing the five Mach 1.1 flow tests, the sample was removed from the test chamber and was instrumented with three Pt 6% Rh/Pt 30% Rh thermocouples in the same manner as described for Sample B3. The thermocouple hole locations for this sample were at the centerline and 1.27-cm above and below the centerline hole, which placed the upper and lower thermocouples about 0.32-cm above and below the narrowed test section area. Post-test measurements to determine ϵ_{TH} were then made in vacuum at 883° K and 1114° K.

8.5.3 Sample B7

This sample was similar to Sample B8, 30.5-cm long by 1.315-cm wide by 0.117-cm thick. The narrowed test section at the center of the strip was 1.843-cm long and 1.050-cm wide. Preliminary tests in vacuum were made at temperatures of 874° K

and 1086° K to indicate the initial emittance characteristics of the sample. For these tests, the sample was instrumented with three thermocouples in the same manner as described for Samples B3 and B8. The thermocouple hole locations were the same as for Sample B8, i.e., 1.27-cm above and below the centerline hole.

After the initial vacuum tests, five Mach 2.1 flow tests were performed with the sample temperatures controlled manually, as for Samples B3 and B8. Optical pyrometer readings were used to indicate the sample temperatures during each test cycle, and analysis of this data indicated that the temperatures obtained were generally within ±10° K of the desired 1089° K, 1366° K, and 1644° K levels desired for these tests. The three thermocouples originally attached to the sample all fell off early in the first flow-test cycle. No post-test measurements in vacuum were made on this sample because its properties appeared to be similar to those for Samples B3 and B8 and the thermocouple holes were difficult to reopen after the original thermo- couple leads fell off. An examination of these holes under a low-power microscope showed them to be partially filled with a hard glassy material which indicates that this particular coating material was highly reactive with platinum thermocouple leads at elevated temperatures.

8.5.4 Results

The visual appearance of all the Cb 754/R512E samples changed noticeably as a result of the test exposures. A photograph of the samples along with an as-received, (Reference), sample is shown in figure 60. The initial color of the untested surface was uniformly light metallic gray. Sample B3 after five static air test cycles was uniformly darker gray. Sample B8 after five Mach 1.1 flow test cycles was a darker brownish-gray above and below the central test area, but the test area was a light yellow-brown color. Sample B7, after five Mach 2.1 flow test cycles was similar in appearance to Sample B8 although the areas above and below the test area were not as dark as for B8.

Most of these changes in appearance were observed after the first test cycle and cor- relate with the changes in emittance that were observed to occur during the preliminary vacuum tests and the first exposure test cycle.
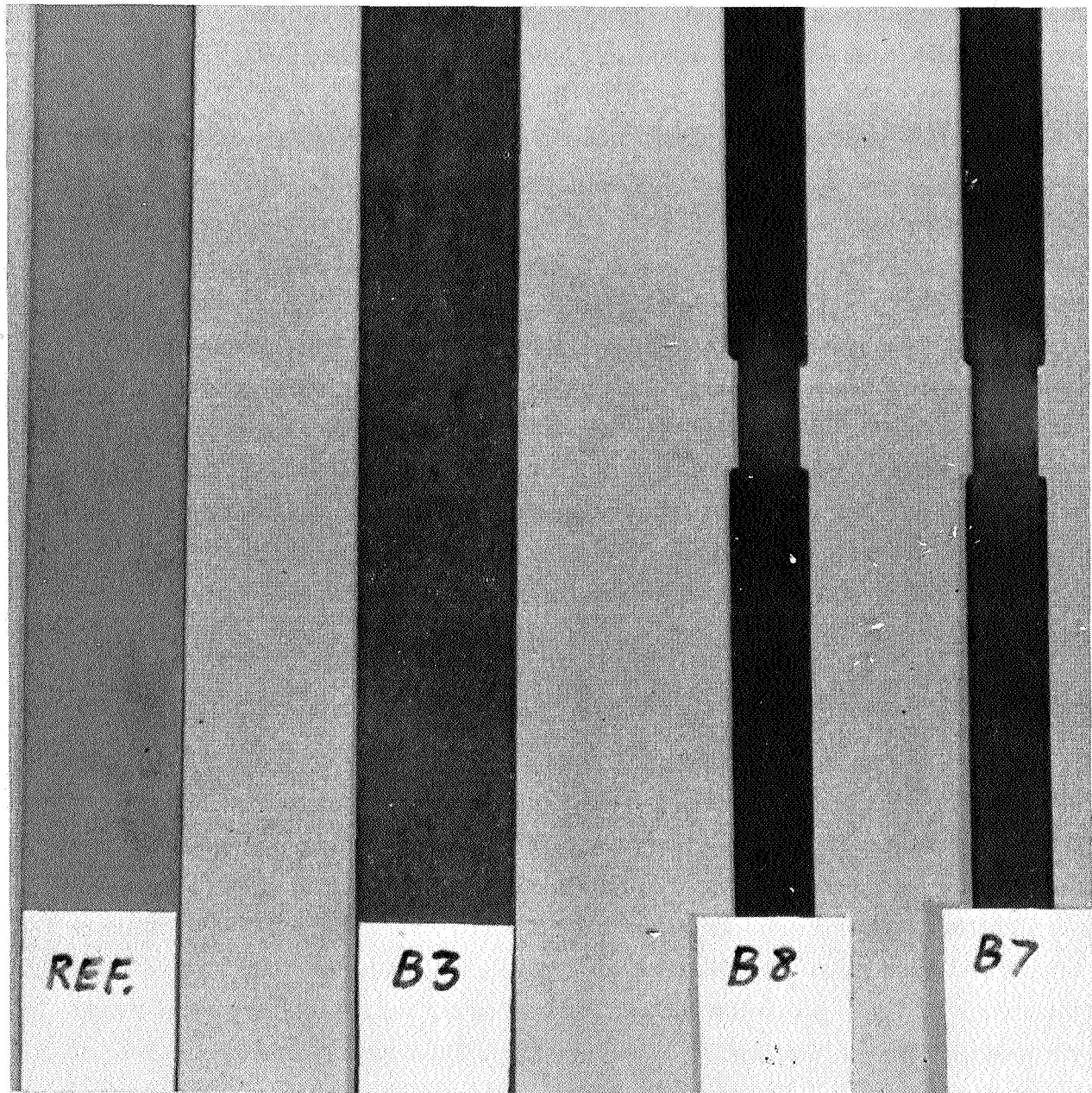
Fig. 60 Visual Appearance of Cb752 Samples with R512E Coating

Initial and final emittance values obtained for these samples at approximately 880° K and 1080° K in vacuum are shown in Table 31 and total normal emittance values measured during each of the five flow test cycles are listed in Table 32. As noted at the bottom of Table 31, ϵ_{TH} values for the two flow-test samples are not as reliable as for the static-air tested sample (B3) because the applied power to the narrowed test section and the average temperature of the test section has to be estimated from the actual power and temperature distribution measurements. The temperatures listed in these two tables are those determined for the center of the test-section area viewed by the radiometer.

Initial ϵ_{TN} values measured at 874° K and 1080° K in vacuum averaged 0.44 and 0.61, respectively, and the corresponding ϵ_{TH} values averaged 0.48 and 0.61. The variations observed can be attributed to the fact that the emittance properties of all three samples were changing rapidly during the initial vacuum tests and the first exposure test cycles. After these initial oxidizing exposures, little change in the emittance properties was noted and the variations that were measured can reasonably be attributed to sample temperature and radiometer measurement errors. The final ϵ_{TN}

Table 31

TOTAL NORMAL AND TOTAL HEMISPHERICAL EMITTANCE VALUES FOR
Cb 752/R512E SAMPLES BEFORE AND AFTER CYCLING TESTS

Sample No.	Before Testing		After Testing	
	T_s (° K)	$\epsilon_{TH}/\epsilon_{TN}$	T_s (° K)	$\epsilon_{TH}/\epsilon_{TN}$
B3 (Static Air Tests)	873 1074	0.48/0.46 0.62/0.63	880 1073	0.81/0.78 0.79/0.76
B8 (M1.1 Flow Tests)	— —	— —	883 1114	(0.86)/0.77 (0.81)/0.79
B7 (M2.1 Flow Tests)	874 1086	(0.48)/0.41 (0.59)/0.59	— —	— —

Note: ϵ_{TH} values for Samples B7 and B8 (in parenthesis), are based on average T_s and applied power estimates for the narrowed test section area and are less certain than the values obtained for Sample B3.

Table 32

TOTAL NORMAL EMITTANCE VALUES FOR Cb 752/R512E SAMPLES
BEFORE, DURING AND AFTER CYCLING TESTS

Cycle No.	Sample B3 (Static Air Tests)		Sample B8 (M1.1 Flow Tests)		Sample B7 (M2.1 Flow Tests)	
	T_s (°K)	ϵ_{TN}	T_s (°K)	ϵ_{TN}	T_s (°K)	ϵ_{TN}
Preliminary Tests in Vacuum	873[1]	0.46	— [3]	—	874[1]	0.41
	1074	0.63	—	—	1086	0.59
#1	1113	0.84	1062	0.78	1086	0.78
	1269	0.81	1378	0.82	1380	0.83
	— [2]	—	1655	0.74	1644	0.77
#2	1113	0.87	1112	0.78	1102	0.82
	1358	0.85	1369	0.76	1388	0.79
	1563	0.84	1634	0.78	1637	0.85
#3	1102	0.82	1085	0.78	1090	0.82
	1363	0.81	1366	0.77	1385	0.81
	1579	0.83	1630	0.79	1637	0.85
#4	1094	0.82	1079	0.76	1102	0.81
	1397	0.79	1375	0.75	1365	0.81
	1599	0.83	1626	0.78	1637	0.86
#5	1113	0.86	1096	0.77	1102	0.80
	1403	0.82	1374	0.75	1370	0.79
	1580	0.83	1626	0.77	1637	0.85
Post-Cyclic Tests in Vacuum	880[1]	0.78	883[1]	0.77	— [4]	—
	1073	0.76	1114	0.79	—	—

Notes:

(1) These temperatures were determined from thermocouple readings at the edges of the sample strips and are less certain than the remaining T_s values which were determined from optical pyrometer readings at the centers of the sample strips.

(2) No data obtained due to electrode-clamp failure which shut off sample power.

(3) No preliminary test data in vacuum obtained for Sample No. B8.

(4) No post-test data in vacuum obtained for Sample No. B7.

8-70

values for these samples averaged 0.78 at 880°K and 1100°K and the corresponding ϵ_{TH} averages were 0.83 and 0.80.

The ϵ_{TN} values listed in Table 32 indicate that the emittance of all three samples remained stable after the first cyclic tests. The variations observed for each sample at the three temperatures monitored during the tests were not more than ±3% from the average values for the last four cycles. The ϵ_{TN} values determined at 1100°K for Sample B3 during the last four static air test cycles appear to average about 5% higher than the value determined at that temperature during the final vacuum test. This may be due to temperature measurement error since optical pyrometer readings of these sample brightness temperatures were more difficult to determine than at the higher temperatures. Another possible source of error in the cyclic test data was the presence of small temperature gradients from the bottom of the sample test area to the top, due to convection. These gradients were not detectable when the sample was tested in vacuum. Temperature gradients from the hot center of the sample strip to the cooler edges averaged about 8°K at 1100°K, for both the vacuum and the static-air cycle tests. At 1370°K the center-to-edge gradient was about 20°K; and at 1580°K the gradient was about 28°K. In each case most of the edge loss appeared to occur in a region very close to the edge and should not have an appreciable effect on the radiometer readings at the center. No attempt was made to correct the center readings of T_s for the radiometer emittance determinations. For the calorimetric determinations of ϵ_{TH} in vacuum, a correction of -3°K was made to T_s at 1100°K to obtain the average temperature of the test section area.

For the narrower flow-test samples, the center-to-edge gradients were about 50% less than for Sample B3, but the vertical gradients from the top and bottom of the test section to the hot center area were much larger and increased as each test cycle progressed to higher total pressures on the sample. For the Mach 1.1 Flow test sample (B8) these temperature differences averaged 25°K, 55°K and 70°K at the nominal test temperatures of 1100°K, 1375°K and 1630°K. For the Mach 2.1 Flow test sample (B7), the temperatures differences were slightly less, i.e. 20°K, 40°K and 60°K, at the same test temperatures. Each of these gradients varied up to ±10°K from the values above depending upon the particular flow conditions obtained.

Except for the 880° K tests in vacuum, all of the sample T_s values were determined from optical pyrometer brightness temperature readings. To convert brightness temperatures to true temperatures, the initial room–temperature ϵ_λ value at 0.65 μm determined from the reflectance measurements was used. For these samples, this value was 0.69. In addition, a τ_λ factor of 0.92 was used for the transmittance of the pyrex window through which all the pyrometer readings were made.

Post–test reflectance measurements ·indicated that ϵ_λ at 0.65 μm increased significantly for each sample during the air–exposure tests. These changes in ϵ_λ along with the observed changes in solar absorptance (α_s) and room–temperature emittance are shown in Table 33. Most of these property changes are assumed to have occurred by the end of the first cyclic exposure test for each sample, corresponding to the observed changes in visual appearance, therefore T_s values after the first test cycle were redetermined using the post–test ϵ_λ values. For Samples B3 and B7 the effect of the change was to lower T_s by the following amounts: -6°K at 1100°K; -9°K at 1370°K and -11°K at 1600°K. For Sample B8 the corresponding changes amounted to -7°K, -11°K and -16°K respectively. The effect of these temperature corrections on the ϵ_{TN} and ϵ_{TH} determinations for these samples was an increase of 0.01 at 1100°K, 0.02 at 1370°K and 0.03 to 0.04 at 1600°K. These changes have been incorporated into Tables 31 and 32 and serve to indicate the uncertainties in T_s, ϵ_{TH} that exist due to these apparent changes in ϵ_λ at the pyrometer measurement wavelength.

Table 33

INITIAL AND FINAL ROOM TEMPERATURE PROPERTIES OF
Cb752/R512E SAMPLES

	α_s	ϵ_λ(Pyrom) $\lambda=0.65\,\mu$m	ϵ_{TN} (DB–100)	ϵ_λ (0.3 μm $\leq \lambda \leq 1.8\,\mu$m)	ϵ_λ (2 μm $\leq \lambda \leq 16\,\mu$m)
Initial	0.67	0.69	0.36	See Figure 61	See Figure 61
Final					
B3	0.75	0.76	0.83	See Figure 61	Not Measured
B8	0.75	0.78	—	See Figure 61	Not Measured
B7	0.76	0.76	—	See Figure 61	Not Measured

Initial and final spectral emittance results for the three Cb 752/R512E samples at their nominal test temperatures of 875° K, 1110° K, 1370° K and 1630° K are shown in figures 61, 62, 63, and 64. For comparison the room temperature emittance characteristics of the samples before and after testing are also shown. The latter curves were determined from pre- and post-test reflectance measurements of the samples. The elevated temperature data points were determined with the radiometer during the initial vacuum and cycling tests, along with the ϵ_{TN} determinations listed in Table 32, and then again during the final test cycles and post-exposure vacuum tests. Since the characteristics of all three samples were similar at each temperature, the results are combined on one figure where the data point symbols indicate the spread in results at each wavelength, and the curves indicate the average characteristics for the samples.

Figure 61 shows that the initial test data for samples B3 and B7 at 875° K (in vacuum) agreed closely to the initial room temperature reflectance data for these samples. The data for Sample B7 is on the order of 15 percent lower than the data for Sample B3, which corresponds with the initial ϵ_{TN} differences for these samples. These differences are attributed primarily to the rapid change in the emittance of these samples during these initial tests.

The post-test data at this temperature for Samples B3 and B8 show that the final emittance of both samples is essentially the same and in both cases significantly higher than the initial data at all wavelengths except for the 1.45 μm measurements. Changes in the room temperature spectral reflectance characteristics of the samples are shown by the curves labeled (2) and (3) for the wavelength region $0.3 \mu m \le \lambda \le 1.8 \mu m$.

The data in Figure 62 are for the same samples at the 1100° K test temperature in vacuum. The initial ϵ_λ values at this temperature show a greater deviation from the room temperature values than those at 875° K, but they are still much lower than the final measurement values. Both the initial and final sets of data show the spread of ϵ_λ values at each wavelength to be small, indicating that the changes in sample emittance characteristics were similar for all samples.
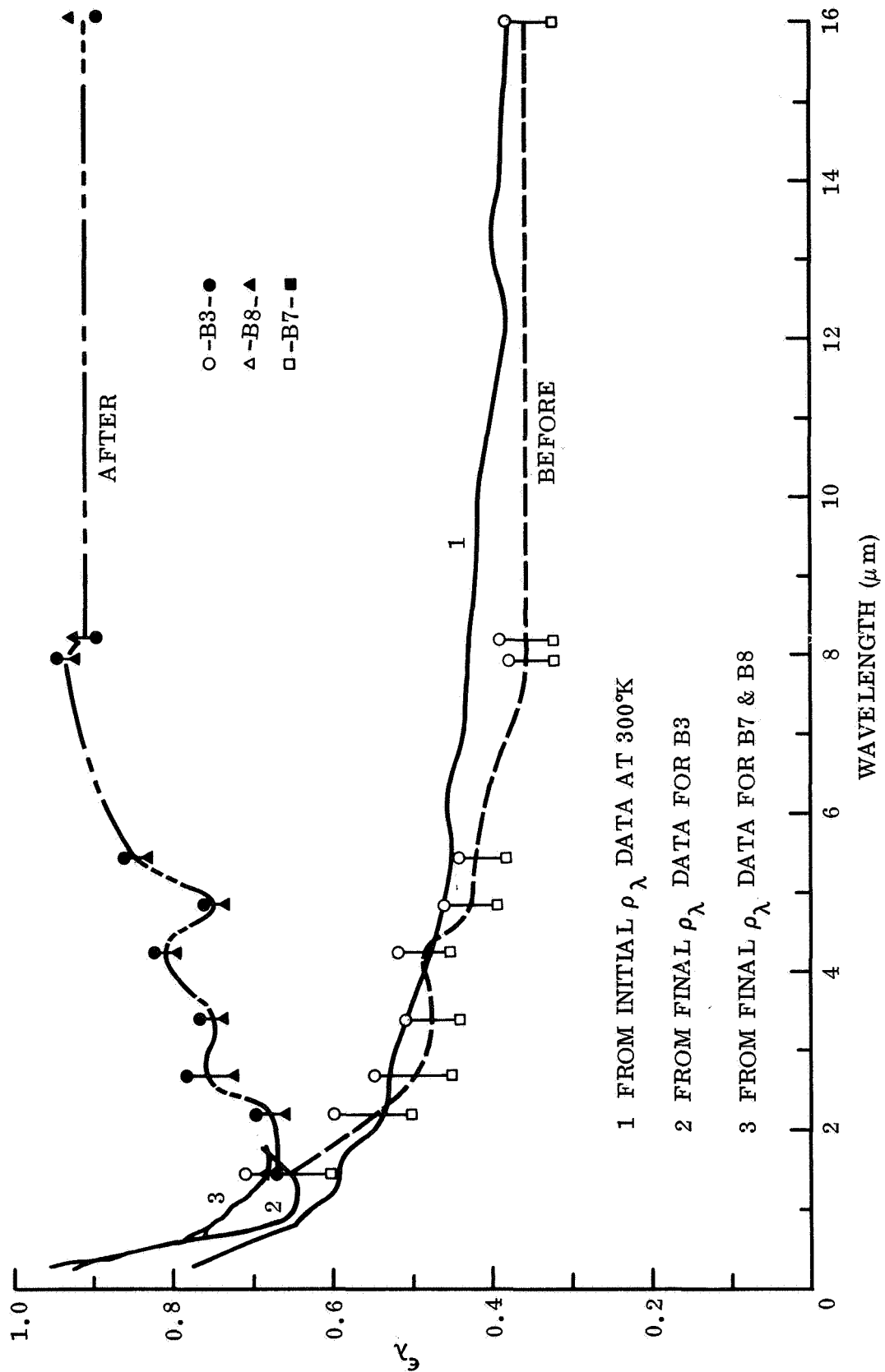
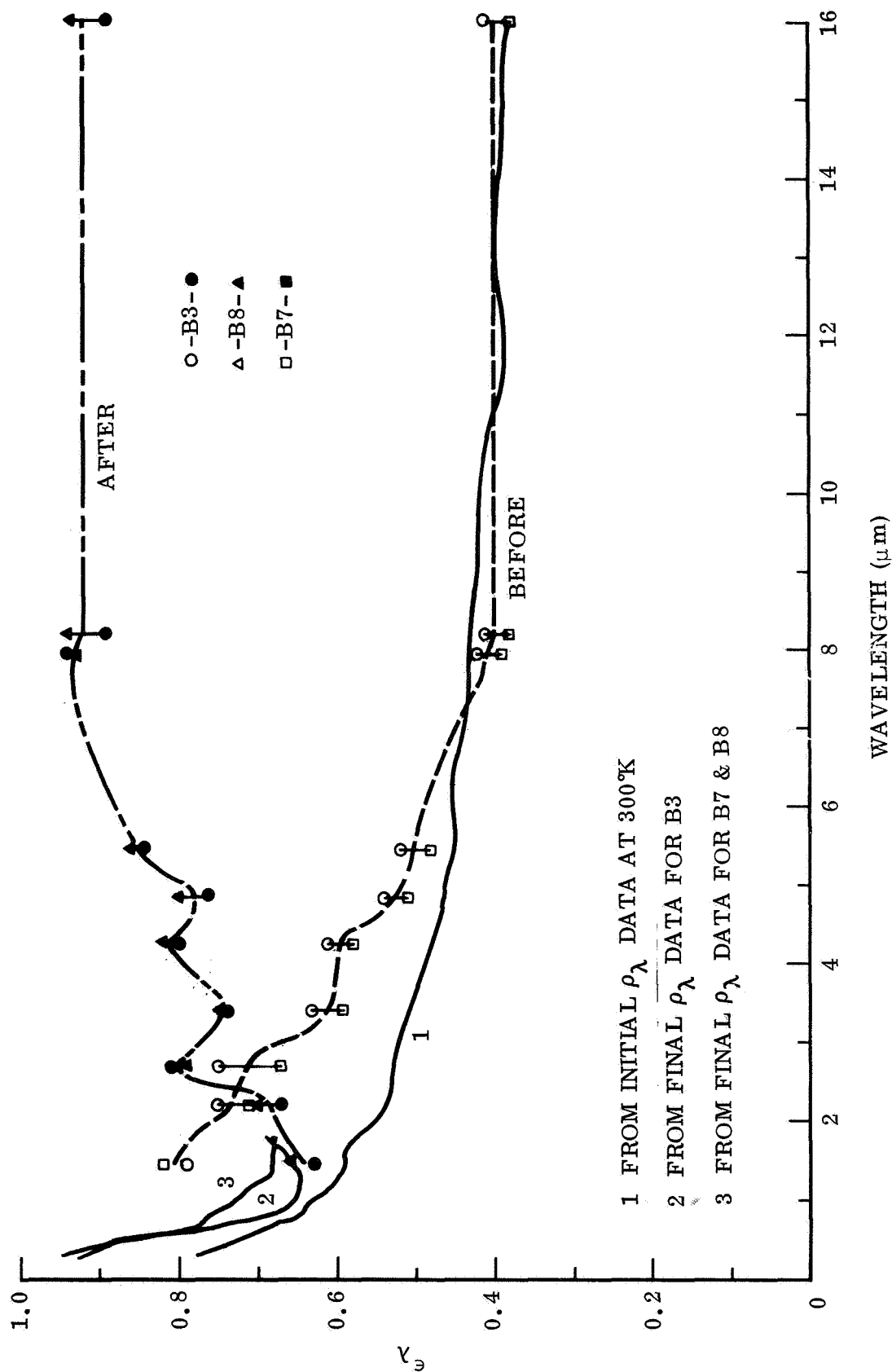Fig. 61 Spectral Emittance of Cb752/R512E Samples at 875°K Before and After Five Test Cycles

Fig. 62 Spectral Emittance of Cb752/R512E Samples at 1100°K Before and After Five Test Cycles
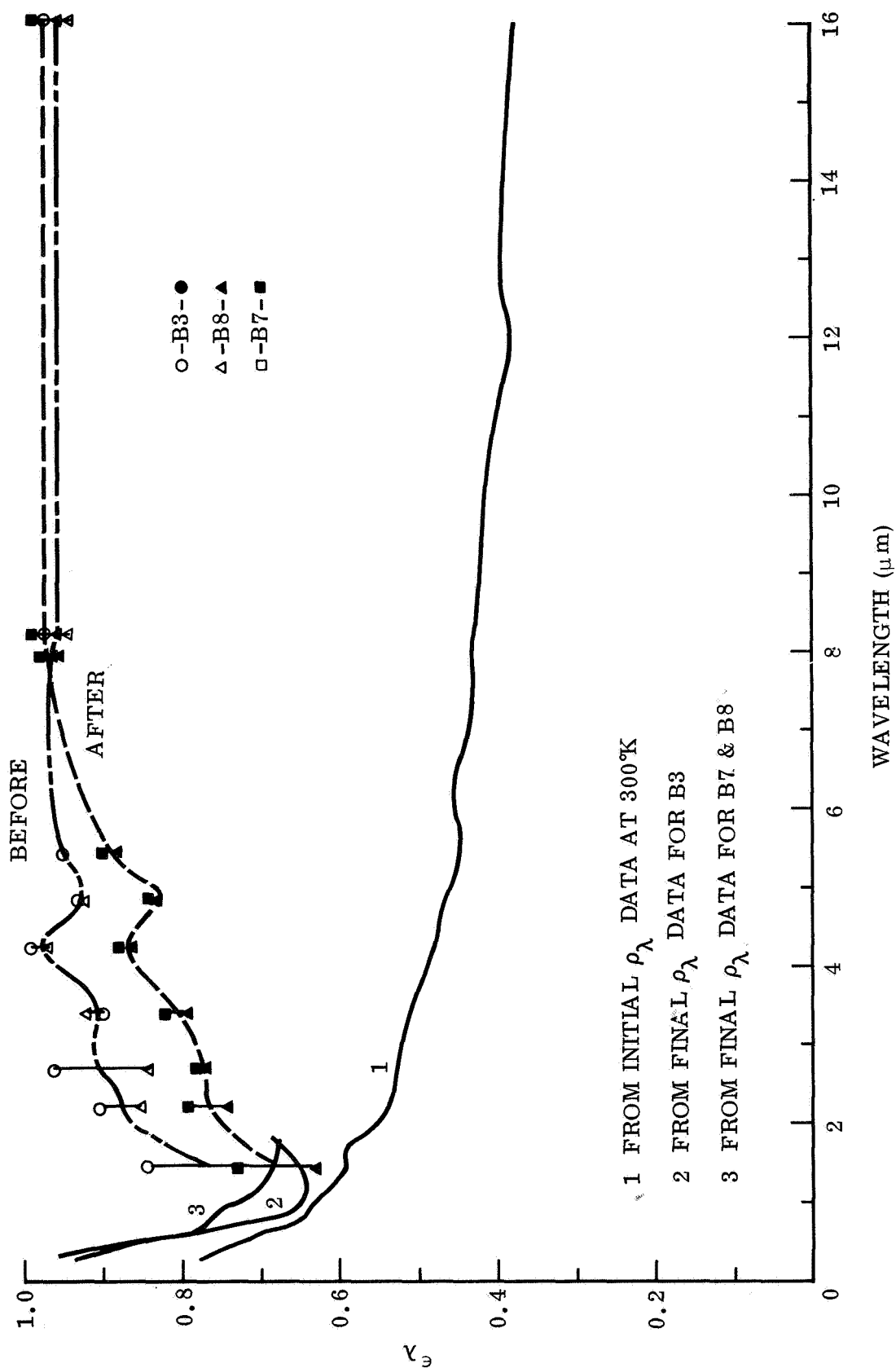
Fig. 63 Spectral Emittance of Cb752/R512E Samples at 1370°K Before and After Five Test Cycles
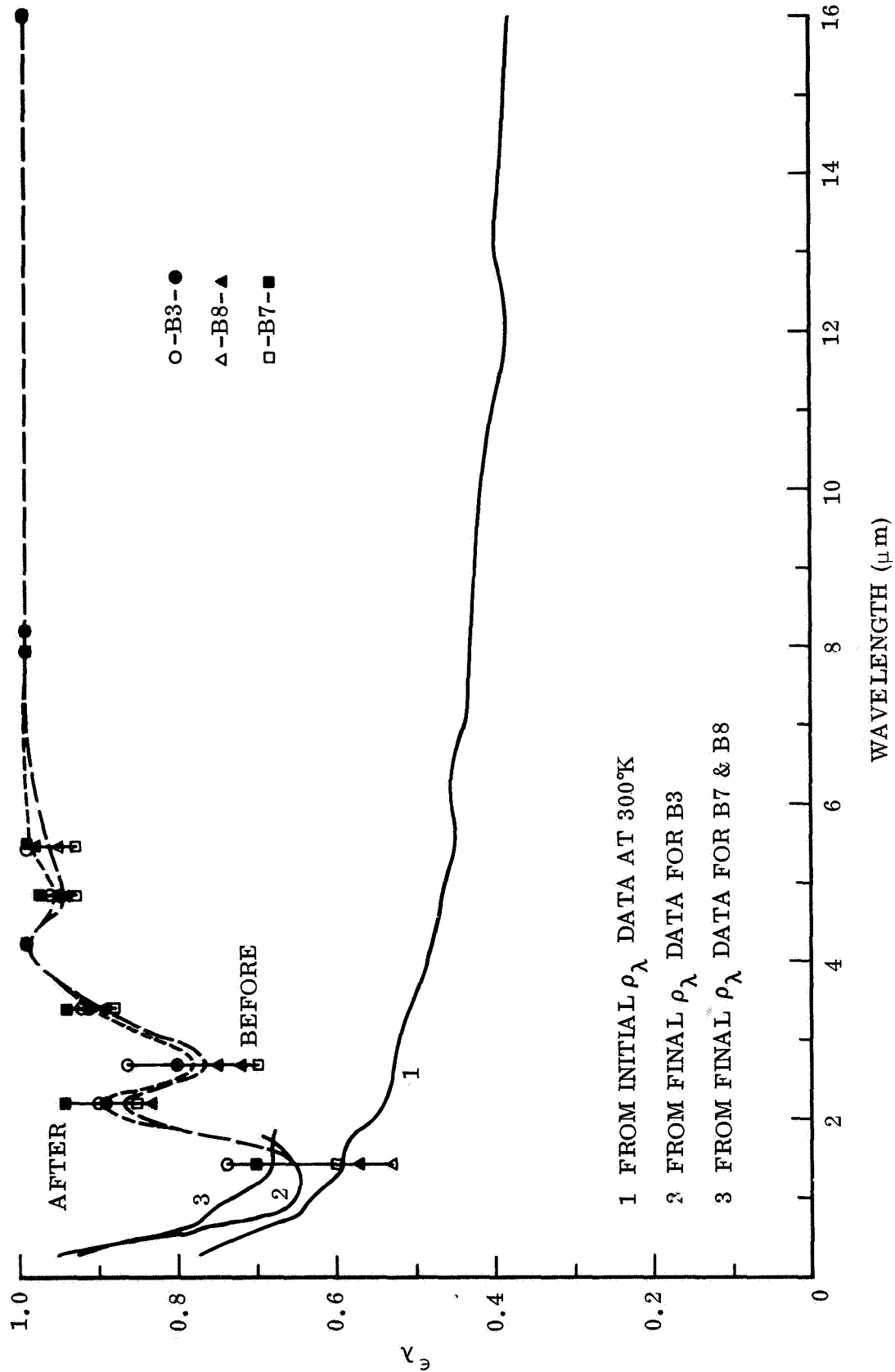
Fig. 64 Spectral Emittance of Cb752/R512E Samples at 1630°K Before and After Five Test Cycles

Figure 63 shows data that were obtained at 1370° K during the initial and final test cycles for these samples. The initial set of data indicates that most of the changes in emittance properties that were observed at the end of these tests had already occurred by the time this test temperature was first attained in the first cycle. The initial set of ϵ_λ values appear to be too high but have the same relative value to one another as in the final set. The most probable reason for these high ϵ_λ determinations is that the temperature of the samples increased during the time that the radiometer measurements were being made. Sample temperatures during the first test cycle of these samples, when the emittance properties were rapidly changing, tended to drift more than during the later test cycles.

Figure 64 shows data that were obtained at approximately 1630° K during the initial and final test cycles for these samples. Both sets of data are essentially the same, indicating that the emittance characteristics of these samples remained stable after this temperature was achieved. The spread in the ϵ_λ data at this temperature is about the same as at the lower temperatures except at the 1.45 μm and 2.2 μm wavelengths where it appears to increase to about ±10 percent of the average value. At these wavelengths the high ϵ_λ values were obtained for Sample B7 and the low ϵ_λ values for Sample B8. This relationship correlates with the ϵ_{TN} data in Table 32 and is the only evidence obtained to indicate a possible dependence of emittance on the different flow-test conditions. Even if true, the dependence is small and the major change in the emittance properties of these samples appear related to the temperature/ pressure parameters of the test cycles rather than the flow-velocity parameter.

A summary of the final emittance characteristics of these samples after their five test cycles is presented in Figure 65 to show the temperature dependency of ϵ_λ between 880°K and 1630°K. At temperatures above 1100°K, ϵ_λ values generally increase with temperature, the largest rise occurring in the vicinity of the 4.25 μm emittance band. Between 1 and 3 μm, emittance bands appear to develop, become more accentuated, and shift towards shorter wavelengths as the temperature increases. Although these changes in ϵ_λ appear to be significant, the net effect on the total emittance of the samples is small. Average ϵ_{TN} values for the three samples at these temperatures are tabulated on the figure and show a rise from 0.78 at 880°K to
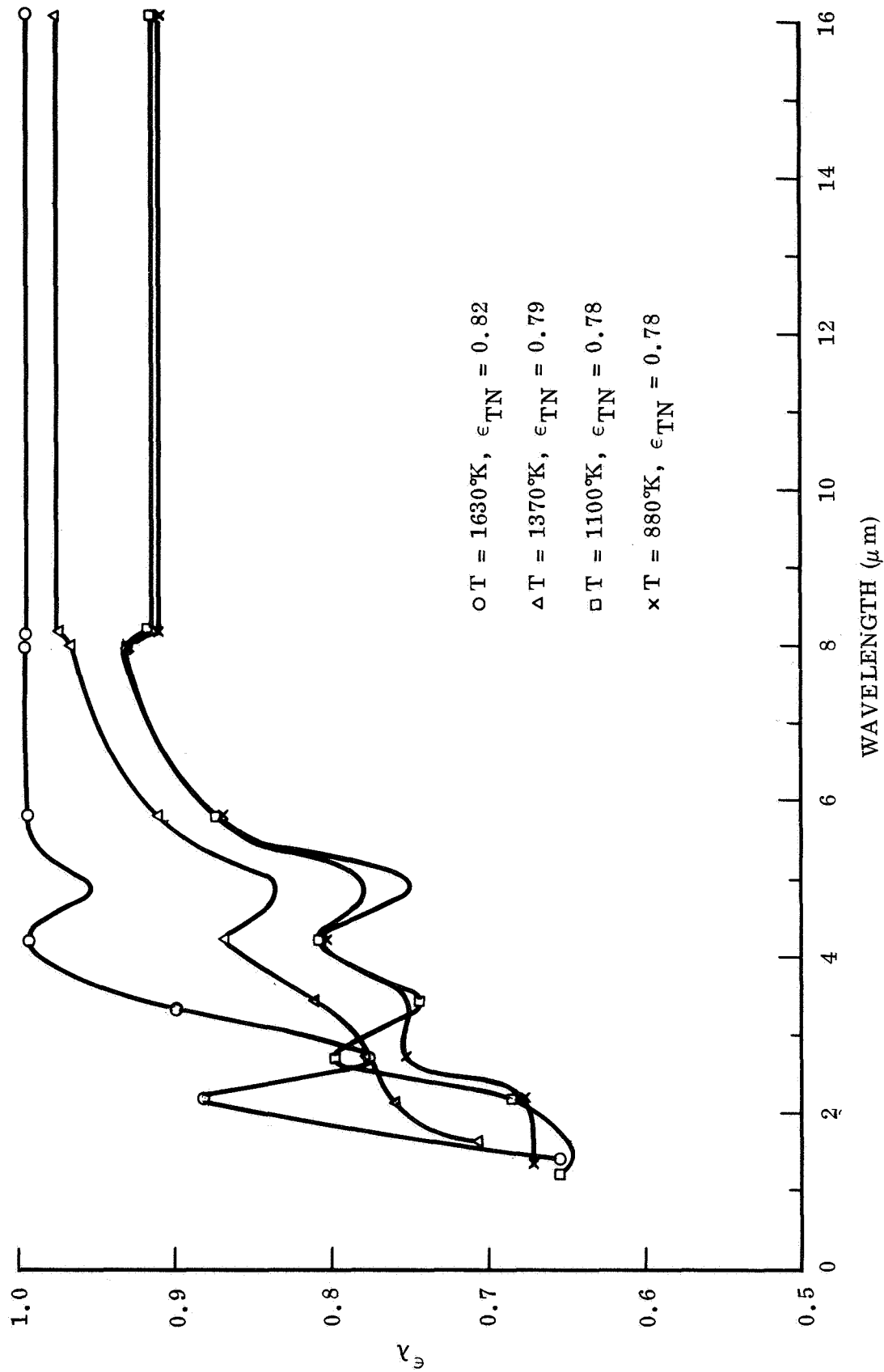
Fig. 65 Temperature Dependence of Spectral Emittance of Cb752/R512E Samples After Five Test Cycles

0.82 at 1630° K. These measured averages are consistent with the spectral curves which, by the integration method, give ϵ_{TN} values that are about 2 percent higher than the measured values.

Concerning the broad-band measurements between 8 and 16 μm, it should be noted that at these temperatures only a small percentage of the total radiation emitted by these samples will be radiated in this band even though the measured emittance values for the band approach 1. For a blackbody at these temperatures the percentages of total energy radiated at wavelengths longer than 8 μm are: 19 percent at 880° K, 11.5 percent at 1100° K, 6.6 percent at 1370° K and 4.4 percent at 1630° K.

8.6 RSI COATINGS

The samples described in this section are thin, ceramic-like coatings which provide high temperature (to 1650° K), high-emittance surfaces for two types of RSI (Reuseable Surface Insulation) materials that have been developed for the Space Shuttle thermal protection system. The first coating, designated as LMSC/0042, is a grey-colored, coating developed by Lockheed Missiles and Space Company, Inc. for use with their LI-1500 and LI-900 types of insulation. The second coating type, designated as MDAC/HCF coating, is a black-colored coating developed by McDonnell-Douglas Aircraft Corp. for use with their HCF type of insulation.

Both coatings are electrical non-conductors with low thermal conductivities which makes their thermal radiation properties difficult to determine by any of the standard test methods, particularly during dynamic exposure conditions. Three different back-face heating techniques were investigated for both types of coatings, and none proved to be entirely satisfactory. The most satisfactory results, in terms of test specimen temperature uniformity, were obtained using a wedge-shaped platinum-cavity heater with the samples mounted in front of the cavity. These test methods and the problems associated with each are described in Section 8.6.2.

The maximum sample temperatures attained during tests of these materials ranged between 1375° K and 1430° K, which is approximately 200° K short of the original test plan goal. The absolute accuracy of the high-temperature emittance determinations

for these samples is less certain than for the oxidized and coated metal samples because of greater uncertainties in the temperature determinations and possible sample transparency. The repeatability of the results, however, serves to indicate that the properties of both coatings remained stable throughout each set of exposure cycles. Calorimetric determinations of total hemispherical emittance were not possible by the methods used for these tests.

8.6.1 Sample Preparation

Samples of each coating were supplied in the form of 1.3-cm wide strips, from 15 to 30-cm long, with the coatings bonded to their respective substrate insulation materials for a total thickness of approximately 0.4-cm. Since both materials have low thermal conductivity, as much of the substrate insulation as possible was removed in order to minimize temperature gradients through the samples during their exposure tests. This was accomplished by lightly sanding the back surface of the strips to re-move the relatively soft insulation material until the hard bond-line between the coating and substrate was reached. This left the final thickness of the samples at between 0.037 and 0.050 cm for the LMSC/0042 coating, and between 0.062 and 0.075 cm for the MDAC/HCF coating. These thin strips were then broken and trimmed into various lengths, usually 1.3-cm square samples, for mounting to the various backface-heater strips used for the sample heating investigations.

Room-temperature reflectance measurements for the region $0.3\,\mu m \leq \lambda \leq 1.8\,\mu m$ were obtained for two of the 'as received,' (before sanding), sample strips of each coating. The results showed the reflectance of both samples to be the same to within ±0.005 units for each coating, and were assumed to be representative for all the samples of each coating. For measurements in the region $2\,\mu m \leq \lambda \leq 25\,\mu m$, one of the thin sample squares of each coating was fastened to a thin, 2.54-cm diameter copper disk with a conducting epoxy cement for measurements with the heated-cavity reflectometer. The results of these measurements are presented later for com-parison with the high-temperature spectral emittance results. Total-normal IR reflectance measurements with the DB-100 reflectometer were not made because the as-received strips were too narrow to fully cover the measurement port for this

instrument, but room-temperature values for ϵ_{TN} were obtained by integration of the spectral measurement data.

8.6.2 Sample Heating Method Investigations

The initial plan for heating the RSI coating samples during their cyclic exposure tests was to tie each sample snugly to the front face of a platinum strip heater, and to control the temperature of the heater strip at sufficiently high levels to maintain the sample temperature at the desired test levels, i.e. 1150°K, 1480°K and 1650°K during each exposure test cycle. Sample temperatures were to be determined by the optical pyrometer method since thermocouple readings would not be reliable for low-conductivity materials such as these and the attachment of thermocouples to the sample surfaces would be difficult.

Initial trials of this method were made in vacuum using a platinum-rhodium alloy heater strip that was 25-cm long by 1.90-cm wide by 0.078-cm thick with five platinum-rhodium thermocouples spot welded to the backface area of the strip behind the sample. A thin rectangular sample of the MDAC/HCF coating, 1.3-cm wide by 2.6-cm long, was tied to the front face of the strip using two wraps of 0.025-cm diameter wire (platinum-rhodium) at the top and bottom of the sample. During the first heating cycle the maximum sample temperature attained was approximately 1225°K with the heater strip operating at a safe (strengthwise) maximum temperature of 1750°K. At this power level the temperature of the center 5-cm length of the heater strip appeared to be uniform to within 15°K, but the surface temperature of the sample appeared to vary by as much as 50°K over small distances (≈ 0.5-cm) that would be difficult to resolve with the radiometer.

Additional trials of this method were made with the sample cemented to the heater strip with a high temperature refractory cement, in hopes of obtaining a better thermal coupling between the sample and heater and thereby attaining higher and more uniform sample temperatures. Uniform bonding of samples to the heater was not achieved, however, and although slightly higher sample-to-heater temperature ratios were obtained, the surface temperatures appeared to be even more variable than before.

Tests similar to those above were made next using a tantalum heater strip, (25-cm long by 1.3-cm wide by 0.10-cm thick), with a sample of the LMSC/0042 coating tied to the front surface of the heater with 0.012-cm diameter tantalum wire, and no cement. By operating the tantalum heater at about 1950° K in vacuum, sample surface temperatures near the desired maximum of 1650° K were obtained in 'hot-spot' areas on the sample, but adjacent sample areas were as much as 250° K cooler and reliable emittance determinations were not possible. Similar tests were also made with one of the MDAC/HCF-coating samples with the results being that slightly more uniform appearing surface temperatures were obtained (about 100° K variations), but the maximum sample temperature attained was about 250° K lower, i.e. about 1420° K with the tantalum heater strip temperature at 2000° K.

Investigations of the flat-strip heating method were dropped at this time because of the following problems:

● The maximum attainable sample temperatures were too low using platinum. Suitably high temperatures could probably be obtained using a tantalum heater, but refractory-metal heaters at 2000° K would not be suitable for the air exposure tests.

● Surface temperature gradients that would seriously compromise the accuracy of any emittance determination occurred with both heaters. Attempts to reduce these gradients by cementing the coating samples to the heater face were not successful.

● 'Hot-spot' locations on the sample changed from time to time, particularly when the heater temperature was changed. This was apparently caused by slight changes in flexure at the center of the heater strip that were not eliminated by the electrode tension setting. In some cases, particularly when the heater power was reduced, these changes in flexure caused the coating samples to crack into two or more separate pieces.

The final heating method investigated, and the one that was used for the tests reported in this Section, involved the use of a wedge-shaped heater with a high-emittance cavity at the front face to radiantly heat the thin sample squares. A sketch of this heater

assembly is shown in figure 66. The wedge was formed from a platinum-rhodium alloy strip which was rolled with initial dimensions of 19-cm length by 7-cm width by 0.032-cm thickness. The wedge was shaped to have a 1.5-cm wide front face and 2.5-cm wide sidewalls with a 0.3-cm wide overlapping seam at the rear to hold the wedge closed. The ends were crushed flat to facilitate clamping the heater to the power-electrode assemblies of the test chamber, and this reduced the overall length of the heater to approximately 18 cm, with 3.5-cm wide, flat ends. A 1.1 cm square cavity was cut out of the center of the front face of the wedge, with small tabs at the edges to support the backface of the sample squares. A small sample-support tab was spot welded to the front face just below the cavity, and a single loop of 0.0076-cm platinum wire was wrapped around the wedge to fit over the top, front face of the sample and loosely hold it against the front face of the cavity. The 1.3-cm sample squares were large enough to cover the entire area of the cavity, but were usually offset slightly so that a small portion of the upper right-hand corner of the cavity could be viewed with the optical pyrometer. Heater temperatures were also measured with small Pt 6% Rh/Pt 30% Rh thermocouples which were spotwelded at various locations on one sidewall of the wedge.

With this heater, sample temperatures up to about 1430° K were obtained in vacuum and during the static-air exposure cycles by operating the heater at temperatures up to 1800° K. Temperatures around the center area of the sample viewed by the radiometer appeared to be uniform to within 10° K (at T_s = 1430° K), although the top, bottom and sides of the sample were as much as 30° K higher or lower, depending on the sample position and test conditions.

Temperature readings at the center of the sidewall were taken as best indications of the effective cavity temperature since most of the radiation impinging on the backface of the sample originates from this region of the wedge. Temperature gradients from the center to the front and back edges of the sidewalls were small except in the region immediately adjacent to the cooler edges. Vertically the gradients were such that temperatures along the vertical centerline of the sidewall dropped about 40° K at points 2.5-cm above and below the center point.
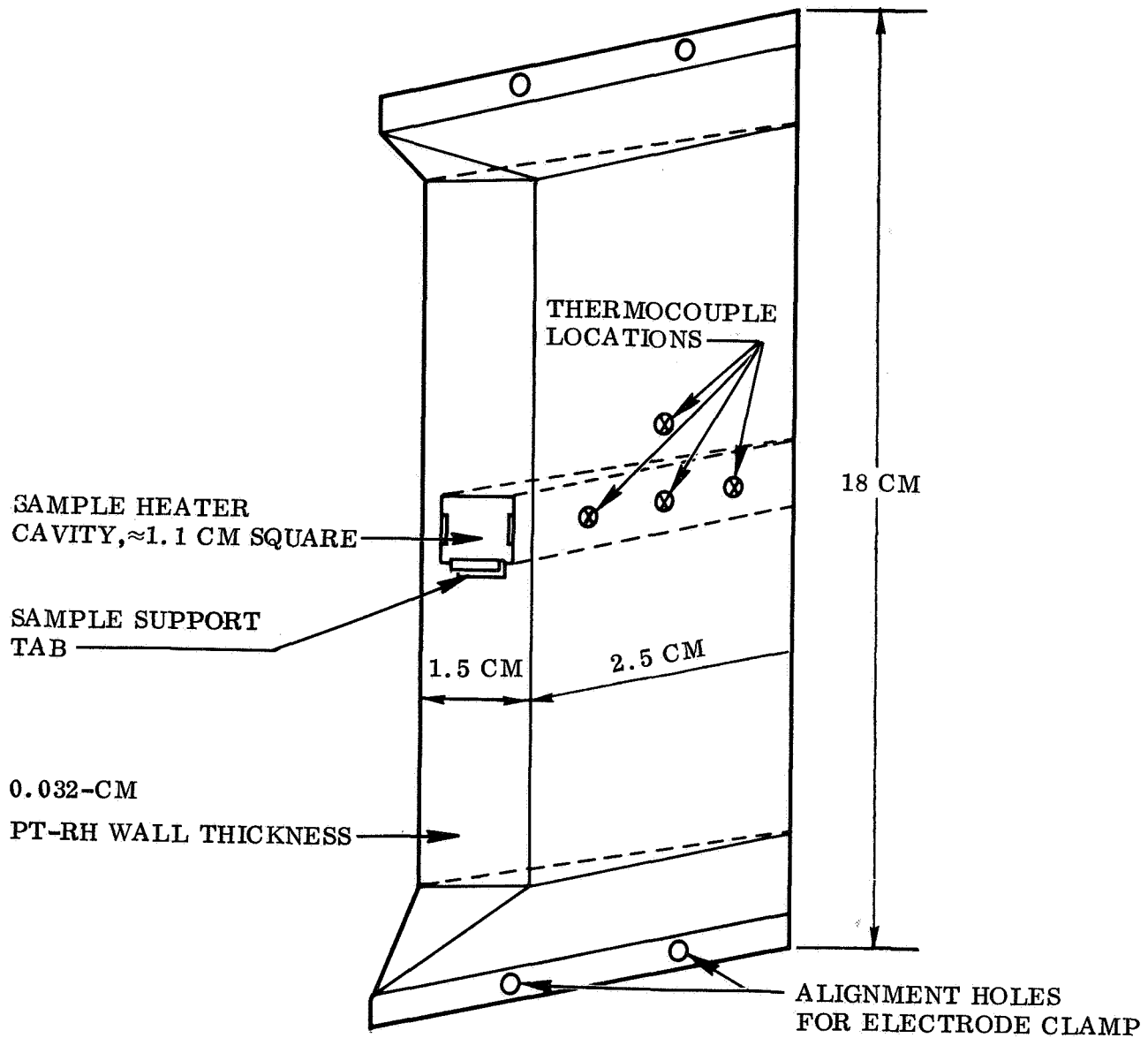
Fig. 66 Sketch of Wedge-Shaped Heater Cavity Used for RSI Coating Sample Tests

8-85

Absolute heater temperatures were determined either from thermocouple readings or, in most cases, from optical pyrometer readings using a value of $\epsilon_\lambda = 0.42$ at $\lambda = 0.65\,\mu$m for the emittance of the platinum-rhodium heater surface. This surface emittance value was determined by comparing thermocouple and pyrometer temperature readings which were obtained at the same time and location for several cases, and appeared to be reliable to within ±0.04 units at temperatures between $1300°$ K and $1800°$ K. By comparing absolute temperature values for the cavity (i.e., the center sidewall temperatures), with optical pyrometer brightness temperature readings of the cavity itself, cavity emittance values at $\lambda = 0.65\,\mu$m were determined to be 0.70 ± 0.05 with no sample in front of the cavity, and 0.82 ± 0.03 with samples blocking off all but the upper right-hand corner of the cavity. This latter value is needed for sample temperature determinations in cases where the sample is partially transparent at the optical pyrometer wavelength, a problem that is discussed next.

8.6.3 Sample Temperature Determinations

As mentioned earlier, sample temperatures for all the RSI-coating samples were determined solely from optical pyrometer readings of the sample brightness temperature. The accuracy of the absolute temperatures determined by this method depends primarily on the accuracy of the ϵ_λ value used for the sample at the pyrometer wavelength ($0.65\,\mu$m), and assumes that all the radiation observed through the pyrometer is emitted from the sample surface, i.e., does not include any reflected or transmitted radiation from other nearby, high-temperature sources. The values used for ϵ_λ at $0.65\,\mu$m for these two coating materials were those determined from the room-temperature reflectance measurements and, in the absence of any independently determined temperature data, the values were assumed to remain constant at temperatures between $300°$ K and the maximum temperatures attained in these tests. This assumption is somewhat risky for both coating materials because of their non-grey spectral emittance characteristics in the region around $0.65\,\mu$m; but since both values are relatively high (0.78 for the LMSC/0042 coating and 0.96 for the MDAC/HCF coating), a change of 5 or 10 percent would not cause a serious temperature determination error.

Of greater concern is the fact that during all of the preliminary sample heating trials, considerable difficulty was experienced in matching the pyrometer filament color to that of the sample surfaces. Although steady-state readings were generally repeatable to within ±5° K, the uncertainty range of the color match was on the order of ±20° K and the problem seemed to be due to a certain amount of sample translucency or transmission of radiation from the hotter substrate heater. To check this possibility, room-temperature spectral transmittance measurements in the region between 0.4 and 2.5 μm were made on samples of each coating using a Gier-Dunkle Model SP210 Integrating Sphere with a transmittance measuring attachment. This instrument measures the spectral hemispherical transmittance, i.e., the sum of the normally transmitted and forward scattered components of incident radiation, of samples for normally directed incident beams of monochromatic radiation.

Measurements of several of the LMSC/0042 coating samples indicated transmittance values on the order of 1.0 to 1.7 percent at 0.65 μm. Measurements of the MDAC/ HCF coating sample indicated no transmittance at 0.65 μm. Since no information was available concerning the temperature dependency of spectral transmittance for either material, it was assumed that the room-temperature properties also applied at the higher test temperatures; consequently the optical pyrometer temperature measurements for the LMSC/0042 coating samples may be in error but measurements for the MDAC/HCF coating samples should be unaffected.

To evaluate the effect of sample transmittance on the optical pyrometer temperature determinations for samples under the test conditions used in this study, the following analysis was made to derive a modified pyrometer equation which relates the true sample temperature to the pyrometer brightness temperature reading.

(1) Let $N_\lambda(T_B)$ be the radiance at 0.65 μm of the pyrometer filament which is calibrated to be equal to the radiance of a blackbody at the indicated temperature, T_B. Then

$$N_\lambda(T_B) = \frac{c_1}{\lambda^5 e^{c_2/\lambda T_B}}$$

8-87

where c_1 and c_2 are the first and second radiation constants. (Note: Wien's law is applicable since λT is less than 3 cm-°K).

(2) Let $N_\lambda(T_T)$ be the radiance of the sample at $0.65\,\mu m$ that reaches the pyrometer, when the sample surface is at some unknown temperature T_T, has a known emittance at $0.65\,\mu m$ of ϵ_s, and is observed through a test-chamber window with a transmittance at $0.65\,\mu m$ of τ_w. Then:

$$N_\lambda(T_T) = \frac{c_1}{\lambda^5 e^{\,c_2/\lambda T_T}}\left(\epsilon_s\,\tau_w\right)$$

(3) Let $N_\lambda(T_c)$ be the radiance of the heater-cavity at $0.65\,\mu m$ that reaches the pyrometer, when the heater-cavity is at a known temperature, T_c, and has a known emittance at $0.65\,\mu m$ of ϵ_c. This radiation must pass through the sample which has a transmittance at $0.65\,\mu m$ of τ_s, and through the test-chamber window with a transmittance of τ_w to reach the pyrometer, therefore:

$$N_\lambda(T_c) = \frac{c_1}{\lambda^5 e^{\,c_2/\lambda T_c}}\left(\epsilon_c\,\tau_s\tau_w\right)$$

(4) Now when the radiance of the pyrometer filament is made to match that of the incoming radiation, then:

$$N_\lambda(T_B) = N_\lambda(T_T) + N_\lambda(T_c)$$

which, after transposing and collecting terms, becomes:

$$T_T = \frac{T_B}{1 - \dfrac{T_B}{c_2/\lambda}\,\ell n\left[\left(\dfrac{1}{\epsilon_s\,\tau_w}\right) - \left(\dfrac{\epsilon_c\,\tau_s}{\epsilon_s}\right)\dfrac{e^{\,c_2/\lambda T_B}}{e^{\,c_2/\lambda T_c}}\right]}$$

This equation serves to demonstrate the effect of sample transmittance on the pyrometer determined sample temperatures, and some results for typical sample test conditions are presented at the end of the next subsection. Before discussing results, however, the following characteristics of the equation should be mentioned:

- When the sample transmittance (τ_s) is zero, the equation reduced to the standard pyrometer equation.

- When the last term in the brackets is small relative to the first, i.e., when τ_s is small and/or T_c is not much larger than T_B, then the error involved when using the standard pyrometer equation is small.

- Finally, as the brackets term approaches zero, T_T approaches zero; and the equation becomes indeterminant when the second term in the brackets is equal to or greater than the first term. This corresponds to the case where all of the incoming radiation originates from the heater cavity and none originates from the sample.

8.6.4 RSI Coating Sample Results

Emittance property test results are reported for two samples of LMSC/0042 coating which were initially tested in vacuum, then exposed to five static-air test cycles (Sample No. 2) and five Mach 1.1 flow-test cycles (Sample No. 3), then retested in vacuum (Sample No. 3 only); and one sample of the MDAC/HCF coating (Sample No. 4) which was tested in vacuum before and after five static-air test cycle exposures. The initial and final room temperature properties of the samples indicated by the reflectance measurements are shown in Table 34. The measurements indicate that no significant property changes occurred in the 0.3 to 1.8 μm spectral region as a result of the test exposures, and this correlates with the observation of no change in the visual appearance of the samples. Post-test reflectance measurements for the region between 2 and 16 μm were not obtained.

Results of the room-temperature spectral transmittance measurements for each of the coating materials are shown in figure 67. The LMSC/0042 coating measurements shows a peak transmittance of 2.7 percent near 0.45 μm which drops off to about 1.7 percent at 0.65 μm and down to about 0.3 percent at 2.5 μm. The MDAC/HCF coating appears to be opaque at wavelengths out to about 0.9 μm and then shows increasing transmittance to about 1.6 percent at 2.5 μm. Assuming that these transmittance characteristics also apply at the elevated test temperatures, it will be shown that the transmittance at 0.65 μm of the LMSC/0042 coating samples can cause significant
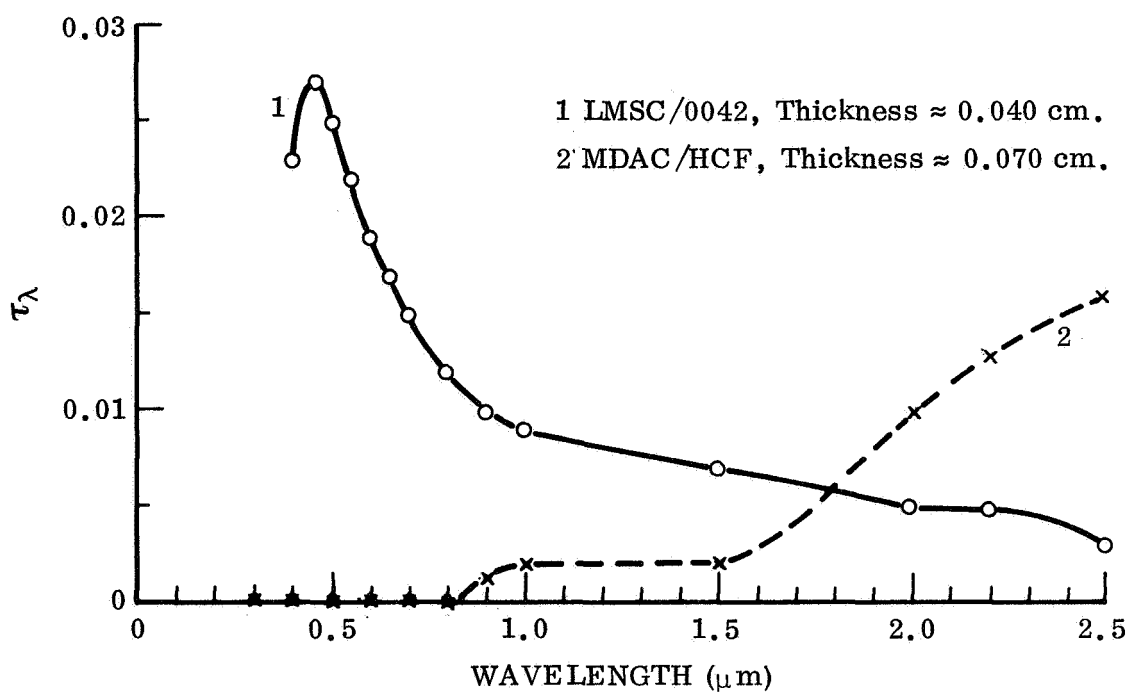
Fig. 67 Room Temperature Spectral Transmittance Data for RSI Coating Samples

Table 34

INITIAL AND FINAL ROOM TEMPERATURE PROPERTIES OF
RSI COATING SAMPLES

Sample I.D. No.	α_s	ϵ_λ (Pyrom) $\lambda = 0.65\,\mu m$	ϵ_{TN}	ϵ_λ $0.3\,\mu m \le \lambda \le 1.8\,\mu m$	ϵ_λ $2\,\mu m \le \lambda \le 16\,\mu m$
LMSC/0042 Coatings					
Initial	0.80	0.78	0.90	See Figure 68	See Figure 68
Final					
No. 2 (5 Static Air-Cycles)	0.81	0.78	N.M.	See Figure 70	N.M.
No. 3 (5 M1.1 Cycles)	0.82	0.79	N.M.	See Figure 70	N.M.
MDAC/HCF Coatings					
Initial	0.90	0.96	0.93	See Figure 69	See Figure 69
Final					
No. 4 (5 Static Air-Cycles)	0.90	0.95	N.M.	See Figure 71	N.M.

N.M.: Not measured.

temperature measurement errors with the optical pyrometer due to transmitted energy from the higher-temperature cavity behind the sample. This source of error is evidently not present for the MDAC/HCF samples, and the difficulty experienced in matching the pyrometer filament to the surface brightness for this material is apparently due to some other cause, possibly to real surface temperature variations since the texture of this coating is coarser and rougher than for the LMSC/0042 coating.

A summary of the test-temperature conditions obtained during the vacuum and exposure-test cycles of the three RSI coating samples is shown in Table 35. The table lists the temperatures at which the heater cavity was operated, the corresponding sample brightness temperature (pyrometer) readings that were obtained, and the 'true'

Table 35

SUMMARY OF HEATER AND SAMPLE TEMPERATURE CONDITIONS
FOR RSI COATINGS SAMPLE TESTS

Sample No. — Test Condition	Heater Cavity Temp. (° K)	Sample Brightness Temp. (° K)	True Sample Temp (For $\tau_s = 0\%$) (° K)
LMSC/0042 — No. 2 (In Vacuum)	1301	1041	1057
	1634	1254	1278
	1804	1401	1431
LMSC/0042 — No. 2 (Static Air Tests)	1292	1040	1056
	1649	1295	1320
	1783	1402	1432
LMSC/0042 — No. 3 (In Vacuum)	1311	1058	1075
	1629	1248	1272
	1769	1347	1375
LMSC/0042 — No. 3 (Mach 1.1 Flow Tests)	1338	1046	1062
	1675	1245	1268
	1792	1308	1334
	1786	1295	1320
	1765	1276	1301
MDAC/HCF — No. 4 (In Vacuum)	1333	1049	1055
	1641	1235	1244
	1778	1343	1354
MDAC/HCF — No. 4 (Static Air Tests)	1323	1049	1055
	1661	1267	1276
	1789	1367	1378

sample temperatures that were used for the sample emittance determinations. The
cavity temperatures listed are the center-sidewall temperatures of the heater that
were indicated either by attached thermocouples or by corrected pyrometer readings.
These temperatures were controlled by manual adjustments of the heater power to
approximately the same levels during each test cycle. The sample brightness
temperature readings are for the center areas of the samples that were viewed by the
radiometer. The 'true' sample temperatures are those determined using the standard
pyrometer equation, i.e. assuming no sample transmittance error, and the room-
temperature values for ϵ_λ at 0.65 μm listed in Table 34. The temperatures shown

for the static-air and Mach 1.1-flow test conditions are averages for the five test cycles for each sample. The three sets of data for LMSC/0042 Sample No. 3 at its maximum test temperature during the Mach 1.1-flow tests are for the three different pressure conditions during this portion of the test cycle (see figure 6). The temperature drops observed during this portion of the test cycle, when the applied heater power was maintained at a constant level, illustrate the effects of increasing convective heat losses from both the sample and the heater due to the higher mass-flow rates in the Mach 1.1-flow test environment.

A summary of the sample temperatures and total normal emittance values obtained for the three coating samples before, during and after their cyclic exposure tests is shown in Table 36. The temperatures listed are 'true' temperatures based on the assumption that the samples are opaque, i.e. τ_s = 0% at 0.65μm. If sample transmittance errors are present in this data, their effect is such that the 'true' temperature values should be lower and consequently, the ϵ_{TN} values should be higher. Examples of these effects are shown at the end of this section for sample transmittance cases of 1 and 1.5 percent and appear to be the most likely explanation for the low ϵ_{TN} values obtained for the LMSC/0042-coating samples at the lowest test temperatures and during the Mach 1.1-flow tests. At the two higher test temperatures, ϵ_{TN} values for LMSC/0042 sample No. 2 averaged 0.83 in vacuum and 0.86 in the static-air test environment. Therefore, the error in these values due to transmittance would not be more than 10 percent, which corresponds to a temperature error of 2.5 percent. Variations in the high temperature ϵ_{TN} determinations for LMSC/0042-Sample No. 2 are small and indicate that no significant change in sample emittance properties occurred as a result of the five static-air exposure cycles.

The ϵ_{TN} values obtained for Coating Sample No. 3 during the Mach 1.1-flow-test cycles are generally about 20 percent lower than those obtained for Sample No. 2. These low values are almost certainly due to larger temperature determination errors resulting from convective cooling of the sample surface in this test environment. Note that for approximately the same heater-cavity temperatures, T_s values at the highest test temperatures during the Mach 1.1-flow test cycles were from 100 to 150° K lower than the corresponding T_s values for Sample No. 2 during the static-air test cycles.

Table 36

TOTAL NORMAL EMITTANCE VALUES FOR RSI COATING SAMPLES BEFORE,
DURING AND AFTER EXPOSURE TEST CYCLES

Test Cycle No.	LMSC/0042 – No. 2 (Static Air Tests)		LMSC/0042 – No. 3 (M1.1 Flow Tests)		MDAC/HCF – No. 4 (Static Air Tests)	
	T_s (° K)	ϵ_{TN}	T_s (° K)	ϵ_{TN}	T_s (° K)	ϵ_{TN}
Initial Tests in Vacuum	1057	0.69	1075	0.68	1055	0.79
	1278	0.82	1272	0.75	1244	0.83
	1431	0.84	1375	0.80	1354	0.87
#1	1052	0.81	1060	0.63	1039	0.77
	1316	0.88	1269	0.83	1265	0.91
	1409	0.86	1329	0.81	1371	0.89
#2	1050	0.81	1063	0.63	1052	0.80
	1307	0.87	1266	0.76	1277	0.90
	1432	0.86	1342	0.76	1388	0.89
#3	1071	0.83	1060	0.64	1061	0.80
	1319	0.87	1263	0.76	1271	0.90
	1451	0.85	1348	0.77	1388	0.89
#4	1027	0.80	1063	0.61	1058	0.75
	1322	0.87	1284	0.72	1287	0.88
	1426	0.87	1323	0.66	1373	0.86
#5	1071	0.84	1054	0.55	1064	0.80
	1328	0.85	1234	0.67	1281	0.87
	1459	0.84	1310	0.76	1398	0.87
Final Tests in Vacuum	(Not Measured)		1065	0.73	1074	0.78
			1272	0.83	1281	0.87
			1362	0.87	1398	0.86

Cooler surfaces in combination with higher cavity-to-sample temperature ratios will result in larger sample temperature determination errors when sample transmittance occurs. The final test data in vacuum for Sample No. 3 indicate that its emittance properties were similar to those of Sample No. 2 and were not significantly affected by the five Mach 1.1 flow test cycles.

8-94

Total normal emittance values obtained for the MDAC/HCF coating sample, both in vacuum and during the five static-air test cycles, indicate that this coating was also unaffected by the static-air exposure cycles. At the two higher test temperatures, ϵ_{TN} values averaged about 0.89 and are presumably free of any temperature determination error due to sample transmittance. Temperature measurement error may be the reason for the lower ϵ_{TN} determinations at the lowest test temperatures since the uncertainty in the pyrometer readings was greater here than at the higher test temperatures.

The effect of sample transmittance at longer wavelengths ($\lambda > 1\mu$m) on the ϵ_{TN} determinations, which is also discussed at the end of this section, is opposite to the effect discussed for pyrometer temperature measurements. In this case transmitted cavity energy will be superimposed on the radiated sample energy that is measured with the radiometer, with the result being erroneously high radiometer readings and ϵ_{TN} determinations. It will be shown that for the highest temperature conditions obtained in these tests, as long as the average sample transmittance in the 1 to 3 μm region does not exceed 2 percent, the error in ϵ_{TN} should not exceed 5 percent.

Spectral emittance measurements were made along with the total normal emittance measurements for each sample during their initial and final tests in vacuum for comparison with the room-temperature measurements and to indicate any changes that may have occurred as a result of the cyclic exposure tests. The initial results for the two LMSC/0042 samples at three test temperatures are compared with the room-temperature ϵ_{λ} curve in figure 68, and similar results for the MDAC/HCF sample are shown in figure 69. The data for both coating materials indicates apparently large increases in the ϵ_{λ} values with increasing temperature, but most of these changes are attributed to sample temperature error, particularly for the LMSC/0042 coating samples at the low test temperatures. It seems highly unlikely that the ϵ_{λ} values would drop by the amount indicated in figure 68 between room temperature and 1075° K, and then increase back to approximately their 300° K values between 1075° K and 1430° K without showing a significant and permanent change in
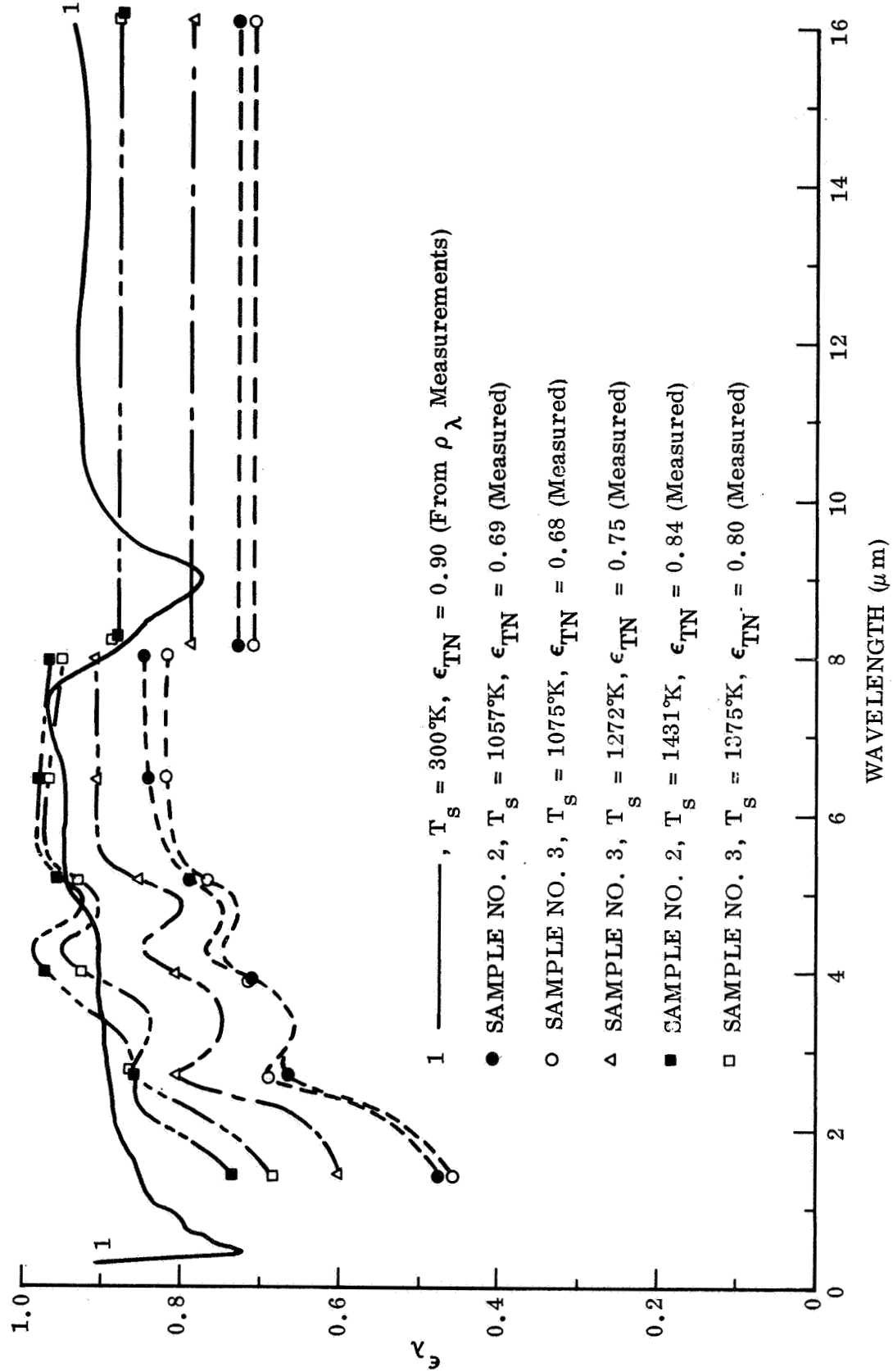
Fig. 68 Initial Spectral Emittance Data for LMSC/0042 Coating Samples at Four Temperatures
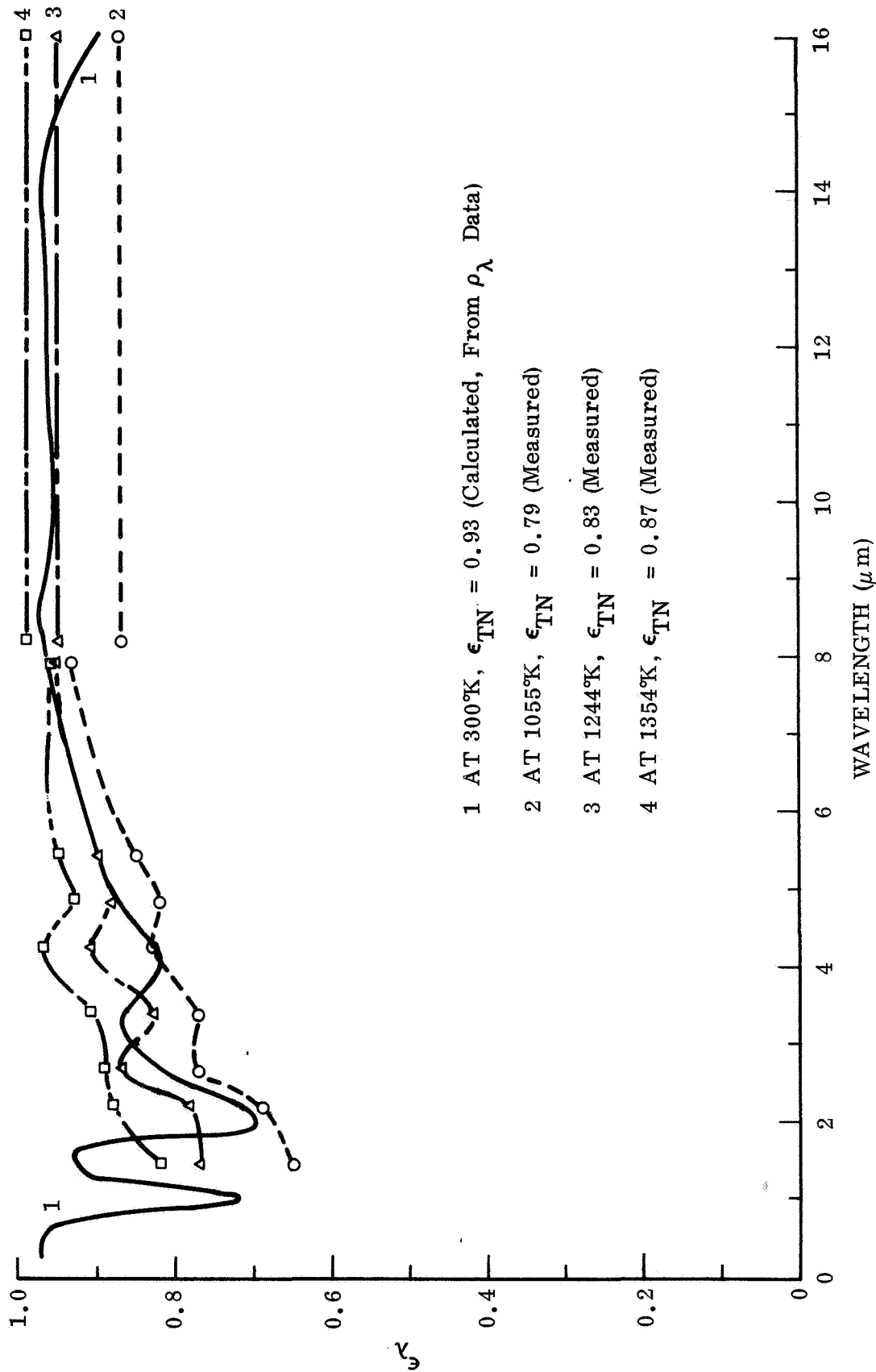
Fig. 69 Initial Spectral Emittance Data for MDAC/HCF Coating Sample at Four Temperatures

1 AT 300°K, ϵ_{TN} = 0.93 (Calculated, From ρ_λ Data)

2 AT 1055°K, ϵ_{TN} = 0.79 (Measured)

3 AT 1244°K, ϵ_{TN} = 0.83 (Measured)

4 AT 1354°K, ϵ_{TN} = 0.87 (Measured)

WAVELENGTH (μm)

ϵ_λ

LOCKHEED PALO ALTO RESEARCH LABORATORY
L O C K H E E D   M I S S I L E S   &   S P A C E   C O M P A N Y ,   I N C .
A   S U B S I D I A R Y   O F   L O C K H E E D   A I R C R A F T   C O R P O R A T I O N

sample properties. No such change was detected however from either the ϵ_{TN} determinations shown in Table 36, or from comparisons of the initial and final ϵ_λ determinations. Also, the fact that the changes are largest at the short wavelengths and smaller at the longer wavelengths is indicative of the differences being due to temperature determination errors.

A comparison of the initial and final ϵ_λ data for the two LMSC/0042 coating samples is shown in figure 70. The final high temperature data for Sample No. 2 was obtained during the last, static-air test cycle whereas the remaining data for both samples was obtained during the initial and final tests in vacuum. The post-test reflectance data for both samples in the region $0.3\,\mu m \leq \lambda \leq 1.8\,\mu m$ is also shown for comparison with the initial reflectance characteristics for these samples. With the exception of the high-temperature data point at $\lambda = 1.45\,\mu m$, the final ϵ_λ characteristics for both samples appear to be essentially the same and indicate little or no difference between the static-air and Mach 1.1-flow test exposures. Differences between the initial and final characteristics of the samples are also small, except for Sample No. 3 at the two shortest wavelengths, and these cannot be considered significant in view of the uncertainties involved in the sample transmittance and temperature determinations.

The initial and final high-temperature ϵ_λ characteristics for the MDAC/HCF coating sample are compared in figure 71 along with the pre- and post-test reflectance data for the $0.3\,\mu m \leq \lambda \leq 1.8\,\mu m$ region. The emittance characteristics of this sample also appear to be unaffected by the five static-air exposure cycles except for the single measurement at $2.7\,\mu m$ and for slight changes in the room-temperature reflectance curve at wavelengths below $1.1\,\mu m$.

While the results shown in figure 70 and 71 serve to indicate that the emittance properties of these two coating materials were not significantly affected by the exposure tests, the absolute accuracy of the emittance determinations remains uncertain because of possible sample transmittance effects. The first and most serious error arises from sample transmittance at $0.65\,\mu m$ which results in sample temperature determinations that are too high and consequently, sample emittance determinations that are too low when measurements are made under the conditions used for these
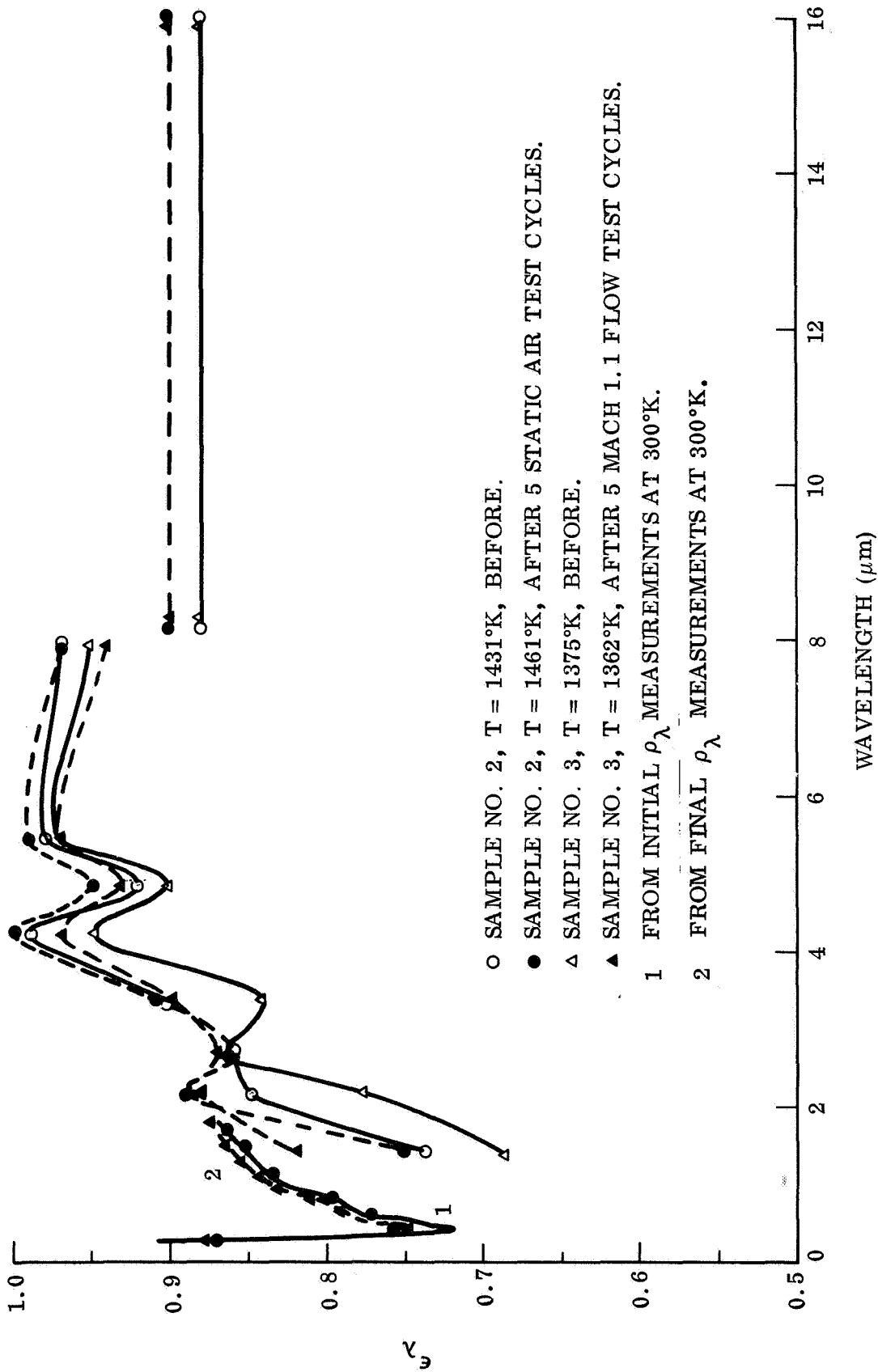
Fig. 70 Comparison of Spectral Emittance Data for LMSC/0042 Coating
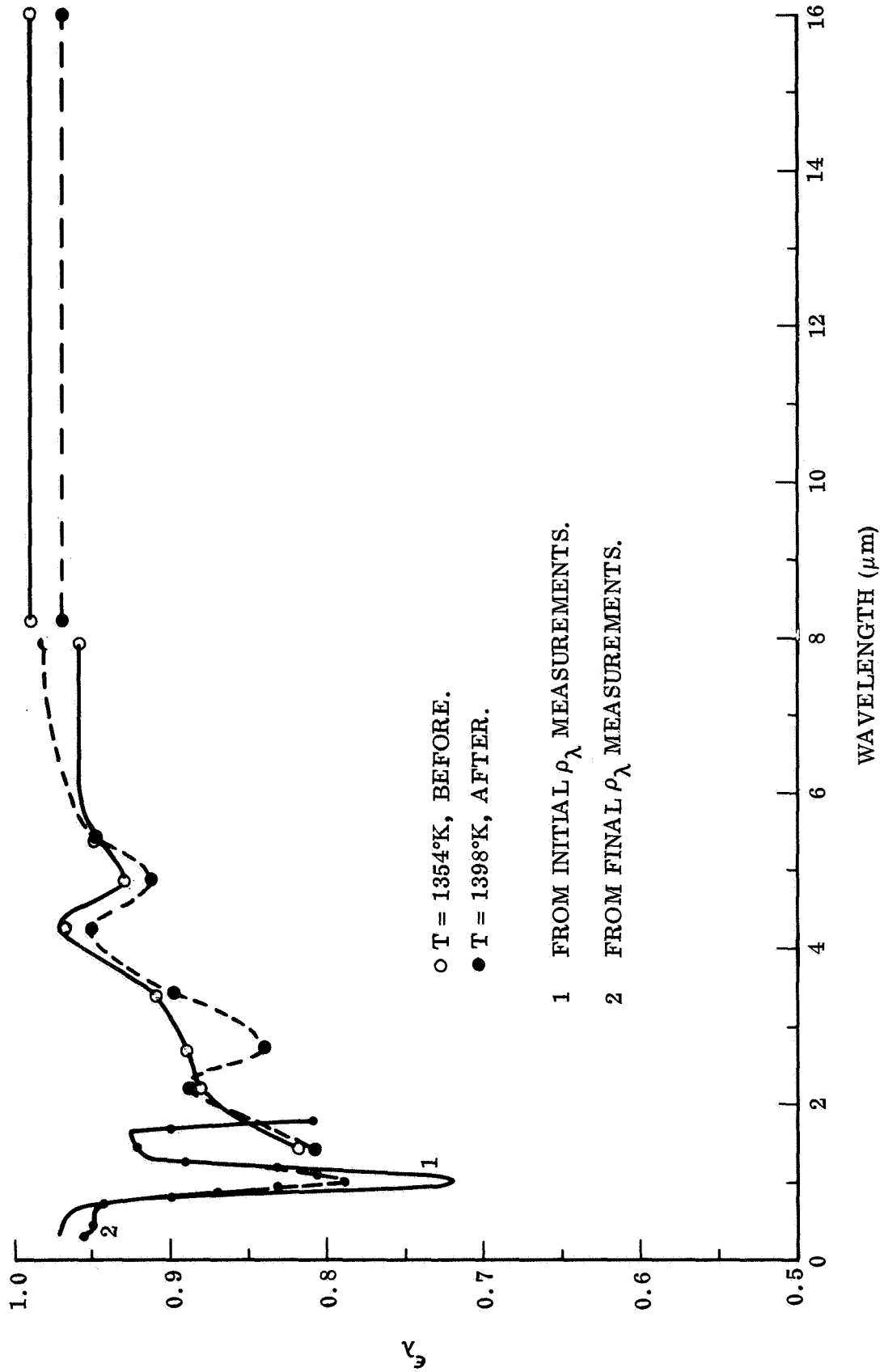Samples Before and After Five Exposure Test Cycles

Fig. 71 Comparison of Spectral Emittance Data for MDAC/HCF Coating
Sample Before and After Five Static-Air Test Cycles

8-100

tests, i.e., with a high-temperature backface heater. Errors of this type appear to apply to the LMSC/0042 coating samples but not to the MDAC/HCF coating.

The effect of sample transmittance values of 1 percent and 1.5 percent at $0.65\,\mu$m on the sample temperature determinations for LMSC/0042 Sample No. 2, using the typical test-temperature conditions that have been described earlier, are shown in Table 37. Typical heater-cavity temperatures and the corresponding brightness temperature readings for the sample obtained with the optical pyrometer are shown in the first two columns of the table. The third column shows the 'true' sample temperatures obtained using the standard pyrometer equation, which applies when the sample is not transparent. The last two columns show the 'true' sample temperatures that are obtained for the two transmittance cases using the modified pyrometer equation described earlier in this section and the assumptions about cavity emittance, sample emittance and window transmittance that are indicated with the table. At the lowest test temperature, the error resulting from assuming τ_s to be 0 percent is seen to amount to about 3.4 percent if τ_s is really 1 percent; and if τ_s is 1.5 percent, the temperature error increases to 5.8 percent. Therefore, τ_s is highly sensitive to small changes in τ_s for these test conditions; the reason being the large cavity-to-sample radiance ratio that exists at these temperatures. At the highest test temperature the cavity-to-sample radiance ratio is smaller, (even though the temperature ratio is larger), and the sample temperature determination errors for the two transmittance cases decreases to 1.4 percent and 2.3 percent, respectively.

The effect of the temperature differences shown in Table 37 on the spectral emittance determinations for Sample No. 2 are illustrated in figure 72, for the low temperature test case, and figure 73 for the high temperature case. At the low test temperature figure 72 shows that the sample temperature error associated with a sample transmittance of 1.5 percent at $0.65\,\mu$m would easily account for the low ϵ_λ values that were obtained for the LMSC/0042-coating samples. The effect is so sensitive to τ_s that corrections for a sample transmittance of 1.7 percent, as was indicated by the room-temperature measurements shown in figure 67, are too large and result in ϵ_λ values that are greater than 1. At the high test temperature figure 73 shows that corrected ϵ_λ values larger than 1 are obtained even for a sample transmittance value of 1 percent at $0.65\,\mu$m. Therefore it appears that τ_s may decrease with increasing

Fig. 72 Effect of Temperature Errors due to Sample Transmittance at 0.65 μm on Spectral Emittance Determinations for LMSC/0042 Sample No. 2 at Low Test Temperatures

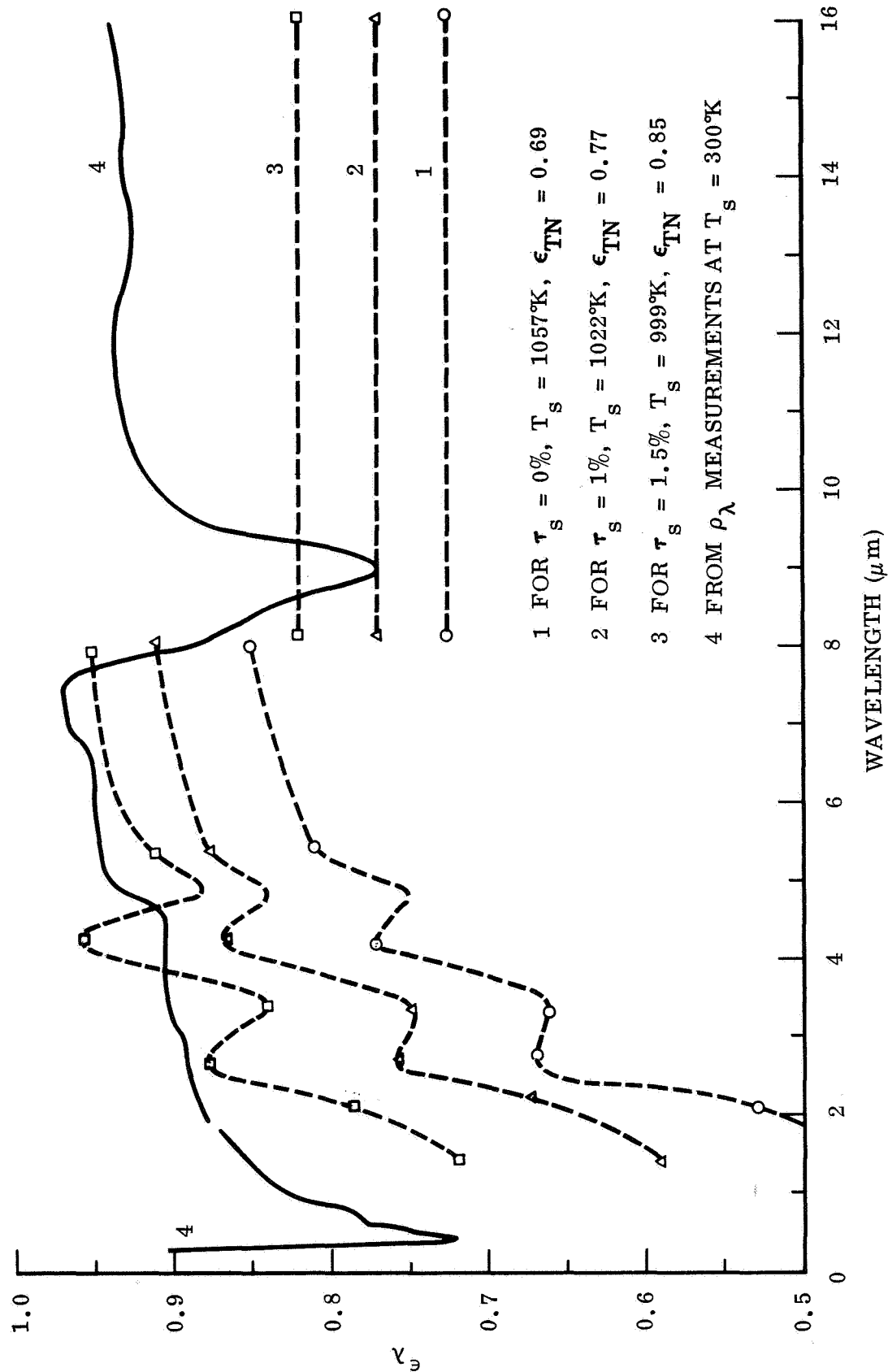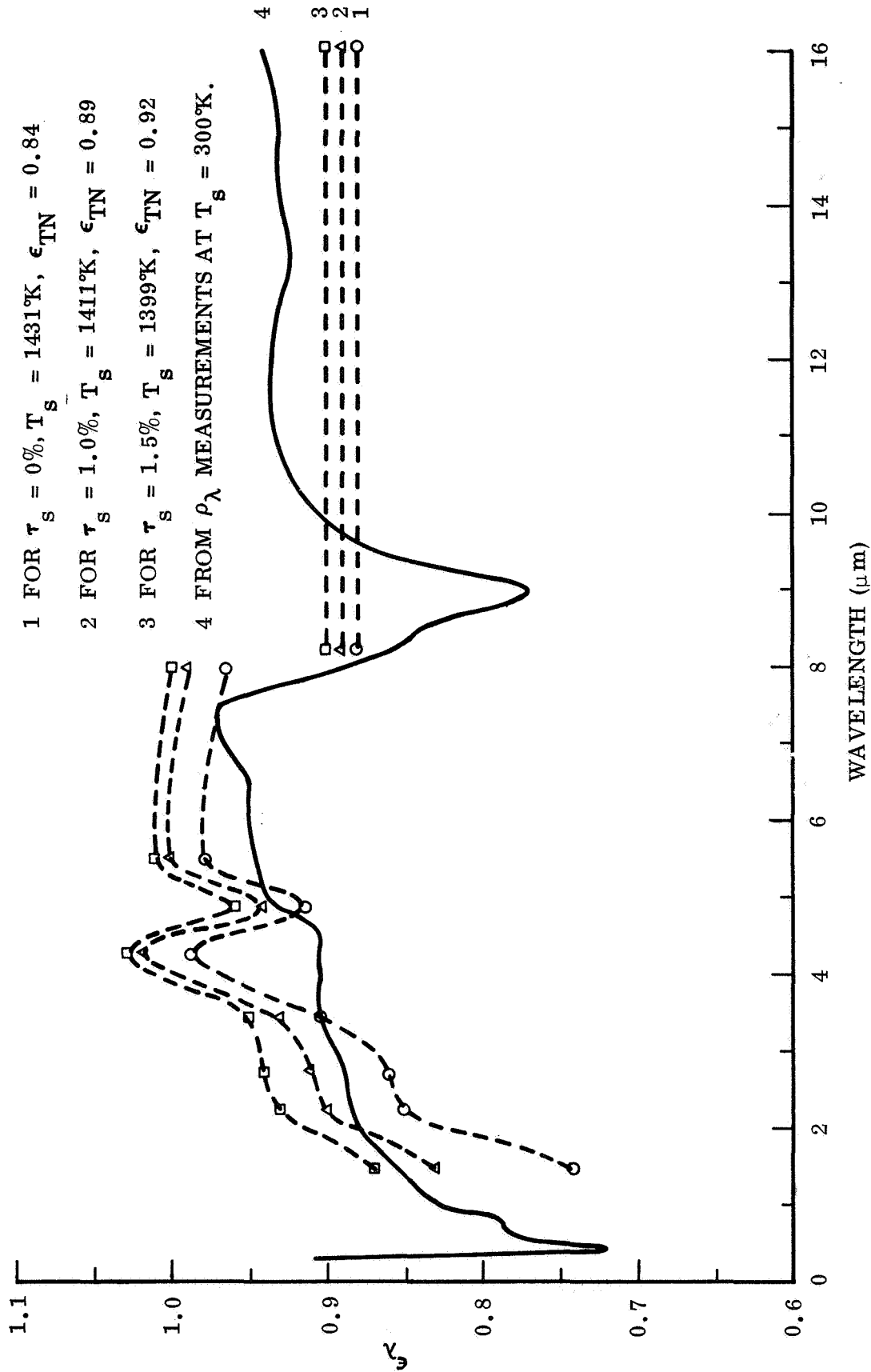Fig. 73 Effect of Temperature Errors due to Sample Transmittance at 0.65 μm on Spectral Emittance Determinations for LMSC/0042 Sample No. 2 at High Test Temperatures

1 FOR τ_s = 0%, T_s = 1431°K, ϵ_{TN} = 0.84

2 FOR τ_s = 1.0%, T_s = 1411°K, ϵ_{TN} = 0.89

3 FOR τ_s = 1.5%, T_s = 1399°K, ϵ_{TN} = 0.92

4 FROM ρ_λ MEASUREMENTS AT T_s = 300°K.

LMSC–D352380

Table 37

CALCULATED EFFECTS OF SAMPLE TRANSMITTANCE AT $0.65\,\mu$m ON TRUE TEMPERATURE DETERMINATIONS FOR LMSC/0042 COATING SAMPLE NO. 2

Heater Cavity Temp. (°K)	Sample Brightness Temp. (°K)	True Sample Temp. (°K) For:		
		$\tau_s = 0\%$	$\tau_s = 1\%$	$\tau_s = 1.5\%$
1301	1041	1057	1022	999
1634	1254	1278	1253	1236
1804	1401	1431	1411	1399

Note: Calculations are based on the following assumptions:

(1)
(1) Emittance of heater cavity is 0.80 at $\lambda = 0.65\,\mu$m.

(2) Emittance of sample surface is 0.78 at $\lambda = 0.65\,\mu$m.

(3) Transmittance of the glass window through which the pyrometer readings are obtained is 0.92 at $\lambda = 0.65\,\mu$m.

temperature and that the temperature and emittance determinations for these samples at the high test temperatures are approximately correct as reported.

A second, less-serious error associated with sample transmittance involves the effect of transmitted cavity energy at the wavelengths measured by the radiometer. When this occurs the radiometer signals and resultant emittance determinations are too high because of the transmitted cavity energy that is superimposed on, and detected with, the energy radiated by the sample. This error will be proportional to the cavity-to-sample radiance ratio, the cavity-to-sample emittance ratio, and to the sample transmittance value — all at the wavelength of interest.

The errors associated with sample transmittance values of 1 percent and 2 percent at each of the narrowband-filter wavelengths for the radiometer have been calculated for the three typical temperature conditions used in these tests and are shown in Table 38. The maximum errors occur for the intermediate test-temperature case because of the larger cavity-to-sample radiance ratios that are obtained at these temperatures,

8-104

Table 38

CALCULATED ERRORS IN RADIOMETRIC ϵ_λ DETERMINATIONS FOR SAMPLES
THAT ARE PARTIALLY TRANSPARENT AT THE FILTER WAVELENGTHS — FOR
THREE TYPICAL TEST-TEMPERATURE CONDITIONS AND TWO SAMPLE
TRANSMITTANCES

λ (μm)	Case A		Case B		Case C	
	$\tau_S = 1\%$	$\tau_S = 2\%$	$\tau_S = 1\%$	$\tau_S = 2\%$	$\tau_S = 1\%$	$\tau_S = 2\%$
1.45	6.4	12.1	7.1	13.2	5.1	9.7
2.2	3.6	6.9	3.8	7.4	3.1	6.0
2.7	2.9	5.6	3.1	6.0	2.6	5.1
3.4	2.4	4.7	2.6	5.0	2.2	4.4
4.25	2.1	4.1	2.2	4.4	2.0	3.9
4.85	2.0	3.9	2.1	4.1	1.9	3.7
5.45	1.8	3.7	2.0	3.9	1.8	3.6
7.95	1.6	3.3	1.8	3.5	1.7	3.3

Case A: For sample temperature of 1050° K and heater cavity temperature of 1300° K.

Case B: For T_S = 1250° K and T_C = 1650° K.

Case C: For T_S = 1400° K and T_C = 1800° K.

Note: The following conditions are assumed for all three cases:

(1) Sample emittance at each wavelength is 0.90.

(2) Cavity emittance at each wavelength is 1.0.

and for all three cases the maximum error occurs at the shortest wavelength. If the room-temperature values of sample transmittance shown in figure 67 are assumed to apply at these test temperatures, it will be seen that at λ = 1.45 μm the maximum error in ϵ_λ attributable to this cause will be on the order of 5 percent for the LMSC/0042 coating samples; and at λ = 2.2 μm will be on the order of 5 percent for the MDHC/HCF coating sample. Errors in the total normal emittance determinations at these temperatures cannot be determined without additional knowledge about the transmittance of the coatings beyond 2.5 μm, but are estimated to be no larger than about 3 percent.

Section 9

DISCUSSION AND RECOMMENDATIONS

The operation of the test apparatus developed under this program was successfully demonstrated as follows:

- The accuracy of radiometric measurements of total normal and spectral normal emittance was verified through data obtained on a NBS platinum-rhodium reference standard. The accuracy of these data is considered to be within ± 0.02.

- Uniform specimen pressures and steady flow conditions were achieved for near sonic $(M = 1.1)$, and supersonic $(M = 2.1)$, free stream Mach numbers. The system has pumping capacity to achieve higher Mach numbers for heated air conditions. Testing can be accomplished over a pressure range of 10^{-5} to 760 Torr.

- Consistent emittance data were obtained for a number of materials over the range of environments from vacuum to $M = 2.1$ flow. Maximum test temperatures were $1650°K$, but this upper limit was imposed by test materials limitations rather than apparatus capability.

The inclusion of a hot gas flow system would be desirable for the testing of electrical insulators such as the ceramic coatings. During this program these specimens were heated using a platinum alloy cavity, and the maximum specimen temperature was limited to approximately $1350°K$ for flow conditions. This maximum temperature was constrained by the necessity to operate at the upper temperature limit of the cavity material, $1900°K$, considering convective heat transfer and low thermal conductivity materials. By using a heated air system, operation could be achieved at temperatures equal to or slightly higher than the cavity temperature.

A second consideration for the use of heated air concerns some ceramic like materials in which there is the possibility of a low level of transmittance in certain spectral band widths. By having to operate the cavity at significantly higher temperatures than the surface temperature, a small fraction of transmitted cavity energy can drastically increase pyrometric temperature measurement errors and subsequently the error in emittance. By using a hot gas stream the surface temperature can be operated slightly above cavity temperature, and for nearly opaque materials a small transmittance is much less significant to the temperature error.

Measurement of surface temperature remains the principal source of error in the emittance data obtained during this program. Under flow conditions temperature gradients generally are present in the test area, and it is necessary to determine this temperature distribution for the radiometer view area. Above $1100°$ K this is readily accomplished using an optical pyrometer.

Little effect of flow conditions on emittance was observed for the materials investigated. Some changes were noted between the "as prepared" condition and the initial exposure to either a static or a flow environment for the coated refractory metals. After the initial exposure to air, however, no further changes in emittance of any significance occurred.

Section 10
REFERENCES

1. "Development of Techniques and Associated Instrumentation for High Temperature Emissivity Measurements," First Quarterly Progress Report, Contract NAS 8-26304, Lockheed Palo Alto Research Laboratory, N-JF-70-1, Vol. 1 and Vol. 2., Oct. 1970.

2. Max, Jacob, Heat Transfer, John Wiley and Sons, New York, N.Y., Vol. 1, 1949.

3. S. T. Dunn and J. C. Richmond, "Survey of Infrared Measurement Techniques and Computational Methods in Radiant Heat Transfer," Thermophysics Specialists Conference, AIAA, Monterey, Calif., Sep. 1965.

4. G. L. Abbott, N. J. Alvares, and W. J. Parker, "Total Normal and Total Hemispherical Emittance of Polished Metals," WADD-TR-61-9A, Part I (1961), Part II (1963), Part III (1963).

5. C. T. Edquist and M. G. Strapp, "A Sphere-Cone Heating Analysis Program, ENVY," LMSC Report TIAD 837, 13 Oct. 1966.

6. C. T. Edquist, "Boundary Layer Thickness Calculations," LMSC Report TIAD 790, 21 Jun. 1965.

7. E. Reshotleo and I. E. Beckwith, "Compressible Laminar Boundary Layer Over a Yawed Infinite Cylinder with Heat Transfer and Arbitrary Prandtl Number," NACA TN 3986, Jun. 1957.

8. I. E. Beckwith and J. J. Gallager, "Local Heat Transfer and Recovery Temperature on a Yawed Cylinder at a Mach Number of 4.15 and High Reynolds Number," NASA TR R-104, 1961.

9. R. A. Perkins and C. M. Packer, "Coatings for Refractory Metals in Aerospace Environments," AFML-TR-65-351, Sep. 1965.

10. L. Kaufman and H. Nesor, "Stability Characterization of Refractory Materials under High Velocity Atmospheric Flight Conditions," AFML-TR-69-84, Part I, Vol. I, Mar. 1970.

11. L. Kaufman and H. Nesor, "Stability Characterization of Refractory Materials under High Velocity Atmospheric Flight Conditions," AFML-TR-69-84, Part III, Vol. III, Feb. 1970.

12. H. Goldstein, private communication, Nov. 1971.

13. W. A. Clayton and J. M. Gunderson, "Calibration of Mass Transport Capability of Re-entry Materials Evaluation Facility X-33," Boeing Report DS-SR-214 MP, Dec. 1963.

14. J. D. Buckley and B. A. Stein, "Preliminary Investigation of the Dynamic Oxidation of JT Graphite Composites at Surface Temperatures Between 4000°F and 5000°F, AFML-TR-66-174, P595, Jul. 1966.

15. "Development of Techniques and Associated Instrumentation for High Temperature Emissivity Measurements," Second Quarterly Progress Report, Contract NAS 8-26304, Lockheed Palo Alto Research Laboratory, N-JF-71-1, Jan. 1971.

16. G. J. Kneissl, and R. B. Kay, "Feasibility of Thermal Radiative Property Measurements Under Simulated Re-entry Conditions," AFML-TR-69-238, Jun. 1969.

17. W. K. Stratton, et al., "Advances in the Materials Technology Resulting from the X-20 Program," AFML-TR-64-396, Mar. 1965.

18. A. G. Emslie and H. H. Blau, Jr., "On the Measurement of the Temperatures of Unenclosed Objects by Radiation Methods," J. Electrochem Soc V6, No. 10, pp. 872-880, Oct. 1959.

19. W. A. Clayton, "A 500° to 4500°F Thermal Radiation Test Facility for Transparent Materials," NASA SP-31, pp. 445-460.

20. R. E. Rolling, A. I. Funai and J. R. Grammer, "Investigation of the Effect of Surface Conditions on the Radiant Properties of Metals," AFML-TR-64-363, 1967.

21. W. J. King, "Free Convection," Mech. Eng. 54, p. 347, 1932.

22. "Certificate of Normal Spectral Emittance," — "Standard Reference Materials 1402 to 1409" and "Standard Reference Materials 1420 to 1428," National Bureau of Standards, U.S. Department of Commerce, April 1966 and Dec. 1965.

Appendix A

EMITTANCE DATA FOR TI-6AL-4V AND COATED RENÉ 41
SAMPLES SUPPLIED BY MSFC

Total and spectral emittance characteristics of nine metal-strip test specimens were measured at temperatures to 1145°K in order to evaluate several coatings and heat-treatment techniques. The specimens, eight René 41 test strips and one anodized titanium-alloy test strip, were prepared at MSFC and forwarded to LMSC for testing in the LMSC High-Temperature Emittance Test Apparatus. Discussions of specimen description, test method, and experimental results are presented in this appendix.

A.1 SPECIMENS

The test specimens were coated or heat-treated metal strips with the following dimensions.

Length: 20.3-cm (nominal)

Width: Uniform, between 1.70 and 2.56-cm

Thickness: Uniform, between 0.043 and 0.163-cm

Sample identification numbers together with brief descriptions of the preparation methods as supplied by MSFC and "as-received" appearances are given in the following paragraphs:

- <u>Sample No. I</u>: René 41 with one coat of Solar SP-43A-I coating. Sample appearance was uniform dull black or dark gray with two vertical streaks down the length of one side.

- <u>Sample No. II</u>: Same as No. I but with dipped-coating of Solar SP-43A-I; uniform dull black color.

- <u>Sample No. 1</u>: René 41, re-solution annealed in air at 1350° K, then oxidized for 16 hrs at 1033° K in air. Sample appearance was dull, mottled gray.

A-1

- <u>Sample No. 2:</u> René 41, oxidized for 16 hrs at 1033°K in air. Sample appearance was fairly uniform, dull gray.

- <u>Sample No. 3:</u> René 41, oxidized for 4 hrs. at 1170°K in air. Sample appearance was fairly uniform, dull, dark gray with a few scratches and small, scattered dark spots.

- <u>Sample No. C2:</u> René 41, heat-treated as follows:

  1/2 hr at 1393°K in air.

  Cooled to room temperature in air.

  4 hrs at 1173°K in vacuum.

  Sample appearance was uniform, slate-gray color.

- <u>Sample No. D2:</u> René 41, heat-treated as follows:

  1/2 hr at 1350°K in air.

  Cooled to room temperature in air.

  16 hrs at 1033°K in vacuum.

  Sample appearance was uniform, slate-gray color.

- <u>Sample No. A2:</u> René 41, heat-treated as follows:

  1/2 hr at 1393°K in vacuum.

  Cooled to room temperature in vacuum.

  3 hrs at 1173°K in vacuum, then

  2 hrs at 1173°K in air.

  Sample appearance was fairly uniform, dull gray color with several scratches and lead-pencil marks on both surfaces. This sample was formed by spot-welding two 0.043-cm thick strips of René 41 together (back to back). One of the strips was only half as thick as the upper section. Also, a 0.6-cm diameter hole had been drilled or punched through the center of the test strip about 6.5-cm above the bottom (thin) end.

- <u>Sample No. E1:</u> Anodized titanium alloy (Ti-6A1-4V). Sample appearance was uniform, dull greenish-gray color.

A-2

Each of the test strips was instrumented with five Pt/Pt-13% Rh thermocouples spot-welded to one edge of the strip – one at the mid-length centerline of the strip, two located ±1.0-cm above and below the centerline thermocouple and two located ±1.5-cm from the centerline. The thermocouples were made from 3-mil diameter bare wire (to minimize thermal conduction losses from the sample), and served to indicate the temperature of the central test-section of the sample. The platinum legs also served as potential measurement taps for determining the voltage drop, and hence I^2R heating power, generated across the test section of the sample. The overall length of each sample thermocouple was approximately 35-cm from the sample to the baseplate feed through, from which extension leads led to a reference junction ice bath, voltage measurement box, and the measuring potentiometer.

A.2 TEST PROCEDURES

The eight René 41 samples were tested at 700°K, 923°K, and 1143°K in vacuum to determine the following emittance properties at each temperature: total hemispherical emittance, ϵ_{TH}; total normal emittance, ϵ_{TN}; and spectral normal emittance, ϵ_λ, at wavelengths between $\lambda = 1\mu$m and $\lambda = 15\mu$m. After being heated to 1143°K, each sample was maintained at that temperature (or power level), for periods of from 20 to 72 hours to evaluate the emittance stability of the sample under these test conditions. The total emittance properties of each sample were then remeasured at each of the three test temperatures as the sample was cooled to room temperature, prior to terminating the test. Exceptions to this general test procedure are noted for Samples #1 and #A2 in the discussion of results which follow.

The test procedure for the anodized titanium sample was the same as described above but at two lower temperatures, 423°K and 700°K, and spectral measurements were obtained only at the 700°K test temperature.

Sample heating and cooling rates were controlled manually with a Variac control to the 10 KVA power transformer, and did not exceed 4°K/sec. All the tests were made in vacuum and the ion-gauge-indicated chamber pressure remained steady at 1×10^{-5} torr at all test temperatures.

A-3

Before and after the elevated temperature emittance tests described above, the following room-temperature emittance properties for each sample were determined:

- Total Emittance, ϵ_T (300°K) inferred from total IR-Reflectance Measurements with a Gier-Dunkle Model DB-100 Reflectometer

- Spectral emittance (or absorptance) from $\lambda = 0.28\mu m$ to $\lambda = 1.8\mu m$, inferred from spectral reflectance measurements with a Cary Model 14 Spectrophotometer with an Integrating Sphere Reflectance attachment.

These supplemental measurements served to verify changes in sample appearance or emittance that were observed during the high temperature tests. The methods used to determine the total and spectral emittance characteristics of these test specimens were the same as described earlier in this report.

A.3 EMITTANCE DATA

Results of the spectral emittance tests for the nine MSFC-supplied test specimens are shown in figures A1 through A9. Figure A1 shows the spectral emittance characteristics of the anodized Ti-6Al-4V sample (No. E1) at a test temperature of 700°K and at wavelengths from 1.5 to 15 μm. Short wavelength emittance characteristics inferred from room-temperature reflectance measurements of the center test-section area of the sample before and after the high-temperature emittance test are also shown. The infrared emittance values are in good agreement with the independently-measured total normal emittance values obtained for this sample at 433°K and 700°K, and show that the reason for the observed drop in ϵ_{TN} with increasing temperature is due to lower ϵ_λ in the region from 1.5 to 8 μm relative to the higher ϵ_λ values at $\lambda > 8 \mu m$. The pre- and post-test reflectance data indicated a slight increase (about 1%) in emittance (or absorptance) in the $0.6 \mu m \leqq \lambda \leqq 1.8 \mu m$ spectral region as a result of the emittance-test exposure of 69 hours at 700°K in vacuum (10^{-5} Torr).

A-4

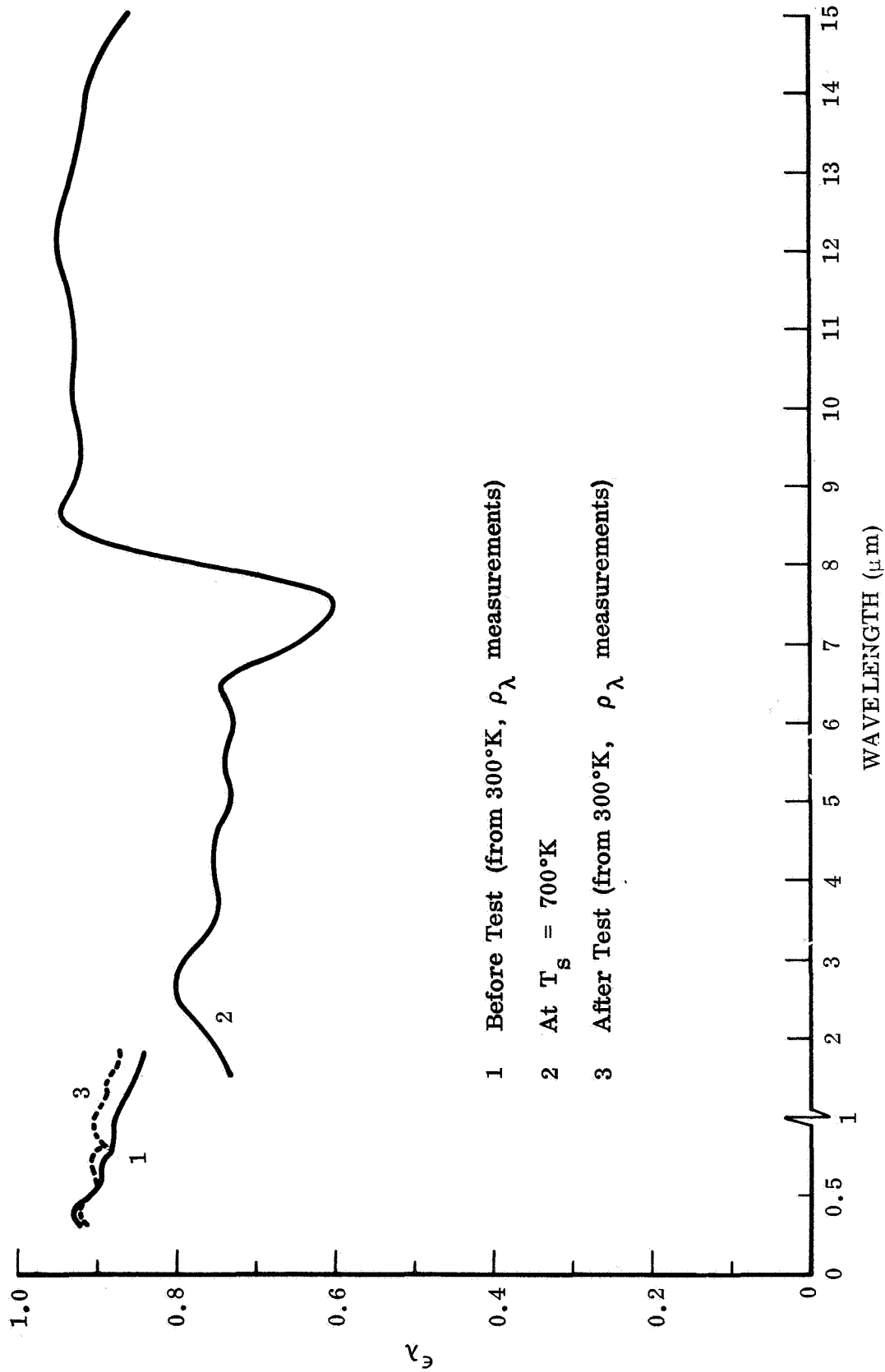Fig. A-1 Spectral Emittance of MSFC Anodized Ti-6AL-4V Sample No. E1, 700°K

1 Before Test (from 300°K, ρ_λ measurements)
2 At T_s = 700°K
3 After Test (from 300°K, ρ_λ measurements)

WAVELENGTH (μm)

ϵ_λ

A-5

Figures A2 and A3 show spectral emittance data for the two Solar SP-43A-I coated Rene samples (No. I and No. II) at test temperatures of 700°K, 923°K, and 1143°K. These curves indicate that significant changes in ϵ_λ occurred during the emittance tests of these samples; however, the net effect of these changes or the total emittance properties of the samples is small, and the data is in good agreement with the independently-measured ϵ_{TN} values at each temperature.

It should be noted that several of the determinations result in ϵ_λ values greater than 1, and these errors could be due to one or a combination of measurement errors in the following parameters: (1) sample temperature determination, (2) KBr window transmittance, (3) reference blackbody temperature, (4) blackbody mirror reflectance, or (5) blackbody and/or sample signal measurement errors. Errors in the window transmittance and mirror reflectance values used for these tests would be systematic for all the sample emittance determinations made in this study and are believed to not exceed ±1 percent. Similarly, blackbody temperature indication errors would also be systematic for all the tests and are believed to not exceed ±3 K (±0.3% at 1143°K). Signal measurements are believed accurate to ±1%, consequently errors in the signal ratios should not exceed ±2%. The most likely source of error is in the sample temperature determinations; however, thermocouple and optical pyrometer readings have been carefully analyzed for each sample in order to minimize these errors, and they are believed to not exceed ±1% at each test temperature. (Note: T_s errors for the total emittance determinations at 923°K and 700°K during the cooling portion of the test cycle may be slightly higher due to thermocouple-calibration changes after the 1143°K stability-test exposures and the inability to verify the thermocouple readings at these temperatures with optical pyrometer readings.) If the high ϵ_λ values for these two samples are indeed due to low T_s determinations, the "corrected" ϵ_λ values in the 1 to 5 μm region will be significantly lower than are shown in figures A2 and A3.

Pre- and post-test reflectance data for Sample No. I indicates that the room-temperature emittance of this sample in the 0.3 μm $\leq \lambda \leq$ 1.8 μm region was essentially flat at 0.95 and did not change more than ±2% after 69 hours at 1143°K in vacuum. The initial room-temperature emittance curve for Sample No. II dropped off considerably at $\lambda >$ 1.0 μm to a low of 0.83 at λ = 1.8 μm. After a 20-hour exposure at 1143°K in
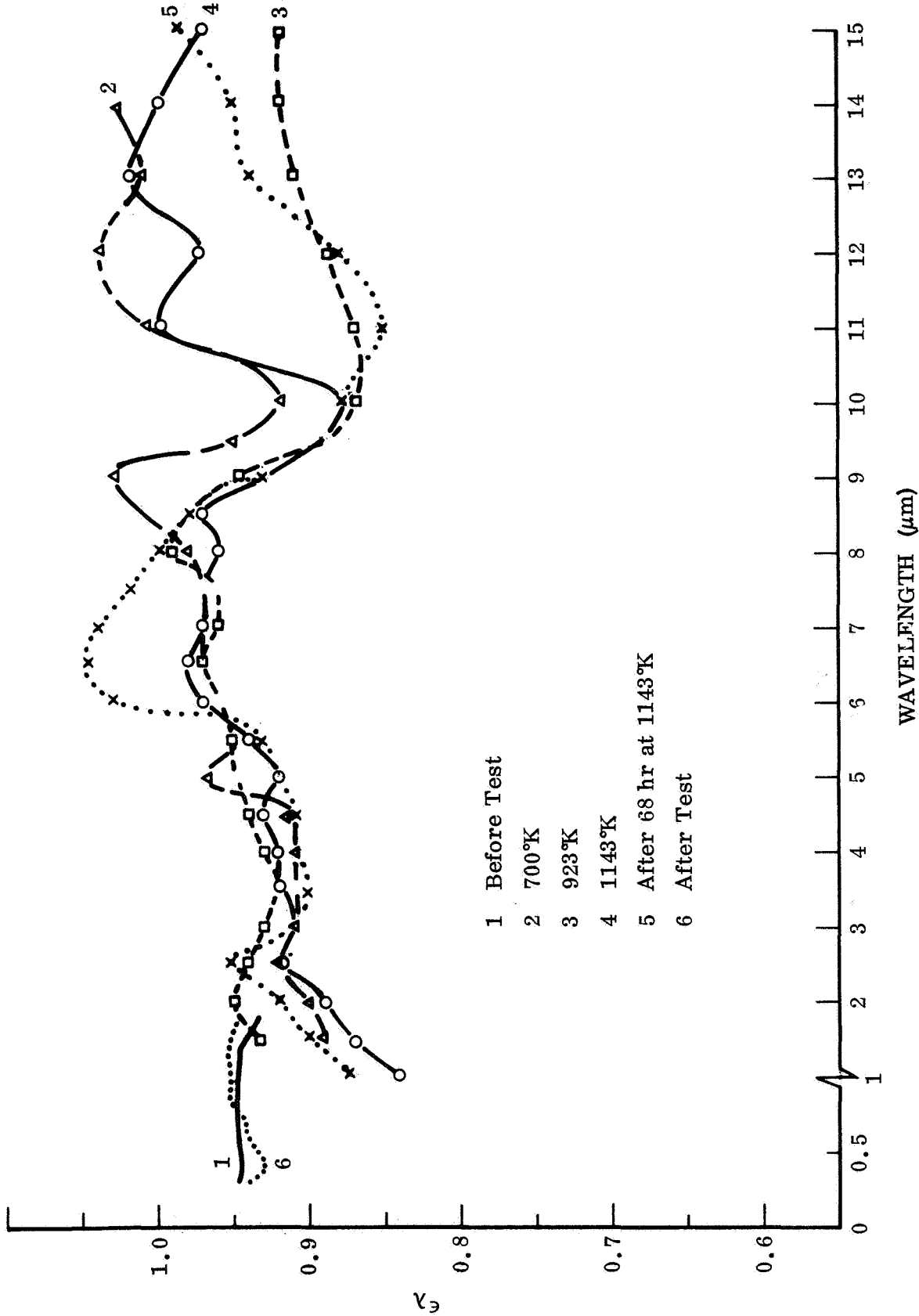
A-6

Fig. A-2 Spectral Emittance of MSFC René Sample No. I with Single
Coat of Solar SP-43A-I

1 Before Test
2 700°K
3 923°K
4 1143°K
5 After 68 hr at 1143°K
6 After Test
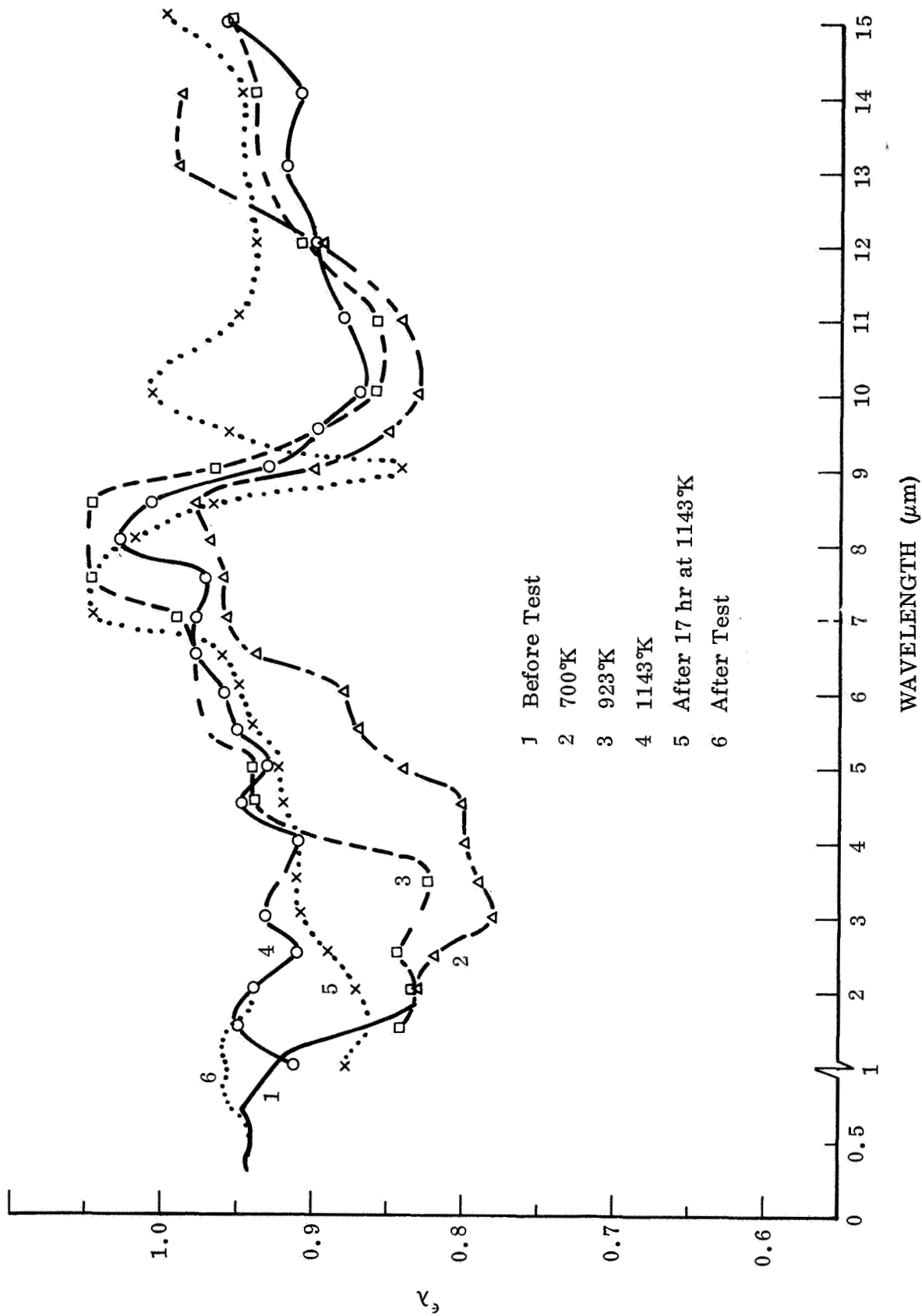
Fig. A-3 Spectral Emittance of MSFC René 41 Sample No. II with Single Coat (Dipped) of Solar SP-43A-I

1   Before Test
2   700°K
3   923°K
4   1143°K
5   After 17 hr at 1143°K
6   After Test

A-8

vacuum, however, the room-temperature emittance curve was similar to that for Sample #I. This change correlates with the initially lower total emittance values obtained for this sample, and the subsequent increase in total emittance after the 20-hr stability test exposure.

Spectral emittance characteristics for the various oxidized René 41 test samples are shown in figures A4 through A9. The data for Sample No. 1, figure A4, indicates that at wavelengths greater than 2μm. ϵ_λ for this oxide coating was not highly temperature-dependent and did not change significantly after 70 hours at $1143°$ K in vacuum. A large change in the room-temperature values between $0.3~\mu$m and $1.8~\mu$m was indicated, however, by the post-test reflectance measurements. This change correlates with the significant color change that was observed for this oxide coating at the conclusion of the high-temperature emittance test.

The initial ϵ_λ characteristics for Sample No. 2, figure A5, differed considerably from those for Sample No. 1 at $700°$ K and $923°$ K and featured a broad, low-emittance band in the region from 7 to 15μm. At $1143°$K, however, ϵ_λ was observed to increase dramatically at wavelengths longer than 5μm, and after 27 hrs at $1143°$ K, ϵ_λ in the 2μm $< \lambda < 5~\mu$m region also increased. These changes correlate well with the independently-measured total emittance values for this sample.

The initial ϵ_λ characteristics for Sample No. 3, figure A6, were similar to those for Sample No. 2, with the exception that the large increase in ϵ_λ at wavelengths longer than 7μm was not observed until after the 69-hr stability-test period for this sample at $1143°$K. After this time, both the spectral and the total emittance properties of these two samples were observed to be closely alike. Unusual color-change patterns were observed for the oxide coating on Sample No. 3 after the high-temperature emittance tests. Post-test reflectance data for the lighter, yellow-green areas and the darker gray areas which developed on the front (viewed) face of the sample strip are shown by curves 6a and 6b on figure A6.

The initial and final ϵ_λ characteristics for Samples No. C2 and No. D2, figures A7 and A8, were observed to be almost identical to one another and to those described earlier for Sample No. 1. Changes in the appearance of these samples after their
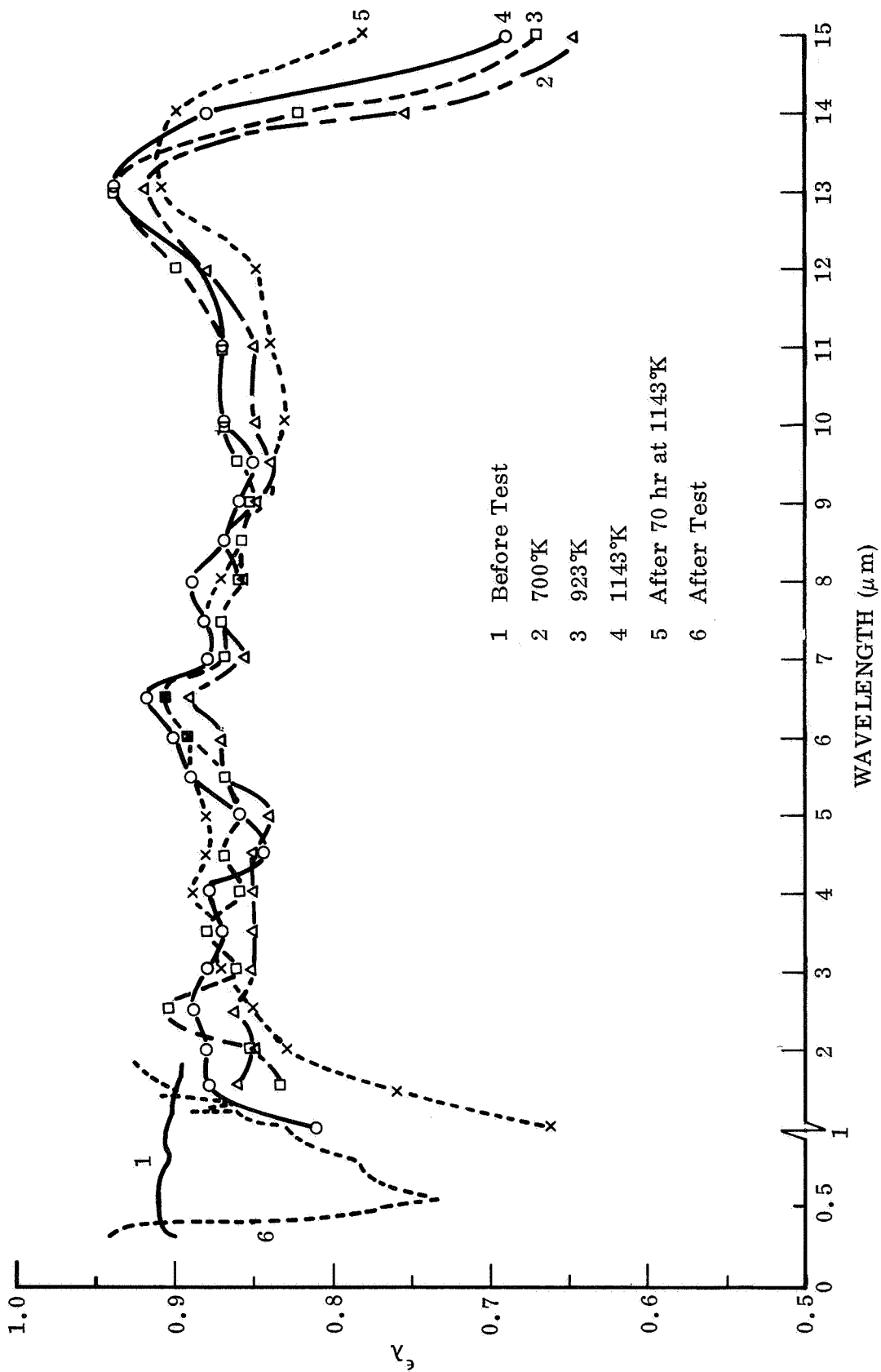
A-9

Fig. A-4 Spectral Emittance of MSFC Oxidized René 41 Sample No. 1
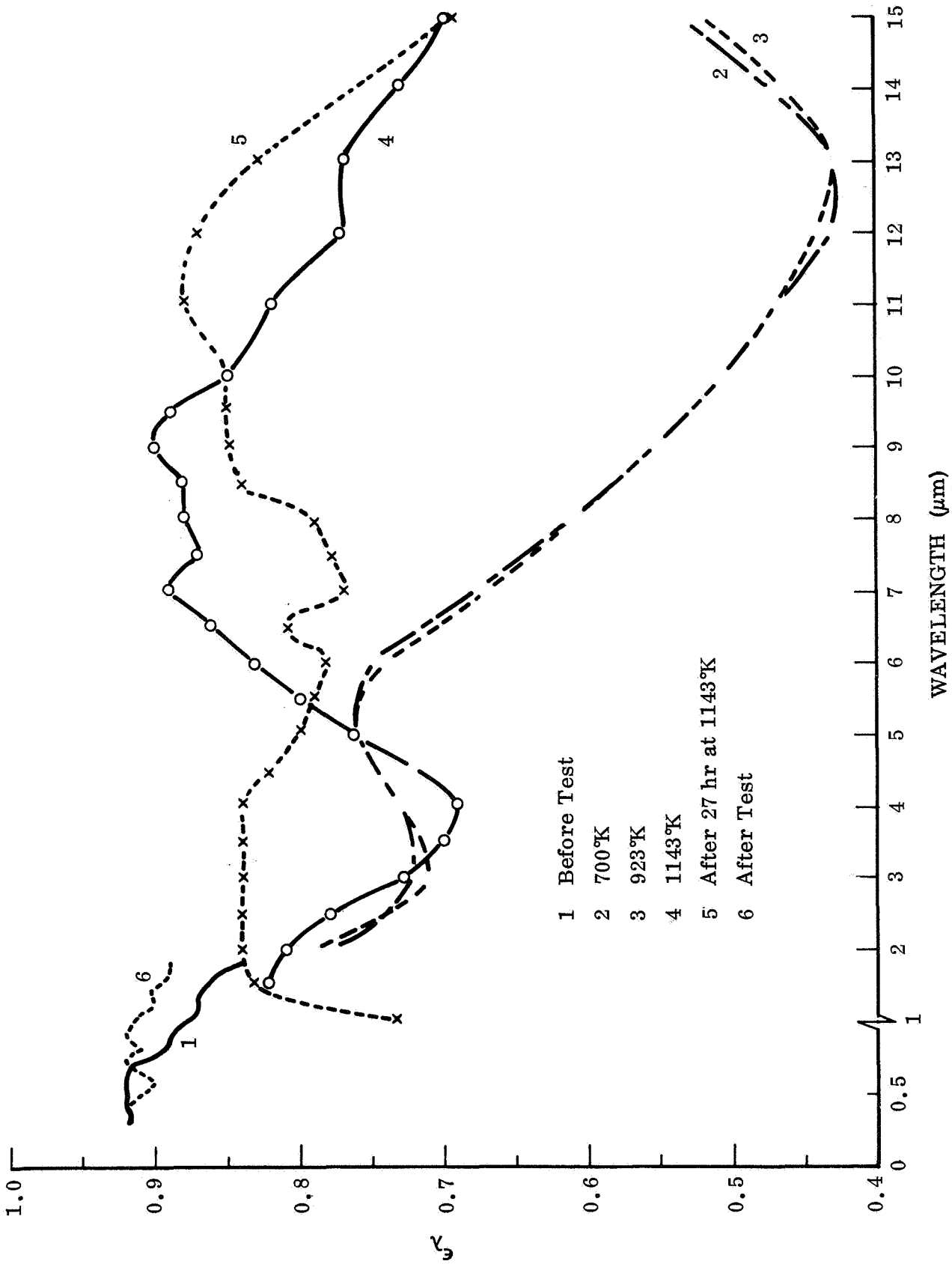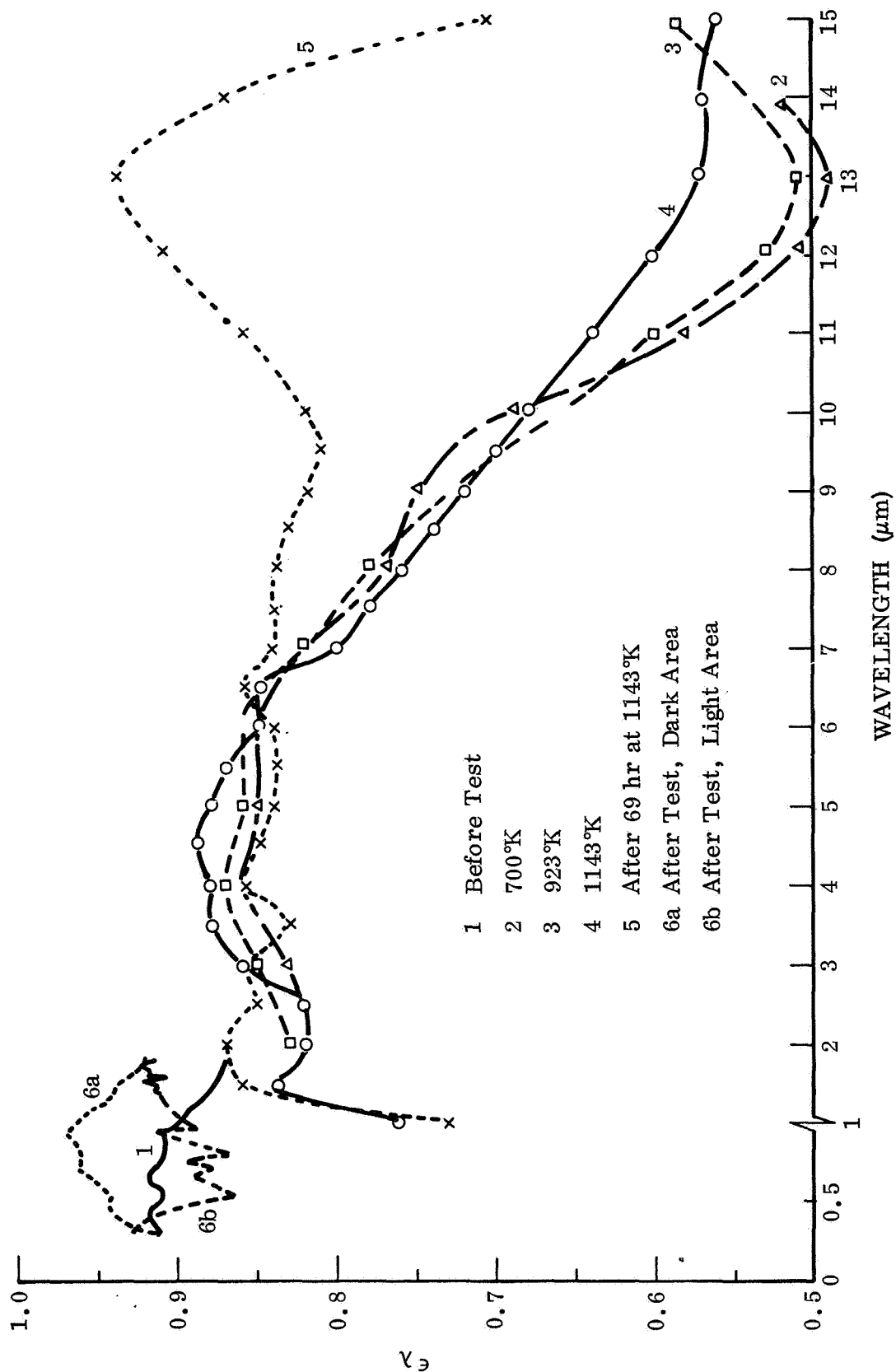
1   Before Test
2   700°K
3   923°K
4   1143°K
5   After 70 hr at 1143°K
6   After Test

WAVELENGTH (μm)

ϵ_λ

A-10

Fig. A-5 Spectral Emittance of MSFC Oxidized René 41 Sample No. 2

1 Before Test
2 700°K
3 923°K
4 1143°K
5 After 27 hr at 1143°K
6 After Test

WAVELENGTH (μm)

ϵ_λ

A-11

Fig. A-6 Spectral Emittance of MSFC Oxidized René 41 Sample No. 3

1 Before Test
2 700°K
3 923°K
4 1143°K
5 After 69 hr at 1143°K
6a After Test, Dark Area
6b After Test, Light Area

WAVELENGTH (μm)

ϵ_λ

Fig. A-7 Spectral Emittance of MSFC Oxidized René 41 Sample No. C2

1 Before Test
2 700°K
3 923°K
4 1143°K
5 After 47 hr at 1143°K
6 After Test

WAVELENGTH (μm)

ϵ_λ
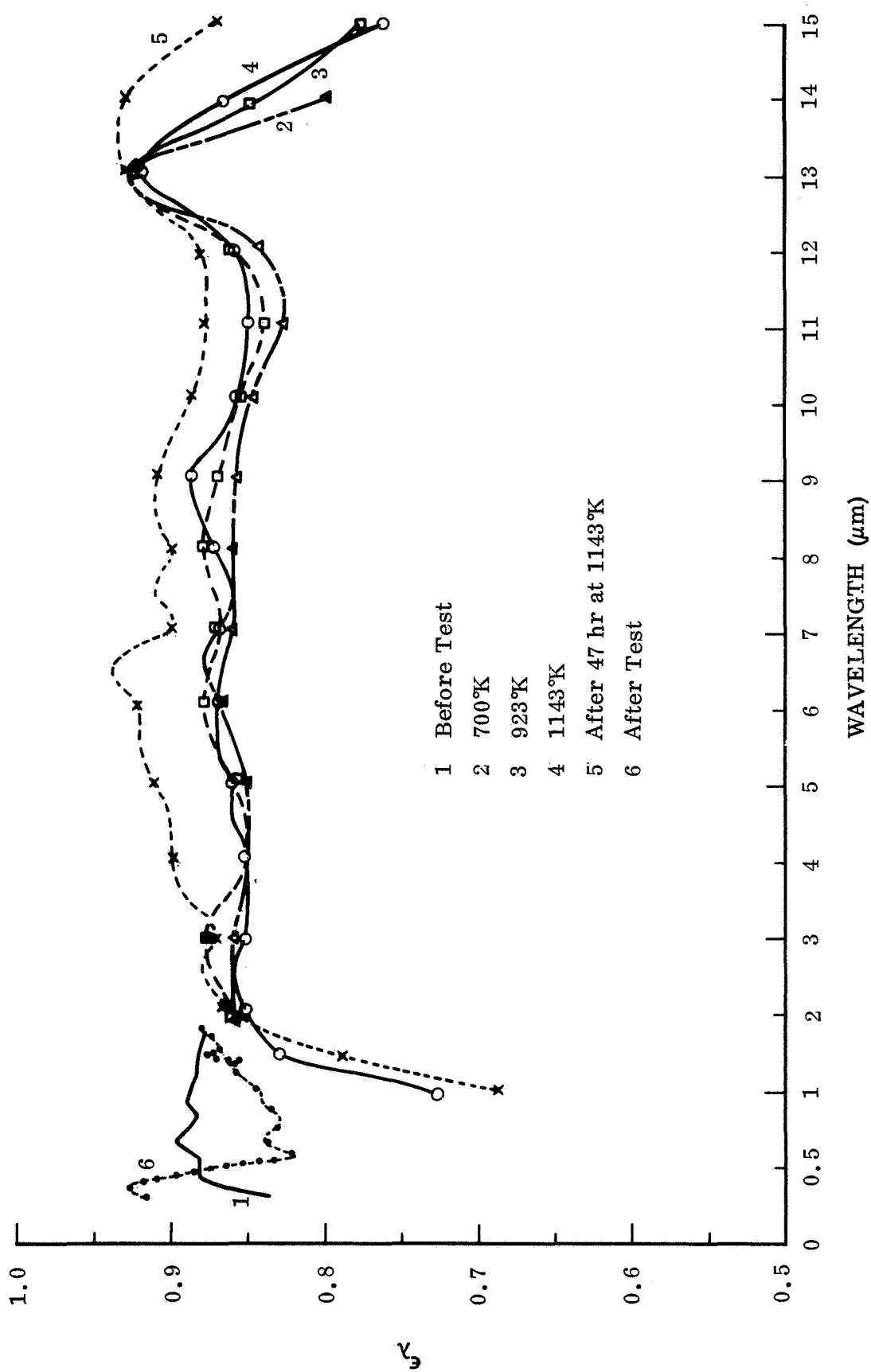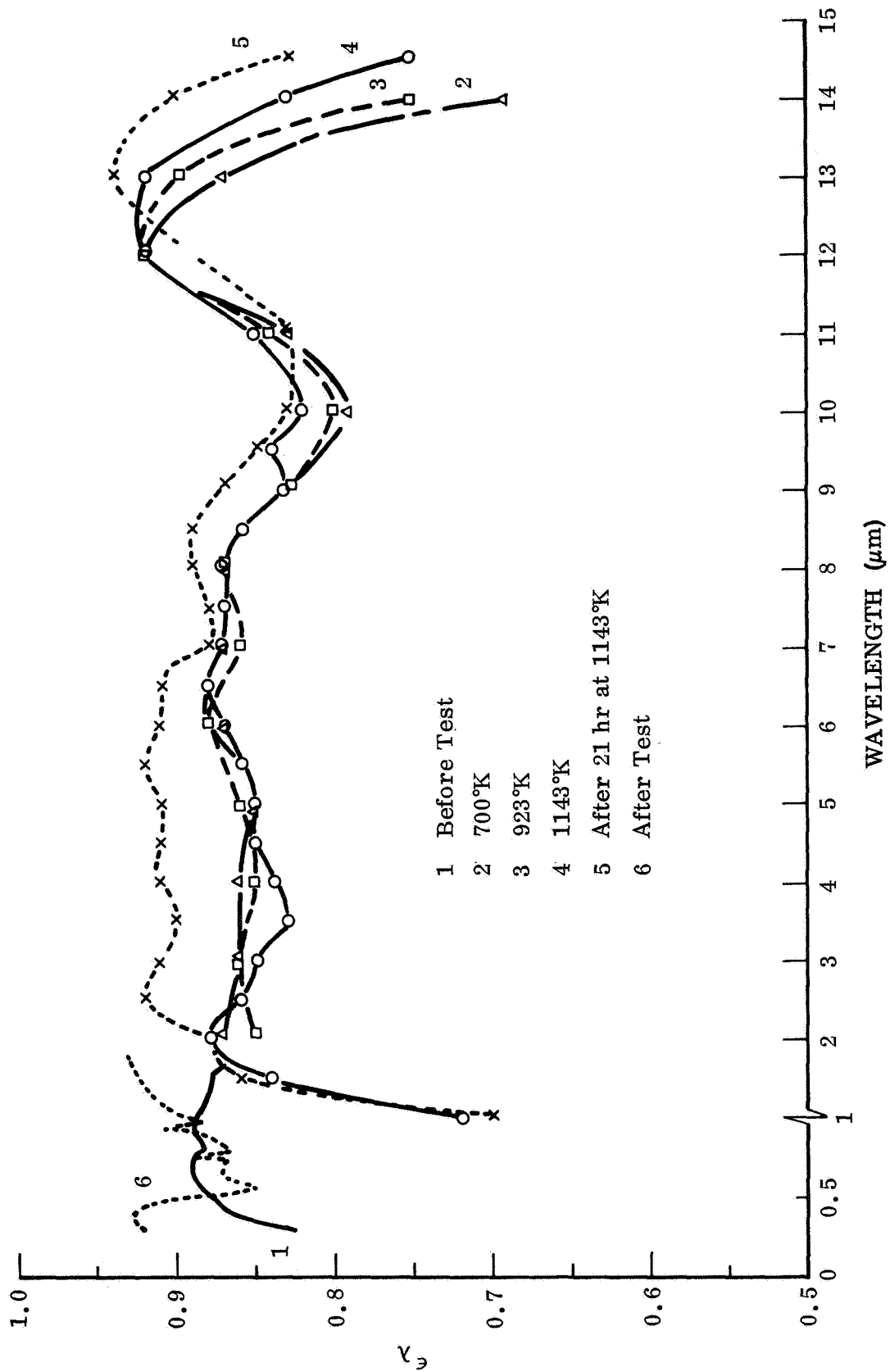
Fig. A-8 Spectral Emittance of MSFC Oxidized René 41 Sample No. D2

1 Before Test
2 700°K
3 923°K
4 1143°K
5 After 21 hr at 1143°K
6 After Test

WAVELENGTH (μm)

ϵ_λ

A-14
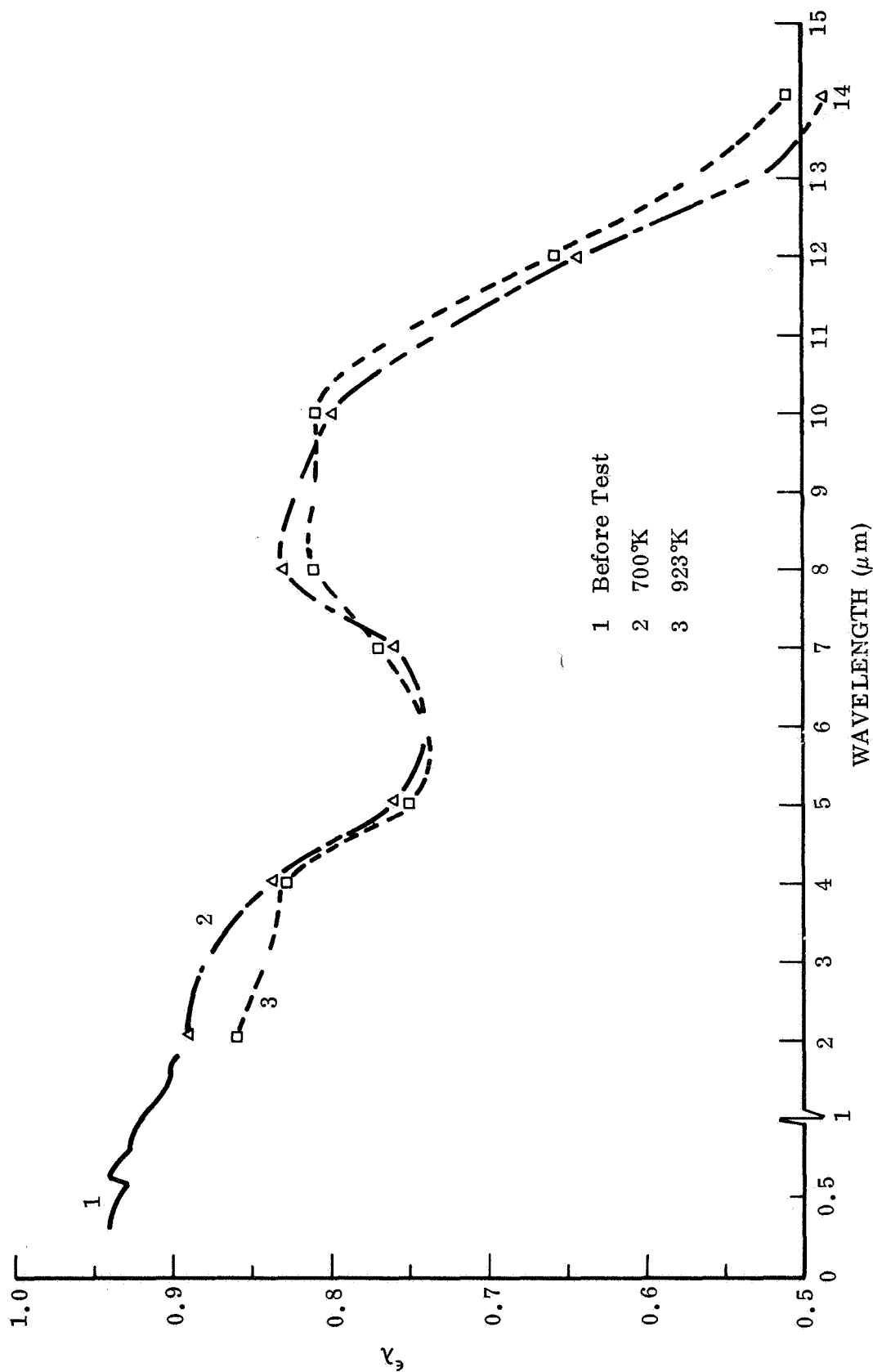
Fig. A-9 Spectral Emittance of MSFC Oxidized Rene´41 Sample No. A2

1 Before Test
2 700°K
3 923°K

A-15

high–temperature emittance tests was from an initial slate-gray color to a mottled yellow–green/gray color. These changes correlate with the differences indicated by the pre- and post-test reflectance data for these samples.

The initial ϵ_λ characteristics for the oxide coating on Sample No. A2 are shown in figure A9 and are seen to be similar to those for Samples 2 and 3 at 700°K and 923°K. No additional emittance data was obtained for this sample because of a sample failure as it was being heated to 1100°K.

As mentioned earlier in the discussion of errors associated with the results for Samples I and II, comparisons were made of the absolute sample temperature indications by optical pyrometer readings at 1143°K, using ϵ_λ values at $\lambda = 0.65\,\mu$m indicated by the room-temperature reflectance measurements for each sample, with the temperature indications obtained from the sample thermocouple readings. The results of these comparisons are as follows:

1) The initial 1143°K test temperatures indicated by the sample thermo- couples are generally low by about 0.5% (5°K), relative to the pyrometer temperature indications. This difference is in addition to the edge-to- center temperature differences for each test strip which were observed with the optical pyrometer.

2) After each of the sample stability test periods at 1143°K, the pyrometer to thermocouple temperature indication difference increased to between 1.0 and 1.5% (10 to 15°K), presumably due to changes in the thermal emf cali- bration for the 3-mil, bare-wire thermocouples.

The emittance results presented in Table A-1 include corrections to T_s for the above- mentioned thermocouple errors. It should also be noted that the 923°K and 700°K test values listed in Table A-1 which were determined after the 1143°K test exposures do not include any additional corrections to T_s to account for possible changes in the thermocouple calibration and are therefore suspected to be from 1 to 3 percent too high.

Table A–1

SUMMARY OF TEST RESULTS FOR NINE MSFC EMITTANCE TEST SAMPLES

Sample	Test Cycle	α_s	ϵ_T (300°K)	$\epsilon_{TH}/\epsilon_{TN}$ at (700°K)	$\epsilon_{TH}/\epsilon_{TN}$ at (923°K)	$\epsilon_{TH}/\epsilon_{TN}$ at (1143°K)	Hours at T (max)
René I	Heating	0.95	0.88	0.87/0.94 ↑	0.87/0.93 ↑	0.87/0.92 ↑	69
	Cooling	0.94	0.86	0.89/0.94 ↓	0.90/0.93 ↓	9.87/0.92 ↓	
René II	Heating	0.92	0.86	0.82/0.87 ↑	0.83/0.88 ↑	0.85/0.89 ↑	20
	Cooling	0.95	0.86	0.87/0.94 ↓	0.87/0.92 ↓	0.86/0.89 ↓	
René 1	Heating	0.91	0.74	0.80/0.85 ↑	0.81/0.83 ↑	0.83/0.85 ↑	71
	Cooling	0.83	0.77	—	—	0.84/0.86 ↓	
René 2	Heating	0.90	0.53	0.64/0.67 ↑	0.69/0.72 ↑	0.74/0.77 ↑	28
	Cooling	0.91	0.73	0.78/0.85 ↓	0.80/0.87 ↓	0.79/0.85 ↓	
René 3	Heating	{ 0.90 / 0.90	0.60	0.71/0.78 ↑	0.76/0.82 ↑	0.80/0.84 ↑	70
	Cooling	0.94	0.73	0.79/0.85 ↓	0.80/0.86 ↓	0.80/0.85 ↓	
René C2	Heating	0.88	0.74	0.78/0.84 ↑	0.79/0.86 ↑	0.79/0.85 ↑	48
	Cooling	0.86	0.80	0.83/0.89 ↓	0.83/0.90 ↓	0.82/0.89 ↓	
René D2	Heating	0.88	0.73	0.78/0.83 ↑	0.78/0.84 ↑	0.78/0.84 ↑	22
	Cooling	0.90	0.77	0.81/0.89 ↓	0.83/0.91 ↓	0.82/0.88 ↓	
René A2	Heating	0.92	0.67	0.70/0.79 ↑	0.76/0.83 ↑	—	—
	Cooling	—	—	—	—	—	

Sample	Test Cycle	α_s	ϵ_T (300°K)	$\epsilon_{TH}/\epsilon_{TN}$ at 422°K	$\epsilon_{TH}/\epsilon_{TN}$ at 700°K	Hours at T (max)
Ti-6A1-4V E1	Heating	0.88	0.80	0.75/0.79 ↑	0.72/0.78 ↑	69
	Cooling	0.90	0.80	—	0.74/0.82 ↓	

Note: $\epsilon_{TH}/\epsilon_{TN}$ values obtained at 923°K and 700°K after the 1143°K test exposures are believed to be 1 to 3 percent too high due to thermocouple calibration changes. See Discussion.

Appendix B
DISTRIBUTION LIST FOR FINAL REPORT
LMSC-D352380

Copies

National Aeronautics and Space Administration
George C. Marshall Space Flight Center
Marshall Space Flight Center, Alabama 35812
Attn: A&TS-MS-IL   1
    A&TS-TU   1
    A&TS-MS-IP   2
    S&E — Attn: MCS, Mr. R. Harwell   10

Lockheed Missiles & Space Company
P.O. Box 504
Sunnyvale, California 94088
Attn: Mr. John Lloyd, Manager, Alternate Space Shuttle Concept Study
    Dept. G1-51-Bldg. 538

Space Division
North American Rockwell Corporation
12214 Lakewood Boulevard
Downey, California 90241
Attn: Mr. Joe Monroe

The Boeing Company
P.O. Box 1470
Huntsville, Alabama 35807
Attn: Maxie Brown (Space Shuttle)

Space Division
North American Rockwell Corporation
12214 Lakewood Boulevard
Downey, California 90241
Attn: Mr. B. Hello
    Vice President, Corporate Wide General Manager
    Space Shuttle Program

McDonnell Douglas Astronautics Company
P.O. Box 516
St. Louis, Missouri 63166
Attn: Mr. Sherman L. Hislop
    Director of Booster/Orbiter Integration

B-1

CCSD
Michoud Operation
P.O. Box 29200
New Orleans, Louisiana 70129
Attn: Mr. C. E. Tharrott, Dept. 2760

Grumman Aerospace Corporation
Plant 25 — Space Shuttle
Bethpage, L.I., New York 11714
Attn: Mr. Fred Raymer

NASA Langley Research Center
Langley Station
Hampton, Virginia 23365
Attn: Mr. Bland Stein

NASA, Ames Research Center
Moffett Field, California 94035
Attn: Mr. H. Goldstein

NASA, Lewis Research Center
21000 Brookpark Road
Cleveland, Ohio 44135
Attn: Mr. John Merutka

Air Force Materials Laboratory
Air Force Systems Command
Wright-Patterson Air Force Base, Ohio 45433
Attn: Mr. N. Geyer

Arthur D. Little, Inc.
20 Acorn Park
Cambridge, Massachusetts 02140
Attn: Mrs. Jean-Berkowitz-Mattuck

The Boeing Company
P.O. Box 3707
Seattle, Washington 98124
Attn: Mr. W. A. Clayton

McDonnell-Douglas Corporation
Box 516, Dept. 256C
Building 102
St. Louis, Missouri 63166
Attn: Mr. T. Allen

University of California
Thermal Systems Division
Berkeley, California 94720
Attn: Professor C. L. Tien

Grumman Aerospace Corporation
Thermodynamics, Plant 35
Bethpage, Long Island, New York 11714
Attn: Mr. L. Hemmerdinger

Thermophysical Properties Research Center
Purdue University Research Park
2595 Yeager Road
West Lafayette, Indiana 47906
Attn: Mr. D. P. DeWitt/Dr. R. E. Taylor